

THE UNIVERSITY OF CALGARY

Prestressed Composite Girders with Corrugated Steel Webs

by

Ahmed Salah El Metwally

A THESIS

SUBMITTED TO THE FACULTY OF GRADUATE STUDIES  
IN PARTIAL FULFILMENT OF THE REQUIREMENTS FOR THE  
DEGREE OF MASTER OF SCIENCE

DEPARTMENT OF CIVIL ENGINEERING

CALGARY, ALBERTA

DECEMBER, 1998

© Ahmed Salah El Metwally 1998



National Library  
of Canada

Acquisitions and  
Bibliographic Services

395 Wellington Street  
Ottawa ON K1A 0N4  
Canada

Bibliothèque nationale  
du Canada

Acquisitions et  
services bibliographiques

395, rue Wellington  
Ottawa ON K1A 0N4  
Canada

*Your file Votre référence*

*Our file Notre référence*

The author has granted a non-exclusive licence allowing the National Library of Canada to reproduce, loan, distribute or sell copies of this thesis in microform, paper or electronic formats.

The author retains ownership of the copyright in this thesis. Neither the thesis nor substantial extracts from it may be printed or otherwise reproduced without the author's permission.

L'auteur a accordé une licence non exclusive permettant à la Bibliothèque nationale du Canada de reproduire, prêter, distribuer ou vendre des copies de cette thèse sous la forme de microfiche/film, de reproduction sur papier ou sur format électronique.

L'auteur conserve la propriété du droit d'auteur qui protège cette thèse. Ni la thèse ni des extraits substantiels de celle-ci ne doivent être imprimés ou autrement reproduits sans son autorisation.

0-612-38626-0

## **ABSTRACT**

An increasing interest in using composite prestressed girders with corrugated webs in bridges has been recognized. The objective of this study is to theoretically investigate the shear strength of corrugated steel webs, and to experimentally investigate both the shear and flexural behaviour of the composite structure. Five, 5.5 m long and 0.73 m deep, prestressed simple span I-girders with zigzag corrugated webs have been built and tested.

The theoretical study shows that the geometry of such webs can be chosen to provide the highest shear strength for the least volume of steel with negligible sensitivity to initial imperfections in the corrugation angle. The existence of a post-buckling shear strength that can be as high as 82 % of the total strength was experimentally confirmed. The experimental results show that while the web supports the shear, the bottom flange prestressing steel supports the tension, and the concrete top flange supports the compression.

## **ACKNOWLEDGEMENTS**

Praise and thanks be to Allah, the Most Gracious, the Most Merciful, and peace be upon His Prophet.

I am extremely grateful to my supervisor, Dr. Robert E. Loov for his support, encouragement, and endless patience and guidance throughout the course of the program. I also deeply appreciate the interest in the project that was expressed by Dr. Amin Ghali and Dr. Gamil Tadros, and I would like to thank them for these fruitful discussions.

I would like to express my deep gratitude to the technical staff of the Department of Civil Engineering especially Mr. Don McCullough, Mr. Terry Quinn, and Mr. Don Anson for their invaluable help, guidance, and donation of time throughout the experimental part of the study. Specifically, I would like to thank Mr. Terry Quinn and Mr. Don Anson for their role in machining the forms, casting flanges, prestressing, and setting up the test and instrumentation; Mr. Paul Houle for the calibration and operation of the MTS loading system; Mr. Don McCullough for his expertise with the instrumentation and the MTS system, and for setting up the data acquisition program. I would also like to express my thanks to Mr. Harry Pollard for smoothly arranging the procurement of the materials. The help offered by my colleagues Mahmoud Reda, Liying Peng, Brian Sjoberg, David Dechka, Florian Spitzner, and Mostafa Hassanain in casting the concrete flanges is greatly appreciated.

The donation of the prestressing strands by Con-Force Structures Limited, Calgary, Canada; and of the superplasticizer by Master Builders Inc., Calgary, Canada is greatly appreciated.

The financial support of Concrete Canada (The Network of Centres of Excellence on High-Performance Concrete), NSERC (The National Sciences and Engineering Research Council), and the Department of Civil Engineering is gratefully acknowledged.

***To My Parents***

***for their continuing love and support***

## TABLE OF CONTENTS

Approval Page .....	ii
Abstract .....	iii
Acknowledgements .....	iv
Dedication .....	v
Table of Contents .....	vi
List of Tables .....	xi
List of Figures .....	xii
List of Symbols .....	xv
 CHAPTER 1 : INTRODUCTION .....	 1
1.1 General .....	1
1.2 Scope of Research Program .....	1
1.3 Thesis Organization .....	2
 CHAPTER 2 : LITERATURE REVIEW .....	 3
2.1 General .....	3
2.2 Shear Strength of Thin Flat Plates .....	3
2.2.1 Buckling Strength .....	3
2.2.2 Post-Buckling Strength .....	6
2.3 Buckling Strength of Shear Diaphragms .....	8
2.4 Research on Steel Beams with Corrugated Webs .....	11
2.4.1 Chalmers University of Technology (Sweden) 1983 - 1987 .....	11
2.4.1.1 Shear Buckling of Girder Webs .....	12

2.4.1.2	Shear, Compression, and Combined Shear and Compression Buckling of Panels . . . . .	14
2.4.1.3	Load-Bearing Capacity Under Patch Loads . . . . .	16
2.4.2	Chalmers University of Technology (Sweden) 1991 - 1996 . . . . .	17
2.4.3	University of Maine - Drexel University (USA) . . . . .	19
2.4.3.1	Shear Tests . . . . .	19
2.4.3.2	Flexure Tests . . . . .	20
2.4.3.3	Corrugated Webs Under Partial Compressive Edge Loading . . . . .	22
2.4.4	University of Warwick (UK) . . . . .	23
2.4.4.1	Flexural Behaviour . . . . .	23
2.4.4.2	Shear Behaviour . . . . .	24
2.4.4.3	Fabrication of Steel Girders for Bridges . . . . .	25
2.4.5	Technical University of Berlin (Germany) . . . . .	25
2.4.5.1	Lateral Torsional Buckling . . . . .	25
2.4.5.2	Shear Strength of Beams with Web Openings . . . . .	26
2.4.6	Other Studies on Steel Beams with Corrugated Webs . . . . .	27
2.5	Research on Composite Beams With Corrugated Webs . . . . .	29
2.5.1	Advantages of Using Corrugated Webs in Bridge Girders . . . . .	29
2.5.2	Campenon Bernard BTP (France) . . . . .	30
2.5.3	Proposed High-Speed Railway Bridges (Germany) . . . . .	33
2.5.4	Japan Highway Public Corporation - Waseda University (Japan) . . . . .	33
2.5.5	National Cheng Kung University (Taiwan) . . . . .	38
2.5.6	New Bridge with Corrugated Webs in Stockholm (Sweden) . . . . .	38
2.6	Summary . . . . .	39
CHAPTER 3 : SHEAR RESISTANCE OF CORRUGATED STEEL WEBS . . . . .		40
3.1	General . . . . .	40
3.2	Geometry of Corrugated Steel Profiles . . . . .	40

3.3 Analysis for Shear - The Concept .....	41
3.4 The Buckling Strength .....	44
3.4.1 The Local Buckling Criterion .....	44
3.4.2 The Global Buckling Criterion .....	44
3.4.3 The Shear Yielding Criterion .....	46
3.4.4 The Interaction of Buckling Modes .....	47
3.4.5 The Optimum Dimensions of a Corrugation Profile .....	49
 CHAPTER 4 : EXPERIMENTAL PROGRAM .....	 54
4.1 General .....	54
4.2 The Parametric Study .....	54
4.3 The Test Girders - Preliminary Dimensioning .....	55
4.4 The Test Girders - Material and Structural Details .....	57
4.4.1 Material Properties .....	58
4.4.1.1 Concrete .....	58
4.4.1.2 Prestressing Strands .....	60
4.4.1.3 Corrugated Webs .....	62
4.4.2 Dimensions and Structural Details .....	62
4.4.2.1 Corrugated Webs .....	62
4.4.2.2 Shear Connectors .....	64
4.4.2.3 Longitudinal Reinforcement Details .....	68
4.4.3 Construction of Girders .....	68
4.4.3.1 Formwork and Web Preparation and Alignment .....	68
4.4.3.2 Prestressing .....	68
4.4.3.3 Casting and Curing .....	70
4.5 Instrumentation and Data Acquisition .....	71
4.5.1 Phase I : Girders A-285 and A-215 .....	72
4.5.2 Phase II : Girders A-175, A-110, and A-80 .....	75
4.6 Test Setup and Loading Procedure .....	78



CHAPTER 5 : DISCUSSION OF EXPERIMENTAL RESULTS .....	82
5.1 General .....	82
5.2 Load-Deflection Behaviour .....	82
5.3 Web Buckling Patterns .....	87
5.4 Shear Behaviour and Strength .....	92
5.5 Flexural Behaviour and Strength .....	104
CHAPTER 6 : CONCLUSIONS AND RECOMMENDATIONS .....	114
6.1 Summary .....	114
6.2 Conclusions .....	115
6.2.1 Findings of The Theoretical Study .....	115
6.2.2 Findings of The Experimental Study .....	117
6.3 Recommendations for Future Research .....	120
REFERENCES .....	122
APPENDIX A : Mathcad Worksheet for Calculating The Shear Strength of Trapezoidally Corrugated Webs in Composite Girders .....	131
APPENDIX B : Mathcad Worksheet for Calculating The Optimum Trapezoidally Corrugated Web Profile in Composite Girders .....	135
APPENDIX C : Mathcad Worksheet for Calculating The Optimum Zigzag Corrugated Web Profile in Composite Girders .....	140
APPENDIX D : Mathcad Worksheet for Calculating The Shear Strength of Zigzag Corrugated Webs in Composite Girders .....	145

APPENDIX E : Stress Calculation and Transformation Formulas for Three-Way $45^\circ$	
Strain Rosettes .....	150
APPENDIX F : Complete Experimental Results .....	152

## LIST OF TABLES

Table		Page
2.1	Different tension-field theories, [ref. 51] . . . . .	7
2.2	Bridges constructed using corrugated webs . . . . .	37
4.2	Concrete mixture proportions . . . . .	59
5.1	Experimental and theoretical shear strengths of the test girders . . . . .	98

## LIST OF FIGURES

Figure	Page
2.1 Thin plate in a pure shear state . . . . .	4
2.2 Shear buckling coefficient, $k_T$ , for different boundary conditions . . . . .	5
2.3 Tension-field action, [ref. 51] . . . . .	6
2.4 Repeated unit corrugations for test specimens, [ref. 9] . . . . .	8
2.5 Geometry of test diaphragm, [ref. 9] . . . . .	9
2.6 Unit corrugation for orthotropic plate analysis, [ref. 9,17] . . . . .	10
2.7 Different series of girder tests, [ref. 34] . . . . .	13
2.8 Panel testing under combined shear and compression, [ref. 35] . . . . .	16
2.9 Geometry of test specimen for shear tests, [ref. 12] . . . . .	20
2.10 Geometry of test specimen for flexure tests, [ref. 14] . . . . .	21
2.11 Geometry of test specimen for partial edge loading tests, [ref. 11] . . . . .	23
2.12 Test setup for flexure and shear tests, [ref. 28] . . . . .	24
2.13 Testing of the large scale box-girder model, [ref. 31] . . . . .	31
2.14 A possible typical cross section of a corrugated web, [ref. 6,20] . . . . .	32
2.15 Cognac bridge - Typical mid-span cross section, [ref. 6,20] . . . . .	32
2.16 Maupre viaduct - Typical mid-span cross section, [ref. 6,20] . . . . .	32
2.17 Bridge cross section proposed to the German Federal Railway, [ref. 30] . . . . .	34
2.18 Different shear connector configurations, [ref. 23] . . . . .	36
3.1 Trapezoidal corrugations (a) coordinate system (b) geometrical relations . . . . .	42
3.2 Zigzag corrugations (a) coordinate system (b) geometrical relations . . . . .	42

3.3	Shear strength for local buckling, global buckling, and shear yield . . . . .	48
3.4	Interaction of the local and global buckling limited by the shear yield . . . . .	49
3.5	$w_{eff}$ for a trapezoidally corrugated web for different $\alpha_i$ values . . . . .	52
3.6	$w$ and $w_{eff}$ for the optimum sub-panel width . . . . .	52
4.1	A cut-through perspective view of the test girder . . . . .	57
4.2	Typical elevation view of the test girder and the loading transfer beam . . . . .	57
4.3	Typical cross section of the test girder . . . . .	58
4.4	Concrete stress-strain curve . . . . .	61
4.5	Stress-strain curve for prestressing strands . . . . .	61
4.6	Stress-strain curve for the corrugated steel web material . . . . .	62
4.7	Expected shear resistance of the zigzag corrugated web of the test girders . . . . .	63
4.8	Typical cross section of the zigzag corrugated web . . . . .	64
4.9	Shear connector details, girder A-285 . . . . .	65
4.10	Shear connector details, girder A-215 . . . . .	65
4.11	Shear connector details, girder A-175 . . . . .	66
4.12	Shear connector details, girder A-110 . . . . .	66
4.13	Shear connector details, girder A-80 . . . . .	67
4.14	Shear connector details in the bottom flange, girder A-285 . . . . .	67
4.15	Typical arrangement of conventional steel for the test girder, elevation view . . .	69
4.16	Girder A-285 in prestressing bed before casting of bottom flange . . . . .	70
4.17	Girder A-285 ready for casting the top flange and the end blocks . . . . .	71
4.18	Instrumentation details, girders A-285 and A-215 . . . . .	74
4.19	Instrumentation details, girders A-175, A-110, and A-80 . . . . .	77
4.20	Loading setup and instrumentation, girder A-80-b . . . . .	78
4.21	Schematic side view of the loading apparatus and test setup . . . . .	79
4.22	Completed girder A-175 ready for testing, elevation view . . . . .	80
4.23	Completed girder A-175 ready for testing, side view . . . . .	81

5.1	Applied load vs mid-span vertical deflection, girder A-285 .....	84
5.2	Applied load vs mid-span vertical deflection, girder A-215 .....	84
5.3	Applied load vs mid-span vertical deflection, girder A-175 .....	85
5.4	Applied load vs mid-span vertical deflection, girder A-110 .....	85
5.5	Applied load vs mid-span vertical deflection, girder A-80 .....	86
5.6	Applied load vs mid-span vertical deflection, girder A-80-b .....	87
5.7	Girder A-175 at the end of testing .....	88
5.8	Web buckling pattern at end of testing, girder A-285 .....	89
5.9	Web buckling pattern at end of testing, girder A-215 .....	89
5.10	Web buckling pattern at end of testing, girder A-175 .....	90
5.11	Web buckling pattern at end of testing, girder A-110 .....	90
5.12	Web buckling pattern at end of testing, girder A-80 .....	91
5.13	Web buckling pattern at end of testing, girder A-80-b .....	91
5.14	Calculation of the shear force $V$ at any stage of loading .....	93
5.15	Applied load vs horizontal web buckling, girder A-175 .....	94
5.16	Applied load vs relative inward movement of flanges, girder A-175 .....	95
5.17	Applied load vs relative inward movement of flanges (zoomed), girder A-175 ..	95
5.18	Principal membrane stresses in shear span (rosette R2), girder A-175 .....	96
5.19	Angle of $\sigma_{\max}$ w.r.t. horizontal direction (rosette R2), girder A-175 .....	96
5.20	Experimental shear force results compared with theoretical calculations .....	99
5.21	Geometry of the column-like fold lines .....	103
5.22	Stresses in concrete flanges vs mid-span deflection, girder A-215 .....	105
5.23	Average stress in prestressing strands vs mid-span deflection, girder A-215 ...	105
5.24	Strain profile at mid-span at different stages of loading, girder A-285 .....	106
5.25	Strain profile at mid-span at different stages of loading, girder A-215 .....	107
5.26	Strain profile at mid-span at different stages of loading, girder A-175 .....	108
5.27	Strain profile at mid-span at different stages of loading, girder A-110 .....	109
5.28	Strain profile at mid-span at different stages of loading, girder A-80 .....	110

## LIST OF SYMBOLS

$a$	=	Sub-panel width for a corrugation profile that has equal sub-panel widths
$a_1$	=	Width of the sub-panel parallel to the beam in a trapezoidally corrugated web
$a_2$	=	Width of the inclined sub-panel in a trapezoidally corrugated web
$A$	=	Sub-panel width between the fold corners (mm)
$A_{lim}$	=	The limiting width for a sub-panel to fully act as a vertical compressive element (mm)
$b$	=	Effective width for a sub-panel acting as a vertical compressive element (mm)
$B$	=	Coefficient controlling the ascending portion of the concrete stress-strain curve
$c$	=	Horizontal projection of the length of a unit corrugation
$D_x$	=	Flexural stiffness per unit corrugation along the beam depth (about the x-axis)
$D_y$	=	Flexural stiffness per unit corrugation along the beam length (about the y-axis)
$E$	=	Young's modulus of elasticity of the web material
$E_p$	=	Young's modulus of elasticity of the prestressing strand material
$f_c$	=	Compressive stress in concrete
$f'_c$	=	Concrete compressive cylinder strength at the time of testing
$f_p$	=	Tensile stress in the prestressing strands
$f_{pu}$	=	Ultimate strength of the prestressing strands
$f_{py}$	=	Yield strength of the prestressing strands
$F_b$	=	Critical buckling shear stress of the web
$F_s$	=	Ultimate shear stress of the web
$F_t$	=	Additional post-buckling shear stress of the web
$F_y$	=	Yield stress of the web material
$h$	=	Clear height of the corrugated web

$H$	=	Corrugation depth
$I_x$	=	Second moment of inertia of a unit corrugation about the x-axis
$I_{xx}$	=	Second moment of inertia of the column-like fold lines about its centroidal x-x axis (mm <sup>4</sup> )
$k$	=	Buckling coefficient for an individual sub-panel, stiffened on each edge by a web or a flange, acting as a vertical compressive element under uniform stress
$k_g$	=	Global shear buckling coefficient
$k_l$	=	Local shear buckling coefficient
$L$	=	Longer dimension of the sub-panel
$n$	=	Interaction exponent for local buckling, global buckling, and shear yielding
$n$	=	Coefficient controlling the descending portion of the concrete stress-strain curve
$n$	=	Exponent controlling the transition from the elastic portion to the strain-hardening portion of the strand stress-strain curve
$P$	=	Applied ram load for the test girders
$P_{cr}$	=	Euler column capacity for a column-like fold lines
$s$	=	Total length of a unit corrugation
$S$	=	Shorter dimension of the sub-panel
$V_b$	=	Shear force corresponding to $F_b$
$V_f$	=	Maximum factored shear force to be carried by the web
$V_{in}$	=	Shear force corresponding to $\tau_{in}$
$V_{le}$	=	Shear force corresponding to $\tau_{le}$
$V_n$	=	Nominal shear strength of the web
$V_r$	=	Factored shear strength of the web
$V_u$	=	Shear force corresponding to the experimental first load peak
$w$	=	Thickness of the corrugated web
$w_{eff}$	=	Effective thickness of the corrugated web
$w/c$	=	Water cement ratio of the concrete mix
$\beta$	=	Corrugation angle in a zigzag corrugated profile



$\varepsilon$	=	Strain
$\varepsilon'_c$	=	Concrete strain at maximum compressive strength
$\varepsilon_m$	=	Strain in the prestressing strands at $f_{pu}$
$\phi$	=	Strength reduction factor
$\nu$	=	Poisson's ratio for the web material
$\theta$	=	Corrugation angle in a trapezoidally corrugated profile
$\sigma_c$	=	Applied uniform compressive stress (MPa)
$\sigma_{hor}$	=	Horizontal membrane stress in the top and bottom of the corrugated web beneath the two loading points of the test girders
$\sigma_{max}$	=	Principal tensile membrane stress in the corrugated web in the shear-span
$\sigma_{min}$	=	Principal compressive membrane stress in the corrugated web in the shear-span
$\sigma_{ver}$	=	Vertical membrane stress in the top and bottom of the corrugated web beneath the two loading points of the test girders
$\tau_{ge}$	=	Elastic critical shear buckling stress corresponding to global buckling
$\tau_{in}$	=	Interactive critical shear buckling stress taking shear yielding into account
$\tau_{le}$	=	Elastic critical shear buckling stress corresponding to local buckling
$\tau_y$	=	Huber-von Mises-Hencky shear yielding stress

## ***CHAPTER 1***

### **INTRODUCTION**

#### **1.1 GENERAL**

Corrugated steel panels are characterized by their high in-plane and out-of-plane geometrical stability. One of the well known structural applications for such panels is in the construction of shear diaphragms. Another important character of a corrugated panel is its very low axial stiffness due to its accordion-like behaviour under axial forces. This character directed researchers in the last decade to investigate the possibility of using such panels as webs in prestressed box-girders for bridges, especially with post-tensioned external prestressing. This application was mainly based on the research that was performed on the use of corrugated webs in steel beams.

#### **1.2 SCOPE OF RESEARCH PROGRAM**

The research program conducted at the University of Calgary was focused on three directions. The first is reviewing the research performed worldwide on different applications of corrugated webs as shear-carrying structural elements as well as reviewing the equations that were suggested to be used for design purposes. The second is providing a general procedure to be used in selecting the optimum corrugation shape and its thickness for the case of corrugated web applications. The third direction is conducting a series of tests on

prestressed concrete composite girders in order to identify the governing buckling mode for each girder's web, investigate its post-buckling strength, calibrate the governing strength equations, and finally look into the general behaviour of the girders.

A total of five, 5.5 m total length and 0.73 m total depth, prestressed concrete girders with custom-made corrugated steel webs have been built and tested. The zigzag profile was chosen for the steel web due to its ease of fabrication. The webs for the five girders are of the same thickness of 0.91 mm and the same corrugation angle of 20 °. The only variable is the sub-panel width. The concrete cylinder strength for the top and bottom flanges is of average 55 MPa. Only the bottom flange is prestressed with three, 13-mm diameter, 7-wire strands.

### **1.3 THESIS ORGANIZATION**

Chapter 2 is a review of the previous research on corrugated panels of different shapes either as shear diaphragms or as webs in steel or composite beams. Chapter 3 details the analysis of the shear resistance of corrugated webs and the mathematical procedure developed for choosing the optimum corrugation profile and thickness. Chapter 4 describes the test specimens, the construction method, the instrumentation, and the loading procedure. Chapter 5 includes the discussion of the test results while chapter 6 summarizes the conclusions and the recommendations.

Appendix A contains a Mathcad worksheet that computes the shear strength of trapezoidally corrugated webs in composite beams based on the analysis presented in chapter 3. A Mathcad worksheet that determines the optimum trapezoidal profile is given in Appendix B. Appendices C and D contains the Mathcad worksheets that has been used in choosing the optimum zigzag profile for the test girders and in choosing the variables of the experimental parametric study. The stress calculation and transformation formulas for the three-way 45 ° strain rosettes are included in appendix E. The complete test results for all of the five girders are given in Appendix F.

## **CHAPTER 2**

### **LITERATURE REVIEW**

#### **2.1 GENERAL**

Research on using corrugated panels as shear-carrying structural members has gone through three stages. The first is research on the behaviour of corrugated steel shear diaphragms. The second is the research on the behaviour of steel beams with corrugated webs. The third stage involves investigating the behaviour of prestressed concrete box-girders, or I-girders, with corrugated steel webs. The later two topics are dominating the current interest in the research on corrugated steel sheets. In this literature review, the three stages will be covered along with a brief discussion of the shear strength of thin flat plates.

#### **2.2 SHEAR STRENGTH OF THIN FLAT PLATES**

##### **2.2.1 Buckling Strength**

When a flat plate is subjected to edge uniform shear stresses as shown in figure 2.1, it is said to be in a state of *pure shear*. Tension and compression stresses which are equal in magnitude to the shear stress and inclined at  $45^\circ$  exist in the plate. The destabilizing effect of the compressive stresses is resisted by the perpendicular tensile stresses. The buckling mode involves a formation of several diagonal waves.

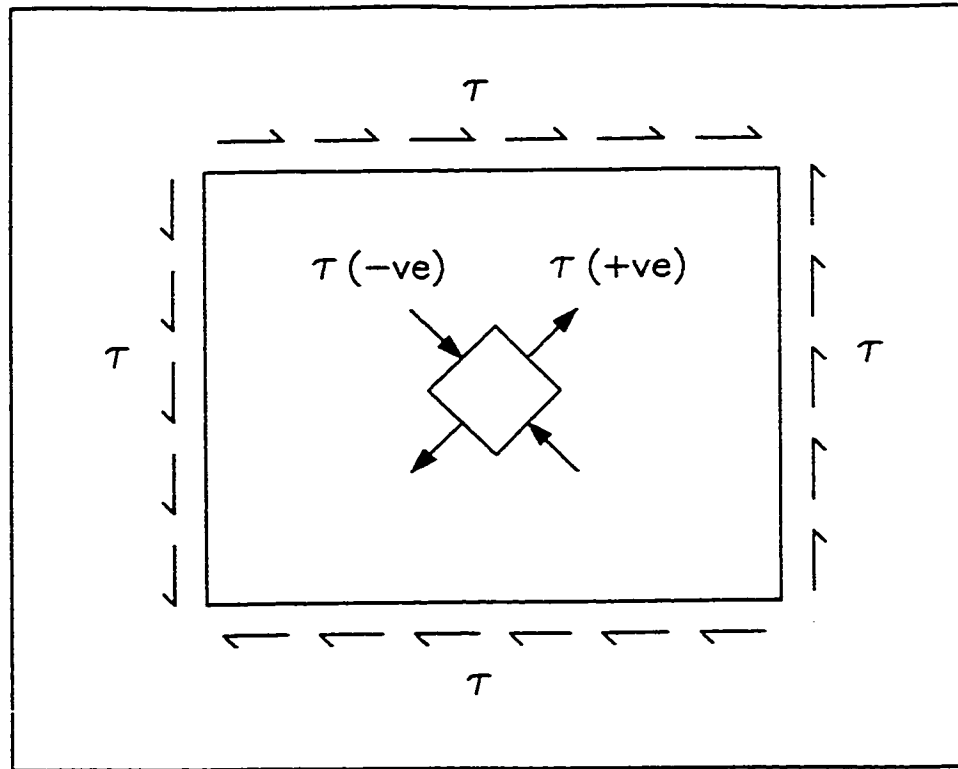


Figure 2.1 Thin plate in a pure shear state

Timoshenko [53] provided an approximate solution, using the theorem of stationary potential energy, for rectangular plates under pure shear. For a rectangular plate of thickness  $w$ , shorter dimension  $S$ , and longer dimension  $L$ , the elastic critical shear buckling stress  $\tau_{le}$  will be given by

$$\tau_{le} = k_l \frac{\pi^2 E}{12(1 - \nu^2)(S/w)^2} \quad (2.1)$$

where  $E$  and  $\nu$  are Young's modulus of elasticity and Poisson's ratio for the plate material respectively.  $k_l$  is the shear buckling coefficient which is a function of the plate aspect ratio and boundary conditions. Equations 2.2 to 2.5, plotted in figure 2.2, can be used to calculate the values of  $k_l$  in the following cases, [51,53]

(A) For four edges simply supported

$$k_t = 5.34 + 4.0 (S/L)^2 \quad (2.2)$$

(B) For long edges simply supported and short edges clamped

$$k_t = 5.34 + 2.31 (S/L) - 3.44 (S/L)^2 + 8.39 (S/L)^3 \quad (2.3)$$

(C) For long edges clamped and short edges simply supported

$$k_t = 8.98 + 5.61 (S/L)^2 - 1.99 (S/L)^3 \quad (2.4)$$

(D) For four edges clamped

$$k_t = 8.98 + 5.60 (S/L)^2 \quad (2.5)$$

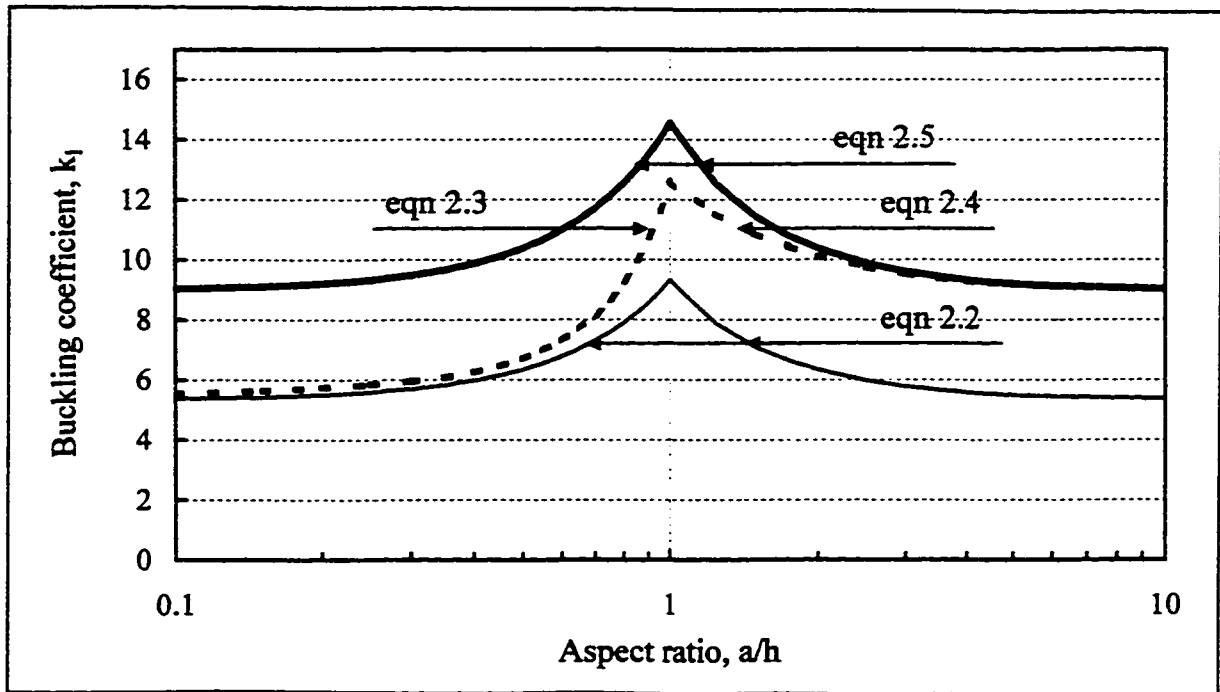


Figure 2.2 Shear buckling coefficient,  $k_t$ , for different boundary conditions

### 2.2.2 Post-Buckling Strength

The observation of the existence of a post-buckling strength in thin plates under shear stresses goes back to the nineteenth century [51]. In stiffened steel plate girders, it was observed that transverse shear which is not sufficiently large to cause a wave formation in the web is transmitted by the web to the bearings in a  $45^\circ$  shear field as described above. This is referred to as *beam action*. When the wave formation occurs as a result of larger loads, the stiffeners start to take up the duty of compressive resistance like the posts of a Pratt truss while the web is divided into panels equivalent to those of an open truss where each web panel acts as an inclined tie. This later mechanism is now referred to as *tension-field action*, figure 2.3.

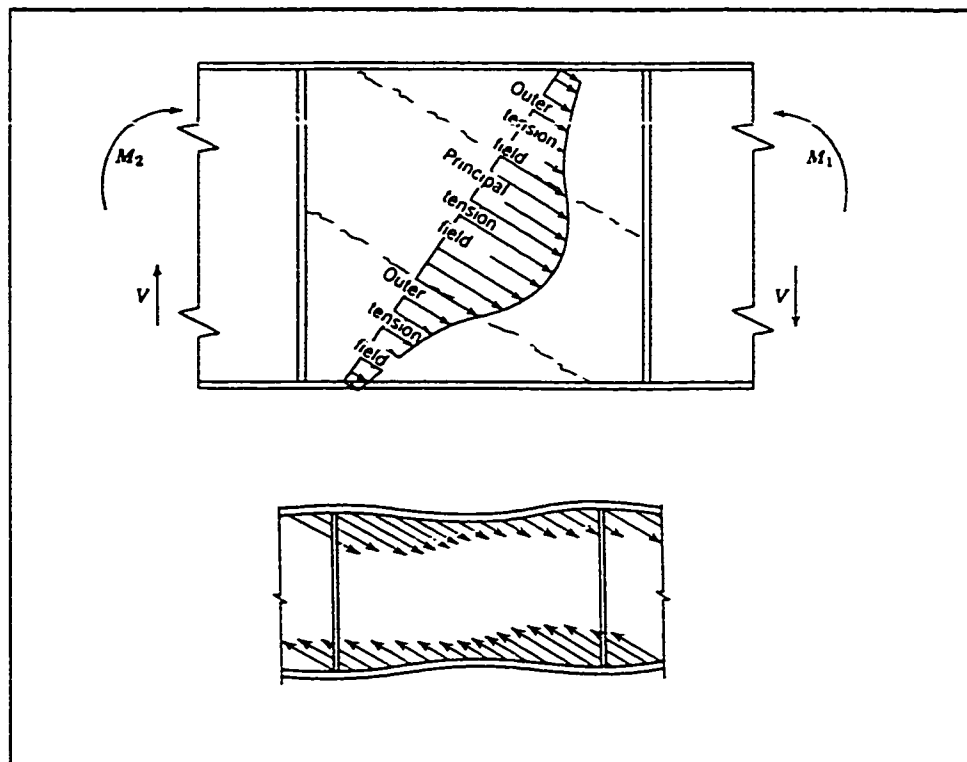

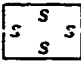

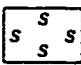
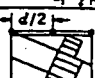
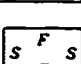

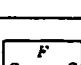

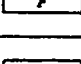

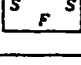

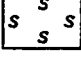

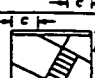
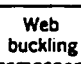
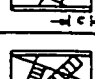
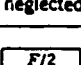


Figure 2.3 Tension-field action, [ref. 51]

The first successful formulation of the tension-field strength of plate girder webs was developed by Basler and Thürlimann in the early sixties of the twentieth century [1,2,51]. It is obvious from figure 2.3 that the tension-field in the web is anchored to the flanges and the

stiffeners. The resulting lateral loads on the flanges causes them to bend inward. Therefore, the nature of such tension-field is greatly influenced by their bending stiffness. Extensive research has been done since the sixties to apply the tension-field theory to different stiffener and flange boundary conditions as shown in table 2.1. Although Basler's model assumes a limited middle tension band, its formulation gives the strength of a complete tension field. This error was recognized and corrected by different researchers [51]. The modified formulation of Basler's model is considered the basis of the current design practice of stiffened plate girders in the United States and Canada.

Table 2.1 Different tension-field theories, [ref. 51]

Investigator	Mechanism	Web Buckling Edge Support	Unequal Flanges	Longitudinal Stiffener	Shear and Moment
Basler (1963-a)			Immaterial	Yes, Cooper (1965)	Yes
Takeuchi (1964)			Yes	No	No
Fujii (1968, 1971)			Yes	Yes	Yes
Komatsu (1971)			No	Yes, at mid-depth	No
Chem and Ostapenko (1969)			Yes	Yes	Yes
Porter et al. (1975)			Yes	Yes	Yes
Hoglund (1971-a, b)			No	No	Yes
Herzog (1974-a, b)		Web buckling component neglected	Yes, in evaluating c	Yes	Yes
Sharp and Clark (1971)			No	No	No
Steinhardt and Schroter (1971)			Yes	Yes	Yes



### 2.3 BUCKLING STRENGTH OF SHEAR DIAPHRAGMS

In 1969, Easley and McFarland [9] published results from a theoretical investigation verified with experimental testing of two different profiles of corrugated shear panels. The tests were conducted at the University of Kansas, USA, and the purpose was to determine the buckling strength of rectangular panels made with corrugated steel sheets under in-plane shear load. In their analysis, Easley-McFarland assumed continuous simply supported panel edges. In the test setup, they reflected their assumption by providing very closely spaced fasteners in connecting the panels to the surrounding frame that was used to apply the shear loading. The chosen corrugation profiles, as can be seen in figure 2.4, were from commercially available sheets which were used in practical production of shear diaphragms. Because of the relatively small corrugation height for both profiles, the predicted failure pattern was a formation of a number of buckled diagonal waves across the entire diaphragm due to elastic buckling. This pattern is referred to as *an elastic global (overall) buckling failure mode*.

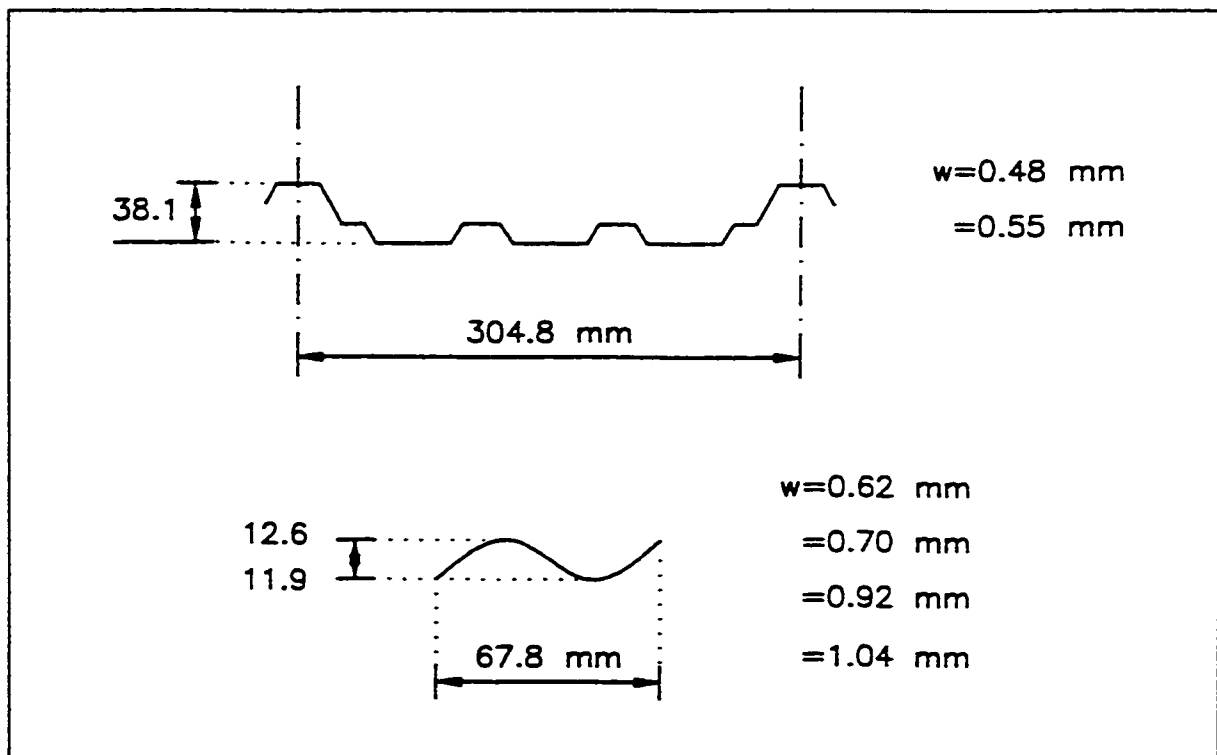


Figure 2.4 Repeated unit corrugations for test specimens, [ref. 9]

In order to be analyzed for such a global behaviour, the corrugated panels were modeled as thin orthotropic flat plates with material properties equal to the gross material constants of one repeating cross section. Figure 2.5 shows the geometry of the diaphragm used in the experimental testing while figure 2.6 shows the unit corrugation used in the orthotropic analysis.

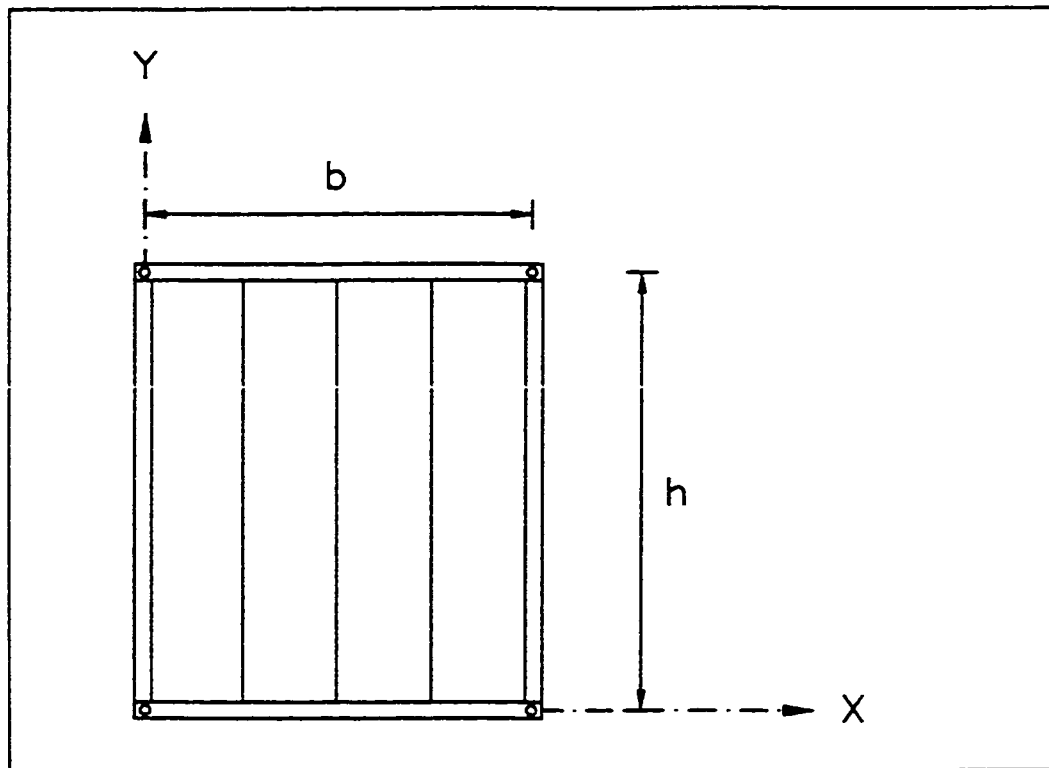


Figure 2.5 Geometry of test diaphragm, [ref. 9]

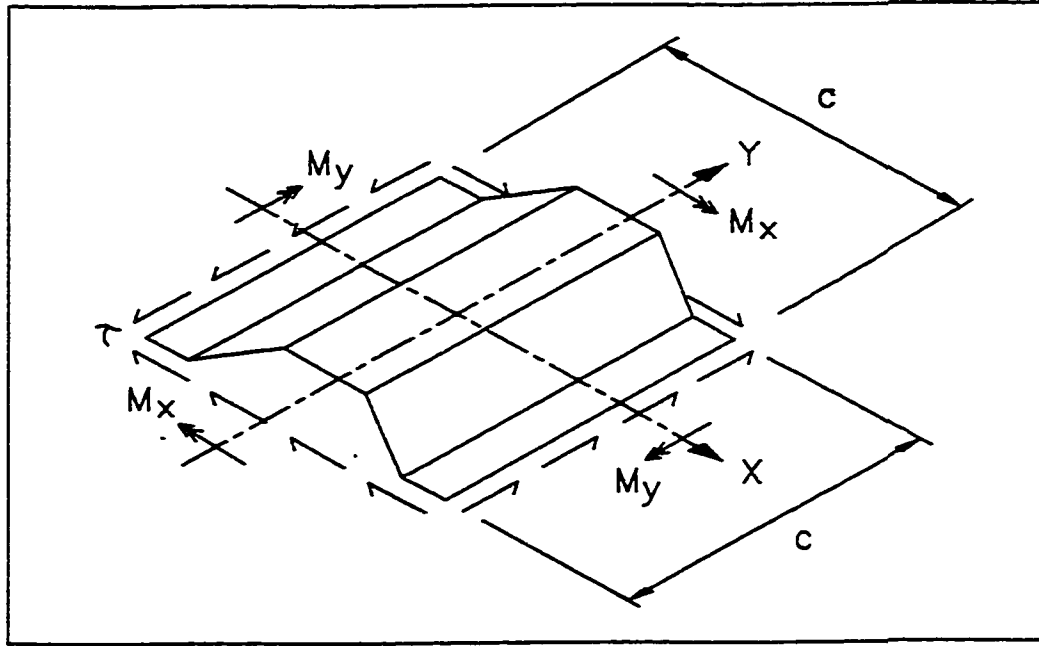


Figure 2.6 Unit corrugation for orthotropic plate analysis, [ref. 9,17]

The equation derived by Easley-McFarland to calculate the elastic critical global buckling shear stress,  $\tau_{ge}$ , was rather complex. In 1975, Easley [8] revised that equation based on two facts. Firstly, for a light-gauge corrugated panel, the flexural stiffness per unit corrugation about the y-axis is usually much smaller than that about the x-axis. This should make some terms in the equations negligible. Secondly, the edge restraint in the test diaphragm, and in practice, can not fully reflect the ideal simple support assumed in analysis. Therefore, the revised equation took the following simplified form:

$$\tau_{ge} = 36 \gamma \frac{(D_y)^{0.25} (D_x)^{0.75}}{wh^2} \quad (2.6)$$

where:

$D_x$  = flexural stiffnesses per unit corrugation about the x-axis

$D_y$  = flexural stiffnesses per unit corrugation about the y-axis

$h$  = diaphragm height parallel to corrugation folds (figure 2.5)

$w$  = corrugated sheet thickness

$\gamma$  = factor to represent different end restraint conditions (  $1 \leq \gamma \leq 1.9$  )

Easley [8] reported two similar formulas for calculating the elastic global buckling loads for shear diaphragms. Bergmann and Reissner used the same orthotropic treatment in 1929 to develop the following formula:

$$\tau_{ge} = 4 \lambda \frac{(D_y)^{0.25} (D_x)^{0.75}}{wh^2} \quad (2.7)$$

in which  $\lambda$  is a multiplier dependent upon the different stiffnesses of the corrugated panel, and is given in a form of curves by Timoshenko and Gere [53]. Also in Poland in 1968, Hlavacek investigated the behaviour under pure shear forces of flat sheets reinforced by separate equally spaced stiffeners symmetrically attached to both faces of the sheet. He then derived the governing strength equation and mentioned its applicability to corrugated webs. Hlavacek's formula was analyzed by Easley [8] and was reduced to:

$$\tau_{ge} = 41 \frac{(D_y)^{0.25} (D_x)^{0.75}}{wh^2} \quad (2.8)$$

It can be noticed that equations 2.6, 2.7, and 2.8 are of the same form but differ in their numerical coefficients.

## 2.4 RESEARCH ON STEEL BEAMS WITH CORRUGATED WEBS

### 2.4.1 Chalmers University of Technology (Sweden) 1983 - 1987

In the late sixties, manufacturing of steel girders with trapezoidally corrugated webs was started in Sweden. The commercial production of these girders was based on some experimental testing performed by the manufacturer. However, most of the produced girders were of small span intended to serve for roofs with light loads. In the early eighties, and

associated with the intention of those manufacturers to increase their production and to include long span girders, L. Leiva-Aravena [3,4,33,34,35] started an experimental program at Chalmers University of Technology in order to investigate several stability problems as will be presented below.

#### 2.4.1.1 Shear Buckling of Girder Webs

Three test series have been carried out, as shown in figure 2.7, to investigate the different shear buckling modes of steel girder webs. The pilot series, *series L*, consisted of six tests conducted on commercially produced girders. *Series B*, named as low girder test series, consisted of four commercially produced girders with smaller web depths than the pilot tests. The model girder test series, *series M*, consisted of four girders with relatively small corrugation height. For series M, the girders were specially manufactured with the intention to study the global buckling mode. For all the above three series, vertical stiffeners were provided at the points of load application. The observations from the tests are summarized as:

- The observed failure pattern was due to either an interaction of local and global buckling as in the case of series L and M, or due to local buckling only as in series B. the local buckling mode was defined as buckles that go along a single sub-panel.
- The load-deflection curves for all of the tested girders showed that the drop of load after the peak was sudden with residual strength roughly about half of the peak load. However, this residual strength was found to be equal to the strength of a flat plate web that has the same thickness as the corrugated web. The deflection in the post-buckling range reached high values while maintaining the same residual strength.
- No high values were measured for horizontal membrane stresses in the web except at the beam mid span in the vicinity of the flanges. This confirms that the bending moment was carried almost totally by the flanges.
- No difference in the shear stresses was found between the folds parallel to the beam and the inclined ones.
- Only a large imperfection can result in a significant decrease of the strength of the girders. This decrease was observed only with webs that had a change in the corrugation

angle, due to imperfections, from  $45^\circ$  to  $30^\circ$ .

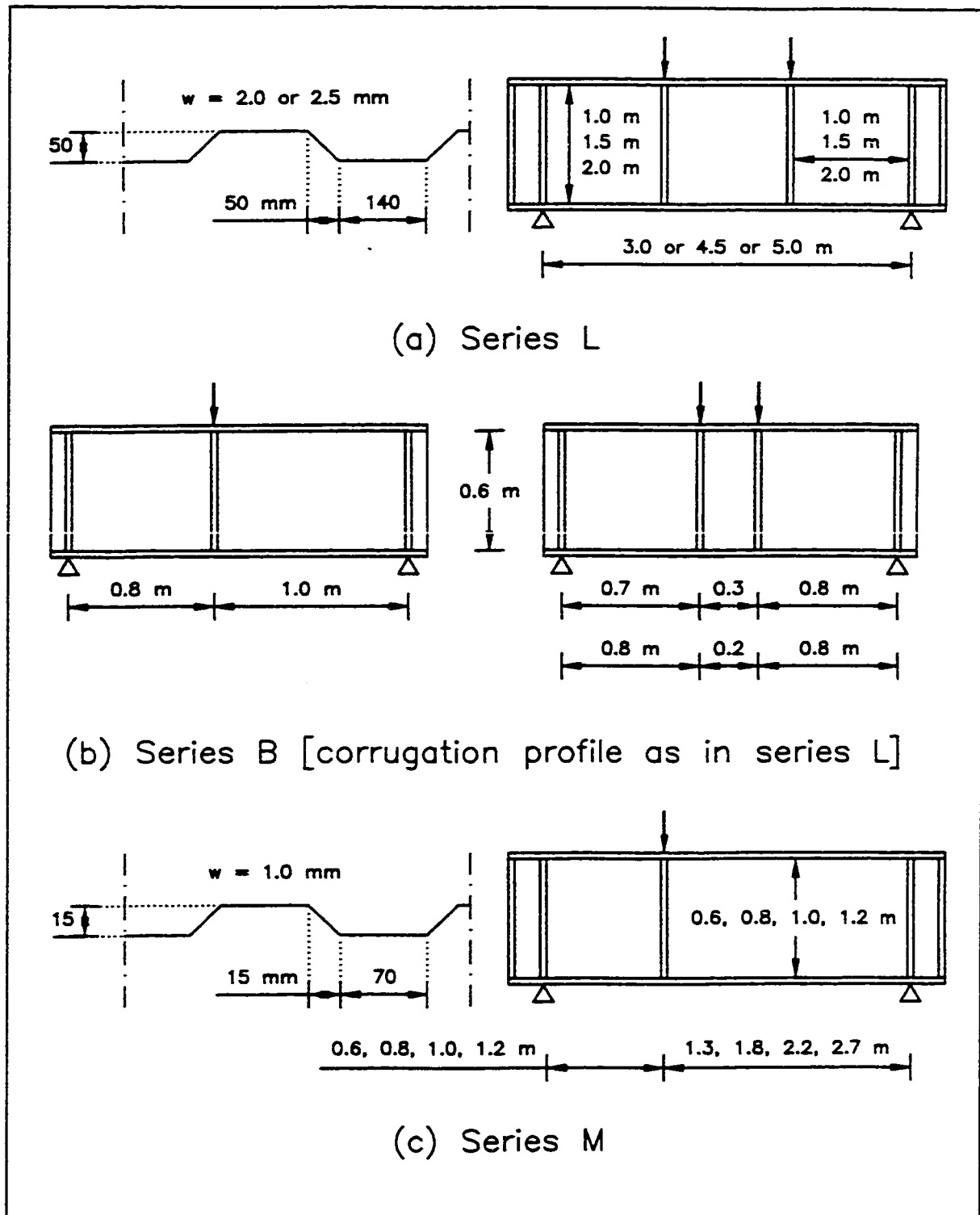


Figure 2.7 Different series of girder tests, [ref. 34]

Based on the test results, the following interaction curve was suggested to calculate the strength of corrugated webs against shear buckling

$$\frac{1}{\tau_{in}} = \frac{1}{\tau_d} + \frac{1}{\tau_g} \quad (2.9)$$

where  $\tau_{in}$  is the maximum shear stress that can be carried by the web,  $\tau_g$  is the elastic global buckling stress given by equation 2.6 with  $\gamma = 1.9$ , and  $\tau_d$  represents the design local buckling stress specified in the Swedish code.  $\tau_d$  is given in a form of table depending on the slenderness of the web sub-panels and the yield strength of the web material [3]. Both  $\tau_g$  and  $\tau_d$  should not be greater than the shear yield stress  $\tau_y$  given by:

$$\tau_y = F_y / \sqrt{3} = 0.577 F_y \quad (2.10)$$

#### 2.4.1.2 Shear, Compression, and Combined Shear and Compression Buckling of Panels

Two more series of tests, both named *series P*, were carried out by Leiva-Aravena in order to study the behaviour of corrugated panels under different kinds of loadings. The first series included testing of ten identical panels: three panels under pure vertical compression, two under pure shear, and five panels under combined shear and compression. The second series consisted of six panels of the same geometry and dimensions as before but with different edge conditions. It was divided into: one panel under pure vertical compression, one under pure shear, and four panels under combined shear and compression. Figure 2.8 shows the test setup for the first series for the case of combined shear and compression loading. The second series had the same test setup but with the bottom flange fully welded to the supporting beam. The major observations from the 16 tests can be summarized as:

(A) For the case of pure shear loading:

- Buckles started in a local mode then joined to form major global buckles that extend diagonally from flange to flange. The maximum load was reached when the panel buckled in a global mode.
- The load-deflection curve took the same shape as described in the girder tests, i.e., a

sudden drop after the peak is reached and a residual strength of about 50 - 60% of the peak load that remained constant with increasing deflection.

- The diagonal local buckles started to form at steep angles of about 63° with the horizontal. With the global buckling developing, the steep angles changed slowly into flatter ones of about 50° with the horizontal.
- The formation of tension fields was observed toward the end of testing. However, this was after the panels had suffered large deformations. Therefore, the strength provided by these fields was not taken into account.

(B) For the case of pure compression loading:

- The buckling starts as local buckling of the flat sub-panels, then an overall column-like buckling mode was observed.
- The load carrying capacity from the experimental results, which corresponds to the overall buckling mode, was found to be very close to that calculated using a strut approach where the web was replaced by a series of unconnected column sections representing an effective zone at the folding lines.
- No post-buckling strength was observed.

(C) For the case of combined shear and compression:

- The buckling pattern and the load-deflection curves depend largely on the initial compression loading before applying the shear load. With low initial compression, the observed buckling pattern was more similar to that of the pure shear case, and the load-deflection curve showed a post-buckling plateau. However, with high initial compression, the buckling pattern was more like the pure compression case with no post-buckling strength observed.
- The interaction between shear and compression was represented, with fair accuracy, by a circle with unit radius:

$$\left( \frac{\sigma_{cs}}{\sigma_c} \right)^2 + \left( \frac{\tau_{cs}}{\tau_s} \right)^2 = 1 \quad (2.11)$$

$\sigma_{cs}$  and  $\tau_{cs}$  are the compression and shear stresses at failure for the case of combined loads,



while  $\sigma_c$  and  $\tau_s$  are the failure compression and shear stresses for the cases of pure compression and pure shear respectively. Generally, the difference in the welded length of the bottom edge did not have a great influence on the shear or compression buckling capacity of the panels.

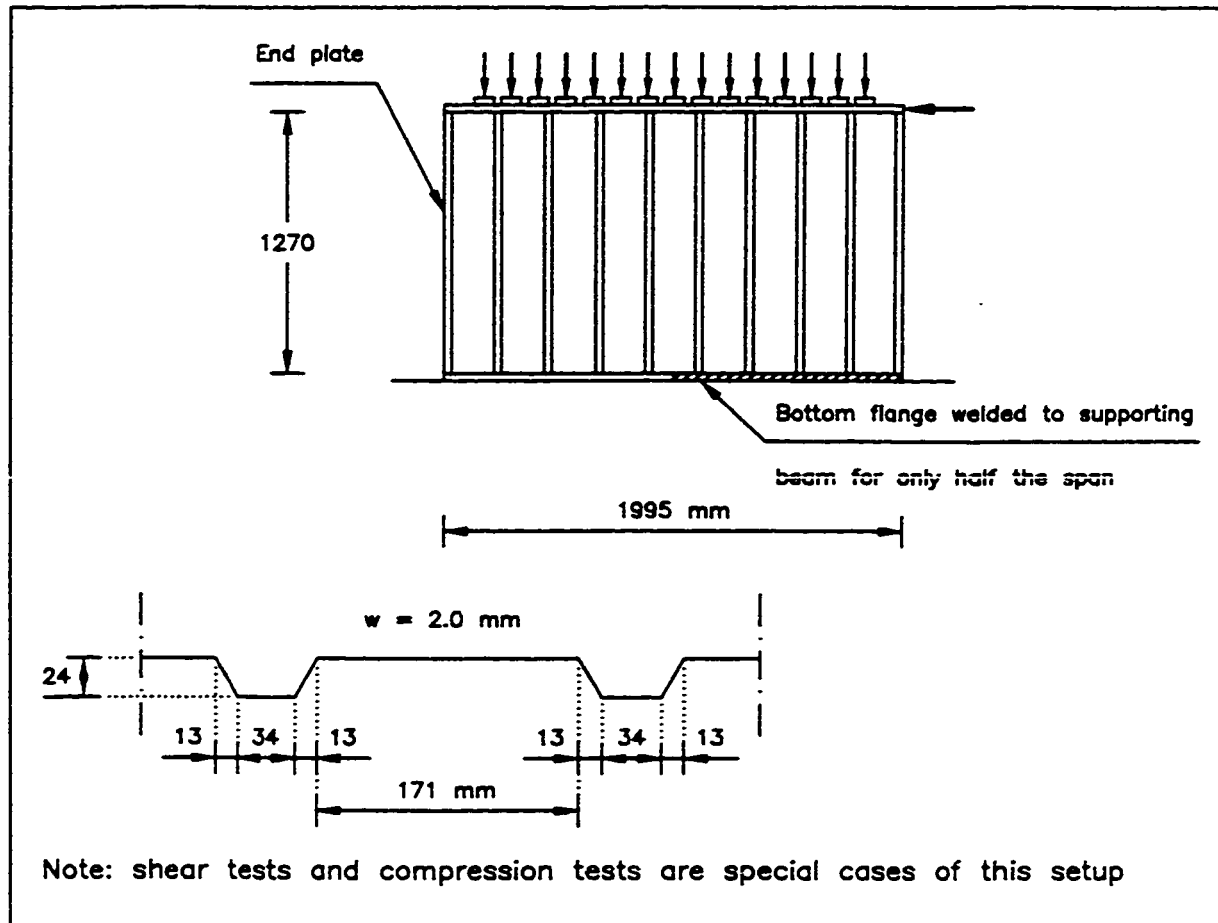


Figure 2.8 Panel testing under combined shear and compression, [ref. 35]

#### 2.4.1.3 Load-Bearing Capacity Under Patch Loads

Six tests were performed on small beams to study the behaviour under patch loads. The beams were of 1 m span and variable web depth 1, 2, and 3 m. The corrugation profile is similar to that of *series L* and *B* in the shear tests with two web thicknesses as well. Top and bottom steel flanges of thicknesses 10 or 12 mm were welded to the web. The applied patch loading has two variables of its own. The first is its location whether it is over the sub-panel

parallel to the beam, the inclined sub-panel, or over the fold line. The second is its distribution length either 5 mm or 50 mm. The major findings can be summarized as:

- The failure in all of the cases did not result from the crippling beneath the point of load application. Instead the load continued to increase non-linearly with the beam deflection until the ultimate peak was reached which ranged from about 1.10 to 1.80 of the first crippling load.
- The web thickness was found to be the most important factor that influenced the strength of this type of girder under patch loads. The ultimate load increased by about 35 - 40 % with an increase in the web thickness from 2 to 2.50 mm.
- The change in the distribution length from 5 mm to 50 mm increased the ultimate capacity of the beams by only 10 %.
- Higher ultimate strength was achieved with the patch load over the inclined sub-panel than when it was over the panels parallel to the beam. However, it should be taken into account that the width of the inclined sub-panels was much smaller.

#### **2.4.2 Chalmers University of Technology (Sweden) 1991 - 1996**

In the early nineties, R. Luo conducted an analytical study, as part of a thesis, to simulate and verify the same experimental tests performed earlier by Leiva-Aravena. Luo performed the analysis both by using the spline finite strip method as well as a geometrically non linear finite element model that takes material elastic-plastic behaviour into account. In addition, Luo also investigated more variables thought to have an influence on the behaviour of girders and panels with corrugated webs. The following is a summary of the comparative study between the analytical and the experimental results for the cases of shear, compression, or combined loading on girders and panels [41,42,44]:

- When initial imperfections were not taken into account, the load-deflection curves obtained from the analytical and the experimental results were almost identical in their post-peak part. In the pre-peak regions, a steeper tangent was obtained from the analytical results. This was attributed to the inevitable existence of initial imperfections

which result in larger deformations than it should be in the ideal case.

- The direct relationship between the ultimate shear capacity and both the web height and web thickness was confirmed.
- For a specific corrugation profile, and in all the three cases of loading, the increase in the corrugation angle was found to change the buckling mode from global buckling to local buckling.
- For all cases of loading, and for the whole range of possible corrugation angles, the highest ultimate load capacity was achieved when all the sub-panels had equal and short widths. However, no limit was set for how short the sub-panel width can be.

In 1996, Luo published an article that discussed the behaviour of steel girders with trapezoidally corrugated webs under patch loading, [43]. In this article, Luo presented her models for Leiva's tests, discussed his variables along with other variables such as initial imperfections, strain hardening, corner effects, and geometric parameters. She finally proposed a tentative empirical formula for the prediction of the ultimate strength. The following were the major findings of the study:

- Contrary to Leiva's results, the ultimate capacity was found to increase by 20 % and 40 % with the change from a knife load to a patch load distributed over 50 and 115 mm respectively.
- The ultimate load was found to increase with the increase in both the web thickness and the flange thickness.
- Small initial global imperfection did not reduce the ultimate strength much. Only a local initial imperfection near the load application point did.
- Taking the strain-hardening into account resulted in increasing the ultimate strength by 8 - 12 %.
- The corner effects due to cold forming did not have any significant effect on the ultimate strength.

### 2.4.3 University of Maine - Drexel University (USA)

In 1990, Elgaaly and Dagher published a paper [10] that included a brief literature review on the research performed worldwide on corrugated webs. The same article included a plan of a research program that was starting at the University of Maine at that time and is currently continuing at Drexel University. The aim of the program was to investigate the behaviour of steel beams with trapezoidally corrugated webs. Several articles and reports describing experimental and analytical results were published [11,12,13,14,15,19]. The following is a brief description of the different series of tests and finite element analyses, and a summary of their results.

#### 2.4.3.1 Shear Tests

Forty two tests on twenty one beams were conducted by R. Hamilton to investigate the effect of the following parameters: thickness of the web, aspect ratio of the shear-span, and corrugation profile dimensions. Figure 2.9 shows a typical elevation view of the tested beams. Non-Linear finite element modeling was also performed in order to obtain a model that can predict experimental results with a practical degree of accuracy. From both the experimental and the finite element investigations, Load-deflection curves similar to Leiva's were obtained with a post-buckling plateau of about 70% of the peak strength. According to the obtained results, corrugated webs under shear loads were found to be governed by either local buckling or global buckling depending on their corrugation profile. The elastic critical global buckling stress  $\tau_{ge}$  is to be calculated using equation 2.6 with  $\gamma = 1.64$ , while the elastic critical local buckling stress  $\tau_{le}$  is calculated using equation 2.1 by considering the longest sub-panel width  $a$  and the web height  $h$  as the shortest and longest dimensions of the rectangular plate respectively. An average value for  $k_f$  from equations 2.3 and 2.5 was found in agreement with the test results. When  $\tau_{ge}$  or  $\tau_{le}$  exceeded the shear yield limit given by equation 2.10, its corresponding inelastic buckling was found to be the governing stress. For an elastic (local or global) buckling stress  $\tau_e$ , the inelastic buckling stress  $\tau_i$  is to be calculated according to the following semi-empirical equation:

$$\tau_i = \sqrt{0.8 \tau_e \tau_y} \leq \tau_y \quad (2.12)$$

For practical applications, it was recommended that both global and local buckling stresses be calculated, and the smaller value controls.

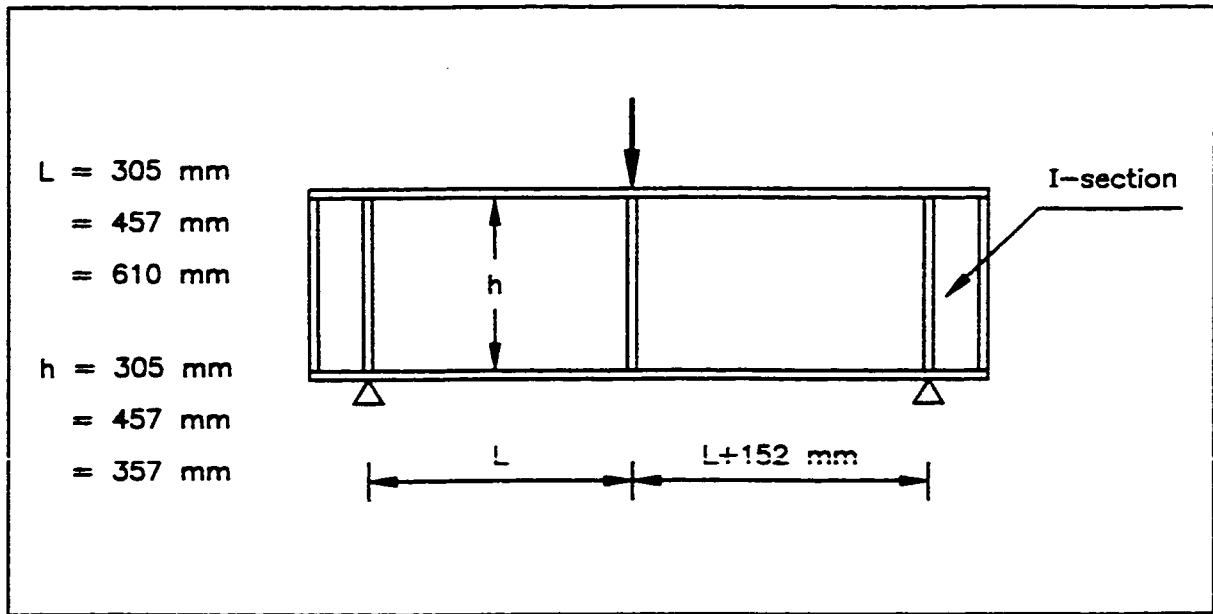


Figure 2.9 Geometry of test specimen for shear tests, [ref. 12]

#### 2.4.3.2 Flexure Tests

Seven beams with a typical elevation view as shown in Figure 2.10 were tested under two point loads. Although the test specimens were built to fail in the middle corrugated web panel, all the seven tests failed in buckling of the 6.35 mm thick flat panels. With continuing loading of the first tested beam, large deformation in the compression flange took place and the flange finally buckled vertically into the middle corrugated panel. This beam was considered a pilot one. For all other six tests, the tests were stopped before failure of the compression flange took place. They were then stiffened by angles welded as cross bracing diagonally across both flat panels. In the second testing, all beams were able to achieve failure loads ranging from 104 % to 140 % of the failure loads achieved in the first testing. The failure mode for this series of tests was due to buckling of the compression flange vertically

into the middle corrugated panel.

The readings from the strain gauges mounted horizontally on different locations at the centre line of the beam span showed almost no membrane or bending strains in the corrugated web except in the vicinity of the flanges where they restrain the web. The strain readings in the top flanges showed that the flanges buckled just after they reached the yield strain. It was then found that the experimental failure moment capacities of all beams can be calculated with negligible error based on the yield strength of the flanges and ignoring any contribution of the web.

In a further investigation, non linear finite element models for beams of the same elevation view as in figure 2.10 were developed in order to test the effect of other parameters. The considered parameters were: the change in corrugation profile, the ratio between the web and flange thicknesses, the ratio between the web and flange yield stresses, and the aspect ratio of the corrugated middle panel. The results from the analysis showed that the ultimate moment capacities of all beams were not dependent on the web material, corrugation profile, or the panel aspect ratio. It was also observed that these ultimate moment capacities ranged between the moment capacities calculated based on the flanges' yield and ultimate strengths neglecting any web contribution.

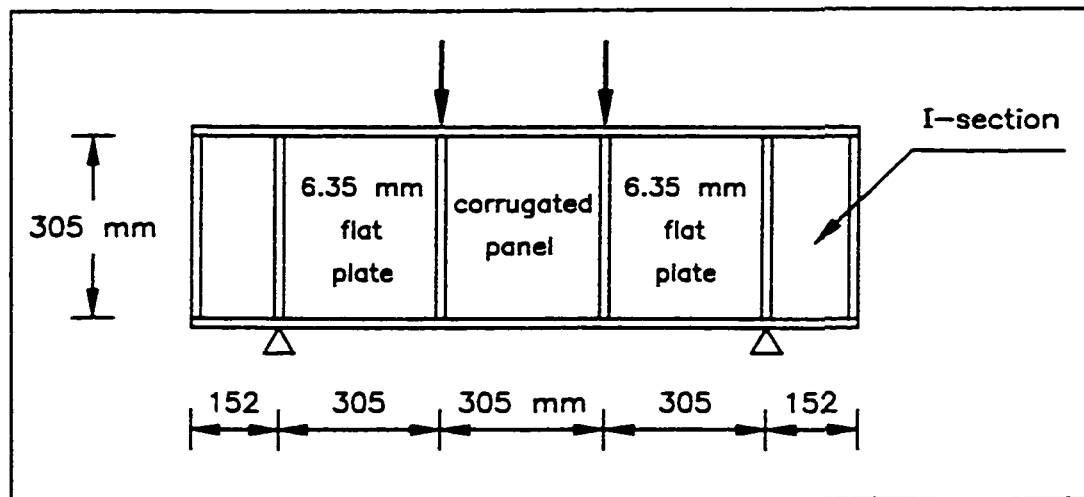


Figure 2.10 Geometry of test specimen for flexure tests, [ref. 14]

#### 2.4.3.3 Corrugated Webs Under Partial Compressive Edge Loading

To study the effect of the various types and locations of compression edge loading on steel beams with corrugated webs, a beam with the dimensions shown in figure 2.11 was built and tested under five different load configurations. Two different loads were used in these five loading configurations, the *patch load* which is a load uniformly distributed over an area that extends the full flange width, and the *line load* which is a load uniformly distributed over a line across the full flange width. The beam was first tested under a patch load over the sub-panel parallel to the beam span, then under a line load over another parallel sub-panel. It was then flipped over and tested under a patch load over the inclined sub-panel, a line load over another inclined sub-panel, and finally a line load directly over a fold line. The beam was also modeled by a finite element model similar to those of the shear tests and the flexure tests. From both the experimental and analytical results, it was observed that the failure in all cases was due to vertical bending of the flange and crippling of the web just beneath the load.

A further study was performed using the same finite element model to investigate other parameters such as: the thicknesses and yield stresses of the flanges and the web, the width and location of the load, the web aspect ratio, and the change in the corrugation profile. A total of seventy beams were modeled, and the results showed that there are two distinct modes of failure: *type I* which includes a collapse mechanism in the loaded flange and local bending or crippling of the web, and *type II* where the failure was due to web yielding followed by web crippling without having any collapse mechanism in the loaded flange. Two equations were proposed to calculate the ultimate capacity of the girder based on these two main modes of failure [11]. It was then suggested that the smaller should control.

The interaction between the compressive edge loading and both shear and in-plane bending was also investigated using the finite element model, and design equations were suggested [11].

A research program that includes preliminary fatigue tests of steel girders with corrugated webs is currently taking place at Drexel University. The tests will investigate the required welding details for the web-flange connection in order to sustain repeated moving loads.

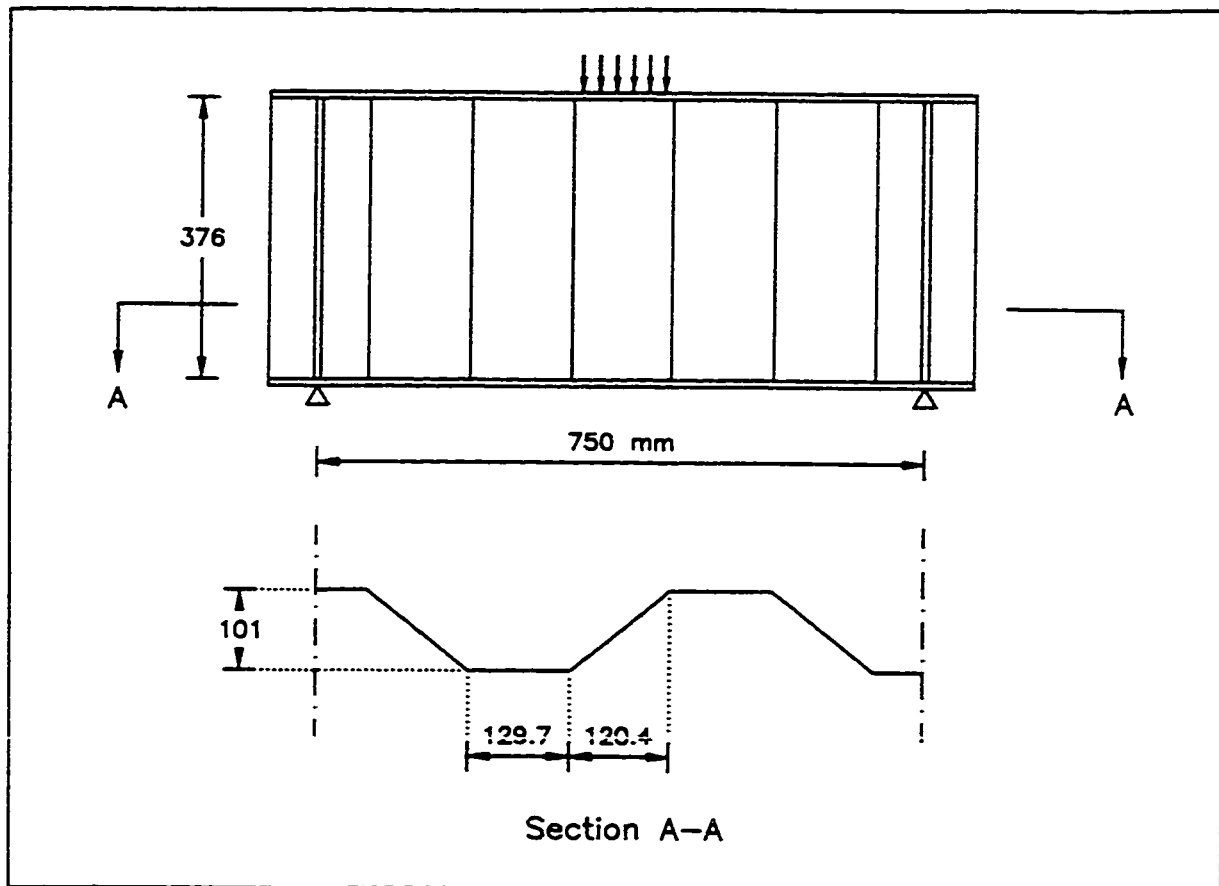


Figure 2.11 Geometry of test specimen for partial edge loading tests, [ref. 11]

#### 2.4.4 University of Warwick (UK)

Three articles were published in 1997 presenting results of an experimental and analytical program conducted at the University of Warwick [26,27,28]. The aim of the program was to study both shear and flexural behaviour of steel beams with trapezoidally corrugated webs. Five test specimens were loaded by pure moment or by a combination of shear and moment, figure 2.12. Finite element modeling of the tests specimens was also performed to allow more detailed analysis.

##### 2.4.4.1 Flexural Behaviour

Both experimental and analytical results confirmed that the capacity of this type of



girder can be predicted with almost no error based on the measured dimensions of the flanges ignoring any web contribution. However, it was also found that the web contribution can be taken into account by using an increased thickness for the flanges which is usually well below 10 %.

The problem of the slenderness class for the compression flange was also addressed. The concern was about choosing the proper compression flange projection that should be used in classifying the flange slenderness. A criterion was finally found, depending on the shape of the corrugation profile, that can allow the use of either the maximum or the mean projection.

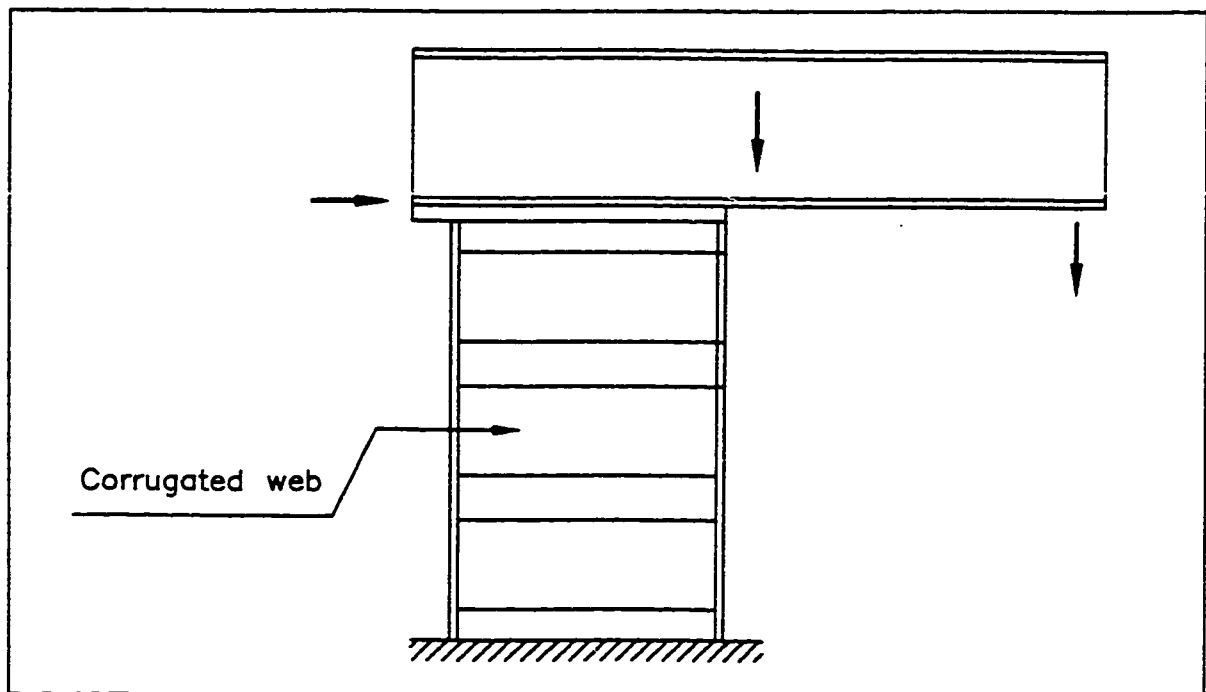


Figure 2.12 Test setup for flexure and shear tests, [ref. 28]

#### 2.4.4.2 Shear Behaviour

The same method of analysis based on the shear yield, local buckling, and global buckling limits was used in predicting and comparing the test and finite element results. From the results it was found that the corrugation profiles of the test specimens were governed by the interaction between local and global buckling. From a practical point of view, it was

recommended that the thickness and the web profile should be selected to enable use of the full yield strength of the steel web. However, no general guide was given to allow the optimum selection of such webs.

An equation to calculate the elastic shear stiffness for a corrugated web in pure shear was also presented with good agreement with both the experimental and analytical results.

#### 2.4.4.3 Fabrication of Steel Girders for Bridges

Part of the study was concerned with a discussion of the practical problems associated with forming the corrugated profiles for bridge girder webs, welding the web and the steel flanges, providing cambering for bridges with a curved soffit, and estimating the needed tolerance for assembling the web panels. The discussion of the above mentioned points focused on the production techniques and the cost estimation.

#### 2.4.5 **Technical University of Berlin (Germany)**

A research program to investigate the behaviour of steel beams with corrugated webs was conducted at the Technical University of Berlin with the goal of improving the design rules specified in the German specifications *DAST-Richtlinie 015:Träger mit schlanken Stegen 1990* and the Eurocode: Steel Structures 1990. Following is a review of the research program and its results.

##### 2.4.5.1 Lateral Torsional Buckling

In 1990, the problem of lateral torsional buckling of such beams was addressed by Linder [36]. Linder pointed out that if vertical buckling of flanges occurs due to bending, the torsional resistance of the beam will be reduced. Therefore, a theoretical and analytical program was conducted in order to investigate the interaction between the vertical buckling of flanges and the lateral torsional buckling. It was found that the torsional section constant for such beams does not differ from that of a beam with flat webs, and will not be affected by the local flange buckling. However, the warping section constant is higher than that of a beam

with flat webs, and will be reduced due to vertical flange buckling. A design method was given and was compared with both the test and the finite element results. A good correlation was obtained when the interaction was taken into account in calculating the ultimate strength of the beams. When the interaction was not taken into account in these calculations, the theoretical strength was found to be on the unsafe side.

#### 2.4.5.2 Shear Strength of Beams with Web Openings

In 1991, Linder published another article describing a research that investigated the shear strength of corrugated webs with openings [37]. Eight beams 400 mm deep with an overall span of 1100 mm were tested under a point load at the mid-span. The trapezoidal corrugated web was 1 mm thick with equal sub-panel widths of 148 mm. Vertical stiffeners were provided at the loading and reaction points. Only one opening, with variable positions vertically and horizontally, was provided for each beam. The diameters of the openings did not exceed the sub-panel width.

Two types were observed for the load-deflection curves. The first type showed a linear relationship until buckles occurred at the edges of the opening and around it, then the slope of the linear part of the curve became flatter. With increasing load, a tension field appeared and the curve became almost flat. However, the load was still increasing with the excessive deformations taking place. The continuous increase of the load was attributed to the strain hardening effects. The second type showed a snap through that occurred very suddenly at the end of the linear part, followed by the ultimate load and the failure.

The experimental results showed that an opening that runs over a fold line is more disadvantageous. Therefore, it was justifiable to have openings with diameters less than the sub-panel width. Even with openings limited to the flat sub-panels, a reduction of up to 30 % in the ultimate shear capacity was observed. It was also observed that the worst vertical position for the opening is at the expected path of the tension field. Based on all the above, an approximate equation for calculating the shear capacity of such webs was proposed. This equation took into account both the strength provided by the web prior to buckling and that provided by the tension field after buckling. A numerical multiplier was introduced in the

tension field part of the equation in order to match the test results.

#### **2.4.6 Other Studies on Steel Beams with Corrugated Webs**

In 1971, Sherman and Fisher [50] conducted experimental tests in order to determine how much weld is needed between the web and the flanges to develop the full strength of such beams in shear. Simple span beams were tested under one point load at the mid-span. The web were of thicknesses 0.91, 0.61, and 0.45 mm. Four weld types have been tested: (1) continuous fillets on both sides of the web, (2) fillets on both side of the parallel sub-panels only, (3) fillets on the outermost side of the parallel sub-panels only, and (4) fillets on only 50 % of the outermost side of the parallel sub-panels. It was observed that welding types 1 and 2 resulted in almost the same ultimate strength. Welding type 3 showed a slight reduction in ultimate strength which was attributed to the decrease in the degree of restraint provided by a one-side welding. Type 4 welding was not recommended due to the high force concentration associated with the decrease of the fillet length. With the thickest webs of 0.91 mm, this force concentration resulted in web tearing prior to the occurrence of buckling or yielding. Sherman and Fisher also concluded that the shear stiffness of beams with corrugated webs constitutes roughly about 60 % - 75 % of the total stiffness (with the higher percentage for the thinner webs). A tentative equation to calculate the beam stiffness based on the conventional beam theory was presented.

In 1977, Hussain and Libove [24] investigated the same problem but with discrete connections between the web and the flanges. A web consisting of two identical corrugated sheets placed face-to-face was connected to rigid flanges built using two back-to-back angles. Two types of attachments were used, wide attachments consisted of large square washers and bolts, and point attachments obtained by removing the washers. It was found that very large increase in stiffness can be achieved by changing from small to large attachments. It was then concluded that the closer to a continuously connected web, the higher the capacity achieved.

In 1984, Hamada *et al.* [18] investigated steel I-beams with partially corrugated webs. Each web was made of a flat steel plate of 2.30 mm thickness with arc corrugations only in

the central part of the web depth formed after welding the it to the flanges. An automated production line was successfully established for the fabrication of these beams in Japan. According to Elgaaly and Dagher [10], the manufacturer of these beams shipped a total of 70000 tons of the product to the United States between 1980 and 1984 to be used in the construction of mobile modular homes. Two problems were experimentally investigated: the web shear buckling strength, and the web crippling under concentrated loads. Equations for calculating the capacity of such beams were given. It was found that the shear capacity of such beams is comparable to that of beams with flat webs with welded stiffeners but with a notable decrease in weight and production time.

In 1997, an article that described two monotonic tests and one cyclic test conducted on steel beams with sinusoidally corrugated web was published by Pasternak and Branka [48]. The tests aimed to investigate the shear strength of the web. The article also presented some technical information about the production of such girders in Austria for the use as rafters and columns of frames in buildings construction, or as crane runway beams.

In Japan in 1997, Honda and Tanaka [22] analytically investigated the static and dynamic behaviour of girders with trapezoidally corrugated webs compared to girders with zigzag webs. The aim of the study was to observe any differences in the load-deflection curve, the shear and bending stress distribution in the web, and the natural frequency and the vibration mode. The researchers were also concerned with determining the limits for applying the conventional beam theory on such beams. From the finite element analysis, it was found out that the distribution of the shear stresses in the web did not change with the change in shape from trapezoidal to zigzag while no bending stresses existed in the web in both cases. No difference was also observed in the load-deflection curve. A limit of the applicability of the conventional beam theory in calculating the static and dynamic characteristics was found. This limit was given as a function of the corrugation profile parameters.

## **2.5 RESEARCH ON COMPOSITE BEAMS WITH CORRUGATED WEBS**

### **2.5.1 Advantages of Using Corrugated Webs in Bridge Girders**

In 1982, the advantages of using corrugated webs in prestressed box or I-girders for bridge construction were recognized by the research team in Campenon Bernard BTP, France. In 1990, M. Cheyrezy and J. Combault [6] reported these advantages. Assuming a composite PC box or I-girder with a stiffened flat steel web, a similar section with a corrugated steel web will have the following advantages:

(A) From a structural behaviour perspective:

- Higher transverse stiffness due to the corrugation depth, combined with higher resistance to in-plane shear forces due to narrow spaced folds. Consequently, more resistance against global and local buckling of webs is achieved.
- As the sensitivity to buckling decreases, the effect of initial geometrical imperfections is less pronounced.
- Owing to the increased transverse stiffness, the number of intermediate diaphragms needed to transmit transverse loads, due to wind pressure for instance, to the concrete flanges is reduced.
- The decreased axial stiffness of the web, due to the accordion effect of the corrugations, prevents it from carrying or transmitting axial forces due to flexure, prestressing, creep, shrinkage, or temperature effects. Therefore, the webs resist only principal stresses caused by shear (and torsional forces for box-girders).
- Longitudinal prestressing forces applied to the bottom flange do not dissipate into the web. Therefore, fewer tendons are needed as well as fewer shear connectors.
- The reduced total weight of the girder and the optimum distribution of forces among its structural components allow lengthening of the feasible maximum span.

(B) From an economic perspective:

- A reduced web thickness, combined with the elimination of welded stiffeners lead to lighter and more economical girder and bearings.
- With the new technique of using transverse reinforcing steel running through the web

as shear connectors (see section 2.4.4), steel flanges can be discarded completely.

(C) From a construction ease perspective:

- The three dimensional flexibility of the web facilitates the construction of curved bridges, and reduces the tolerance necessary for assembling the web panels.
- Lighter temporary supports are allowed.

Compared with a PC box or I-girder, the corresponding composite PC box or I-girder with a corrugated steel web will have the same advantages that results from the decreased self weight such as increasing the feasible span, the saving on piers and on temporary supports. In addition to that, the following advantages were also recognized:

- The right material is used in the right place, i.e., concrete to sustain bending moments and steel webs to carry shear forces.
- The elastic lever arm is increased to its maximum value.
- The difficulties associated with the casting of deep concrete webs are avoided.
- If segmental construction is to be used, the weight of the freshly poured concrete for the bottom and top slabs (or flanges) can be supported by the already placed web element. This greatly simplifies the construction equipment.
- Also in segmental construction, the cast-in-place box elements are much lighter which allows having approximately three times longer elements. This should result in a faster construction pace.

### **2.5.2 Campenon Bernard BTP (France)**

As a part of a national French project that was aimed at improving the current knowledge in the field of bridge engineering, a search for lighter and stronger girders was taking place. Two new innovations were found to achieve the desired lightness and practicability when combined together: external prestressing and corrugated webs. In 1983, tests were successfully performed on a large scale box-girder model that was built by Campenon Bernard BTP and was loaded only by external prestressing. Figure 2.13 shows the

large scale model. Eventually, the French Department of Transportation decided to give Campenon Bernard the opportunity of building an experimental bridge located in the city of Cognac. The 108 m long bridge consisted of a continuous three span prestressed box-girder with trapezoidally corrugated web. The longest span was the middle one of 43 m. the bridge was completed by the end of 1986. Subsequent to the success of the Cognac bridge, three more bridges with trapezoidally corrugated webs were built in France: the Maupre viaduct (325 m long with seven continuous spans varying from 40.95 m to 53.55 m, completed in 1987), the Asterix bridge (a two-span bridge each 36.60 m long, completed in 1989), and finally the Dole bridge (496 m long with seven continuous spans distributed as two 48 m long end spans and five 80 m long middle spans, completed in 1994). For all these bridges, the corrugated web thickness varied from 8 mm to 12 mm depending on the location in the span and on the shear and torsion forces carried by the span. Figure 2.14 shows a possible typical cross section of a corrugated web while figures 2.15 and 2.16 show the mid-span cross sections of the Cognac bridge and the Maupre Viaduct.

Several articles describing the large scale model and the specifications of the bridges built were published either by Campenon Bernard researchers or by others who discussed their work [5,6,7,20,21,31,32,46,49]. However, none of these articles covered any research results or detailed theoretical discussions.



Figure 2.13 Testing of the large scale box-girder model, [ref. 31]



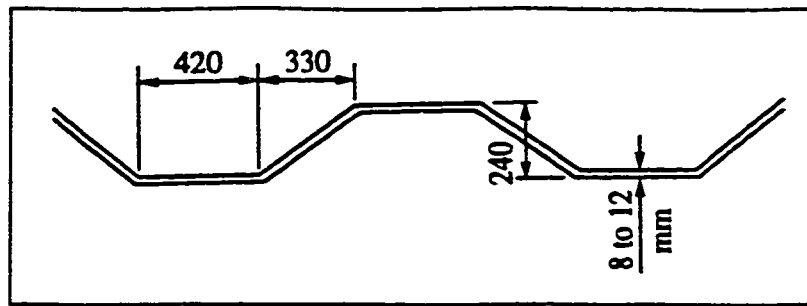


Figure 2.14 A possible typical cross section of a corrugated web, [ref. 6,20]

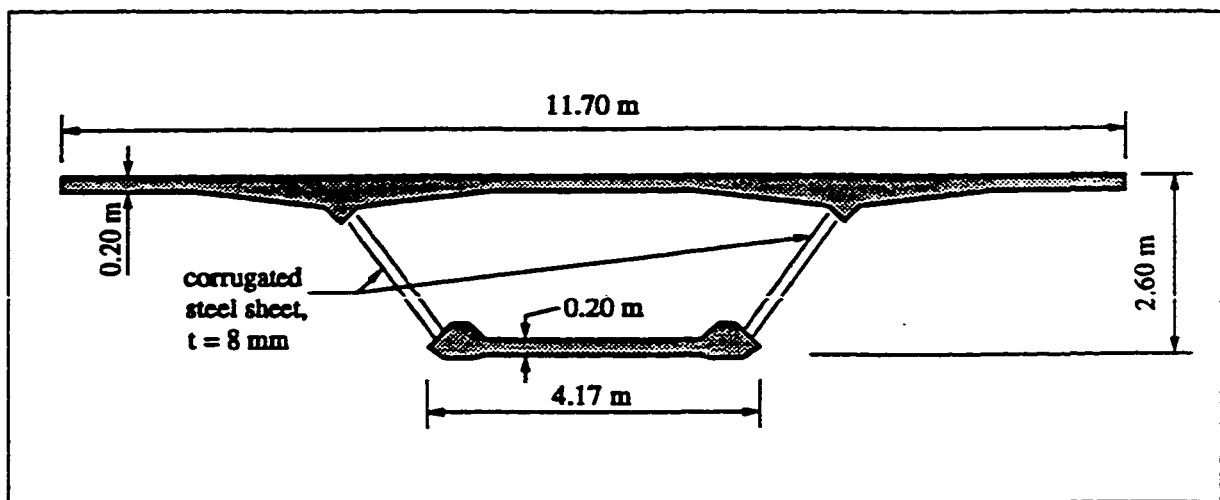


Figure 2.15 Cognac bridge - Typical mid-span cross section, [ref. 6,20]

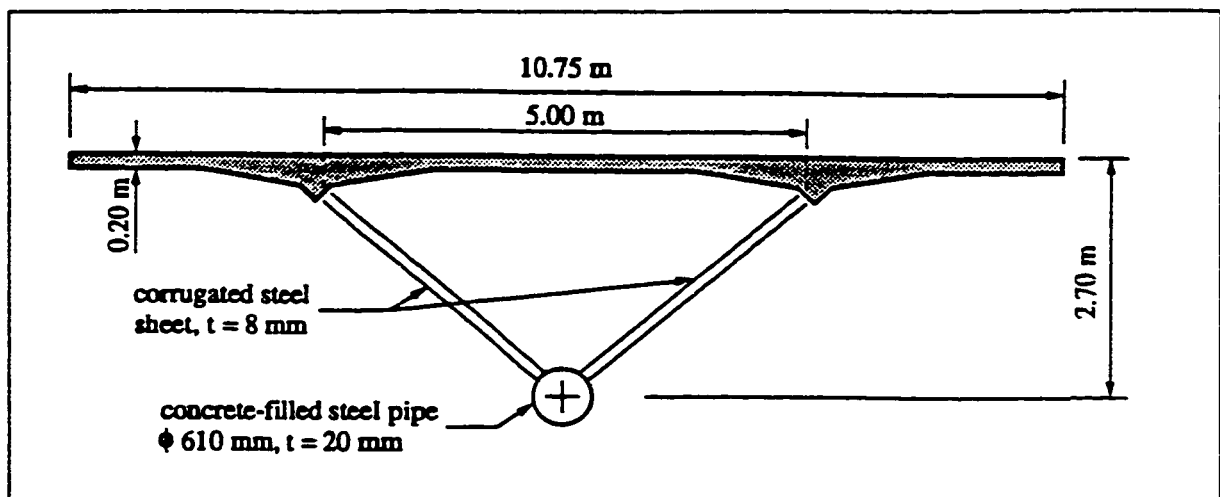


Figure 2.16 Maupre Viaduct - Typical mid-span cross section, [ref. 6,20]

### **2.5.3 Proposed High-Speed Railway Bridges (Germany)**

Associated with the intention to improve the infrastructure systems in Germany in order to meet the enormous increase in transportation among the European countries, new high-speed track systems were under planning in 1994. Among the alternatives that were under investigation was the new composite system that has been used in France, the prestressed box-girders with corrugated steel webs. A comparative study has been conducted using the typical 58 m single span girder which is used in Germany for high speed bridges crossing valleys without rivers [29,30]. The comparison was between the single cell prestressed concrete box-girder section that is typical for that girder, and the proposed new composite prestressed box-girder with corrugated webs. For both cross sections, a concrete strength of 85 MPa was assumed in the design which complies with the trend toward using high strength concretes in Germany since the beginning of the nineties. The following results were obtained:

- With the new system, the girder height was reduced from 5 m to 3.50 m.
- 27 mm thick corrugated steel webs of 520 MPa ultimate strength were found to be needed in order to account for the un-investigated fatigue effects, and to meet the deformation limits in the German specifications.
- Internal longitudinal prestressing was used only for the bottom flange.

The study was proposed to the German Federal Railway. Figure 2.17 shows a sketch of the proposed cross section with the shear connectors details.

### **2.5.4 Japan Highway Public Corporation - Waseda University (Japan)**

In November 1993, the first Japanese box-girder bridge built with corrugated webs was completed [47]. The Shinkai bridge is a one span bridge with total length of 31 m, span length of 30 m, and is 14.80 m wide. Twin box-girders of constant depth 1.90 m and with rigid end diaphragms were used. Both internal and replaceable external cables have been used for longitudinal prestressing. Two articles briefly describing the shear and torsion analysis of the

Shinkai bridge were published [55,56]. It was concluded that more attention should be paid to the warping effects in the design of such box-girders.

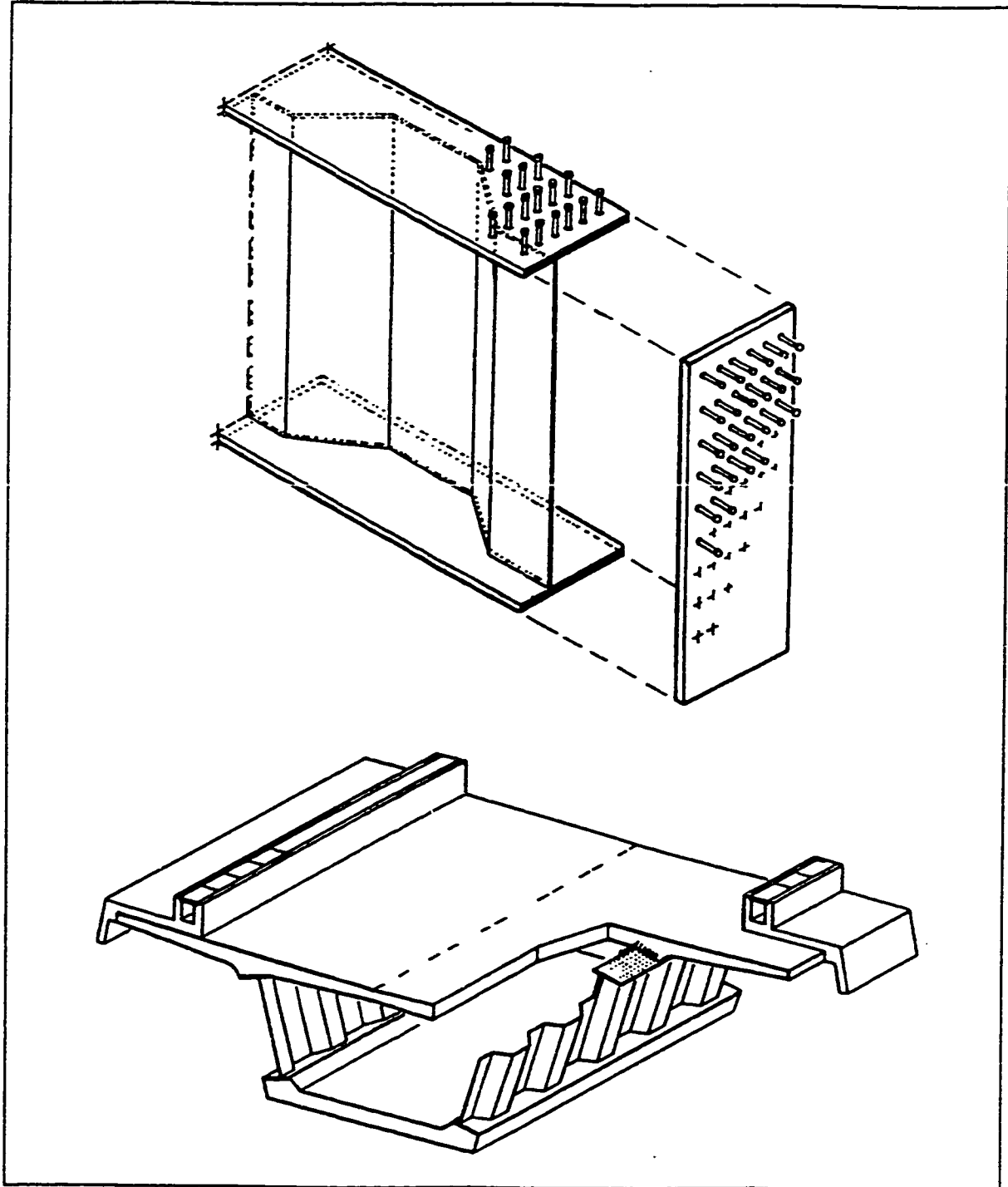


Figure 2.17 Bridge cross section proposed to the German Federal Railway, [ref. 30]

Another bridge built using one externally prestressed box-girder with corrugated webs, the Ginzan-Miyuki (Matsunoki) bridge, was completed in 1996. It is a continuous five-span bridge with a total length of 210 m, a deck width of 9.30 m, and a box-girder depth of 3 m. A diagonally suspended incremental launching technique was used in the construction. The stability of the bridge during construction was briefly discussed in one article [25]. Results from an experimental dynamic analysis performed on the completed bridge were also published [25, 52]. The aim of the analysis was to investigate the vibration characteristics of both the girder and the external prestressing cables under moving vehicles. The Ginzan-Miyuki bridge is considered the longest bridge of its kind to be built in Japan up to this date.

Both the Shinkai and the Ginzan-Miyuki bridges were built using top and bottom steel flanges with welded headed shear studs to provide a mechanical connection between the corrugated webs and the concrete flanges. In 1994, a research program was started at Waseda University in order to investigate the behaviour of composite beams with a new types of shear connectors. In 1995, Yoda and Ohura Published the first results of this program [54]. Six, 3 m long simple span beams, with bottom steel flanges and top reinforced concrete flanges were statically tested under 2 symmetrical point loads 500 mm apart. The top concrete flanges were 100 mm thick, and the trapezoidally corrugated webs were 4.50 mm thick. The six beams were divided into three groups where different type of shear connectors was used for each one:

- Group A used the conventional headed shear studs with a nominal diameter of 6 mm welded directly to the web perpendicular to it.
- Group B used 6 mm nominal diameter transverse steel bars in the top flange running through holes punched in the corrugated web. The bars were placed at 60 to 92 mm intervals.
- Group C used only 30 mm diameter punched holes in the corrugated web arranged at 100 mm intervals. The beams of group C were intended to investigate whether or not the composite action provided by the corrugations and the concrete that runs through the holes will be adequate.

The test results showed that beams of group B had the necessary composite action up to the failure of the top concrete flange in compression. Beams of groups A and C had a complete

composite action up to about 91 % of the flexural strength, then the compression flange failed in horizontal shear. No slippage of the shear studs, the transverse steel bars, or even near the holes was observed prior to failure.

Fatigue tests on similar beams and under similar load configuration, except its dynamic nature, have also been carried out [57]. The promising results obtained from both the first static and dynamic tests led to the use of the new “transverse steel shear connectors” method in the latest Japanese corrugated web bridge, the Hondani bridge. This continuous bridge has total length of 198 m divided into three continuous spans 43.92 m, 97.00 m, and 55.86 m respectively. The bridge cross section is 11.4 m wide, 6.40 m deep at the support, and 2.50 m deep at the centre of the central span. It has been completed in 1997. Figure 2.18 shows both the conventional welded stud shear connectors and the new technique adopted in the construction of the Hondani bridge [23].

The research on this type of shear connectors is still taking place at Waseda university. A design method that can be used to determine the needed transverse bar diameter and hole spacing is being developed.

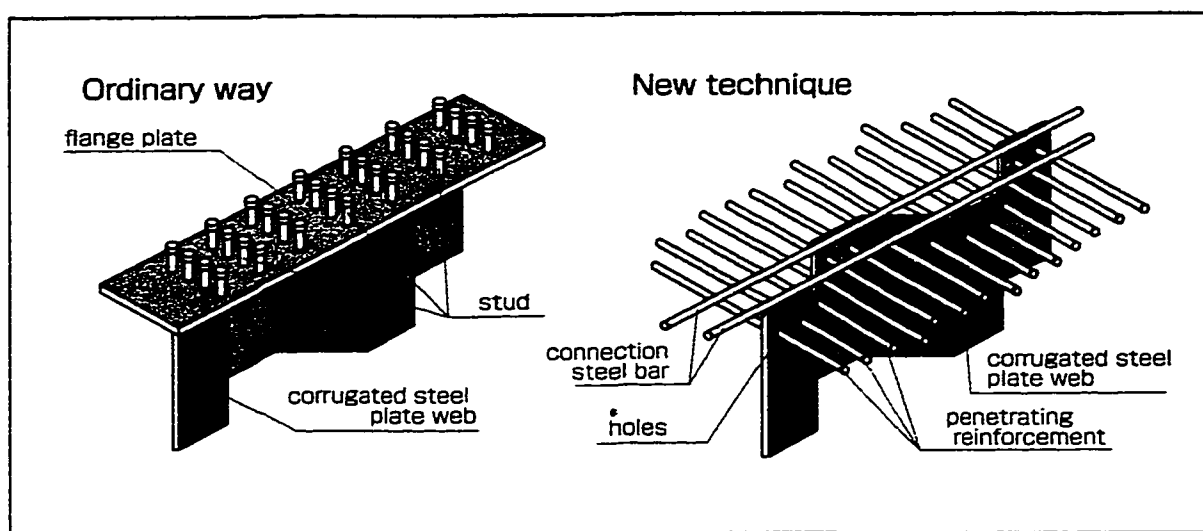


Figure 2.18 Different shear connector configurations, [ref. 23]

Table 2.2 gives a summary of the structural dimensions of the French and Japanese bridges built so far using corrugated steel webs.

Table 2.2 Bridges constructed using corrugated webs

* Bridge * Location & year of completion	* Structural system * Span number	Total length (m)	Span lengths (m)	Deck width (m)	Total depth (m)		Approx. Span / depth		Corrug. web thickness (mm)
					M <sup>†</sup>	S <sup>††</sup>	M <sup>†</sup>	S <sup>††</sup>	
<i>Cognac bridge</i> France 1986	Single P/C box-girder (3-continuous)	107.8	32.45 42.9 32.45	11.7	2.6	2.6	13 ~ 17	13 ~ 17	8
<i>Maupre viaduct</i> France 1987	Triangular P/C box-girder (7-continuous)	324.5	40.95 ~ 53.55	10.75	3	3	14 ~ 18	14 ~ 18	8
<i>Asterix bridge</i> France 1989	P/C slab on 2 steel beams (2-continuous)	74	2 × 37	13	2.1	2.1	18	18	not available
<i>Dole bridge</i> France 1994	Single P/C box-girder (7-continuous)	496	48 5 × 80 48	14.5	2.5	5.5	19 ~ 32	9 ~ 15	8 ~ 12
<i>Shinkai bridge</i> Japan 1993	Twin P/C box-girder (1-simple)	31	31	14.8	1.9	1.9	16	16	9
<i>Matsunoki bridge</i> Japan 1995	Single P/C box-girder (5-continuous)	210	28 4 × 45.5	9.3	3	3	9 ~ 15	9 ~ 15	9 ~ 12
<i>Hondani bridge</i> Japan 1998	Single P/C box-girder (3-continuous)	198.4	44.6 97.2 56.6	10	2.5	6.4	18 ~ 39	7 ~ 15	12

† Typical mid-span section

†† Typical over-support section

### 2.5.5 National Cheng Kung University (Taiwan)

In 1998, Mo *et al.* [45] presented the test results of an experimental program conducted on a scaled prestressed box girder with corrugated webs. As a part of the national project to improve Taiwan's transportation system, a new route 345 km long was planned. The route includes many bridges and viaducts that cover approximately 207 km of its total length. The new structural system that has been successfully used in France and Japan was considered as one of the alternatives, but required further analytical and experimental research. Four box-girders were built and tested under cyclic flexural loading. The box-girders were built as a 1/6 scale of the girder of the Shinkai bridge in Japan. Each girder was of 5.0 m total length, and 0.365 m total depth. The thicknesses of the top and bottom slabs were 85 mm and 60 mm respectively. The main goal of the testing was to investigate the flexural behaviour of such a structural system under cyclic loading and to verify the prediction of its load-deflection curve. The considered experimental parameters were the effective prestressing level ranging from 0.3 ~ 0.8 of the yielding stress of the prestressing strands, and the concrete strength of the top and bottom slabs ranging from 33 ~ 50 MPa. An analytical model that predicts the load-deflection curve of such girders was developed and compared with the test results. The tests were conducted at the structural laboratory of the National Cheng Kung University, and the results showed a good agreement between the predicted and the experimental load-deflection curves. The results also showed the high levels of ductility provided by such a system under cyclic loading. The best results from both the ultimate flexural strength and the ductility points of view corresponded to an effective prestressing level of  $0.5 f_{py}$ .

### 2.5.6 New Bridge with Corrugated Webs in Stockholm (Sweden)

In 1997, a new bridge with corrugated webs was under construction in the Swedish capital, Stockholm. The overall bridge layout and dimensions are not available to the author.

## 2.6 SUMMARY

It has been shown in this chapter that the attention to the use of corrugated steel webs in both steel and composite beams has greatly increased in the past two decades. Important trends in the behaviour of corrugated webs under different kinds of loading were established by several research programs that were conducted at different research institutes worldwide. Formulas that represent the behaviour of such webs were also developed. Although several prestressed composite bridges were built in the last 12 years using corrugated steel webs, there is an obvious lack of research and of published information in this field of application. The lack of information is primarily concerning: (1) the applicability of the strength equations that is based on the studies performed on steel girders with very small span to depth ratios to prestressed composite bridge girders with much higher span to depth ratios, (2) the actual distribution of forces among the different structural components of such a system at the different stages of loading, and (3) a criterion to allow determining the structurally and economically optimum corrugation profile for such an important application.



## ***CHAPTER 3***

# **SHEAR RESISTANCE OF CORRUGATED STEEL WEBS**

### **3.1 GENERAL**

This chapter details the fundamental concept that has been used to describe the behaviour of corrugated webs under pure shear forces. The analysis covers both the cases of webs bounded with steel (flexible) or concrete (rigid) flanges. It will also cover two shapes of corrugations, the trapezoidal and the zigzag profiles. A plotting of the different modes of shear buckling was developed and will be presented. A mathematical procedure for choosing the optimum corrugation profile and thickness was developed and will be presented as well.

### **3.2 GEOMETRY OF CORRUGATED STEEL PROFILES**

The most common corrugation profiles for use as webs in steel or composite beams are the sinusoidal and the trapezoidal profiles. As was discussed in chapter 2, steel I-beams with webs with partial sinusoidal corrugations in the central part of its depth were used in the United States in the eighties for the construction of mobile modular homes, [18]. It was also mentioned that steel beams with sinusoidally corrugated webs are being commercially produced in Austria to be used as rafters and frame columns in buildings construction, [48]. In the meanwhile, trapezoidally corrugated webs have been used in the construction of all the corrugated web bridges that have been built so far in France, Japan, or in Sweden. A third

shape, the zigzag profile, has been used recently in Japan in building composite beams for test purposes, [22]. Geometrically, the zigzag profile can be considered as a special case of the trapezoidal one by removing the sub-panel that is parallel to the beam span. The shear buckling analysis in this research is limited to the trapezoidal and the zigzag profiles. Figures 3.1 and 3.2 show the coordinate system and the geometrical relations that will be adopted through the entire thesis for both shapes.

### 3.3 ANALYSIS FOR SHEAR - THE CONCEPT

Corrugated steel webs are believed to be able to sustain greater loads in shear than flat stiffened steel webs of the same thickness. This ability is usually attributed to two characteristics of corrugated webs: (1) the high transverse stiffness that is provided by the corrugation depth, and (2) the high in-plane stiffness due to the narrow spaced folds that act as vertical stiffeners to the flat sub-panels. Both characteristics should be considered when analyzing corrugated webs against shear forces.

So far, the proposed equations to calculate the strength of corrugated webs in pure shear limit the maximum achieved strength to that corresponding to the critical shear buckling stress or to the shear yielding stress, whichever is less. As was discussed in chapter 2, the total post buckling strength that has been observed through experimental testing of steel beams, was measured to be only about 50 % of the buckling strength. This observation does not agree with the second assumption that has been made, i.e., that folds behave as vertical stiffeners to the flat sub-panels of the corrugated web. It is well known that significant additional amounts of shear past the theoretical buckling load can be carried in the case of vertically stiffened flat webs. The additional post buckling strength is provided by the so called *tension field action* that forms after the initiation of buckling provided that shear yielding did not take place prior to buckling, [1,2,51]. Even, if the observed results are true in the case of steel beams with flexible steel flanges, it is not known whether it is the same in the case of composite beams with rigid concrete flanges or not. In the analysis proposed in this thesis, it will be assumed primarily that the total shear strength of the web is the sum of both the

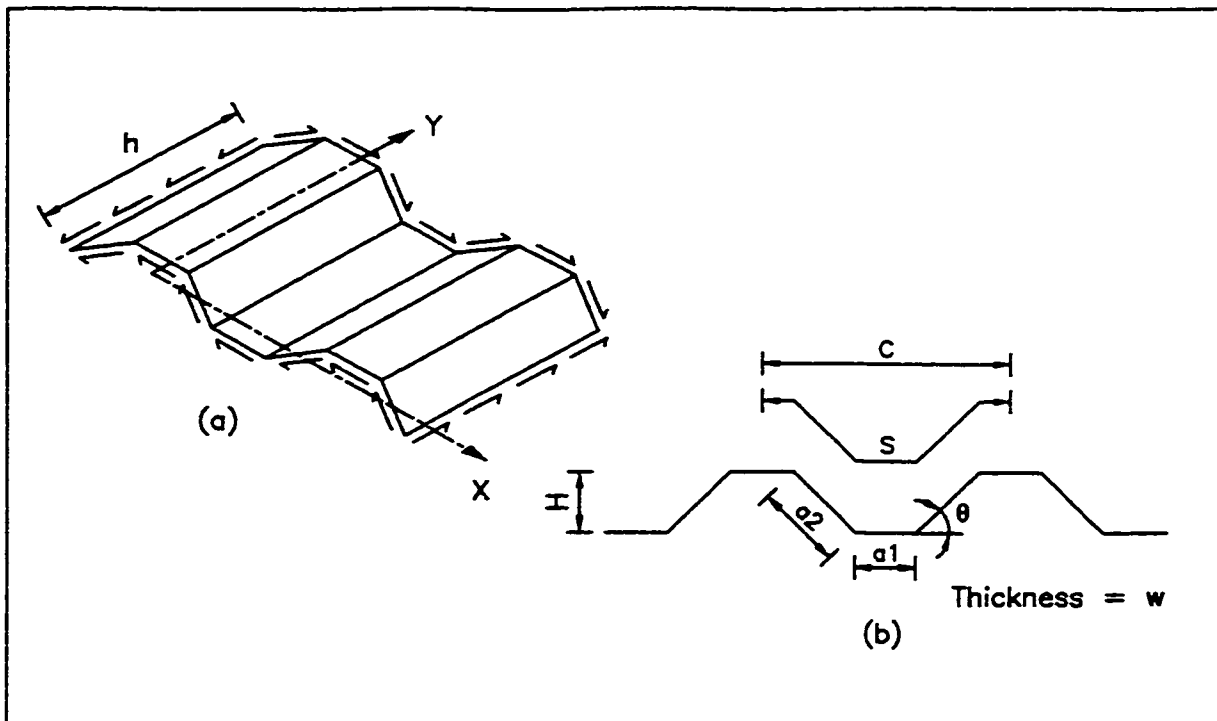


Figure 3.1 Trapezoidal corrugations (a) coordinate system (b) geometrical relations

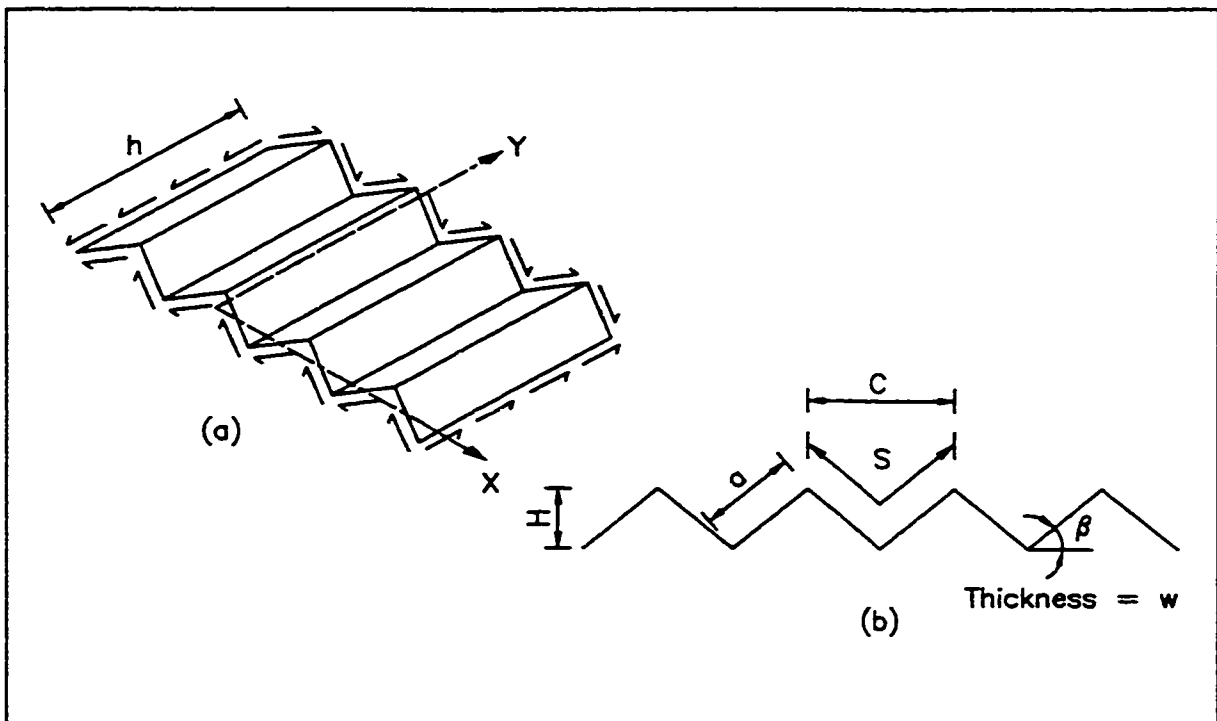


Figure 3.2 Zigzag corrugations (a) coordinate system (b) geometrical relations

buckling and the additional post-buckling strengths. The buckling strength will be calculated taking into account the possible buckling modes that have been recognized by other researchers, namely, the *local buckling* and the *global buckling* modes. The additional post-buckling contribution will be left undetailed until after the results from the experimental testing have been obtained.

Assume a corrugated web of depth  $h$  and thickness  $w$  is subjected to a vertical factored shear force  $V_f$  parallel to the fold lines. The force is assumed to be constant in the x-direction perpendicular to the corrugations, i.e., it forms a field of pure constant shear around an element in the web. With  $V_n$  and  $V_r$  the nominal and factored shear strengths of the web respectively, and  $\phi$  the strength reduction factor, the governing design equation should be

$$V_r = \phi V_n \geq V_f \quad (3.1)$$

The nominal strength of the web is calculated by

$$V_n = w h F_s \quad (3.2)$$

where  $F_s$  is the ultimate shear stress to be carried by the web, which is the sum of the critical buckling shear stress,  $F_b$ , and the additional post-buckling shear stress,  $F_t$ , according to the equation

$$F_s = F_b + F_t \quad (3.3)$$

As mentioned before, the determination of  $F_b$  will be discussed below and will be subjected to any modifications imposed by the experimental results, while  $F_t$  will be defined later according to the data obtained experimentally.

### 3.4 THE BUCKLING STRENGTH

#### 3.4.1 The Local Buckling Criterion

In this buckling mode, the corrugated web is treated as a series of flat rectangular sub-panels mutually supporting each other along their vertical edges, and supported by the flanges at their horizontal edges. The buckling is expected to show in the form of a single buckle along each single sub-panel in the region subjected to high shear stresses exceeding this limit. Equation 2.1 is used to determine the theoretical elastic critical shear buckling stress  $\tau_{le}$ . For the case of a practical corrugated web, the web height  $h$  will always be longer than the widest sub-panel width  $a$  (which is the opposite to the case of a stiffened flat web where usually the web height  $h$  is less than the spacing between the vertical stiffeners  $a$ ). Therefore, equation 2.1 will take the following form

$$\tau_{le} = k_l \frac{\pi^2 E}{12 (1 - \nu^2) (a/w)^2} \quad (3.4)$$

The local shear buckling coefficient  $k_l$  can be calculated using equation 2.2 in the case of a steel girder, and using equation 2.3 in the case of a composite girder. It is clear from all the discussion above that the resistance of a corrugated web against local buckling is independent of whether its corrugation profile is trapezoidal or zigzag. It is also clear that a trapezoidal profile whose sub-panels are all of the same length will be more practical than a profile whose inclined sub-panels are different in length than the ones parallel to the beam span.

#### 3.4.2 The Global Buckling Criterion

In this buckling mode, the corrugated web is treated as an orthotropic plate of uniform thickness with material properties equal to the gross material constants of one repeating cross section (see figure 2.6). The global buckling is characterized by formation of diagonal buckles where each one crosses several corrugations. By substituting our web's dimensions into

Easley's solution [8] for calculating the elastic critical shear stress  $\tau_{ge}$  of the unit corrugation shown in figure 2.6 under pure shear, the following equation can be obtained

$$\tau_{ge} = k_g \frac{(D_y)^{0.25} (D_x)^{0.75}}{w h^2} \quad (3.5)$$

where  $D_x$  and  $D_y$  are the flexural stiffnesses per unit corrugation along the beam depth (about the x-axis) and the beam length (about the y-axis) respectively. Equation 3.5 applies to a web of any corrugation profile. However the terms  $D_x$  and  $D_y$  are functions of the geometry of the profile. Their values for the trapezoidal profile in figure 3.1 are

$$D_x = \frac{E I_x}{c} = \frac{E \left[ 2 a_1 w \left( \frac{H}{2} \right)^2 + \frac{w H^3}{6 \sin \theta} \right]}{2 (a_1 + a_2 \cos \theta)} \quad (3.6-a)$$

$$D_y = \frac{c}{s} \left( \frac{E w^3}{12} \right) = \frac{(a_1 + a_2 \cos \theta)}{(a_1 + a_2)} \left( \frac{E w^3}{12} \right) \quad (3.6-b)$$

For the zigzag profile in figure 3.2, their values are

$$D_x = \frac{E I_x}{c} = \frac{E \left[ \frac{w H^3}{6 \sin \beta} \right]}{2 a \cos \beta} = \frac{E w H^3}{12 a \sin \beta \cos \beta} \quad (3.7-a)$$

$$D_y = \frac{c}{s} \left( \frac{E w^3}{12} \right) = \cos \beta \left( \frac{E w^3}{12} \right) \quad (3.7-b)$$

$k_g$  in equation 3.5 is the global shear buckling coefficient which depends solely on the top and bottom end restraints. For simply supported edges (which can represent flexible steel flanges),  $k_g = 36$ . For clamped edges (which can represent rigid concrete flanges),  $k_g = 68.4$ . It should be noted that when comparing the global buckling strength of trapezoidal and zigzag profiles that have the same plate thickness  $w$  and the same sub-panel width  $a$  (assuming that the trapezoidal profile has a constant sub-panel width), two cases exist. The first is when preserving the same angle between sub-panels where the corrugation angles should satisfy  $\theta = 2\beta$ . In this case, the trapezoidal profile will give a higher resistance over the whole range of the corrugation angles due to the contribution of the sub-panel parallel to the beam to the out-of-plane inertia. The second case is when preserving the same resistance against global buckling which yields  $\beta > \theta$  for any width of the sub-panels due to the same reason. In the meantime, practical considerations limit the range of the available corrugation angle. Practically, the trapezoidal corrugation angle  $\theta$  should not be chosen greater than  $90^\circ$ , and the zigzag corrugation angle  $\beta$  should not be chosen greater than  $45^\circ$ . Therefore, the global buckling strength of the trapezoidal profile will be studied only over the range  $0^\circ < \theta \leq 90^\circ$ , while that of the zigzag profile will be studied over the range  $0^\circ < \beta \leq 45^\circ$ .

### 3.4.3 The Shear Yielding Criterion

As in the analysis of any steel plate under pure shear, the Huber-von Mises-Hencky yield criterion is considered as an upper limit to the ultimate shear stress in the web. This criterion defines the shear stress  $\tau_y$  along the edges of an element in a pure shear state causing it to yield. For a web material with yield strength  $F_y$ , the shear yield is expressed by

$$\tau_y = F_y / \sqrt{3} \approx 0.58 F_y \quad (3.8)$$

### 3.4.4 The Interaction of Buckling Modes

In chapter 2, it was mentioned that the corrugation dimensions that have been used in Leiva-Aravena's tests [3,34] resulted in shear strengths that were best fitted by an interaction curve of the local and global buckling modes taking the shear yield strength into account (equation 2.9). Other equations that have the same form were suggested by Elgaaly *et al.* [15], and by Johnson and Cafolla [26]. In order to visualize how such an interaction can take place, it might be useful to take a look at a numerical example and its strength plotting that shows the governing buckling modes of a corrugated web. Let us consider the trapezoidally corrugated web of the Japanese Shinkai bridge. The web has the following geometrical properties: a vertical height of about 1.70 m, a thickness of 9 mm, a corrugation angle of about  $37^\circ$ , and a constant sub-panel width of 250 mm. The plotting of the  $\tau_{le}$ ,  $\tau_{ge}$ , and  $\tau_y$  against the possible range of sub-panel widths  $0 < a \leq h$  is shown in figure 3.3. From this figure, it is clear that region 1 should be governed by the global buckling, region 3 should be governed by the local buckling, while region 2 (which the corrugation profile belongs to) should be governed by the shear yield. By plotting such a graph, two theoretical conclusions can be drawn. Firstly, a smooth transition between the local and global buckling should take place in region 2 provided that it does not exceed the  $\tau_y$  limit. Secondly, according to our concept, additional post-buckling strength can only exist for sub-panel widths that belong to regions 1 or 3. The following general equation is proposed as an interaction equation of the buckling modes with the shear yield automatically taken as the upper bound in region 2.

$$\frac{1}{(\tau_{in})^n} = \frac{1}{(\tau_{le})^n} + \frac{1}{(\tau_{ge})^n} + \frac{1}{(\tau_y)^n} \quad (3.9)$$

A mathematical property of equation 3.9 is that it will always take the least value of the three limits in the right hand side as an upper limit for the resulting value of  $\tau_{in}$  in the left hand side regardless of the exponent  $n$  value. However, low  $n$  values (say  $n = 1$  or less) will result in  $\tau_{in}$  values that are considerably less than the least of the three limits. High  $n$  values (say



$n = 5$  or more) will result in  $\tau_{in}$  values that are almost identical to the least of the three limits.

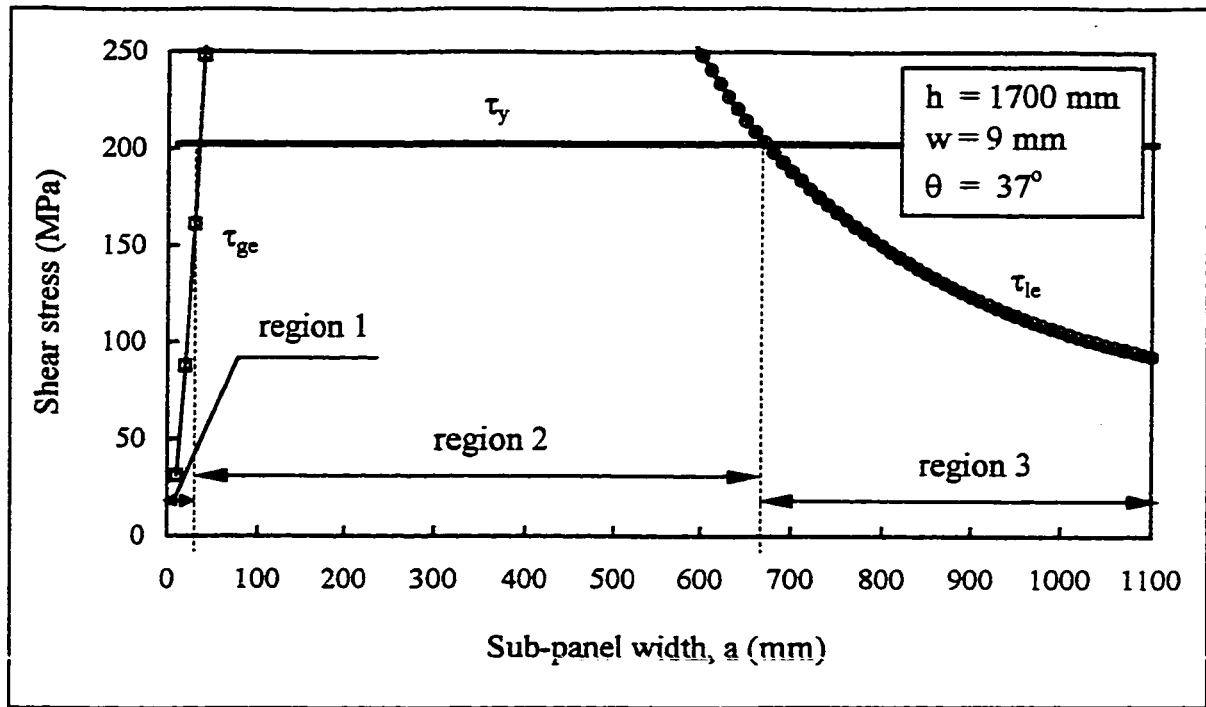


Figure 3.3 Shear strength for local buckling, global buckling, and shear yield

Therefore, theoretically speaking, if a proper exponent  $n$  can be determined to match the experimental results, only the  $\tau_{in}$  curve is needed to define *the buckling stress limit*  $F_b$  in regions 1 and 3, and *the ultimate stress limit*  $F_s$  in region 2. Elgaaly *et al.* [15] suggested an equation that is similar to equation 3.9 with an exponent  $n = 1$ . Figure 3.4 is a re-plot of figure 3.3 with two additional traces corresponding to equation 3.9 with  $n = 1$  and  $n = 2$ . From figure 3.4, it can be seen how an exponent of  $n = 1$  gives a very conservative value for  $\tau_{in}$  in region 2 which is much less than  $\tau_y$ . It can be expected that an exponent of a slightly higher value,  $n = 2$  for instance as shown in the figure, might be more suitable. However, it needs experimental values to confirm this theory. It should be noted that figures 3.3 and 3.4 were plotted using a Mathcad worksheet that was developed for that purpose. The Mathcad worksheet, Appendix A, computes the different strengths of a trapezoidally corrugated web in a composite beam according to equations 3.4, 3.5, 3.8, and 3.9.

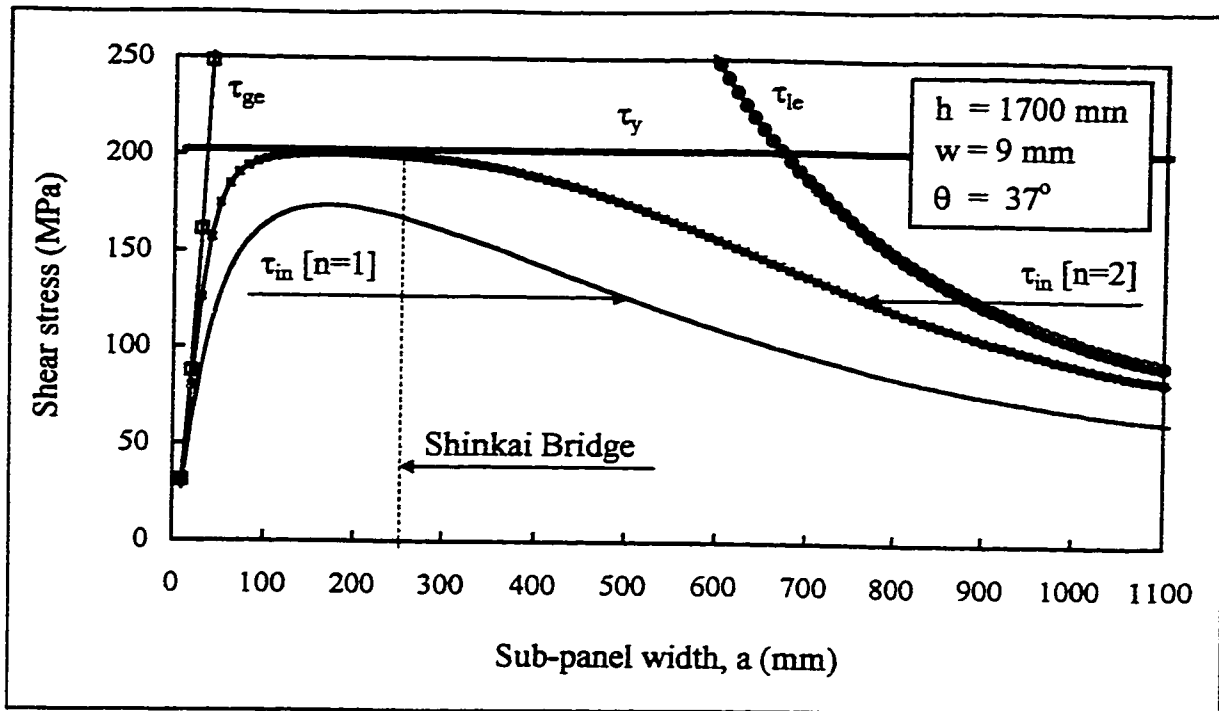


Figure 3.4 Interaction of the local and global buckling limited by the shear yield

### 3.4.5 The Optimum Dimensions of a Corrugation Profile

From figure 3.4, for  $n = 2$ , the maximum interaction shear stress that can be carried by the web is  $\tau_{in} = 201$  MPa corresponding to a sub-panel width  $a = 180$  mm. The curves in this figure were calculated for a corrugation angle  $\theta = 37^\circ$ . However, by choosing another corrugation angle as input,  $\theta = 30^\circ$  for instance, a different  $\tau_{in}$  curve will be obtained, and consequently a different maximum value at a different sub-panel width. Now, which one of the two profiles that correspond to the maximum interaction strengths is stronger and which is more economic? Or generally speaking, what is the definition of an optimum profile, and how can we determine the dimensions of such a profile? The proposed answer to this problem will be described below.

An optimum corrugated profile can be defined as “*the profile that gives the desired shear strength for the least cost*”. The cost should take into account the volume of steel, manufacturing costs, ... etc. In the proposed solution that will be described below, cost has

been assumed proportional to the volume of steel.

Assume a case of a girder with a corrugated web (trapezoidal or zigzag) needed to be designed for a specific nominal shear resistance  $V_n$ , and a specific web height  $h$ . The possible values for  $\alpha$ , and  $\theta$  (or  $\beta$ ) are:

$$0 < \alpha_i \leq h \quad (3.10)$$

$$0^\circ < \theta_j \leq 90^\circ \quad \left( \text{or} \quad 0^\circ < \beta_j \leq 45^\circ \right) \quad (3.11)$$

The interaction equation 3.9 can then be rewritten in a force form as:

$$V_{n_{i,j}} = w h \left[ \frac{1}{\left( \tau_{le_{i,j}} \right)^n} + \frac{1}{\left( \tau_{ge_{i,j}} \right)^n} + \frac{1}{\left( \tau_y \right)^n} \right]^{-\frac{1}{n}} \quad (3.12)$$

By solving this equation for its only unknown  $w$ , the web thickness for all possible combinations of  $\alpha$  and  $\theta$  (or  $\beta$ ) can be determined. All these combinations have the same strength  $V_n$ . Then, in order to determine the most economical profile, which will be then the optimum one, another function  $w_{eff}$  will be introduced to represent the effective thickness of the web which is the thickness of a straight web made with the same volume of material.

For a trapezoidal profile

$$w_{eff_{i,j}} = w_{i,j} \left( \frac{s_i}{c_{i,j}} \right) = w_{i,j} \left( \frac{2}{1 + \cos \theta_j} \right) \quad (3.13)$$

For a zigzag profile

$$w_{eff_{i,j}} = w_{i,j} \left( \frac{s_i}{c_{i,j}} \right) = w_{i,j} \left( \frac{1}{\cos \beta_j} \right) \quad (3.14)$$

A Mathcad worksheet, Appendix B, was developed to compute all possible combinations of  $w$ ,  $\alpha$  and  $\theta$  for a trapezoidally corrugated web in a composite girder according to the procedure described above. By using only the web height of the Shinkai bridge and a nominal shear force of 3.0 MN as input, the corresponding optimum profile was found to have the following geometrical properties:  $\alpha = 250$  mm,  $\theta = 16^\circ$ , and  $w = 9$  mm. This combination gave the smallest effective thickness of only 9.1 mm. The actual corrugation profile that was used in the bridge needed a thickness of 9 mm as well to sustain the same 3.0 MN nominal shear force. However, this corresponds to an effective thickness of 9.8 mm which is about 8 % greater than that of the optimum profile. Using the corrugation angle as the x-axis, and the effective web thickness as the y-axis, figure 3.5 shows the plotting of some of the possible combinations including the optimum one. Each trace represents a sub-panel width. Figure 3.6 shows the plotting of the  $w$  and  $w_{eff}$  curves only for the optimum combination.

One of the important observations of figure 3.5 is the flatness of all the curves at their lower values. If we took the curve for  $\alpha = 250$  mm as an example (which is the curve of the optimum profile), its smallest  $w_{eff} = 9.1$  mm corresponds to  $\theta = 16^\circ$  as it was mentioned before. However, it was found that the maximum calculated effective thickness in the range of  $11^\circ \leq \theta \leq 24^\circ$  is greater than that of the optimum angle by only 1.5 %. Two conclusions can be drawn out of this finding. Firstly, for practical purposes, corrugated webs can be considered insensitive to initial imperfections in the angle of corrugation. Secondly, the assumption that the web will resist only principal stresses caused by shear or torsion should be considered correct even in the regions of the beam that are under both high shear and high moment values. If we considered a case of a composite I-girder with flat stiffened web that suffers high shear and moment actions in some part of it. The interaction between both straining actions will reduce the shear capacity of the web. However, if a corrugated web was

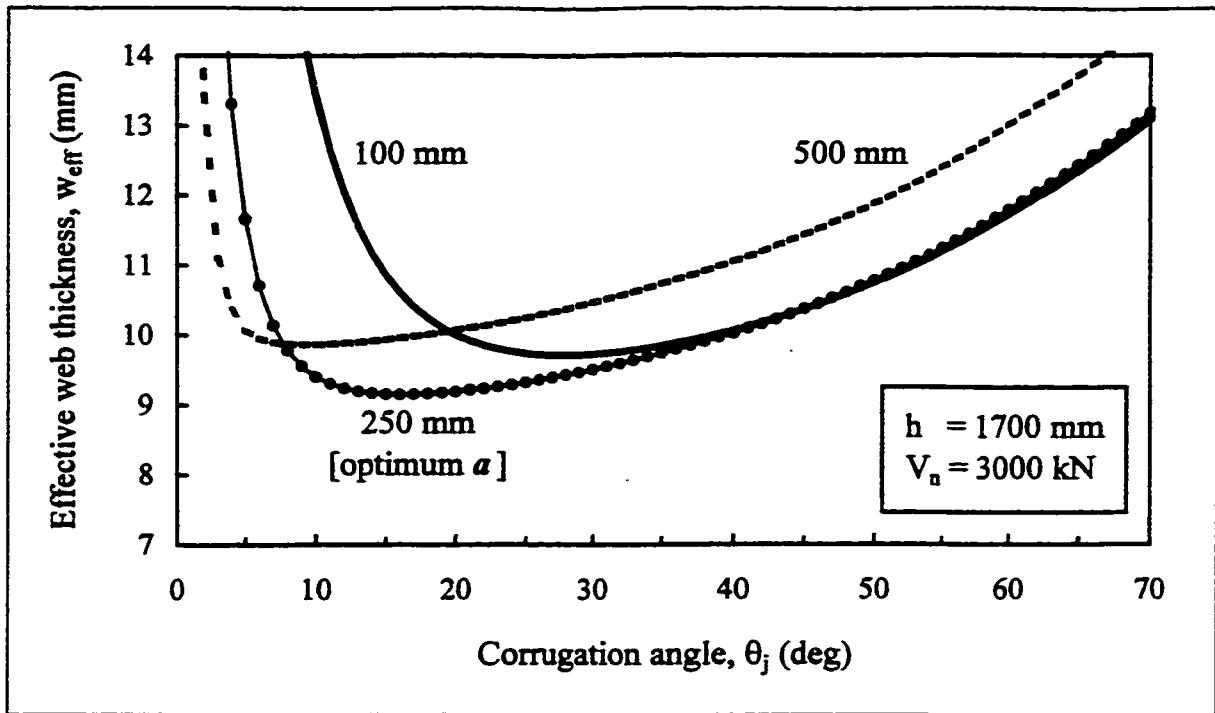


Figure 3.5  $w_{eff}$  for a trapezoidally corrugated web for different  $a_i$  values

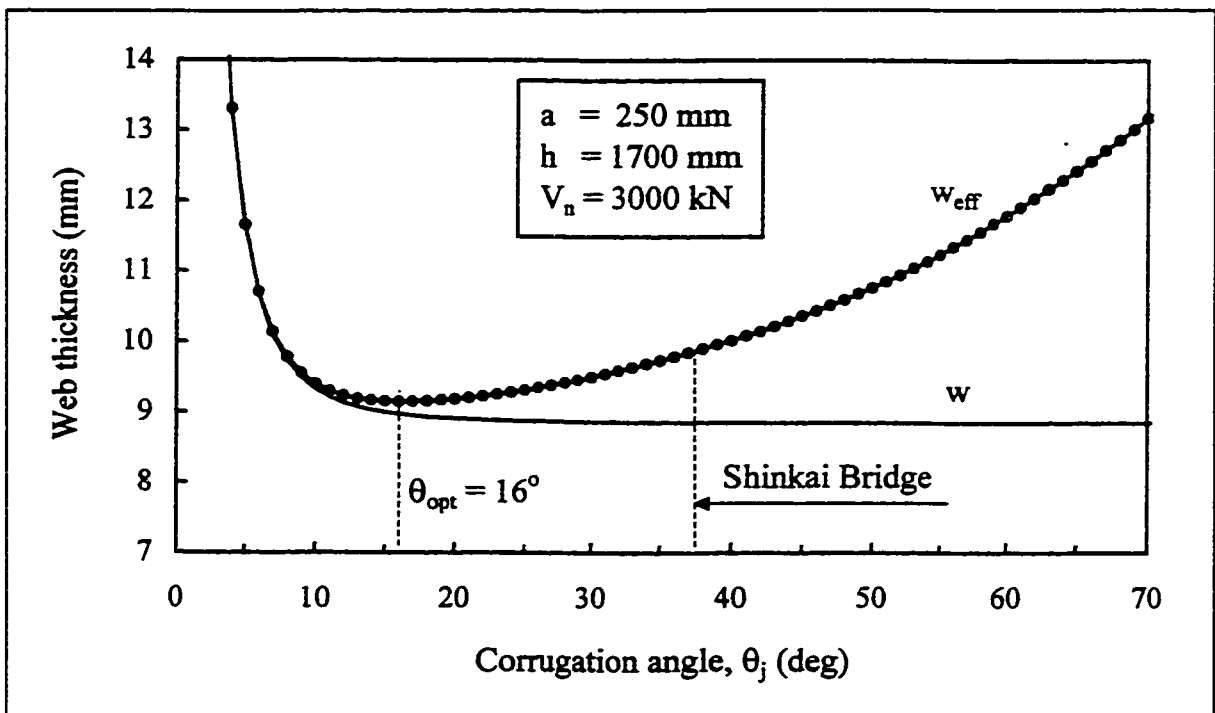


Figure 3.6  $w$  and  $w_{eff}$  for the optimum sub-panel width

used instead, the accordion effect will take place due to the bending moment and will result in increasing the corrugation angle near the flange under compression and decreasing it near the flange under tension. Such a change in the corrugation angle is expected to be minimal. Therefore the decrease in the shear strength should also be minimal and can be ignored. The proposed plotting of the shear strength of corrugated webs and the optimization procedure were presented by El-Metwally and Loov [17].

## ***CHAPTER 4***

### **EXPERIMENTAL PROGRAM**

#### **4.1 GENERAL**

This chapter is divided into five parts. The first part states the problem and the basis of the parametric study. The second part describes the process of choosing the test girder's shape and preliminary dimensions. The third part details the description of the five test girders including the material properties, the dimensions, the reinforcement details, the shear connector details, and the steps of construction. The fourth part describes the instrumentation and data acquisition. The fifth and last part describes the test setup and loading procedure.

#### **4.2 THE PARAMETRIC STUDY**

As was mentioned in chapter 1, the main objective of the experimental program is to investigate the different shear buckling modes and the ultimate shear strength of prestressed composite box or I-girders constructed using corrugated webs. Although the investigation of the flexural behaviour of the girders was included as well, the main variables had to be based on the shear part of the study. Therefore, it was decided to test several girders that have the same overall dimensions and flexural strength but with different shear strengths. In order to be able to draw a shear strength plotting for the web similar to that in figure 3.4, each girder's web has to have the same thickness, corrugation angle, and height. The only changing

parameter should be the sub-panel width so we can represent the three regions shown in figure 3.3. Plotting such a shear strength representation should allow us to determine the shape and the exponent value of the proposed interaction curve.

#### **4.3 THE TEST GIRDERS - PRELIMINARY DIMENSIONING**

The main criterion for choosing the overall shape of the test girder is that the relative dimensions and the span-to-depth ratio should be compared to those of real girders in short and medium span bridges as was summarized in table 2.2.

The first two decisions that have been made in the preliminary dimensioning process concerned the shape of the girder and the web profile. The I-shape was chosen for the cross section. It was found that a composite I-section can be constructed much easier than a box-section. Also for shear and flexure testing, the results obtained by testing the simpler I-section can apply to both sections. Concerning the corrugated web profile, no commercially available sections were found to satisfy our parametric study requirements. Therefore, custom-made webs were the only possible solution. The choice between the trapezoidal and the zigzag profiles was left to the steel fabricator, and the simpler zigzag profile was recommended. Again, the test results using the zigzag profile should be applicable to the trapezoidal one as well. It will be shown later from the discussion of the test results in chapter 5 that such a structural system that consists of P/C composite I-girders with zigzag corrugated webs can be considered a light, strong, and economic alternative for short and medium span bridges.

Due to lab space limitations, a total length of 5.5 m was chosen for the test girders. Preliminary detailing of the longitudinal and transverse reinforcing steel called for a thickness not less than 100 mm and 130 mm for the top and bottom flanges respectively. In order to provide enough space for observing the web buckling patterns, a 0.5 m clear web height was chosen which led to a girder of 0.73 m total depth. This corresponds to span-to-depth and span-to-web height ratios of approximately 7.5 and 11 respectively.



A very simple approach, along with a trial and error process, was used to calculate the ultimate flexural strength of a girder of such dimensions and shape. The flexural capacity was calculated considering that the compression force will be carried by the top flange while the tension force will be carried by the prestressing strands. The required concentric prestressing force in the bottom flange and the concrete 28-day compressive strength of the top flange were chosen to achieve a ductile behaviour of the girder. For the two-point-load setup that has been chosen for testing, the resulting section consisted of three concentric straight 13 mm 7-wire strands in the bottom flange, and concrete of 33 MPa 28-day strength for both flanges. The ultimate moment capacity for such a section was estimated to be approximately 284 kN·m corresponding to a support reaction of 142 kN. After introducing a factor of safety of 1.5 to ensure that the web will fail in shear prior to a flexure failure, the design shear force was reduced to 95 kN. This reduced shear force was used later to define the geometrical properties of the webs in the test girders. An additional check was made according to clause 18.4.1 CSA standard A23.3-94 to ensure that the 7-day strength of the concrete will sustain the prestressing transfer load which called for a 7-day strength of 32 MPa. Therefore a concrete of 55 MPa 28-day strength was used. It should be noted that the combination of this concrete strength and prestressing level for the bottom flange is adequate to prevent any cracking at its bottom fibre in the girder's mid-span up to a moment corresponding to the web shear yield capacity. However, this requires that the basis of the approach used in the flexural analysis and design are maintained up to that point.

#### 4.4 THE TEST GIRDERS - MATERIAL AND STRUCTURAL DETAILS

Figures 4.1 and 4.2 show a cut-through perspective view and a typical elevation view of the actually tested girders. The detailed typical cross section is shown in figure 4.3.

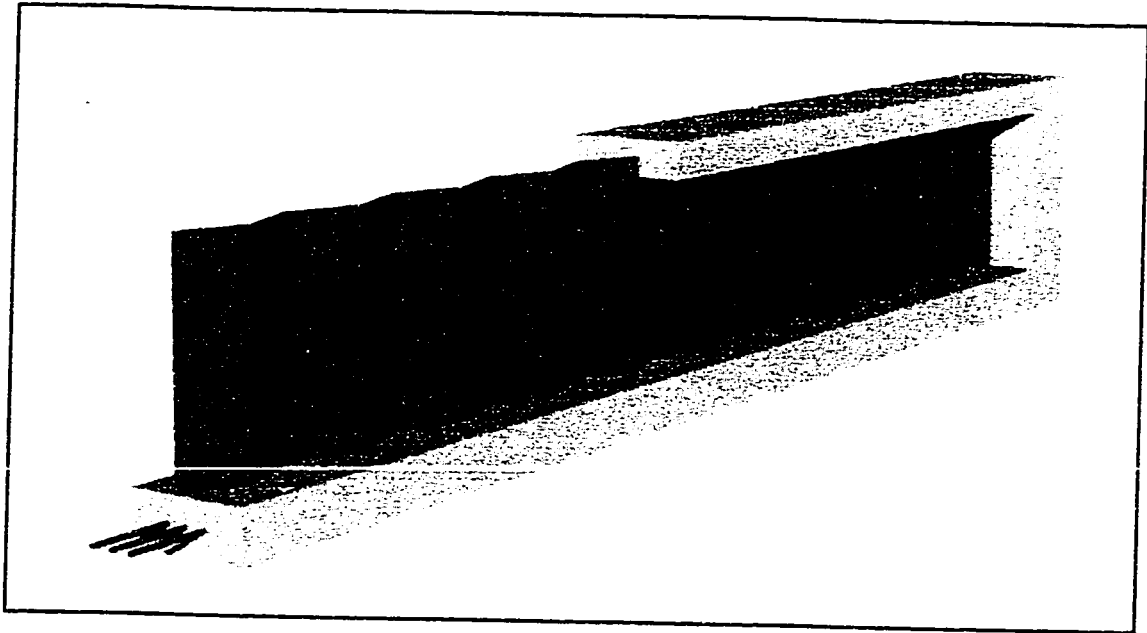


Figure 4.1 A cut-through perspective view of the test girder

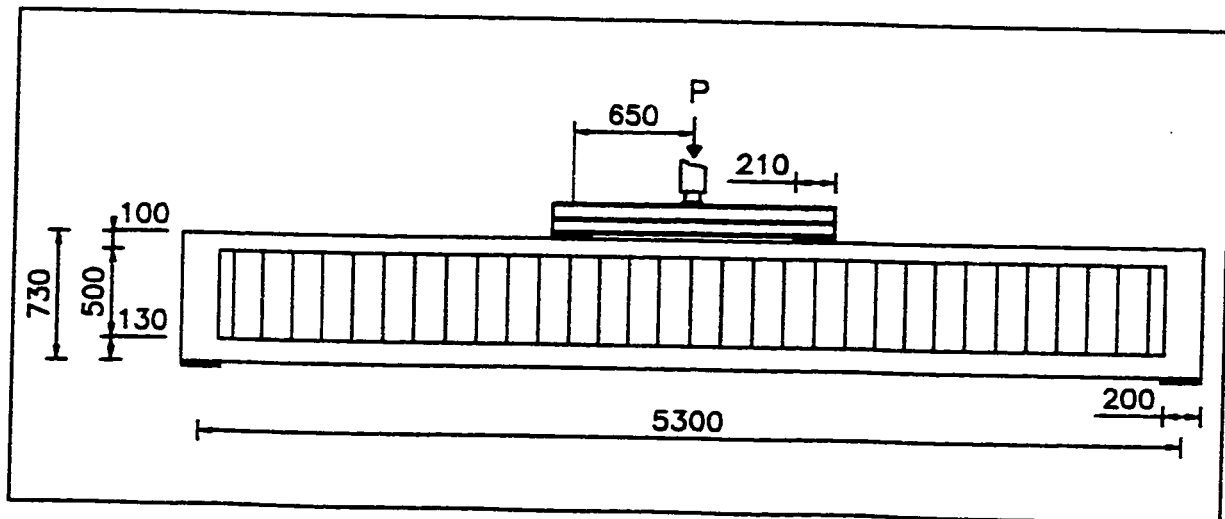


Figure 4.2 Typical elevation view of the test girder and the loading transfer beam

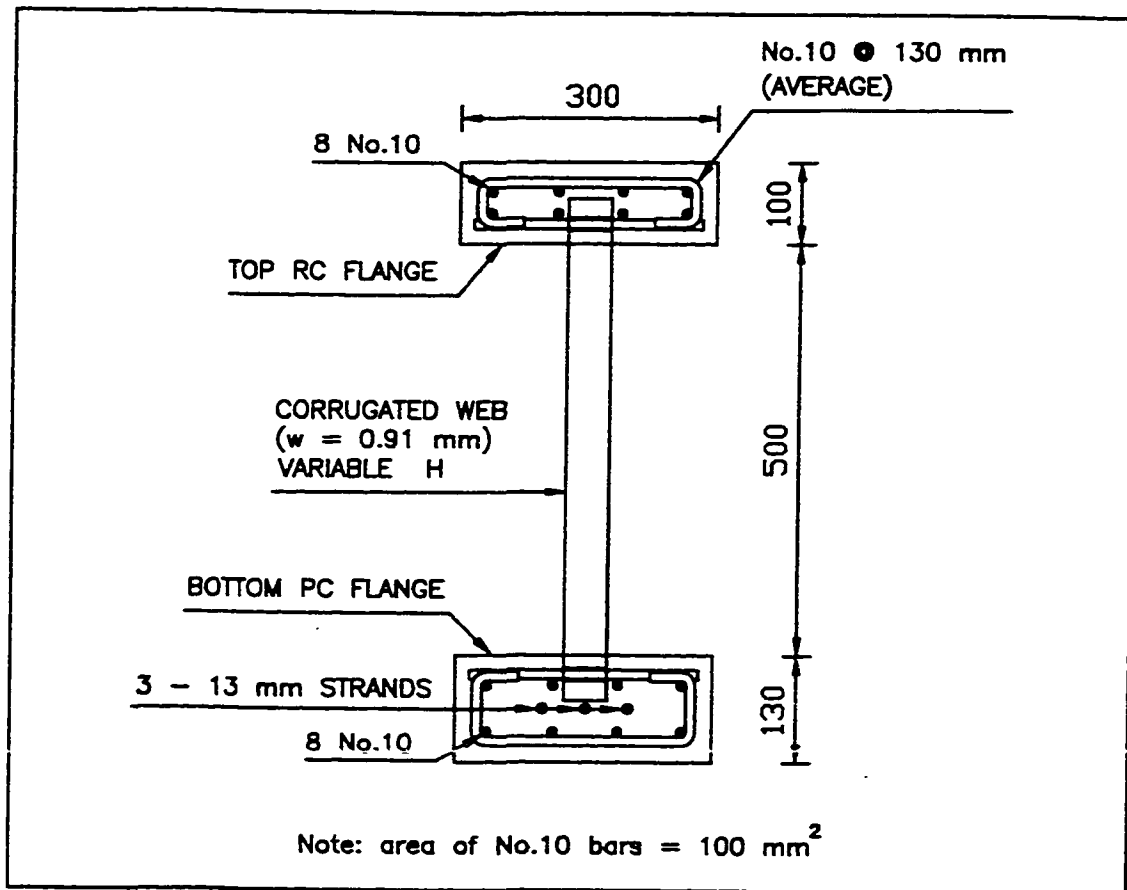


Figure 4.3 Typical cross section of the test girder

#### 4.4.1 Material Properties

##### 4.4.1.1 Concrete

The concrete mix was designed for a target strength of 60 MPa. The cylinders testing was performed according to CSA A23.2-9C and the actual average cylinder compressive strength for the top and bottom flanges of all girders at the time of testing was 55 MPa with sample standard deviation of 2.90. The prestress release time and the testing time differ from one girder to another, but their minimum time was set to 7-day and 28-day respectively of the time of casting the top flange (which was the last part to be cast). Table 4.1 shows the concrete mix proportions and the achieved strengths at prestress release and at testing with their corresponding sample standard deviations.

Table 4.1 Concrete mixture proportions

Portland cement (Type 10) [kg/m <sup>3</sup> ]	450
Water <sup>†</sup> [kg/m <sup>3</sup> ]	175
Coarse aggregate <sup>††</sup> [kg/m <sup>3</sup> ]	1071
Fine aggregate [kg/m <sup>3</sup> ]	685
Superplasticizer [L/m <sup>3</sup> ]	3.5
Average strength [MPa] (at prestressing transfer)	51.5
Sample standard deviation	2.89
Average strength [MPa] (at testing)	55
Sample standard deviation	2.9

<sup>†</sup> w/c = 0.39

<sup>††</sup> maximum aggregate size = 10 mm

In order to calculate the stresses in the concrete flanges from the strain readings during testing, the concrete stress-strain curve had to be established. The young's modulus was determined according to the ASTM C 469-94 test up to 40 % of the compressive strength. Loov's equation, equation 4.1, was then used to predict the complete stress-strain curve of the concrete.

$$f_c = f'_c \left( \frac{A x}{1 + B x + C x^n} \right) \quad (4.1)$$

In this equation,  $x = \varepsilon/\varepsilon'_c$ ,  $C = 1/(n-1)$ , and  $A = 1 + B + C$ .  $f'_c$  and  $\varepsilon'_c$  are the 28-day compressive strength, and the strain at maximum compressive stress respectively. The equation is very flexible and automatically follows the general shape of the concrete stress-strain curve of both ductile low strength concretes and brittle high strength concretes. The

constants  $B$  and  $n$  control the shape of the ascending and the descending portions of the curve respectively. Their values should be properly chosen so that the curve can match the experimentally determined points. A table for the possible values of  $B$  and  $n$  with different concrete strengths is given by Loov [38]. The experimental and fitted curves for the concrete of the flanges are shown in figure 4.4 in which the experimental curve was drawn up to only 70 % of the concrete strength to avoid damaging the strain transducers.

#### 4.4.1.2 Prestressing Strands

The stress-strain curve for the strands was determined according to ASTM A 370-90. The yield strength (taken as the stress corresponding to 1 % extension under load) and Young's modulus were directly obtained from the results. Loov's equation, equation 4.2, was used to draw the complete stress-strain curve, and to determine the stress corresponding to any strain during the testing of the girders, [39]

$$f_p = f_{pu} \frac{\varepsilon}{\varepsilon_m} + \left[ \left( E_p \varepsilon - f_{pu} \frac{\varepsilon}{\varepsilon_m} \right)^{-n} + \left( f_{py} \left( 1 - \frac{\varepsilon}{\varepsilon_m} \right) \right)^{-n} \right]^{-\frac{1}{n}} \quad (4.2)$$

$E_p$  and  $f_{py}$  are the Young's modulus and yield strength of the strands respectively.  $f_{pu}$  is determined by extending the strain-hardening part of the curve up to  $\varepsilon_m = 0.035$ . The exponent  $n$  can then be chosen to properly simulate the actual transition from the elastic portion of the curve to the strain-hardening portion. Both the experimental and the fitted curves are shown in figure 4.5.

It should be noted that the value of  $E_p = 194\,000$  MPa shown in figure 4.5 corresponds to the actual stress-strain relationship of the strands. However, because of the twisted nature of the strands, the strain gauges had to be attached to the strands at an angle to its longitudinal direction. Therefore, a strain gauge was attached to each sample of the strands when performing the tension test to simulate the actual testing case. The calculated modulus of elasticity according to the strain gauge readings was 205000 MPa. This value of

$E_p = 205000 \text{ MPa}$  was used in calculating the stresses from the strain readings during the testing of the girders.

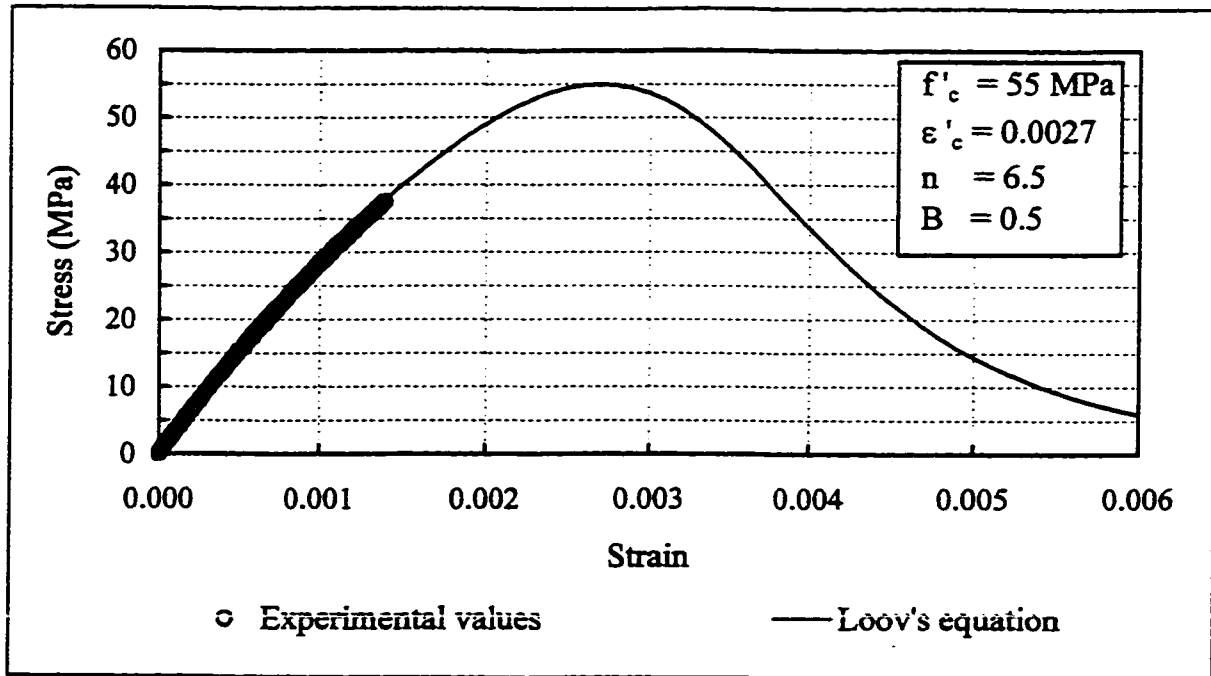


Figure 4.4 Concrete stress-strain curve

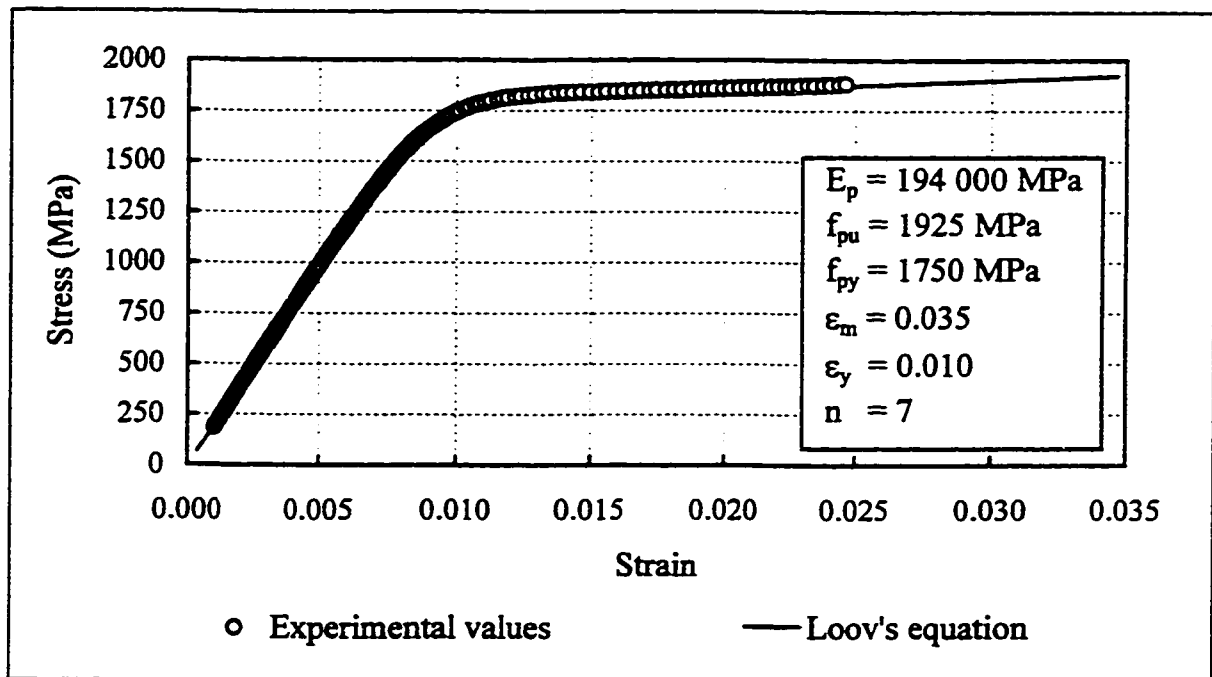


Figure 4.5 Stress-strain curve for prestressing strands

#### 4.4.1.3 Corrugated Webs

The stress-strain curve for the web material, shown in figure 4.6, was determined according to ASTM A 370-90. The curve shows that the galvanized steel exhibits a distinct yield plateau with a value of  $F_y = 350$  MPa and a ductile behaviour after yield up to failure.

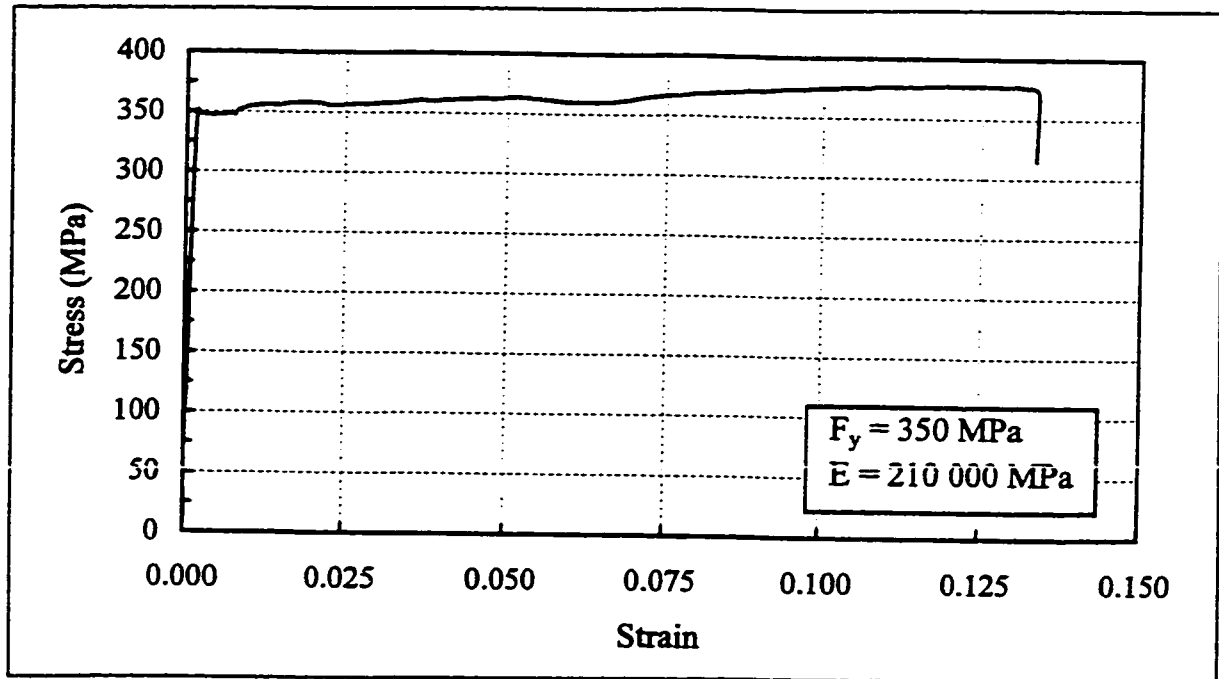


Figure 4.6 Stress-strain curve for the corrugated steel web material

### 4.4.2 Dimensions and Structural Details

#### 4.4.2.1 Corrugated Webs

From the preliminary dimensioning process, the web height and the maximum design shear force were set to 500 mm and 95 kN respectively. Using the actual material properties of the web and using an exponent of  $n = 2$  for the interaction equation (equation 3.9), the optimization procedure was applied to determine the optimum corrugation angle and web thickness. Appendix C is the Mathcad worksheet that was developed for such a purpose. The optimum corrugation parameters were  $w = 1.1$  mm and  $\beta = 23^\circ$ . The choice was then between gauge 18 (1.21 mm) and gauge 20 (0.91mm). The later thickness was chosen for the

web along with a corrugation angle of  $20^\circ$ . It should be noted that coupons from the actual webs were used in performing the tension test and plotting the stress-strain curve for the web material, figure 4.6. Testing such thin specimens from such thin webs along with the fact that it was cold formed can explain why there was almost no strain hardening after the yielding point in the stress-strain curve. Figure 4.7 shows the shear strength plotting of the web as a function of the sub-panel width. It also shows the five sub-panel widths that were chosen for the five test girders presented as five big dots over the x-axis. The five widths are 285 mm, 215 mm, 175 mm, 110 mm, and 80 mm. The girders were named after their sub-panel widths. Therefore, the five girders were designated A-285, A-215, A175, A-110, and A-80. It can be noticed from figure 4.7 that all sub-panel widths belong to region 3 with the smallest width, 80 mm, very close to region 2. The reason for that is because the highest interaction strength for both  $n=1$  and  $n=2$  correspond to a sub-panel width of 50 mm which was not considered a practical width according to the web fabricator. Appendix D is the Mathcad worksheet that was used to plot figure 4.7. The typical cross section of the zigzag corrugated web of the test girders is shown in figure 4.8.

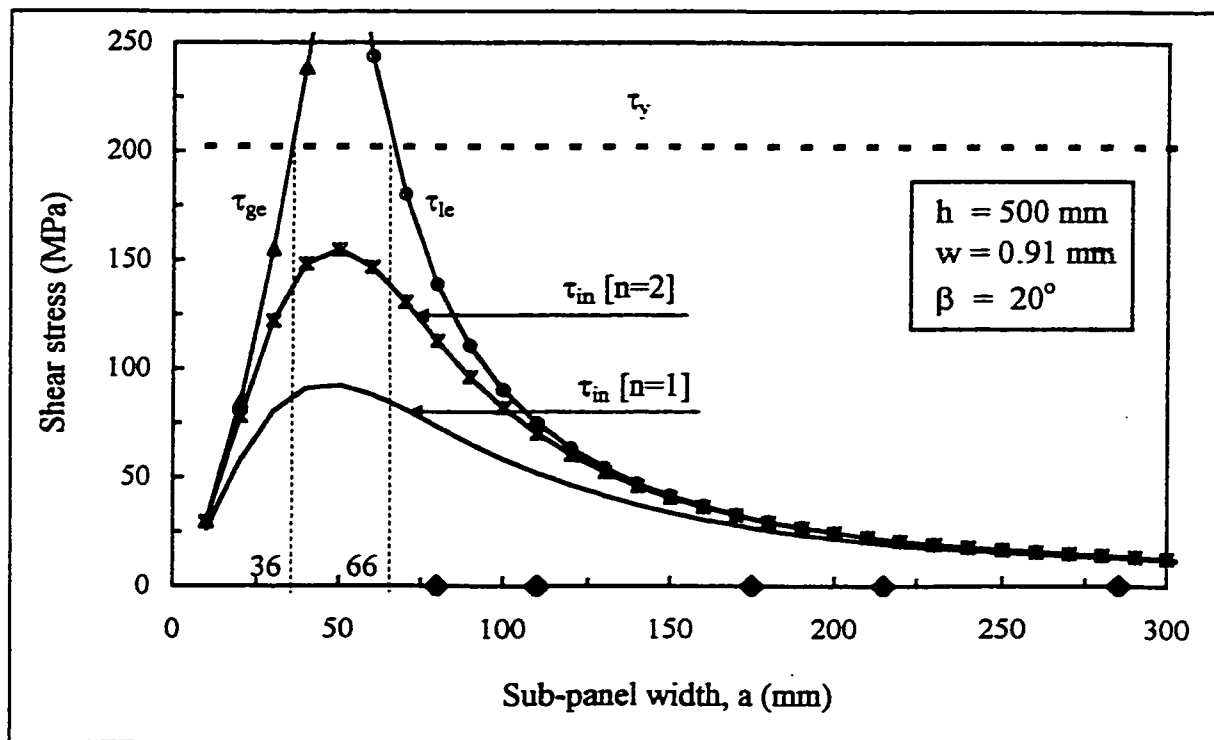


Figure 4.7 Expected shear resistance of the zigzag corrugated web of the test girders



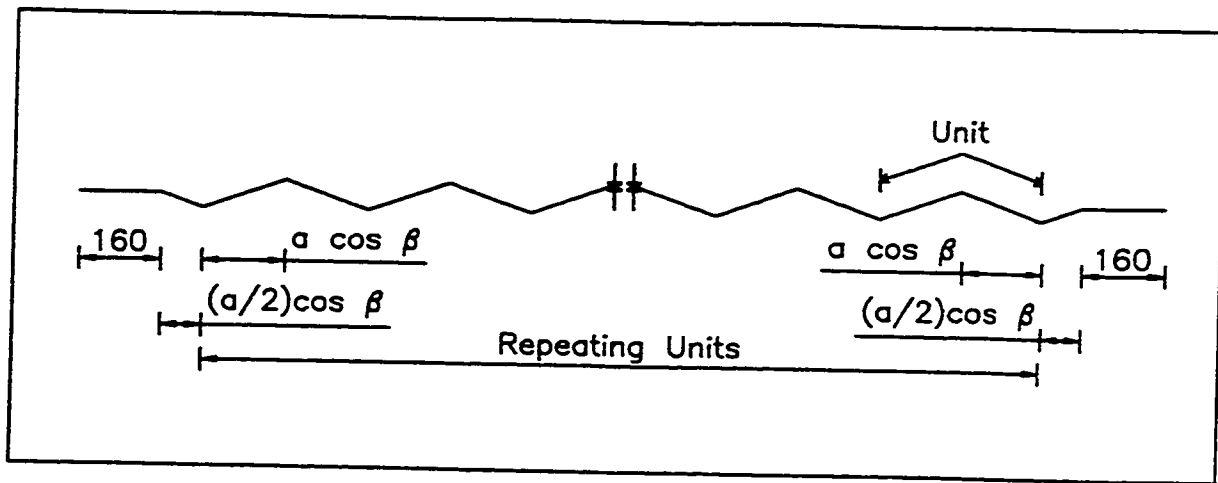


Figure 4.8 Typical cross section of the zigzag corrugated web

#### 4.4.2.2 Shear Connectors

To ensure full composite action in girders with corrugated webs, which are characterized by their flexibility in the longitudinal direction, a relatively flexible mechanical connection will likely be adequate. The new Japanese method which utilizes transverse steel passing through holes in the web was used in the test girders. The design equations for this method are still under development in Japan. Based on the size and the distribution of transverse flange reinforcement that was reported by Yoda *et al.* [54,57], a conservative estimation of the required shear connectors was made. The many uncertainties that exist such as the actual shear and flexural behaviour of the girders, as well as the resistance to horizontal shear that is provided by this new shear connection method justified that conservative estimation. Transverse # 10 bars of grade 400 were used with an average spacing of 130 mm for the whole length of the girders. The bars ran through 14 mm holes drilled in the web. The actual spacing varied from one girder to another depending on the corresponding sub-panel width. Figures 4.9 through 4.13 show the actual hole spacing for each girder while figure 4.14 shows a close-up view of the shear connector details in the bottom flange of girder A-285. The 23 mm distance that is provided from the hole edge to the edge of the web plate in the top and bottom flanges was intended to prevent a hypothetical case of end tearing of the web. For girder A-285, the hole arrangement for the part of the web that is inside the end block that is shown in

figure 4.9 was found very complicated and was abandoned in the other four girders.

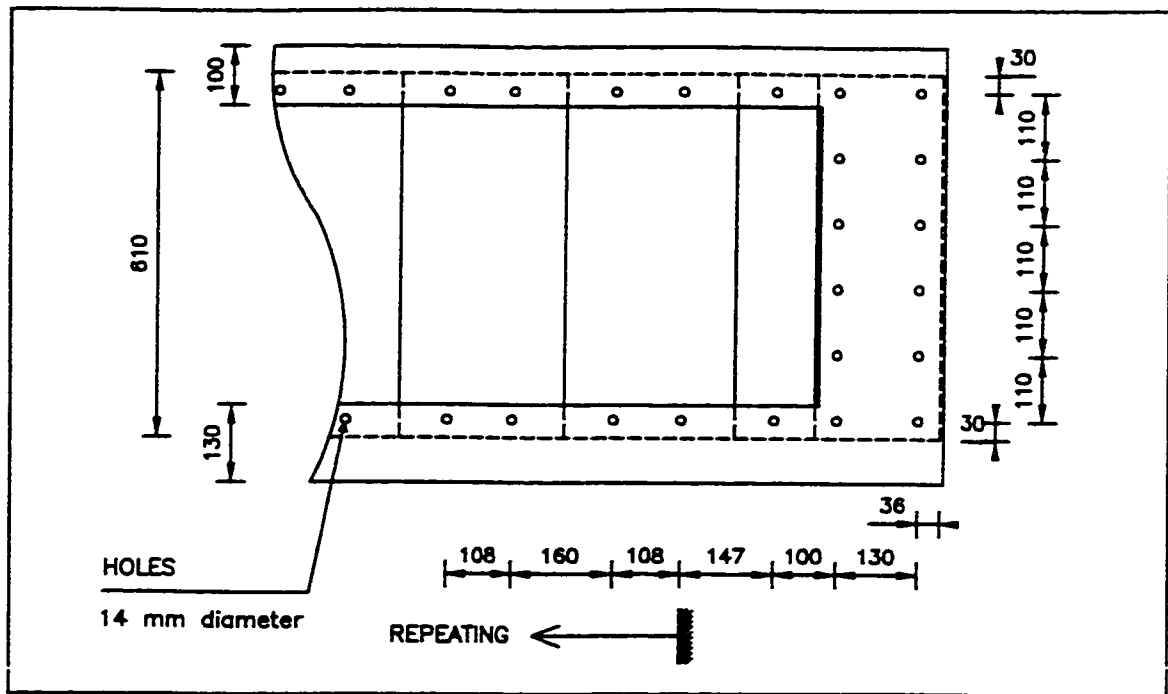


Figure 4.9 Shear connector details, girder A-285

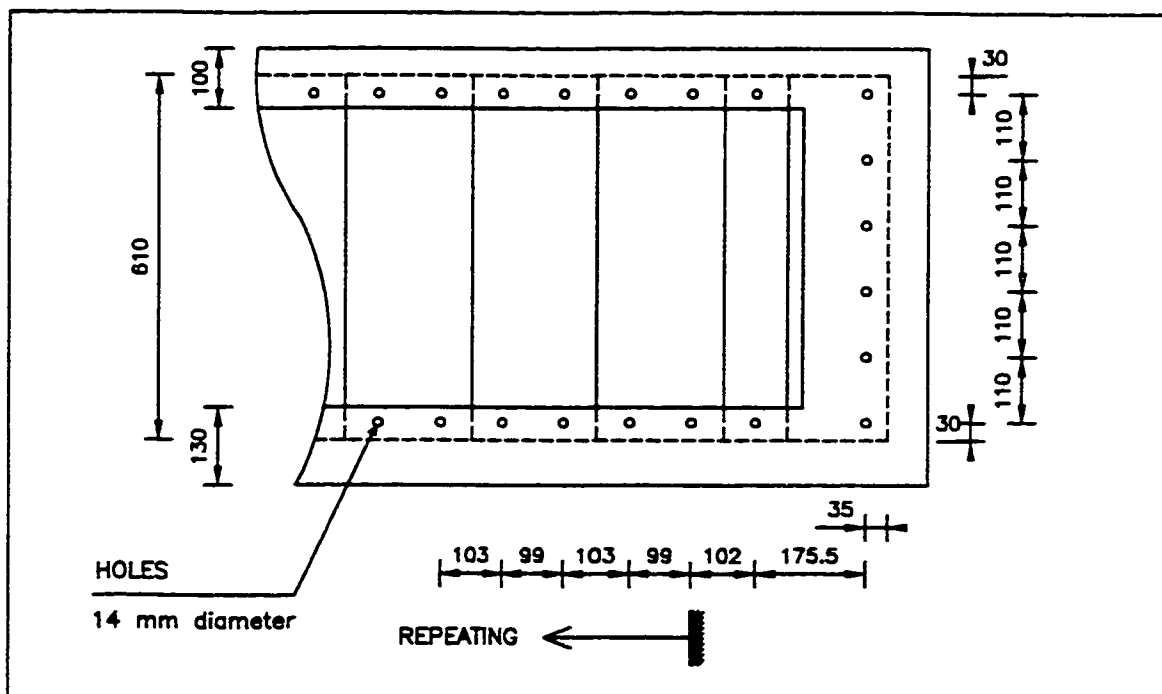


Figure 4.10 Shear connector details, girder A-215

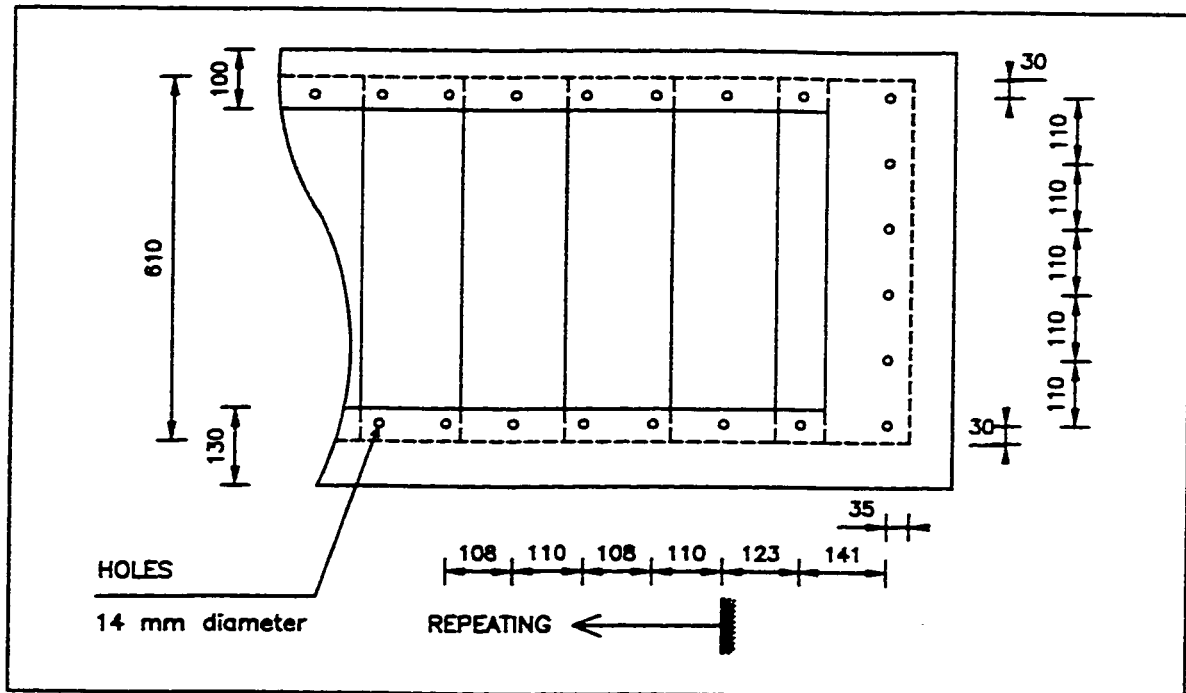


Figure 4.11 Shear connector details, girder A-175

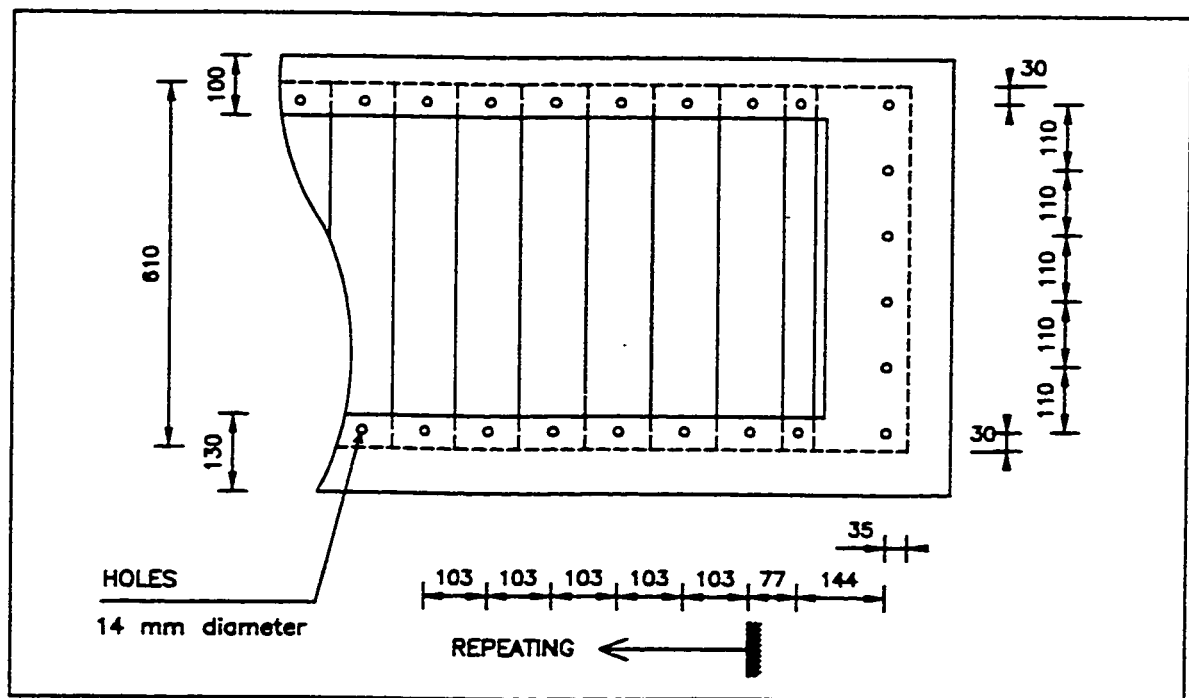


Figure 4.12 Shear connector details, girder A-110



#### 4.4.2.3 Longitudinal reinforcement Details

As was mentioned before, the section of the test girder was designed assuming that the maximum moment at the mid-span will be carried entirely by the top concrete flange in compression and the prestressing strands in tension. In addition, longitudinal conventional reinforcement was used to provide a framing action between the top and bottom flanges and the concrete end blocks. Because the transfer of the prestressing force took place after a minimum of 7 days of casting the top flange, the conventional steel area for the corner sections was calculated to resist the secondary moments due to the concentric prestressing force in the bottom flange. Minimum steel was maintained at other sections in the top and bottom flanges along the full length of the girder. Figure 4.15 shows typical elevation view of the test girder with the longitudinal reinforcement details.

#### 4.4.3 Construction of Girders

The construction of the test girders will briefly be presented here in a step-by-step basis.

##### 4.4.3.1 Formwork and Web Preparation and Alignment

A plywood form was built and used for all girders. A disposable Styrofoam sheet, that was previously cut to the exact shape of the corrugated web profile of the girder being cast, was used to make the bottom form for the top flange. The holes in the corrugated webs were marked and cut using an electrical drill. The conventional steel cage of the bottom flange was then put in place and the corrugated web was aligned and connected to the cage as was shown in figure 4.14.

##### 4.4.3.2 Prestressing

The prestressing of the strands in the bottom flange was the last step before casting it. The structural lab at the University of Calgary has a prestressing bed that consists of two steel frames of 1.2 MN maximum nominal capacity. The stressing load was applied using an ENERPAC single-acting-hollow ram, measured using a 260 kN maximum capacity load cell calibrated to a range of loading 0 ~ 150 kN with accuracy  $\pm 0.5\%$ , and displayed using a

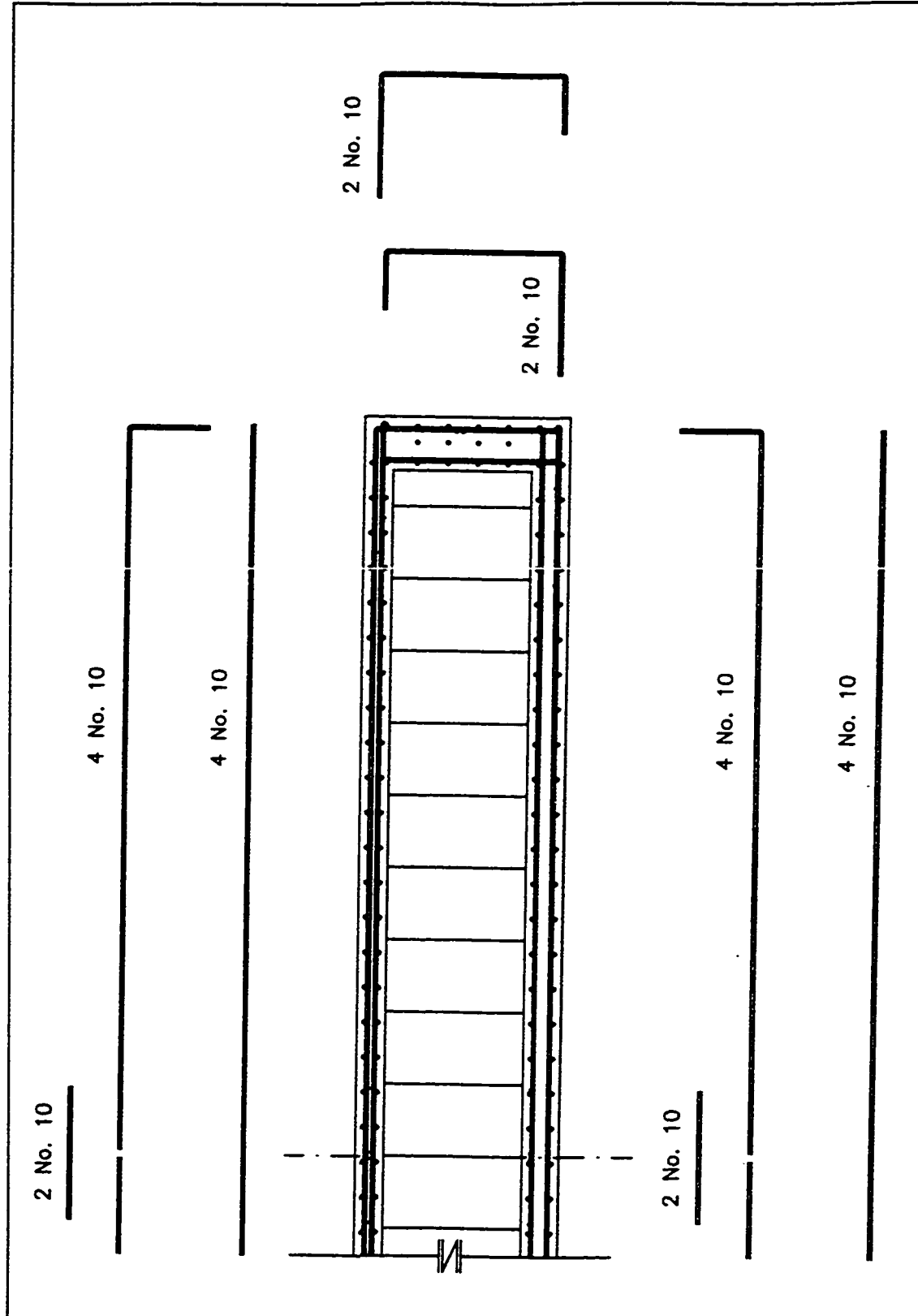


Figure 4.15 Typical arrangement of conventional longitudinal steel for the test girder, elevation view

digital pressure gauge. Each strand was stressed to approximately 1300 MPa before the seating of anchorages which is equivalent to approximately 130 kN. Figure 4.16 shows a test girder in the prestressing bed just after prestressing (prior to casting of the bottom flange).

#### 4.4.3.3 Casting and Curing

After stressing the strands, the bottom flange was cast and then covered by plastic sheets to prevent excessive drying shrinkage. After a minimum of 24 hours, the already prepared conventional reinforcement cage of the top flange was put in place and was connected to the web by inserting bars through the holes. The stirrups of the end blocks were added as well to connect the web and the conventional steel in these parts. The top flange and the end blocks were cast simultaneously and were covered by plastic sheets. Figure 4.17 shows the reinforcement details of the top flange of girder A-285. Moist curing was applied for the first three days, using wet burlap covered with plastic sheets, followed by air curing until the time of testing. The same curing procedure was applied to the concrete cylinders taken from both pours.



Figure 4.16 Girder A-285 in prestressing bed before casting of bottom flange

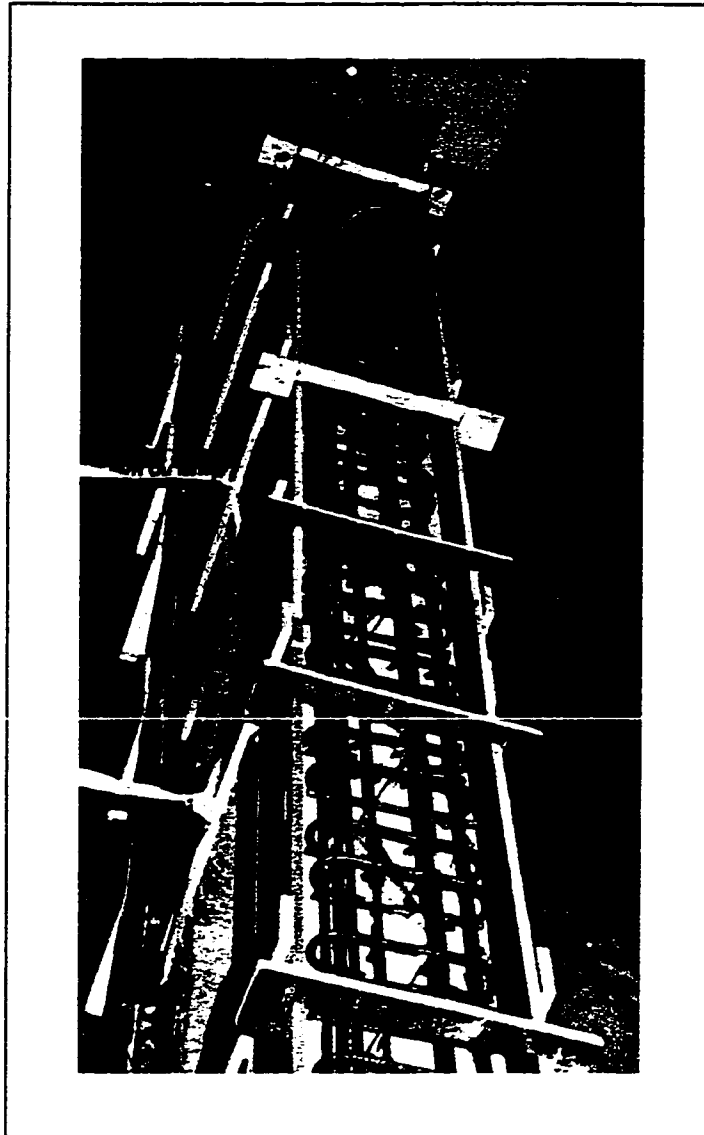


Figure 4.17 Girder A-285 ready for casting the top flange and the end blocks

#### **4.5 INSTRUMENTATION AND DATA ACQUISITION**

The testing of the five girders was performed on two stages. Girders A-285 and A-215 were the first to be constructed and tested. Both girders had the same instrumentation. After analyzing the test results of both girders, the instrumentation arrangement was modified and then applied to the remaining three girders A-175, A-110, and A-80. The testing of girders



A-285 and A-215 will be referred to as *phase I* during the rest of the thesis, while the testing of girders A-175, A-110, and A-80 will be referred to as *phase II*. The concrete strain gauges that were attached to the flanges were TML stain gauges of type PFL-3011 and were manufactured by Tokyosokki Kenkyujo Co., Ltd., Japan. The three way 45 ° strain rosettes that were used to measure the membrane strains in the web and the strain gauges attached to the prestressing strands were of types EA-06-125RA-120 and EA-06-062AK-120 respectively. They were manufactured by Micro-Measurements, Measurements Group, Inc., USA. Horizontal and vertical deflections were measured at different locations using linear stain conversion (LSC) displacement transducers. They were manufactured by Apek Design & Developments Ltd., United Kingdom. During prestressing and up to the time of testing, the strain gauges attached to the prestressing strands were hooked up to a VISHAY P-350A portable strain indicator connected to a switch and balance unit. This enabled us to measure the short term and long term prestressing losses. At the time of testing, the different gauges (for concrete flanges, web, or prestressing strands) and LSCs were connected to a DATASCAN data acquisition equipment which was hooked up to an Intel based Pentium 200 personal computer. The readings of all gauges and LSCs were recorded using the Labtech Notebook 10.0 software. The output data was collected continuously throughout the test with a 10-second sampling rate. The details of the instrumentation arrangements of both testing phases are presented below.

#### **4.5.1 Phase I : Girders A-285 and A-215**

Figure 4.18 shows the typical instrumentation in a half span of girders A-285 and A-215. The instrumentation details are symmetrical about the beam centerline. Five sets of strain gauges, or rosettes, were used to measure strains in different locations in each girder as follows:

1. *Set R* consists of three-way 45 ° strain rosettes mounted on only one side of the web in the centre point of the sub-panels. This set of rosettes was intended to measure the membrane strains in the web along the beam length.

2. *Set E* consists of one-way strain gauges, of the same type as the rosettes, mounted on only one side of the web 25 mm from both the left and right edges. This set of gauges was intended to measure the vertical membrane strain in the web at its connection to the concrete end bearing blocks.
3. *Set L* is another group of the one-way strain gauges mounted on only one side of the web 25 mm below the loading plates. Gauges of set L were intended to measure the vertical compressive strains in the web caused by the direct load application.
4. *Set S* (not shown in figure 4.18) consists of three one-way strain gauges where each gauge was mounted on one prestressing strand at the girder's mid-span. As the observed strain readings of the three strands of each girder were usually very close, the average of the calculated stresses was used to represent the stress state in the strands during testing.
5. *Set C* consists of eight concrete strain gauges that were intended to measure the axial strains in both the top and bottom concrete flanges due to bending. Each pair of gauges was glued to the smooth sides of both flanges 15 mm from their top and bottom edges at the girder's mid-span. This means that strain gauge C1 in figure 4.18 actually represents an average of the readings of two strain gauges mounted on both sides of the top flange at the same level (15 mm from the top edge).

The mid-span deflection of each girder during testing was measured using two LSCs, *D1*, that were placed under the bottom concrete flange. The average of the readings of both LSCs was used to represent the mid-span deflection under applied load. In the testing of girder A-215, two additional LSCs, *D2*, were placed between the interior faces of the of the flanges to measure their relative movement at the girder's mid-span. This relative movement was also represented by the average of the readings of both LSCs. Four load cells, two at each end block, were used to measure the vertical reaction under applied load. The sum of the readings of both load cells at each end represents the reaction at this end.

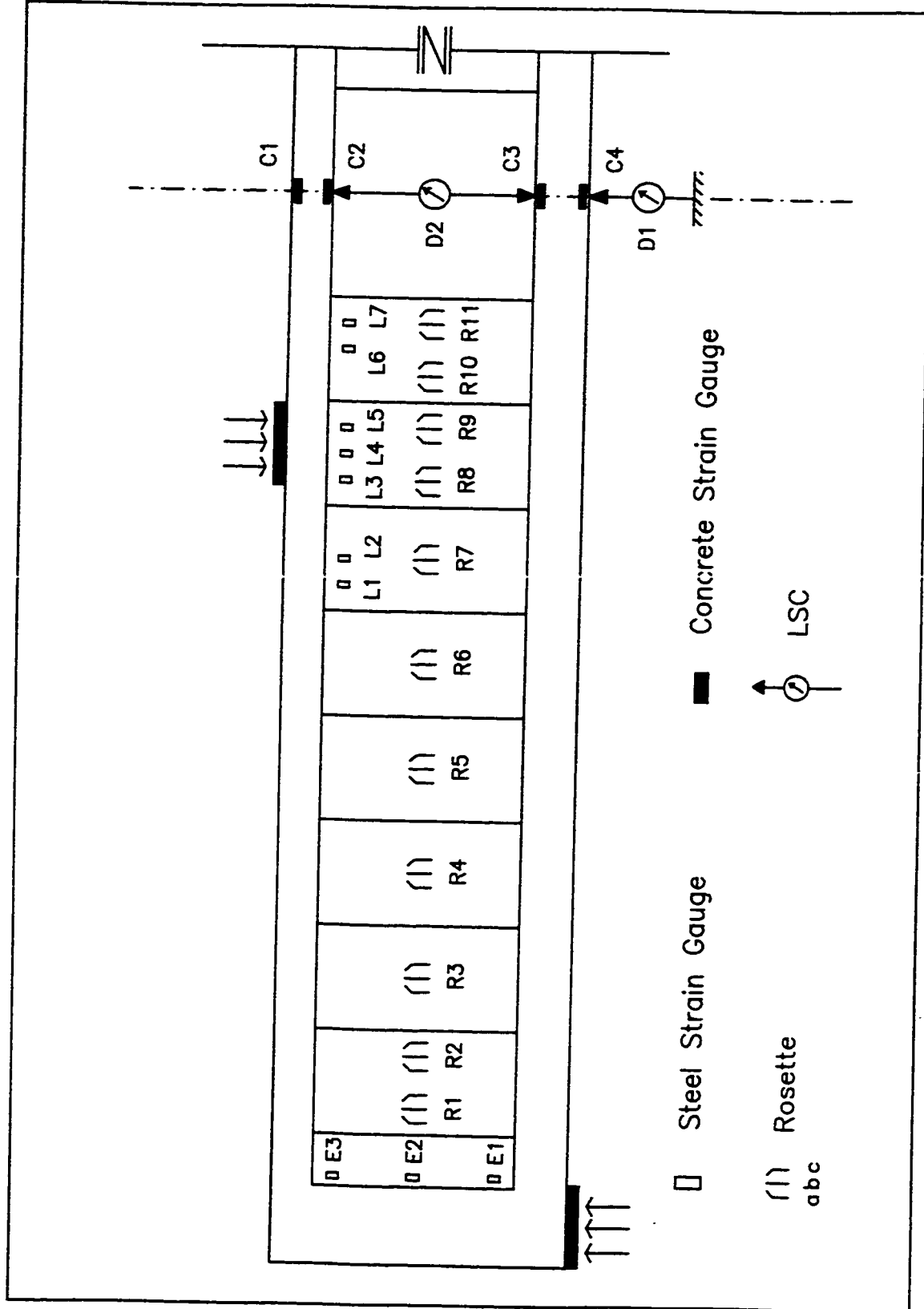


Figure 4.18 Instrumentation details, girders A-285 and A-215

Because all the gauges and rosettes of the three sets R, E, and L were mounted on only one side of the web, their readings were affected by the bending stresses caused by the web buckling which took place at a very early stage in the loading of both girders. Unfortunately this bending effect could not be corrected. Therefore, the pure membrane strains could not be obtained and the pure membrane stresses could not be calculated. The large number of strain gauges and rosettes applied to the webs of both girders was considered lost. Consequently, the plotted results will include only the stresses calculated from the readings of strain gauges of sets C and S, the load cells reactions, and the deflection readings of LSCs D1 and D2. A brief discussion of the test results of both girders A-285 and A-215 was presented by Loov and El-Metwally [16,40].

#### **4.5.2 Phase II : Girders A-175, A-110, and A-80**

Figure 4.19 shows the typical instrumentation setup that was used for the three girders. The applied modifications can be summarized as follows:

1. For *set R*, the strain rosettes were applied to only one shear-span but on both sides of the web. Each pair of rosettes was mounted at the web's mid-height 10 mm from the fold line. In the testing of girders A-285 and A-215 of phase I, a relatively consistent shear buckling pattern was observed in both shear-spans of each web. This justified having rosettes on only one shear-span for the girders of phase II. The contribution of the bending stresses due web buckling was eliminated by taking the average of the readings of the two rosettes of each pair to represent the strain readings at their mounting point. The pure membrane strains were then obtained, and the pure membrane stresses were calculated.
2. For *set L*, the strain gauges were replaced by eight strain rosettes mounted on both sides of the web at four locations as shown in figure 4.19. The pair L1 was mounted 25 mm from the bottom face of the top flange beneath the right loading point, while the pair L2 was mounted 25 mm from the top face of the bottom flange in a vertical line from the pair L1. The pairs L3 and L4 are similar but for the left loading point. By having 3-way

rosettes instead of 1-way gauges, both the horizontal and vertical pure membrane stresses beneath the loading points were calculated. Again, any bending contribution due to web buckling was eliminated by taking the average of the strain readings of the two rosettes of each pair.

4. The strain gauges of *set E* were eliminated.
5. The LSCs measuring the relative movement of the flanges were increased to ten LSCs placed on both sides of the web at five locations: under the two loading points, in the middle of both shear-spans, and in the mid-span. The average of the readings of each pair was calculated and used to represent the relative movement at their mounting point. These averages were referred to as D2, D3, D4, D5, and D6 as shown in figure 4.19.
6. From the two tests of phase I it was found that the visual observation of the load corresponding to the shear buckling of the web is extremely difficult. Therefore, four LSCs, *set H*, were placed horizontally perpendicular to the web at four different locations as shown in figure 4.19. The LSCs were placed so that they can measure the buckling displacement in either sides, i.e, a concave or a convex buckling. The value of the buckling displacement and its direction are not of interest. Rather, it is the load corresponding to the initiation of buckling.

The testing of girder A-80 was associated with a longitudinal slip of the whole girder 20 mm to the left side during testing. This resulted in severe buckling deformations in only the right shear-span while the left shear-span remained without noticeable buckles (see Appendix F). This difference was only in the buckling pattern and was not observed in the strain readings which indicates that it was merely a geometrical nonlinearity phenomenon and that no significant difference existed in the shear force taken by the web in each shear-span. To make use of the remaining unbuckled shear span, an additional test, denoted A-80-b, was conducted. The elevation view of the new loading arrangement and instrumentation of test A-80-b is shown in figure 4.20. The only data acquisition in this test were the mid-span deflection and the applied load. Unlike the previous five tests where the overlapped web splice was located at the region of zero shear, the splice in the new test was located almost in the middle of the

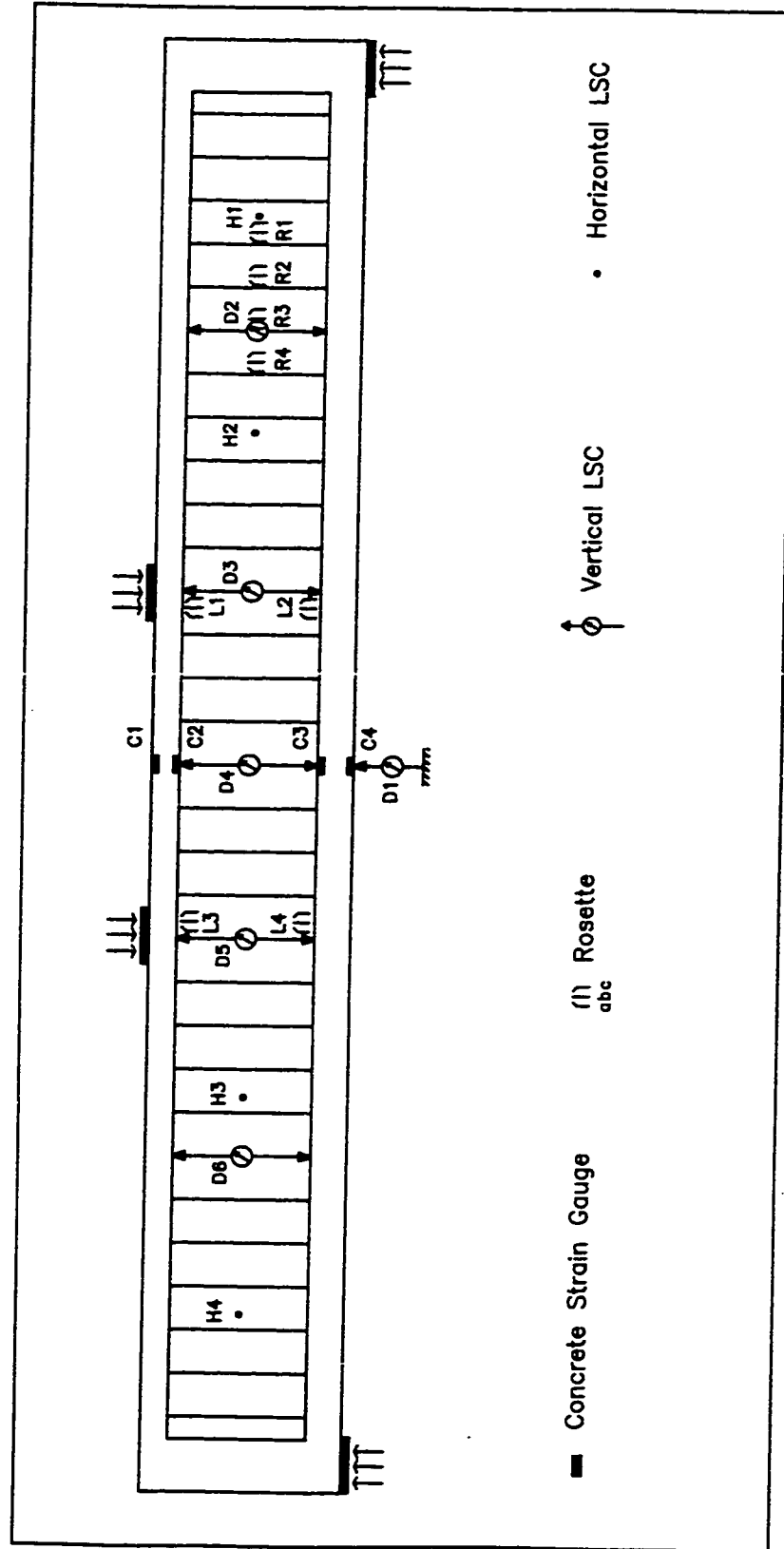


Figure 4.19 Instrumentation details, girders A-175, A-110, and A-80

shear-span. The test should therefore help to verify whether or not it is necessary to weld the web panels in actual bridge girders where the web splice should be carrying shear forces.

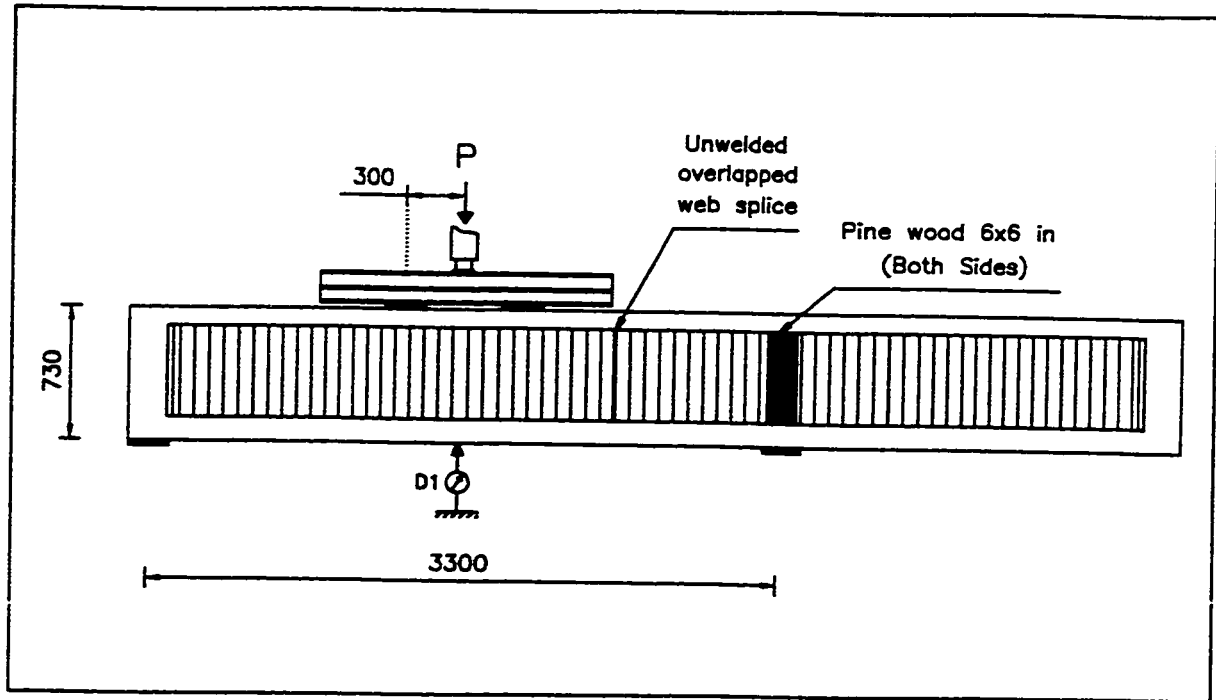


Figure 4.20 Loading setup and instrumentation, girder A-80-b

#### 4.6 TEST SETUP AND LOADING PROCEDURE

Figure 4.21 shows the side view of the loading apparatus and the test setup for phase II. In this setup, both the right and left supports of the girder were arranged to provide free rotation and free horizontal movement. Such arrangement was intended to provide better consistency in the buckling pattern in both shear-spans. The horizontal movement was provided by the roller tray B, while the rotation was allowed by using the 50 mm diameter cylinder welded to the 12.5 mm thick lower plate A. The girder and the transfer beam were restrained to move horizontally as a rigid body by the loading ram at the point of loading. The same setup was used in phase I but with a hinge at the left support (made using a 50 mm cylinder welded to a 12.5 mm plate) and a roller at the right support (made using the roller tray). Both the upper and lower plates in figure 4.21 were of 120 mm width. Four load cells

were also used in phase I to measure the reaction at the two supports (two at each support).

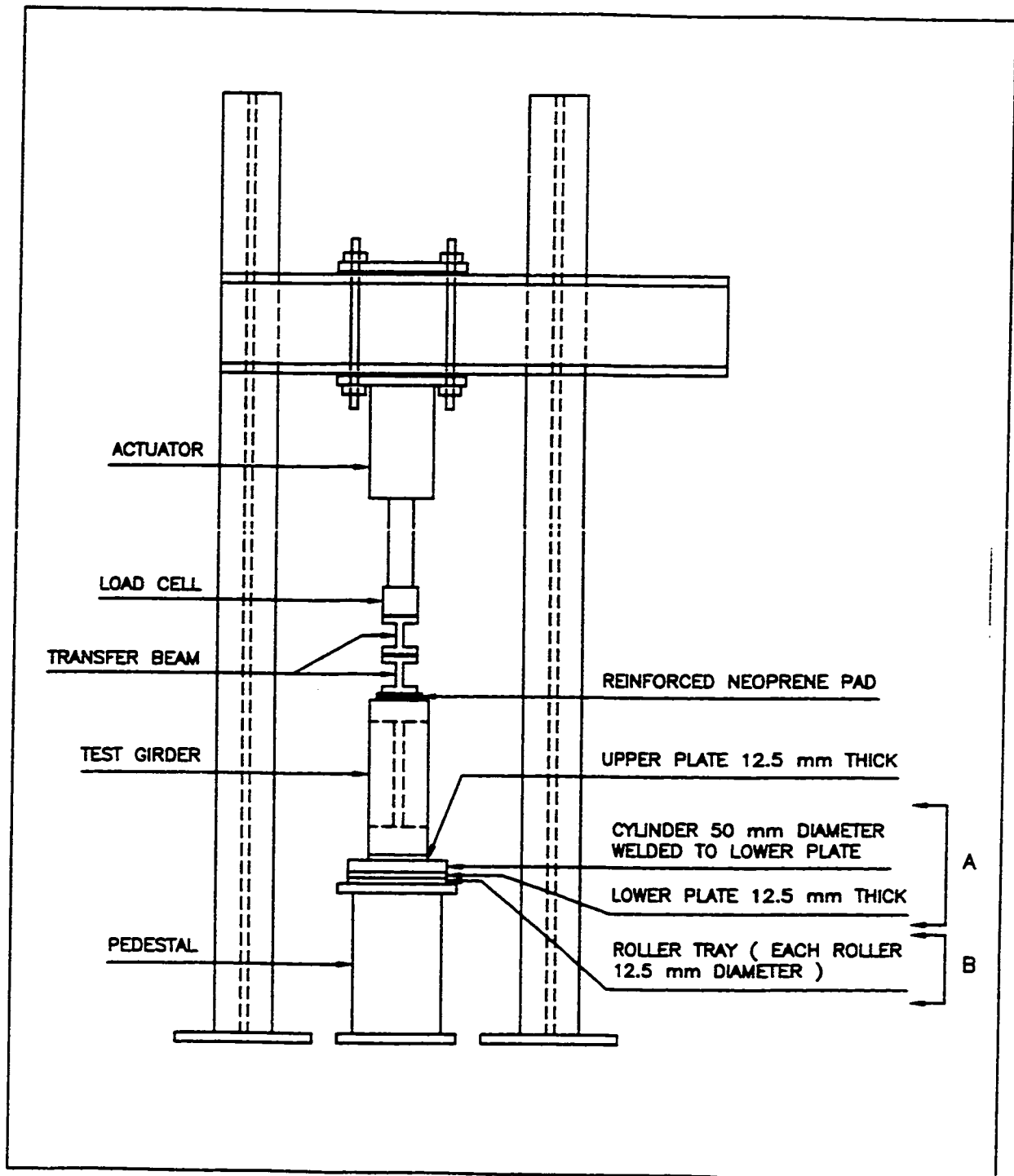


Figure 4.21 Schematic side view of the loading apparatus and test setup



The load was applied through the MTS closed-loop system that is available at the structural lab of the University of Calgary. It was applied in a stroke-control procedure with an initial stroke rate of 1 mm per minute up to the first drop in load, i.e., the first load peak. After the first peak, the stroke rate was doubled to 2 mm per minute, and after a 40 mm deflection it was doubled again to 4 mm per minute. The hydraulic actuator was of 500 kN capacity. The applied load was measured using a load cell of 250 kN maximum capacity calibrated to an accuracy of  $\pm 0.5\%$  throughout its range. The reaction load cells used in phase I were of 260 kN maximum capacity each. They were calibrated to an accuracy of  $\pm 0.5\%$  through a loading range of 0 ~ 150 kN. The output of the loading, stroke, and reaction readings were recorded using the same data acquisition system described above. Figures 4.22 and 4.23 show elevation and side views of girder A-175 under the test frame ready for testing.

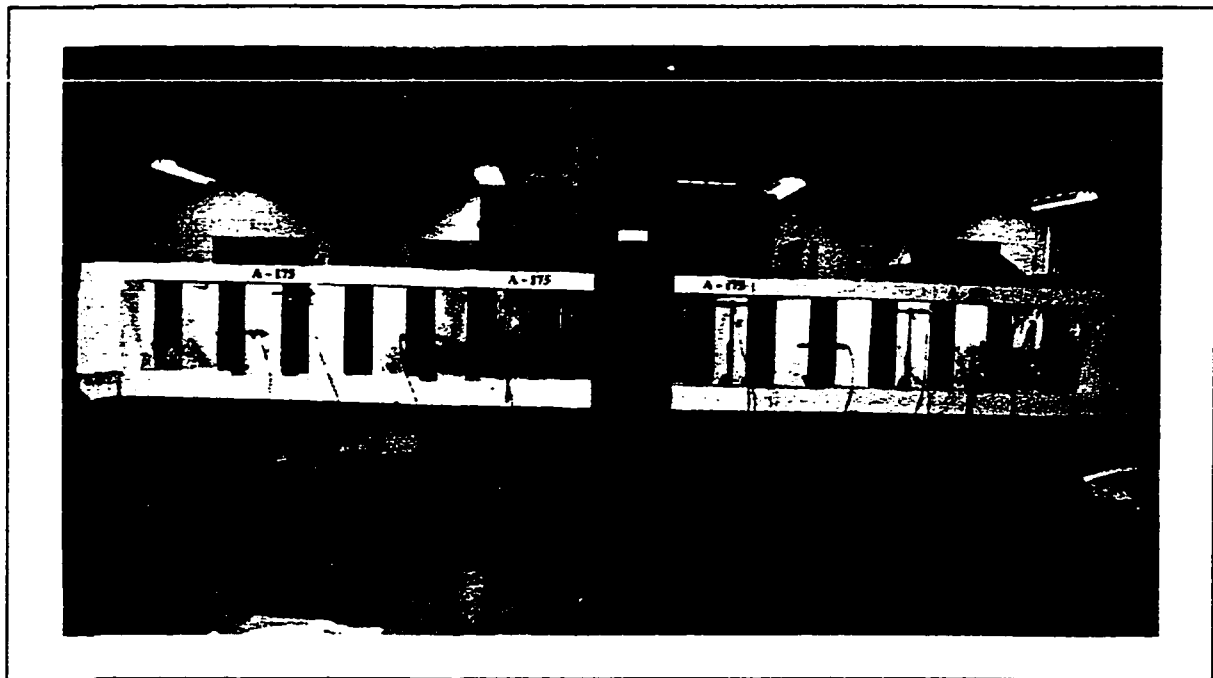


Figure 4.22 Completed girder A-175 ready for testing, elevation view



Figure 4.23 Completed girder A-175 ready for testing, side view

## ***CHAPTER 5***

### **DISCUSSION OF EXPERIMENTAL RESULTS**

#### **5.1 GENERAL**

This chapter is divided into four parts. The first part describes the load-deflection behaviour of the five test girders. The second part describes the observed sequence of the web buckling for each girder during testing and the patterns at the end of testing. The third part discusses both the buckling and the post-buckling shear strengths of the five corrugated webs. The third part also includes a comparison between the theoretically calculated strength that was presented in chapter 4 and the experimentally determined one. The fourth and last part discusses the flexural behaviour and strength of the five test girders based on the information obtained experimentally.

#### **5.2 LOAD - DEFLECTION BEHAVIOUR**

The load vs mid-span deflection curves for the five test girders are shown in figures 5.1 through 5.5. The limit for terminating the testing for the five girders was the achievement of a relatively high mid-span deflection. None of the first four girders A-285, A-215, A-175, and A-110 showed a continuing reduction in the applied load or a severe cracking or concrete crushing up to the time the testing was stopped. For girder A-80, a longitudinal slip of the whole girder 20 mm to the left side caused the web buckling to concentrate in the right shear-

span of the girder, and caused the top flange in that right side to bend vertically creating high bending moments on its connection to the right concrete end block. A short time before the test was stopped, the concrete crushed in the inner face of this connection and the load dropped again creating a third peak shown in figure 5.5. For all of the five test girders, the load-deflection curve can be divided into three main parts. The first part is limited by the first load peak, and is characterized by being close to a linear load-deflection relationship. The second part lies between the first and second load peaks. In this part, the applied load drops suddenly after the first peak then gradually rises until it reaches the second load peak. The third part of the curve is that following the second load peak, and is characterized by a gradual increase in the applied load up to the termination of the testing except for girder A-80 as was mentioned above.

The most important of the three parts of those load-deflection curves is the first one up to the first load peak. Although explanations of each of the three parts will be suggested, it is thought that for design purposes, the ultimate nominal strength of such girder should be taken as the first load peak. The excessive web buckling and mid-span deflection that take place after this first load peak can justify this choice. If a reasonable strength prediction of this type of girder was found based on the experimental results and with good correlation with that first load peak, a strength reduction factor can be used to define the design ultimate strength.

In the testing of the girders of the first phase A-285 and A-215, the maximum achieved mid-span deflections were 27.1 and 45.9 mm respectively. The unloading of both girders was characterized by a very rapid recovery of most the deflection which indicated the great amount of energy that can be stored by such a system. For the girders of the second phase A-175, A-110, and A-80, the unloading load-deflection curve was recorded and plotted. For those three girders which were tested up to very high mid-span deflection values (77.5 mm for girder A-110), the recovered deflection was 55 %, 51 %, and 32 % respectively. Based on the visual observation of the excellent deflection recovery of girders A-285 and A-215, it is believed that a much higher recovery could be achieved if the testing was stopped just after the first load peak.

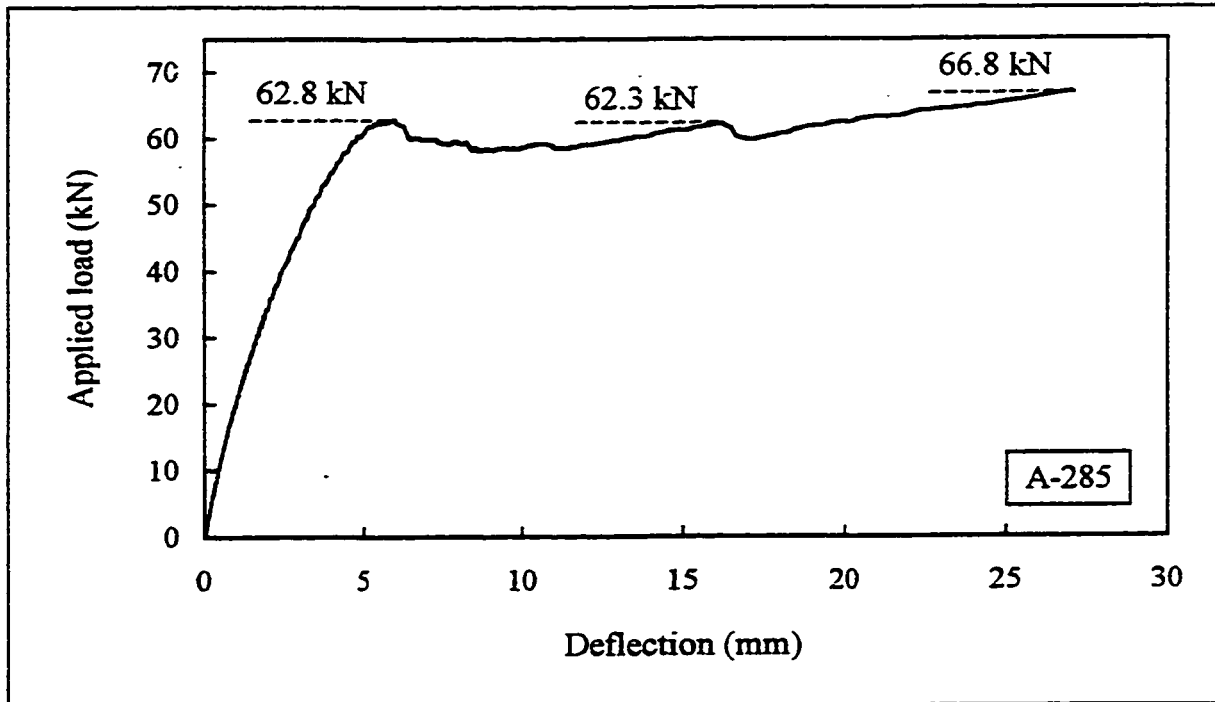


Figure 5.1 Applied load vs mid-span vertical deflection, girder A-285

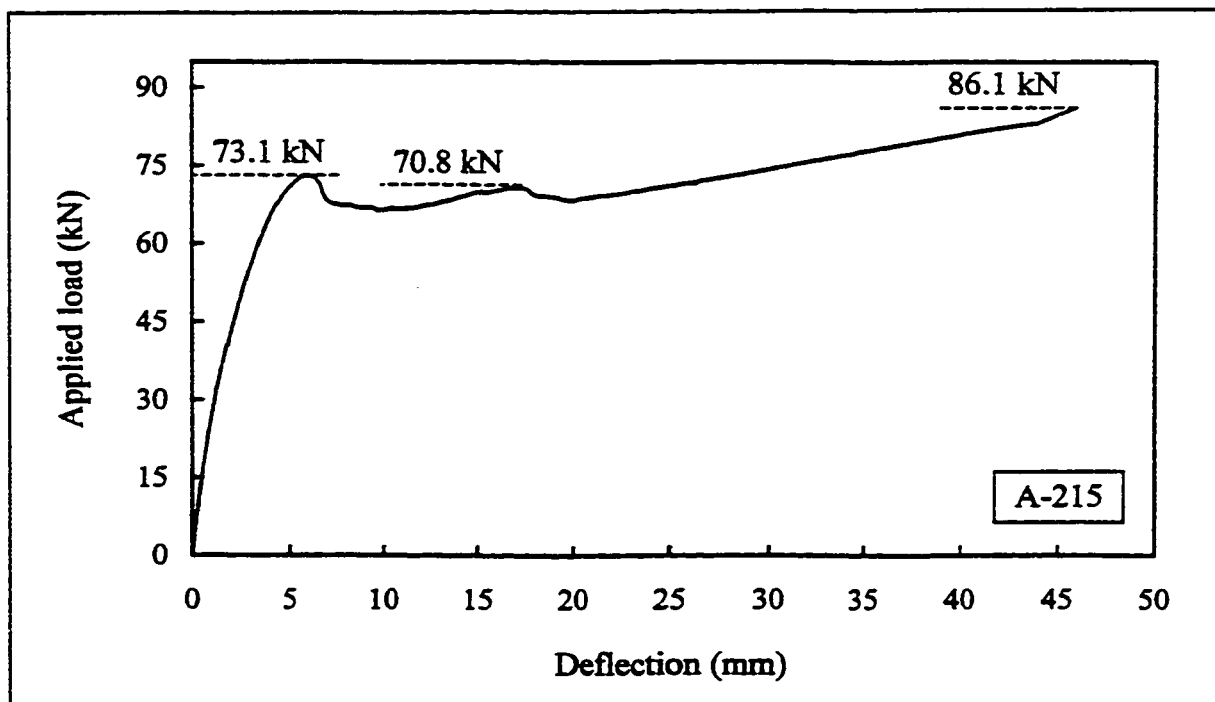


Figure 5.2 Applied load vs mid-span vertical deflection, girder A-215

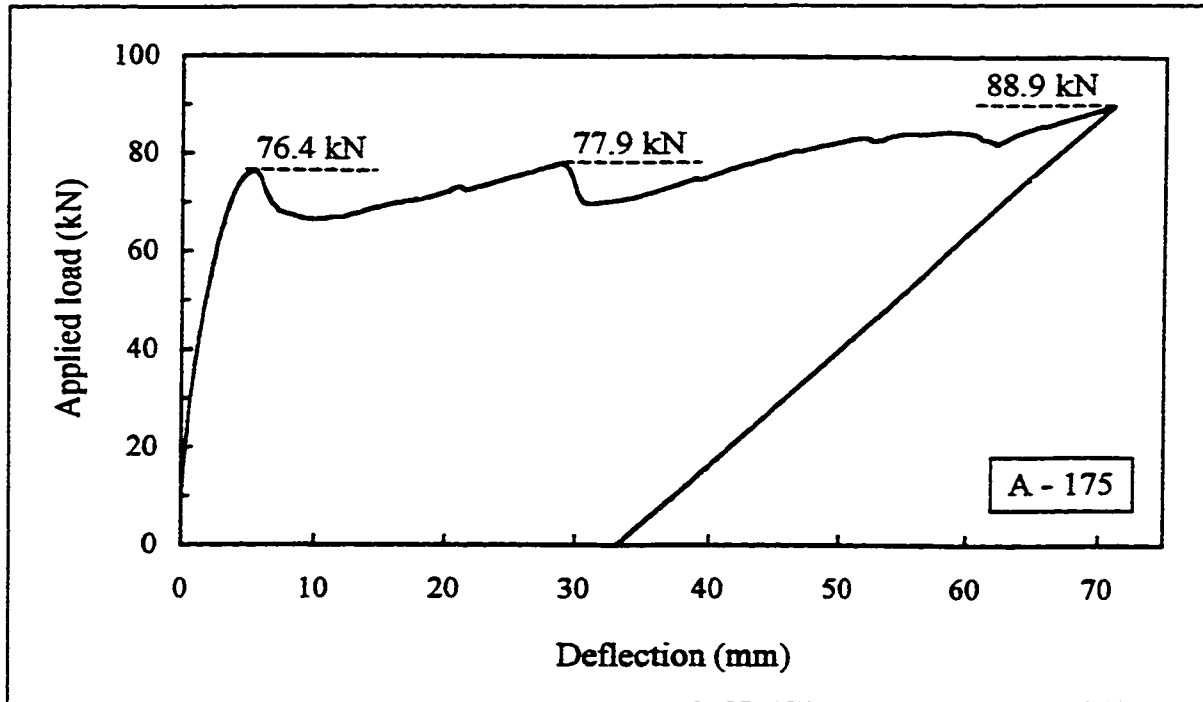


Figure 5.3 Applied load vs mid-span vertical deflection, girder A-175

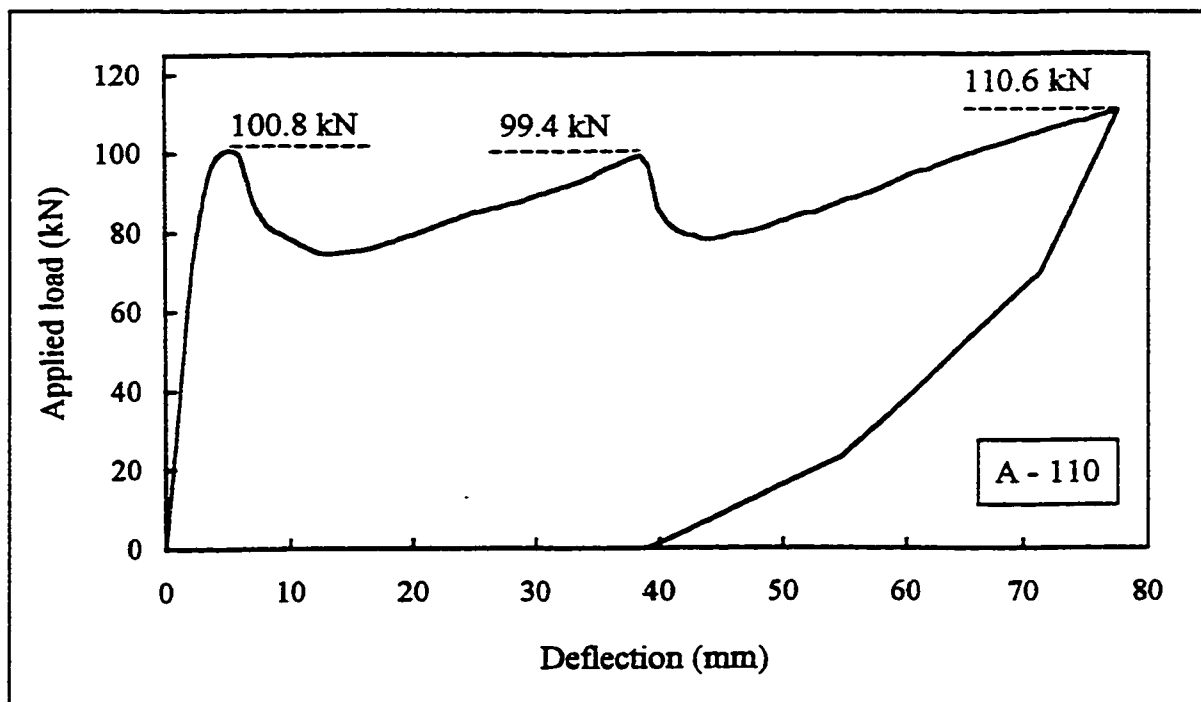


Figure 5.4 Applied load vs mid-span vertical deflection, girder A-110

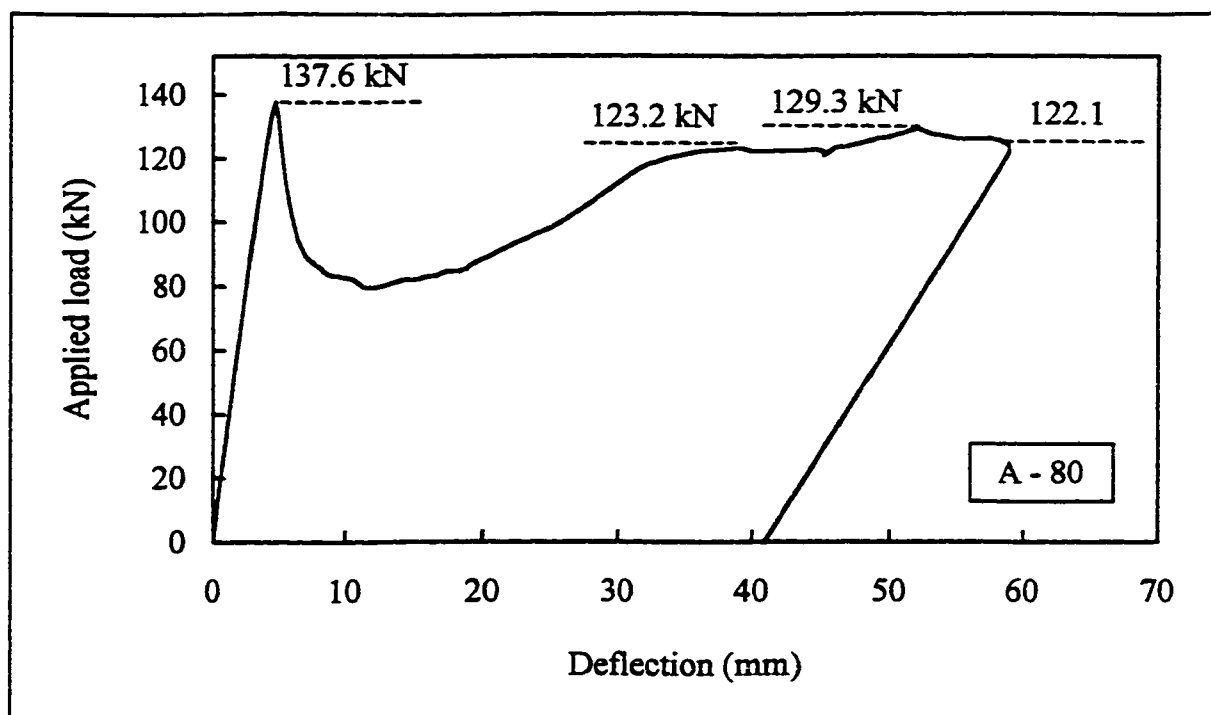


Figure 5.5 Applied load vs mid-span vertical deflection, girder A-80

In the test designated A-80-b, the overlapped unwelded web splice was in the shear-span. The load-deflection curve shown in figure 5.6 indicates that the web can carry a considerable amount of shear even if the web splices are not welded. The low stiffness that appears in the beginning of the curve can be attributed to the great amount of distortion that existed in the flanges due to the first testing of this girder. At the end of testing, the web splice showed a considerable distortion as will be shown later in figure 5.12.

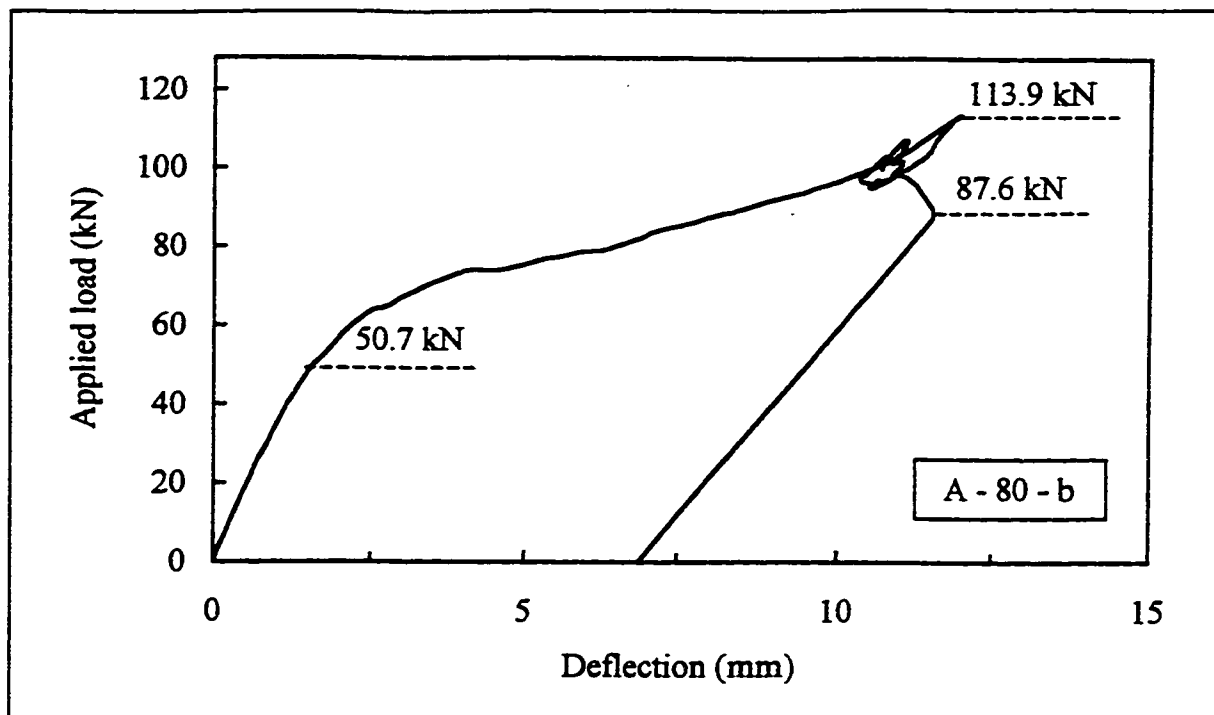


Figure 5.6 Applied load vs mid-span vertical deflection, girder A-80-b

### 5.3 WEB BUCKLING PATTERNS

For the girders with webs that have relatively wide sub-panel widths A-285, A-215, and A-175, a similar sequence of web deformation took place. Individual diagonal buckles started to appear in each sub-panel in both shear-spans at an early stage of loading corresponding to the buckling load. With the increase of load, the buckles started crossing the fold lines and extending to the next sub-panel. At the end of testing, the diagonal buckles in the shear-spans for the three girders were in the range of  $51^\circ$  to  $43^\circ$ ,  $58^\circ$  to  $32^\circ$ , and  $57^\circ$  to  $37^\circ$  to the horizontal respectively. The steep angles were closer to the concrete end blocks while the flatter ones were closer to the loading points. No compression buckles due to web crippling were observed beneath the loading points up to the termination of the testing except those appeared beneath the left load in girder A-285 at a very late stage of loading (see figure 5.8). Instead, horizontal buckles due to vertical compression appeared above the bottom flange beneath the two loading points. Those buckles were first noticed just after the applied load



reached its first load peak. With the increase in load, the buckles became more visible and extended toward the girder's mid-span. At the end of testing, a continuous horizontal buckle extends along the full length of the region of zero shear and maximum moment between the two loading points. Figure 5.7 shows a pictures of girder A-175 at the end of testing. Figures 5.8 through 5.10 show drawings of the web buckling pattern at the end of testing of the three girders respectively.

For the two last girders with webs that have narrower sub-panel widths A-110, and A-80, the sequence of the web buckling was similar to that described above with the exception that the initiation of the diagonal buckles did not take place along the individual sub-panels. The diagonal buckles in the shear-span started in a mode that is some what between the local and the global modes. This observation was particularly applicable to girder A-80 with the narrowest sub-panel width. At the end of the testing, the diagonal buckles in the shear-spans for the two girders were in the range of  $58^{\circ}$  to  $35^{\circ}$  and  $53^{\circ}$  to  $30^{\circ}$  to the horizontal respectively. Figures 5.11 and 5.12 show drawings of the web buckling pattern at the end of testing of the two girders respectively. The web buckling at the end of testing girder A-80-b is shown in figure 5.13.

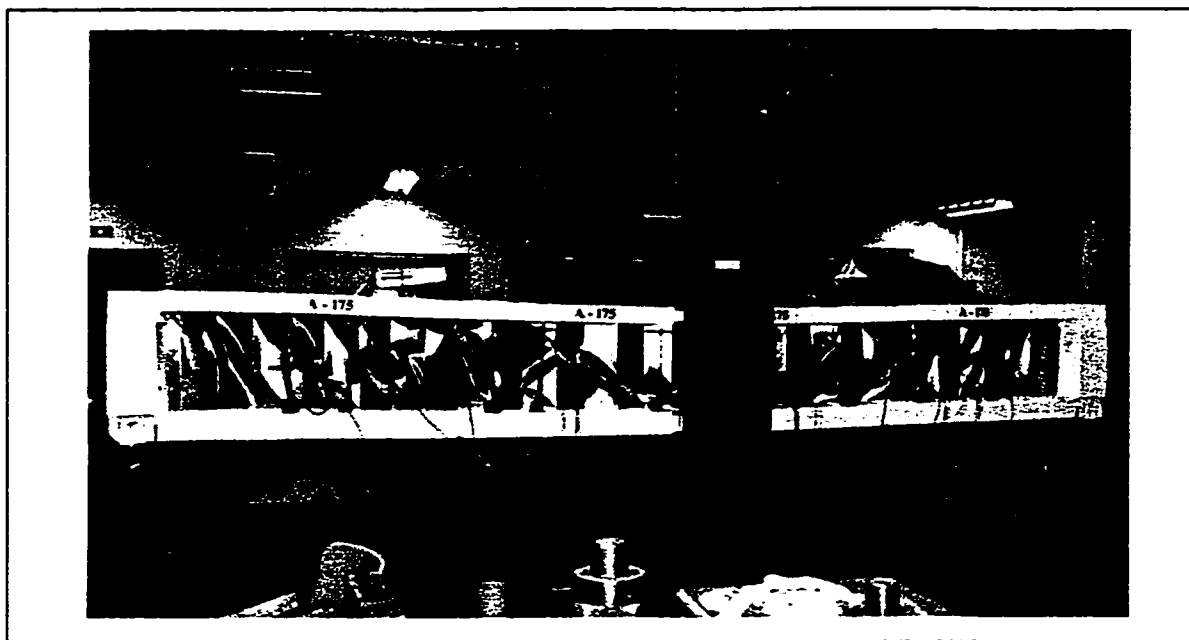


Figure 5.7 Girder A-175 at the end of testing

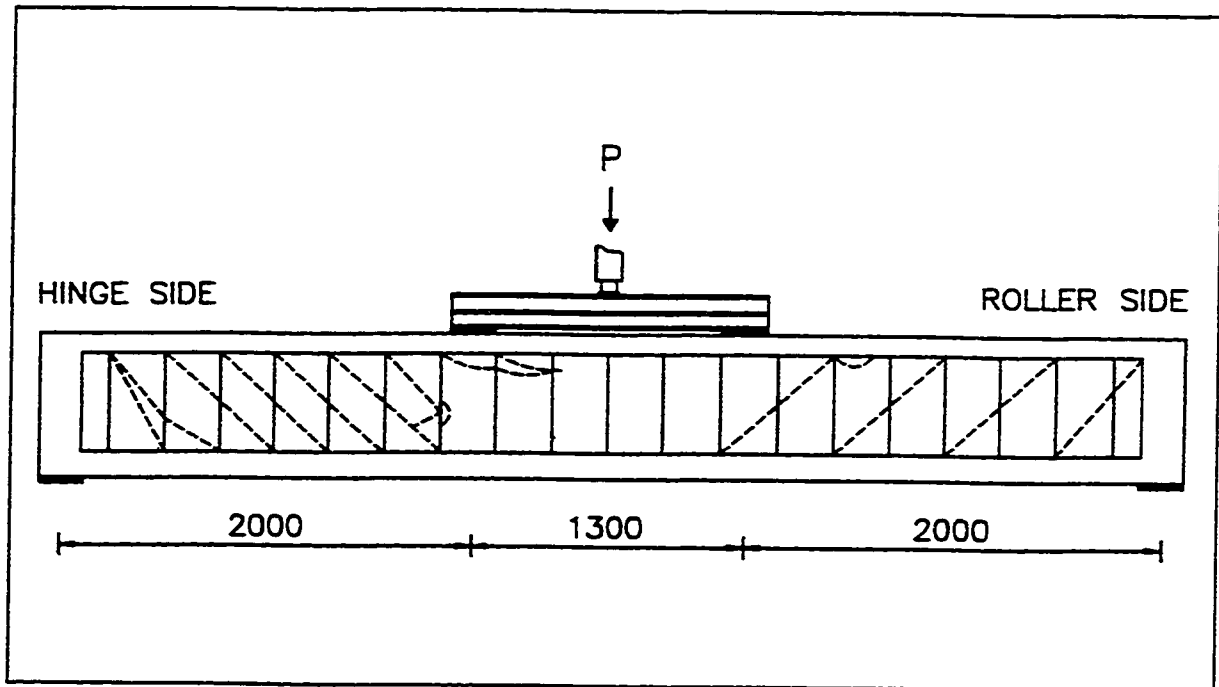


Figure 5.8 Web buckling pattern at the end of testing, girder A-285

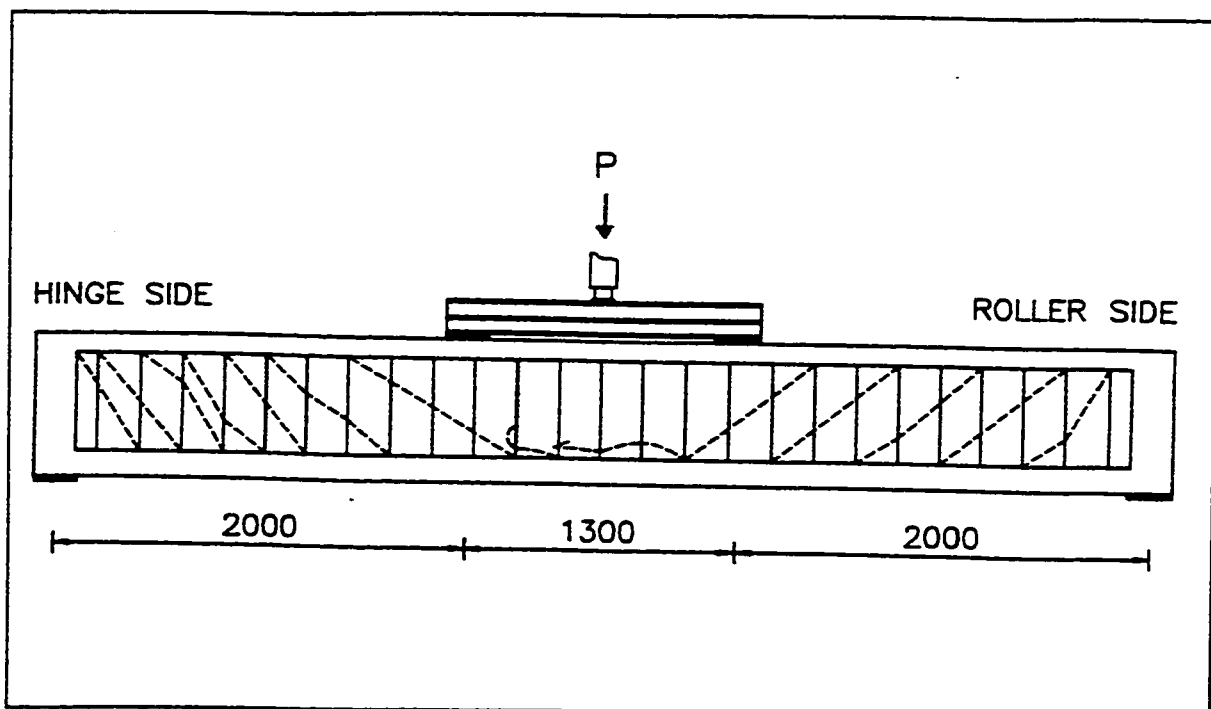


Figure 5.9 Web buckling pattern at the end of testing, girder A-215

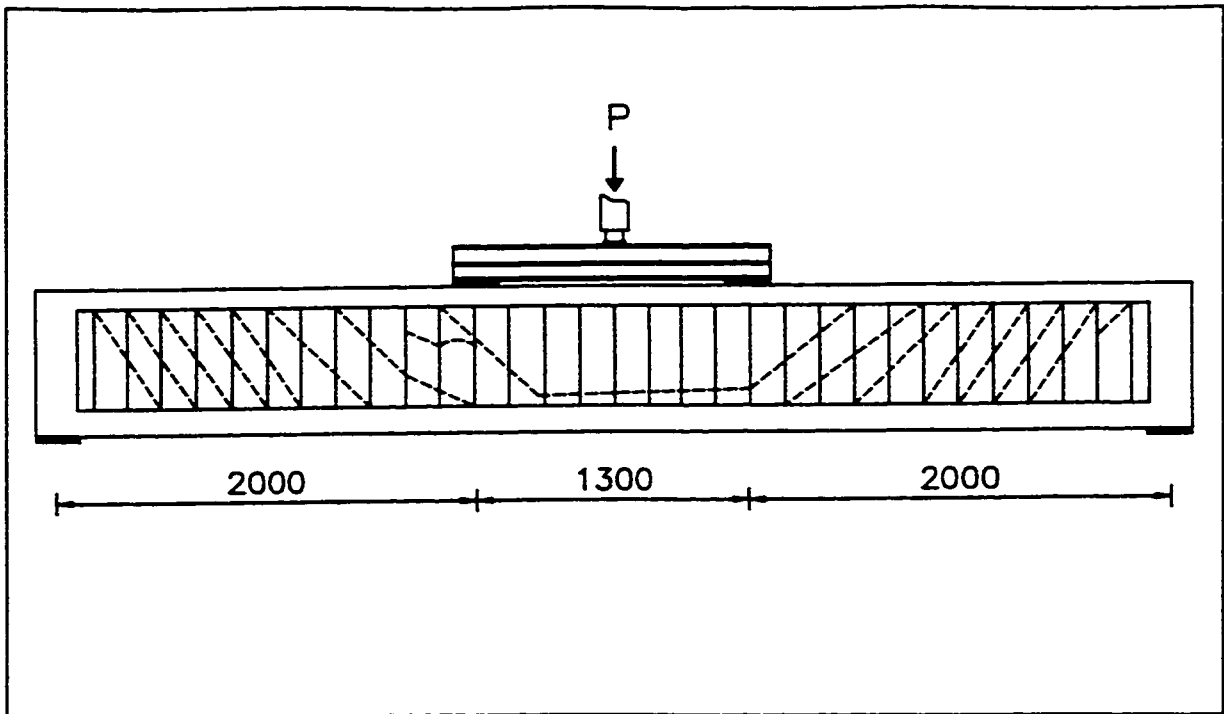


Figure 5.10 Web buckling pattern at the end of testing, girder A-175

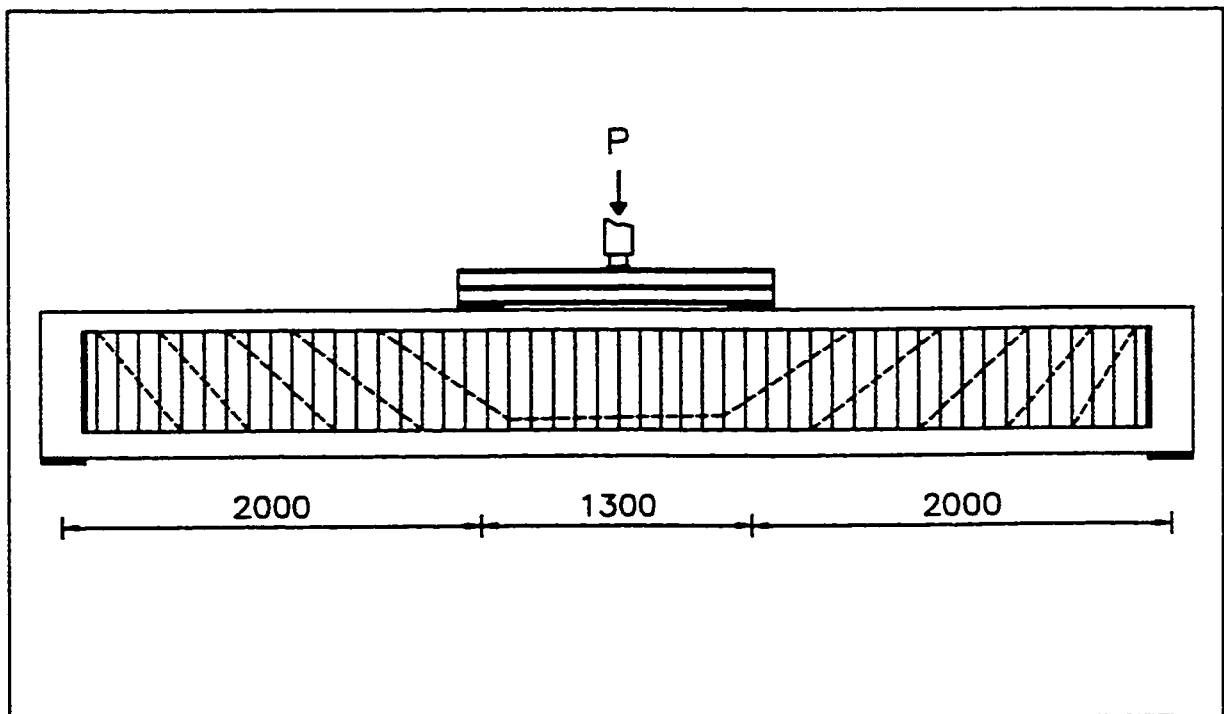


Figure 5.11 Web buckling pattern at the end of testing, girder A-110

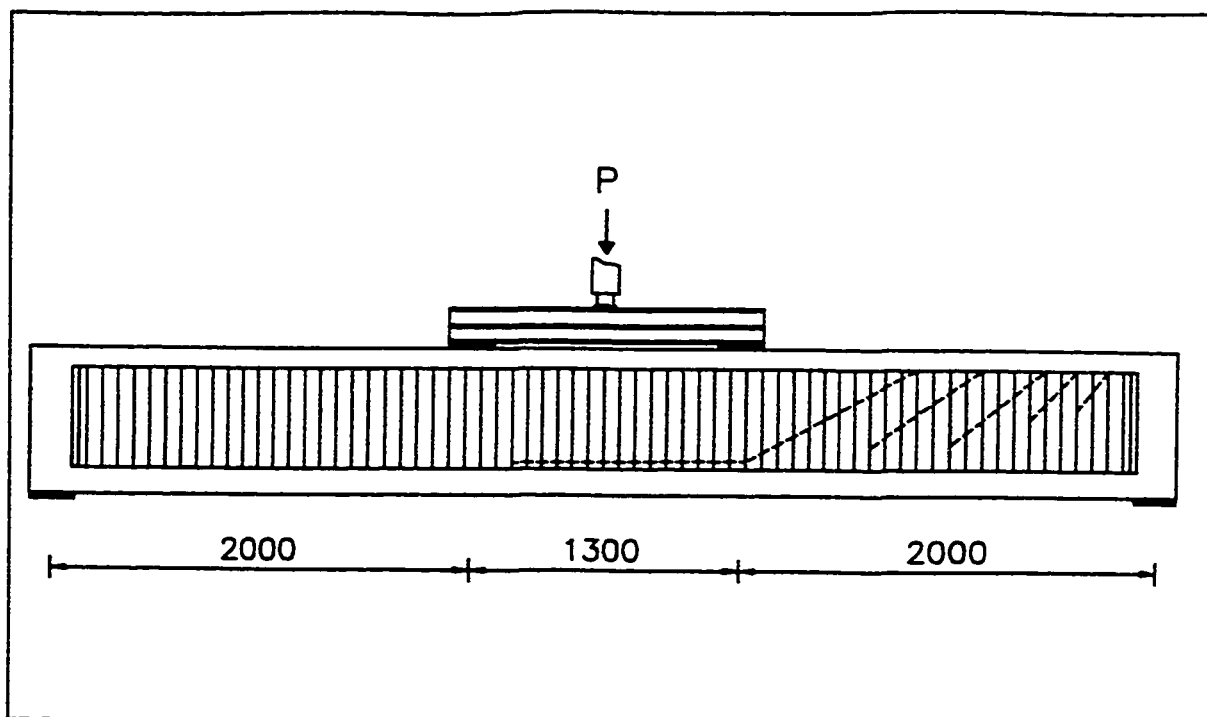


Figure 5.12 Web buckling pattern at the end of testing, girder A-80

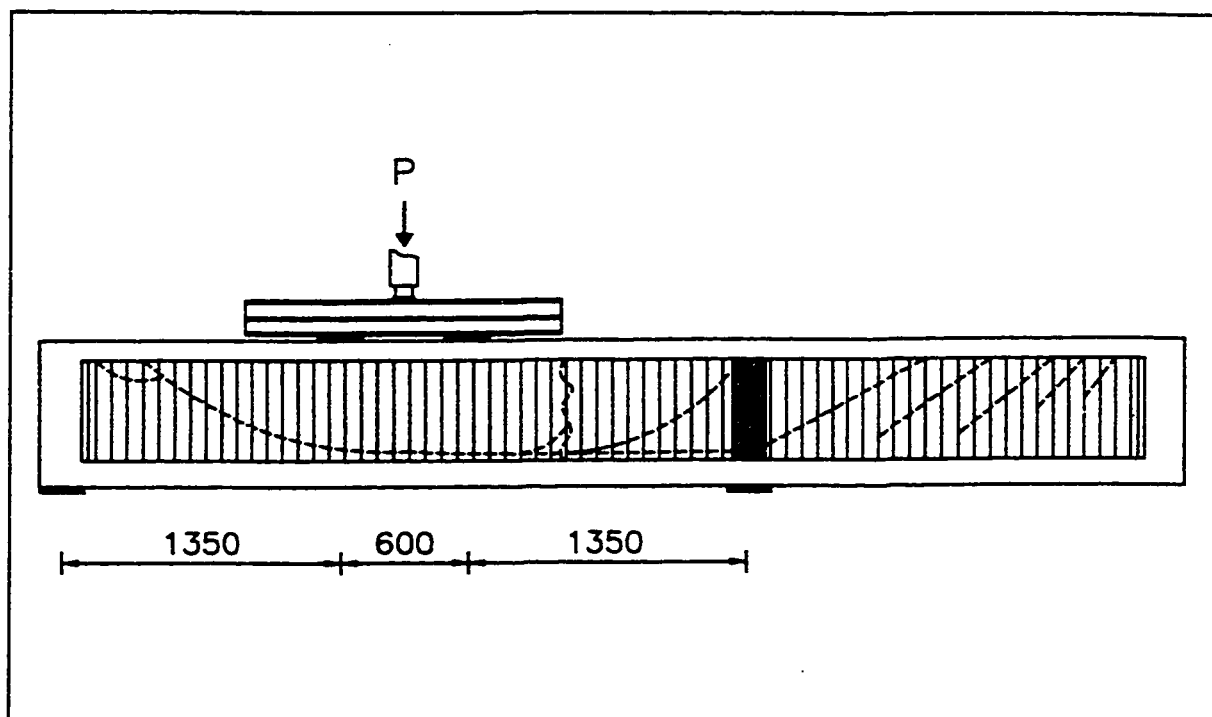


Figure 5.13 Web buckling pattern at the end of testing, girder A-80-b

## 5.4 SHEAR BEHAVIOUR AND STRENGTH

In the theoretical discussion of the shear strength of corrugated steel webs that was presented in chapter 3, the shear strength was assumed to be the sum of the buckling and the additional post-buckling strengths. The prime goal of the testing was to identify both the buckling and the total strengths in order to determine the post-buckling contribution, if any. However, in testing the phase I girders (A-285 and A-215) only the total shear strength was determined. The modifications applied to the instrumentation of the three girders of phase II (A-175, A-110, and A-80) enabled the determination of both the total and the buckling strengths. The applied load corresponding to buckling was identified by three different means which show excellent agreement with each other. In the following discussion of the experimental results, the case of girder A-175 will be detailed as a typical example. The complete results for all girders are given in Appendix F.

Because all girders were over-designed in flexure as was described in chapter 4, the experimental ultimate total shear strength of the web  $V_u$  was taken as the shear corresponding to the first load peak. In order to take the self weight of the girder into account, figure 5.14 was drawn. In this figure, the forces acting on the girder are shown including the self weight of the flanges and the web as a uniform load, the self weight of the end blocks as two concentrated loads, and the self weight of the transfer beam as two concentrated loads acting at the loading points. In the typical shear force diagram shown in the same figure, the average shear force in the middle of the shear-span will be used from now on to represent the shear force at any stage of loading.

To identify the load corresponding to the initiation of the web shear buckling for the three girders A-175, A-110, and A-80, the readings of the horizontal LSCs H1 through H4, the vertical LSCs D2 through D6, and the rosettes of set R were analyzed and compared. Figure 5.15 shows the typical readings of the horizontal LSCs H1 through H4 plotted against the applied load. The initiation of the buckles can be identified by the first sharp deviation in each LSC reading. Figures 5.16 and 5.17 show the typical readings of the vertical LSCs D2 through D6 that measure the relative vertical movement of the concrete flanges plotted (un-zoomed

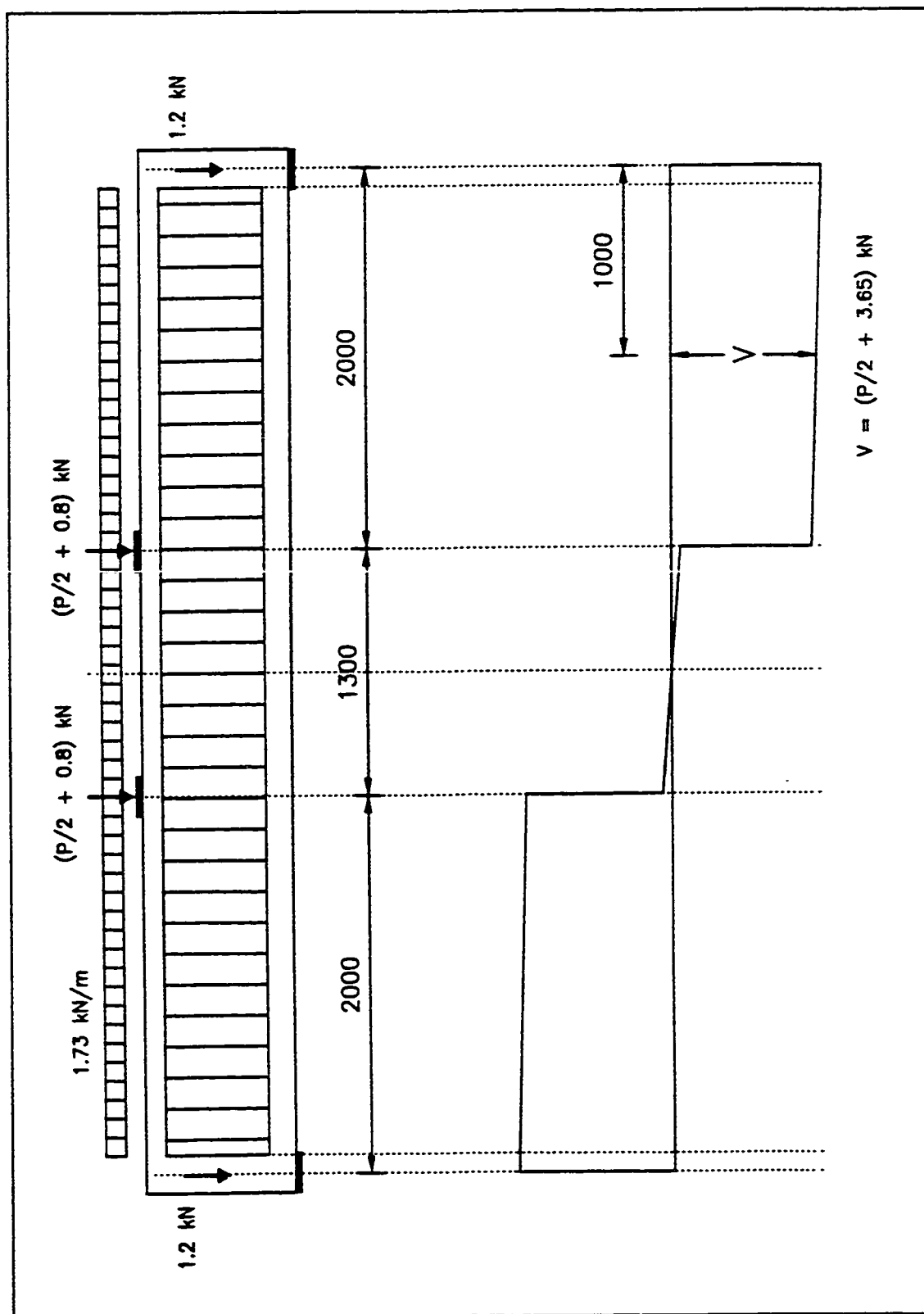


Figure 5.14 Calculation of the shear force  $V$  at any stage of loading

then zoomed) against the applied load. In figure 5.17, LSCs D3 and D5 at the points of load application show a gradual inward movement of the top flange toward the bottom flange from the beginning of loading. The LSC D4 at the mid-span shows the two flanges moving apart from each other up to the first load peak. The flanges continue moving apart until they reach a maximum movement of approximately 0.05 mm then they start approaching each other in a snap-through manner forming a loop-like part of the curve that can be seen in the figure. LSCs D2 and D6 located in the two shear-spans of each girder show the most interesting readings. They do not show any movement of the flanges toward or apart from each other up to some point. Then, they start indicating a gradual inward movement of the flanges. The load corresponding to point where LSCs D2 and D6 start to show the inward movement is very close to the load corresponding to the first sharp deviation in the readings of LSCs H1 through H4. Both loads are almost equal to the theoretically calculated load based on local buckling.

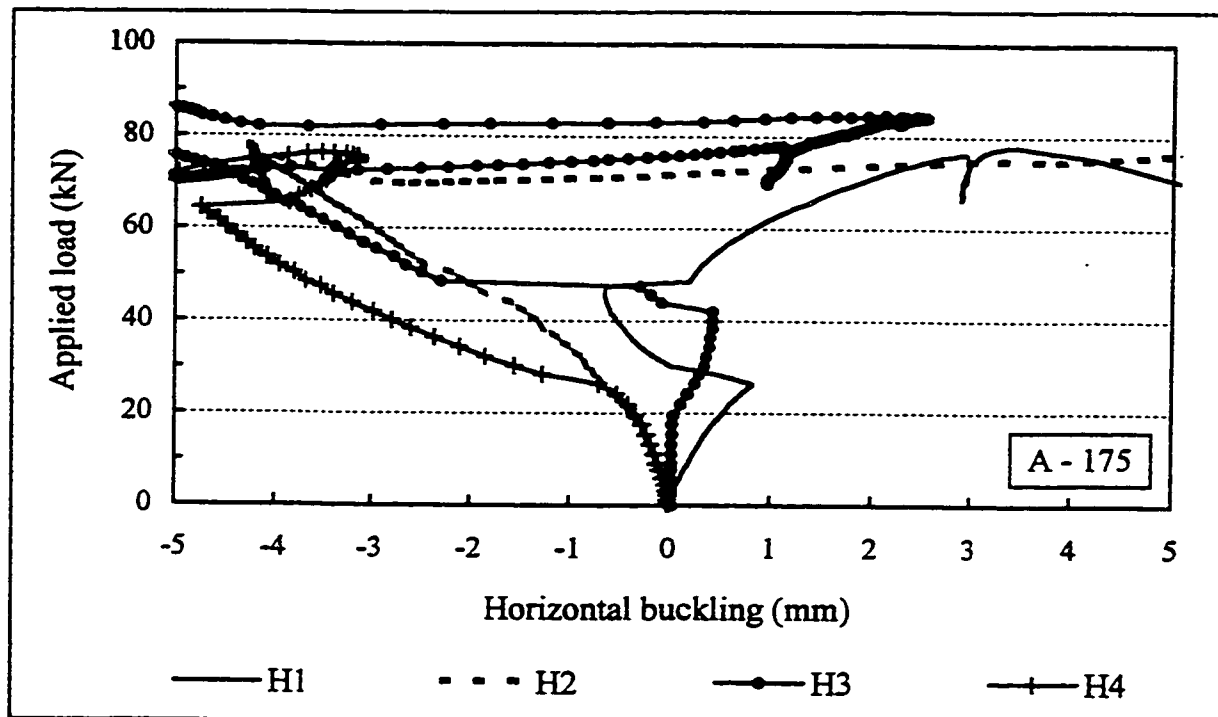


Figure 5.15 Applied load vs horizontal web buckling, girder A-175

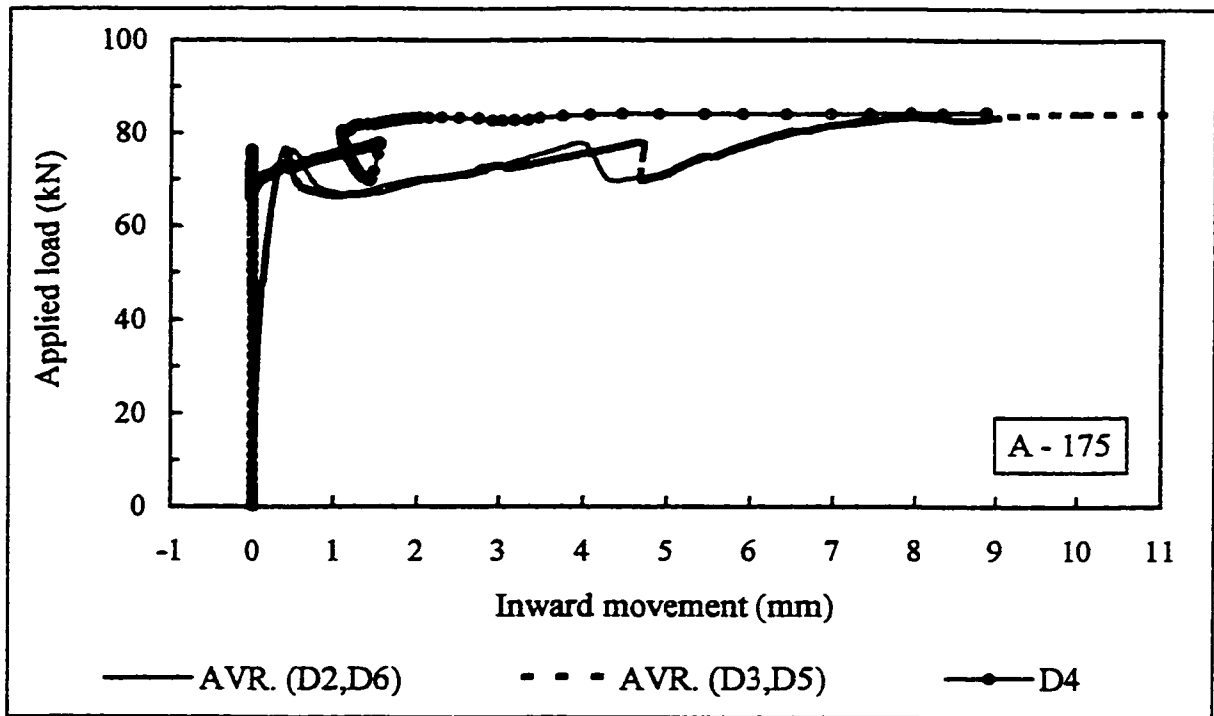


Figure 5.16 Applied load vs relative inward movement of flanges, girder A-175

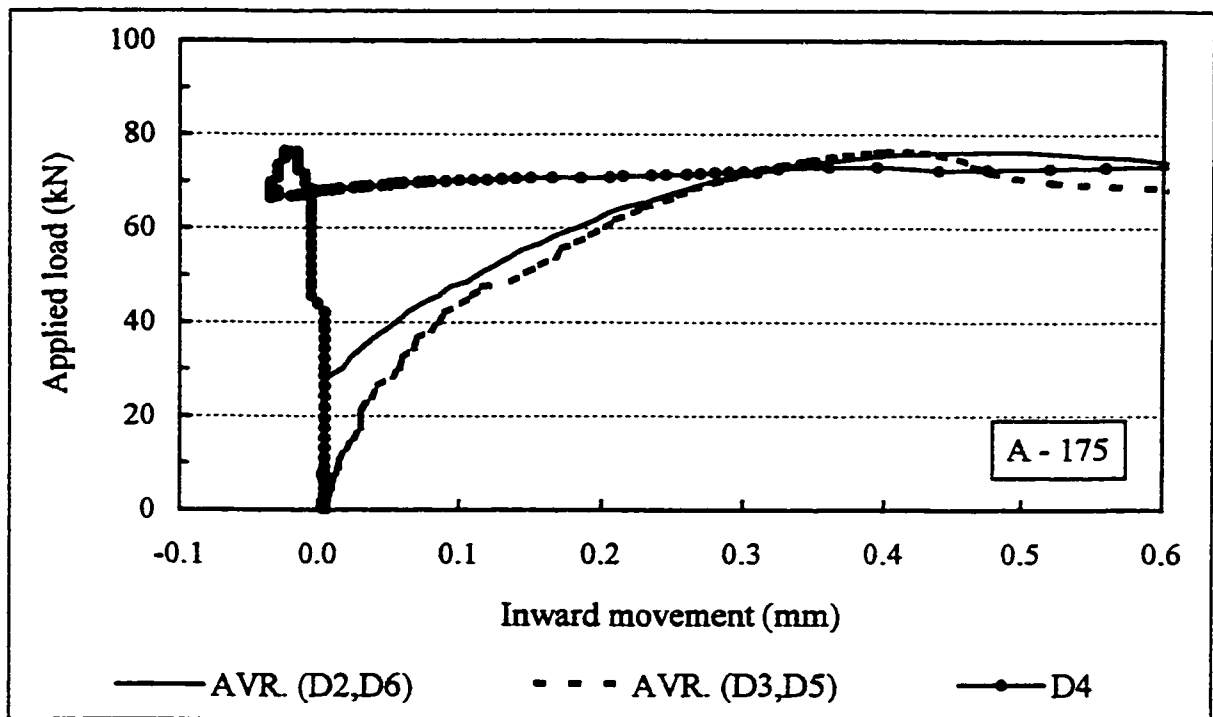


Figure 5.17 Applied load vs relative inward movement of flanges (zoomed), girder A-175



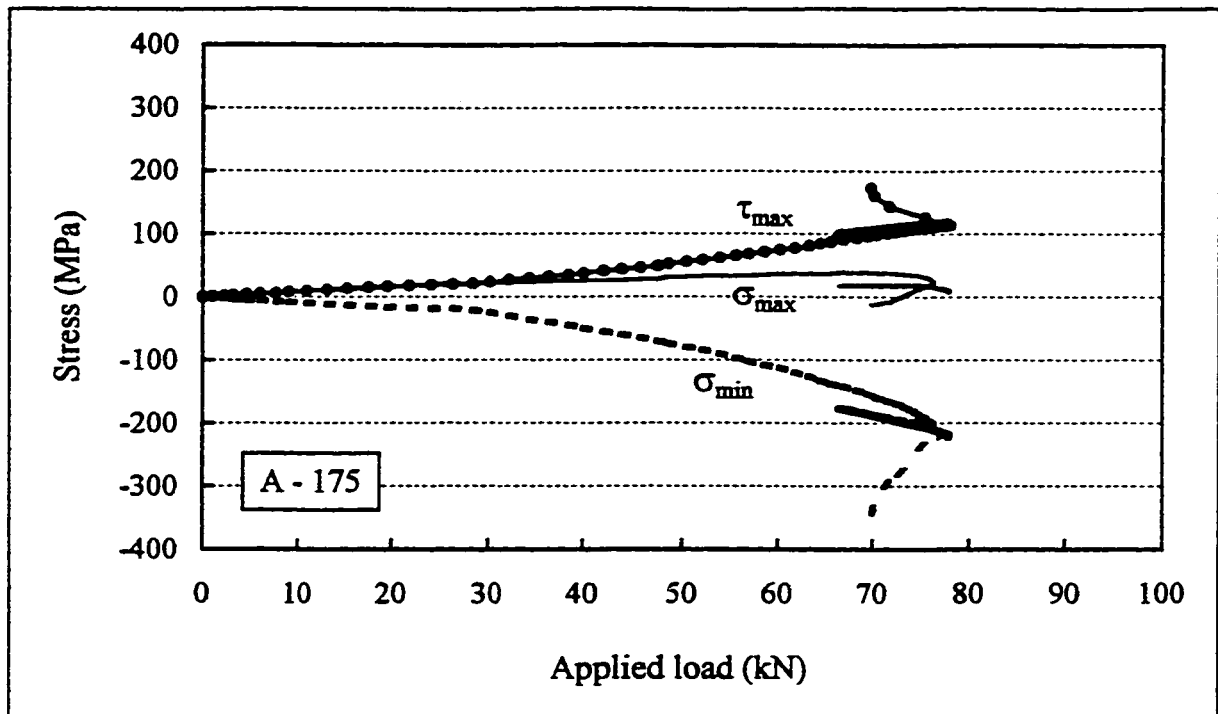


Figure 5.18 Principal membrane stresses in shear span (rosette R2), girder A-175

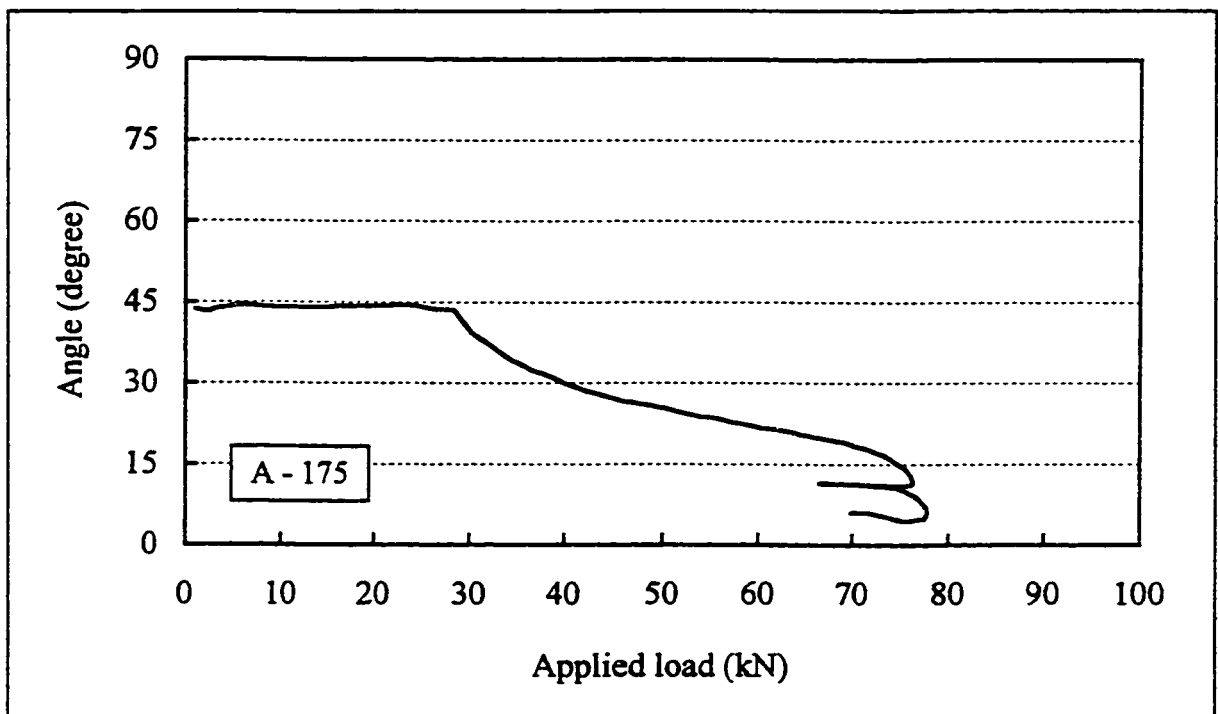


Figure 5.19 Angle of  $\sigma_{max}$  w.r.t. horizontal direction (rosette R2), girder A-175

The third and most important method of identifying the buckling load is the readings of the strain rosettes of set R. Figures 5.18 and 5.19 show a typical plotting of the principal normal and shear stresses, and the angle of the principal tension to the horizontal, against the applied load. The load corresponding to the initiation of buckling can clearly be identified from both figures. Up to the elastic buckling, the principal tension and the principal compression stresses should be equal and equivalent to the principal shear stress. This can be represented as a Mohr circle with its centre at the origin (0,0). The angle of principal tension should be equal to  $45^\circ$  with the horizontal. Both criteria were satisfied as shown in the figures. At the buckling load, the traces of  $\sigma_{\max}$  and  $\tau_{\max}$  started to separate and the angle of principal tension started to decrease. Again, the identified buckling load from the readings of all of the shear-span rosettes agreed very well with the buckling load identified by the other two methods and with the theoretically calculated load based on local buckling. The shear buckling load  $V_b$  was then determined using the shear force diagram previously presented in figure 5.14.

It should be noted that the shear stress corresponding to the initiation of buckling obtained from the rosettes readings was also very close to that calculated for the local shear buckling which confirms the relation between the shear stress in the web and the shear force  $V = w h F$ . It should also be noted that the principal stress and principal angle figures for rosettes R1 through R4 for all the three girders of phase II were plotted either up to the end of testing or up to reaching the yield strain in one or more rosette branches, whichever is first. The yield strain was reached in only six out of the twelve rosettes of the three girders, and this usually occurred well after the second load peak. At least one rosette for each girder did not show yield strain in any branch up to the end of testing. This agrees with what will be shown later in figure 5.20 that none of the girders reached the shear force corresponding to the shear yield limit, although girder A-80 was very close. In fact, the yield strain that is shown by those six rosettes can be attributed to the excessive distortion of the web in the shear-span, close to the end of testing, which produces high bending stresses at the concave and convex surfaces of the diagonal buckles.

Table 5.1 shows the experimental values of the total applied load at buckling and at the first load peak and their corresponding shear forces  $V_b$  and  $V_u$  respectively. The theoretically calculated buckling loads are also presented for comparison. The last column to the right side in the table shows a comparison between the experiment and theoretical local shear buckling loads. The shear strength plotting for the webs of the five test girders which was shown in figure 4.7 as the shear stress against the sub-panels widths will be re-plotted in figure 5.20 as the shear force against the sub-panel widths. The same figure 5.20 shows the experimentally determined  $V_b$  and  $V_u$  values.

Table 5.1 Experimental and theoretical shear strengths of the test girders

Girder	Experimental Results					Theoretical Calculations			
	$P$ Buckling (kN)	$P$ 1 <sup>st</sup> Peak (kN)	$V_b$ (kN)	$V_u$ (kN)	$\frac{V_b}{V_u}$	$V_{le}$ (kN)	$V_{in}$ [n=2] (kN)	$V_{in}$ [n=3] (kN)	$\frac{V_b}{V_{le}}$
A-285	N/A	62.8	N/A	35.1	N/A	6.4	6.4	6.4	N/A
A-215	N/A	73.1	N/A	40.2	N/A	10.3	10.2	10.3	N/A
A-175	26.5	76.4	16.9	41.9	40 %	15	14.8	15	1.13
A-110	67.8	100.8	37.6	54.1	70 %	34.1	31.9	33.5	1.10
A-80	131.6	137.6	69.5	72.5	96 %	63.2	51.3	57.4	1.10

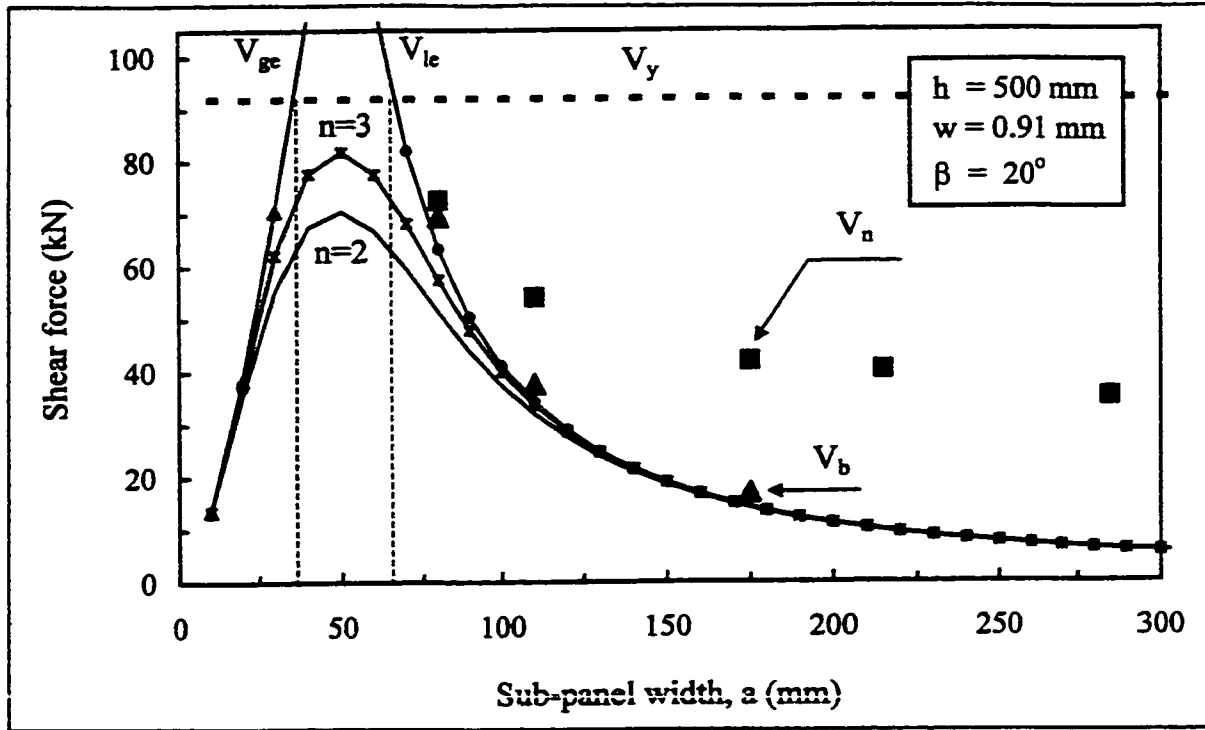


Figure 5.20 Experimental shear force results compared with theoretical calculations

It can be seen from figure 5.20 how close the experimentally determined buckling shear forces for three girders A-175, A-110, and A-80 are to the curve that represents the local shear buckling strength. The considerable additional post buckling strength especially in the first three girders A-285, A-215, and A-175 can also be seen. From figure 5.20, it can be concluded that the buckling load  $V_b$  for the girders A-285 and A-215 (which were not determined experimentally) should also be close to that calculated based on the local shear buckling. In this case, the ratios of  $V_b$  to  $V_u$  for those two girders will be about 18 % and 26 % respectively.

Let us now discuss the interaction curve  $V_{in}$  ( or  $\tau_{in}$  ). As was mentioned before, the interaction curve will not only represent the strength of the sub-panels in the transition zones between the three limits. In addition, it will allow the representation of the three limits by only one equation. Before recommending a specific value for the exponent  $n$  of the interaction curve, let us discuss the differences between two shear strength representations for two

different profiles: figure 3.4 for the trapezoidal corrugation profile of the Shinkai bridge in Japan, and figure 5.20 for the zigzag corrugation profile of the test girders. In our comparison, the three regions (1, 2, and 3) shown in figure 3.3 will be used as reference. In figure 3.4, the angle of corrugation was taken as  $37^\circ$  instead of the optimum corrugation angle that was calculated in Appendix B and found to be  $16^\circ$ . All the other properties of the web profile were equal to those of the optimum profile. This resulted in a higher global shear buckling strength, and consequently a relatively wide region 2 that is governed by the shear yield. Therefore, a small value of only  $n = 2$  was enough for the highest strength corresponding to a sub-panel width  $a = 180 \text{ mm}$  to reach the shear yield limit. If the optimum corrugation angle of  $\theta = 16^\circ$  were used, the elastic global shear buckling curve would then become more flatter, region 2 would be narrower, and a higher value of  $n$  would be needed for the interaction curve to reach the shear yield limit in region 2. The case is slightly different for the corrugation profiles of the test girders. The optimum angle was found to be equal to  $23^\circ$ , and the chosen angle was  $20^\circ$  with almost no difference in the global shear buckling strength. This, along with the fact that the zigzag profile is generally of lower global shear buckling strength than the trapezoidal profile, allowed region 2 to become relatively narrow and required a considerably high  $n$  value to reach the shear yield limit in region 2. Therefore, based on the experimental results of the test girders and on the theoretical study of chapter 3, a value of  $n = 3$  appears to be suitable for use with the zigzag profiles, while a value of  $n = 2$  can be recommended for use with the trapezoidal profiles. However, more testing with sub-panel widths that belong to region 2 is still needed to confirm the above suggestions. Generally speaking, an  $n$  value that is higher than the actual one will result in an interaction curve that changes from one limit to the other without showing a transition zone, while an  $n$  value that is smaller than the actual one will underestimate the strength of the corrugated web.

In order to explain how the web carries the additional shear force past the buckling load, the attention should first be paid to the readings of the shear-span rosettes R1 through R4. Figures 5.18 and 5.19 show that *after the buckling load and up to the first load peak*:

- (1) the angle of principal tension started to decrease from about  $45^\circ$  to about  $15^\circ$ .
- (2) the principal tension stress stabilized at almost the same value that corresponds to the buckling load.
- (3) the principal compression and the principal shear stresses kept increasing steadily.

So, by keeping in mind that the strain rosettes are located at the mid web height 10 mm from the fold lines, an explanation can be drawn. With the initiation of buckling, the web wanted to accommodate itself to carry more load. The principal compression stress started to switch to steeper angles toward the stiff fold lines, while the perpendicular direction of the principal tension became flatter. According to these observations, the fold lines started to act as columns and continued to carry additional load until they buckled under vertical compression. As was mentioned in describing the buckling pattern earlier in this chapter, the first vertical buckling was noticed above the bottom flange in a vertical line extending from both of the two loading points. This means that the web crippling took place near the bottom flange where there are low vertical compression stresses instead of near the top flange where there are high vertical compression stresses (see the stress plotting from rosettes L1 through L4 for phase II girders, Appendix F). It seems that the geometrical distortion caused by the extension of the diagonal shear buckles from the neighboring shear-span into the girder's mid-span near the bottom flange weakened the fold lines below the loading points. With the failure of the web in vertical buckling beneath the loading points, the applied load dropped creating the first load peak.

For girder A-110 the same observations apply except that the post-buckling range was not as wide which allowed the principal angle to switch from  $45^\circ$  to an average of only  $25^\circ$ . For girder A-80, the buckling load was very close to the first load peak and there was no room for the principal stresses to change their values or angles. This indicates that the shear strength of the web and the strength of the fold lines acting as columns especially beneath the load application points were almost equal to each other in this last girder A-80.

Following the strut approach presented by L. Leiva-Aravena [35], a calculation of the capacity of the web against vertical compression stresses will be proposed here. According to

clauses 5.6.2.1 and 5.6.2.2 in the CSA Standard S136-94 *Cold Formed Steel Structural Members* which defines the effective width of elements in compression, only a portion of the web around the fold lines is effective in carrying the vertical compressive stress. Figure 5.21 (a) and (b) shows the basis of the calculations below. In this figure, the corner length is assumed to be 5 mm. The limiting width  $A_{\text{lim}}$  in mm which allows the whole web to act a continuous column is defined by

$$A_{\text{lim}} = 0.644 w \sqrt{\frac{k E}{\sigma_c}} \quad (5.1)$$

in which

$E$  = Young's modulus of elasticity for the web material (MPa)

$k$  = buckling coefficient for the individual sub-panel as a compressive element = 4

$w$  = web thickness (mm)

$\sigma_c$  = applied compression stress (MPa)  $\leq F_y$

If the actual width  $A$  shown in figure 5.21 was found to be greater than the limiting width  $A_{\text{lim}}$ , the effective column width should be used. The effective width  $b$  in mm is defined by

$$b = 1.47 A_{\text{lim}} \left[ 1 - \frac{0.208}{(A/w)} \sqrt{\frac{k E}{\sigma_c}} \right] \quad (5.2)$$

The Euler column capacity  $P_{cr}$  of the individual columns can then be calculated assuming fixed-fixed boundaries, that represents the concrete flanges, by

$$P_{cr} = \frac{\pi^2 E I_{xx}}{(0.5 h)^2} \quad (5.3)$$

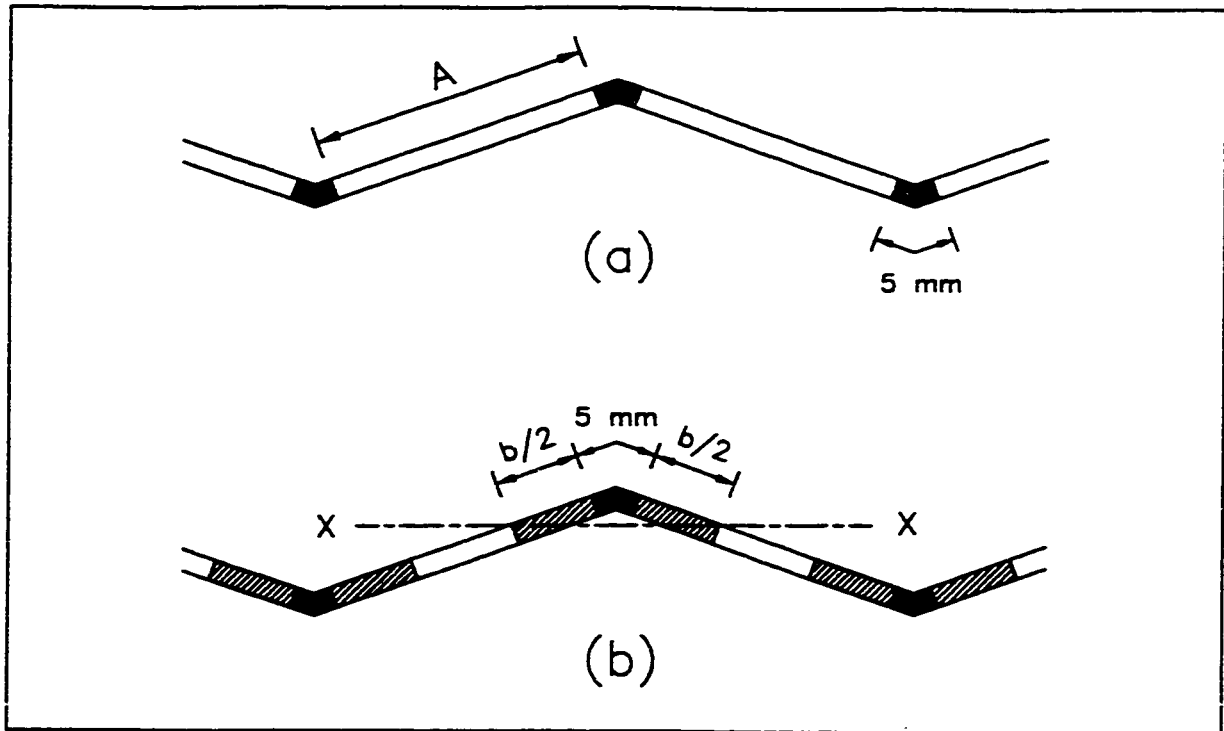


Figure 5.21 Geometry of the column-like fold lines

where  $I_{xx}$  is the second moment of inertia of the column about its centroidal  $x-x$  axis shown in figure 5.21. The value of  $\sigma_c$  can be taken as the compressive vertical stress just beneath the top flange at the points of load application. Taking the average of the two readings of each girders, the values of  $\sigma_c$  is 130 MPa, 98 MPa, and 136 MPa for the three girders A-175, a-110, and A-80 respectively. Working with a hypothetical web whose sub-panel width is the average of those of the three girders and with a hypothetical stress that is equal to the average of the three  $\sigma_c$  stresses mentioned above, the following results were obtained.

$$a = 122 \text{ mm}, \quad A = 117 \text{ mm}, \quad \text{and} \quad \sigma_c = 121 \text{ MPa}$$

$$\text{which yields} \quad A_{\text{lim}} \approx 49 \text{ mm} < A$$

$$\text{and} \quad b \approx 63 \text{ mm}, \quad I_{xx} = 588 \text{ mm}^4, \quad \text{and} \quad P_{cr} = 19.5 \text{ kN}$$

With a distribution angle of 1:1.5 (horizontal to vertical), the width of the bearing plate at



each loading point can cover 2, 3, and 4 fold lines for the three girders respectively. These folds can carry a compression loading of 39 kN, 58.5 kN, and 78 kN corresponding to a total applied load of 78 kN, 117 kN, and 156 kN respectively. The ratios of these predicted loads to the experimentally determined loads that corresponds to the first load peak are 1.02, 1.16, and 1.13 respectively which shows a good agreement. For a practical design case, the value of the compression stress  $\sigma_c$  can be assumed based on the kind of loading and its distribution length.

The fact that the girder was able to carry such high shear in testing girder A-80-b without having a fully connected web in the shear-span indicates that the load-carrying mechanism in this case in both the pre-buckling and the post buckling stages does not differ from that of the previous cases. In this particular case, the principal tension in the shear-span can not be transferred from a web panel to the other through the unwelded splice. However, by having this principal tension anchored to the concrete flanges at the splice region, the fold lines of the splice can still act as a vertical stiffener (column) but with the compressive stress transmitted to it only at the top and bottom ends not along the entire web height as for the other fold lines.

## 5.5 FLEXURAL BEHAVIOUR AND STRENGTH

For the five test girders, the axial stresses in the concrete flanges and in the strands, at each girder's mid-span, are plotted against the applied load and are included in Appendix F. It can be seen from all ten plottings that the stresses are fairly proportional up to the point of the first load peak. Following that first peak, a dramatic change in the way the girder behaves in flexure took place. In this discussion, figures 2.22 and 2.23 show the re-plotting of the concrete and strand stresses for girder A-215 against the mid-span deflection, which gives a better view of the stress changes. Being tested in a displacement controlled setup, no disruptions or fluctuations in the stress traces appear in both figures. Three vertical dotted lines are drawn on each figure to indicate (I) the web buckling point, (II) the first peak point, and (III) the second peak point. Following these two figures, the strain profiles at different stages of loading are drawn for each of the five test girders, figures 5.24 through 5.28.

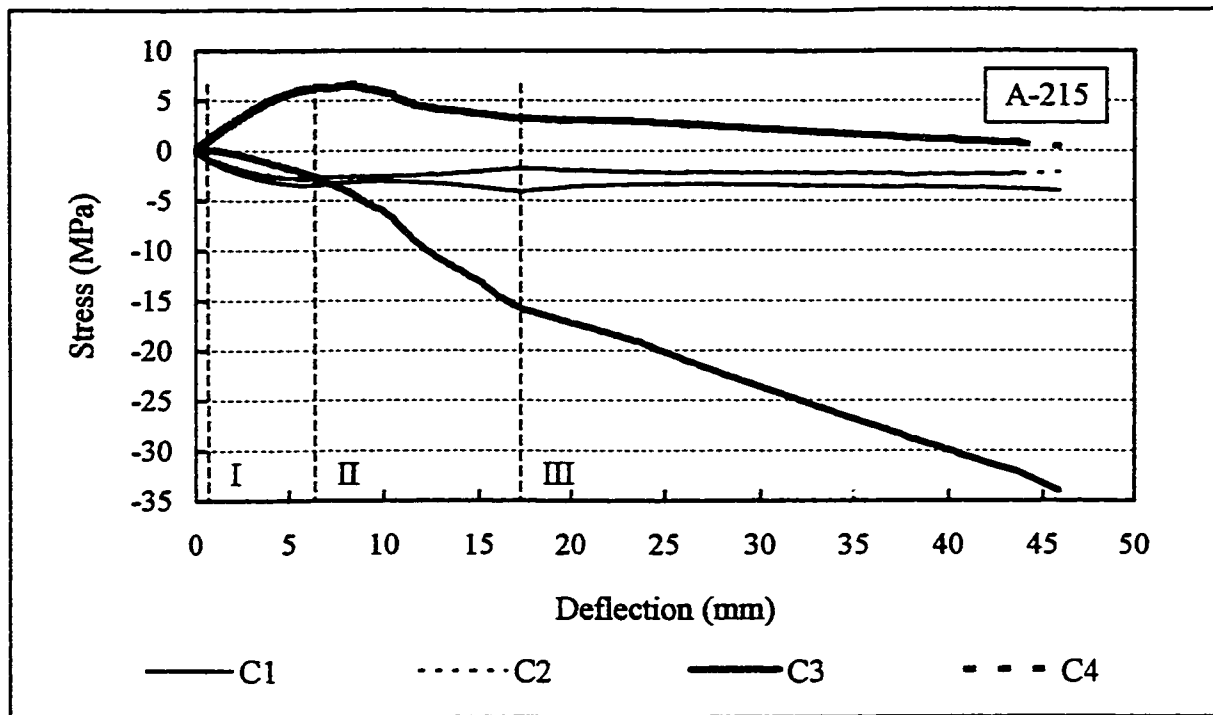


Figure 5.22 Stresses in concrete flanges vs mid-span deflection, girder A-215

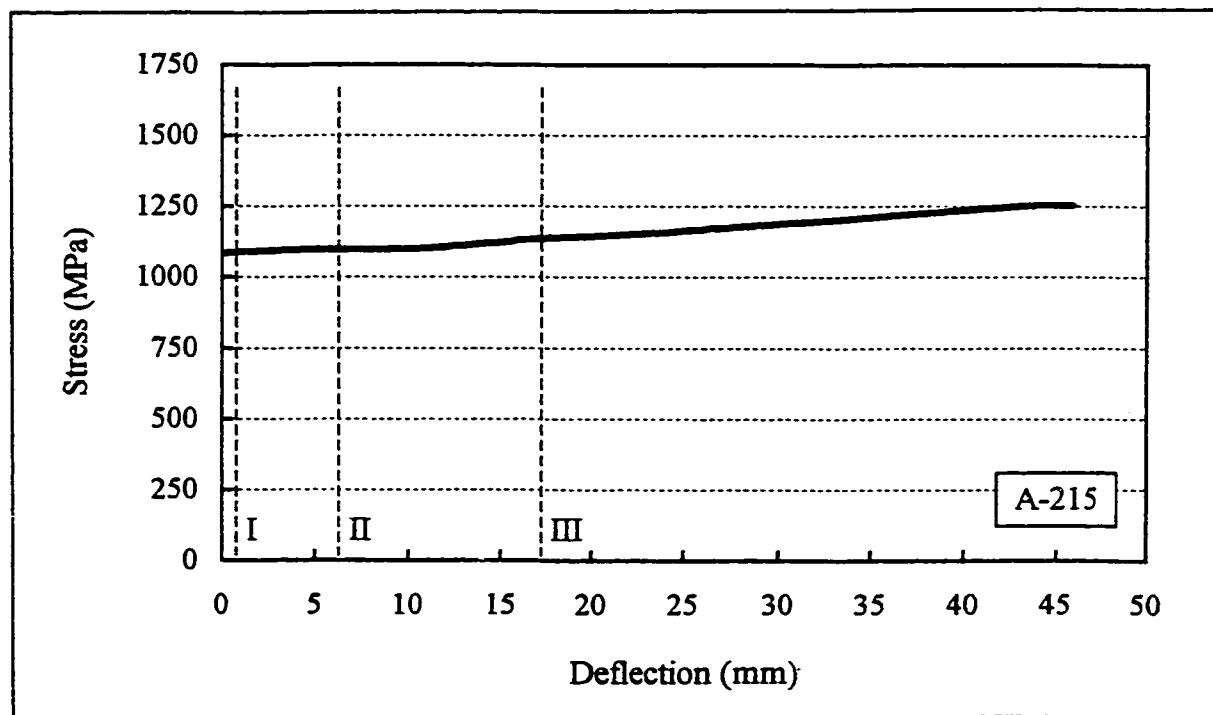


Figure 5.23 Average stress in prestressing strands vs mid-span deflection, girder A-215

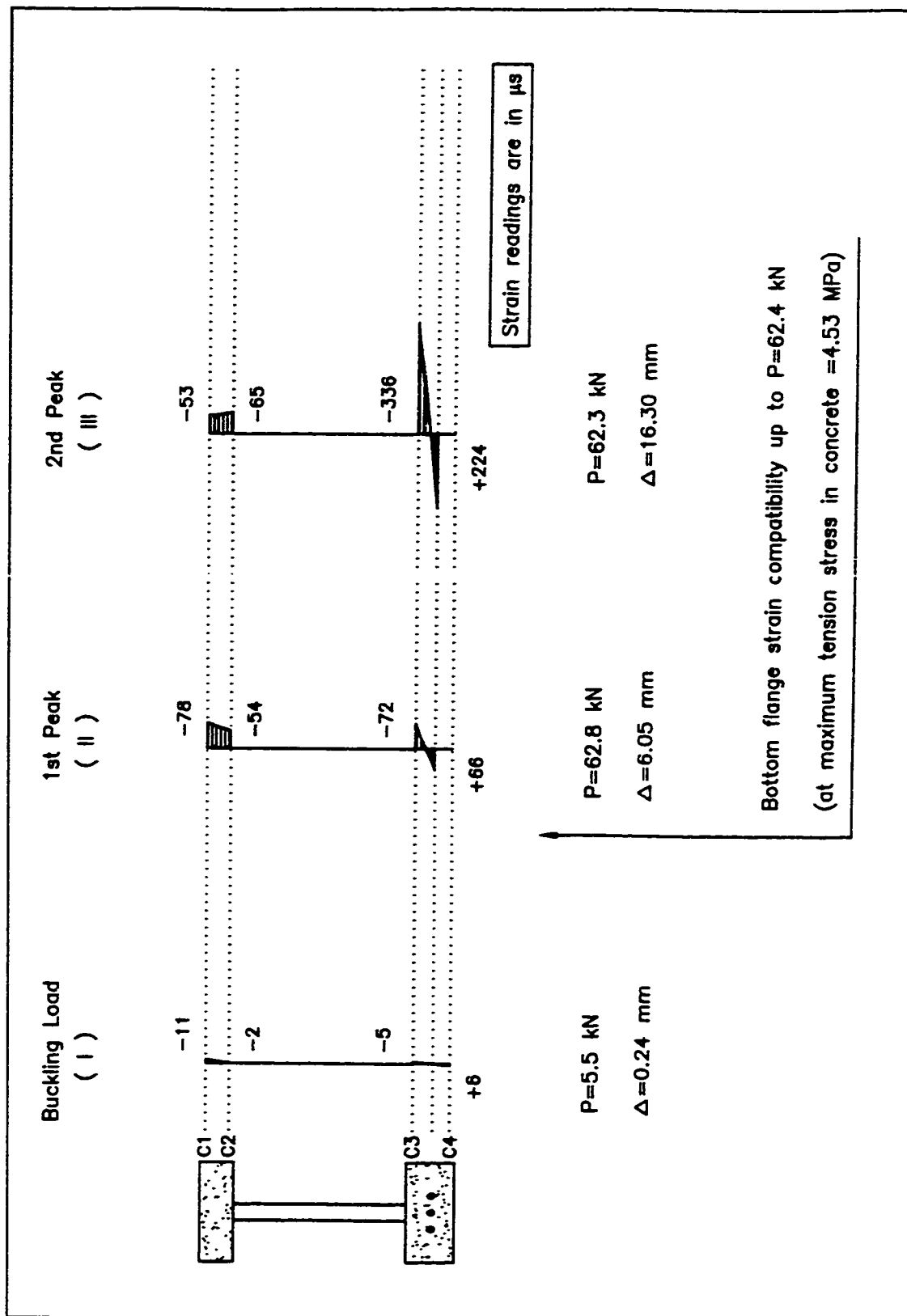


Figure 5.24 Strain profile at mid-span at different stages of loading, girder A-285

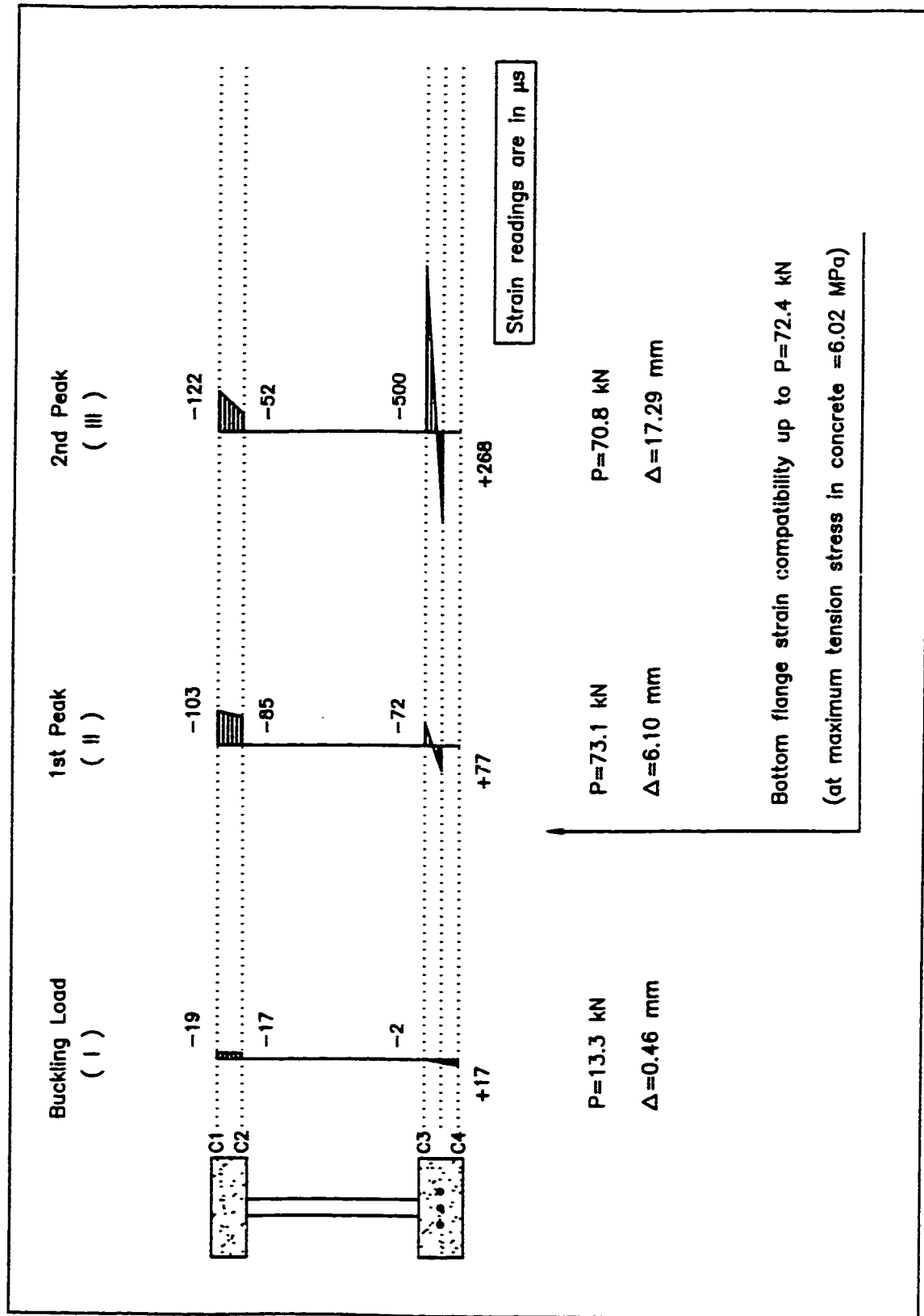


Figure 5.25 Strain profile at mid-span at different stages of loading, girder A-215

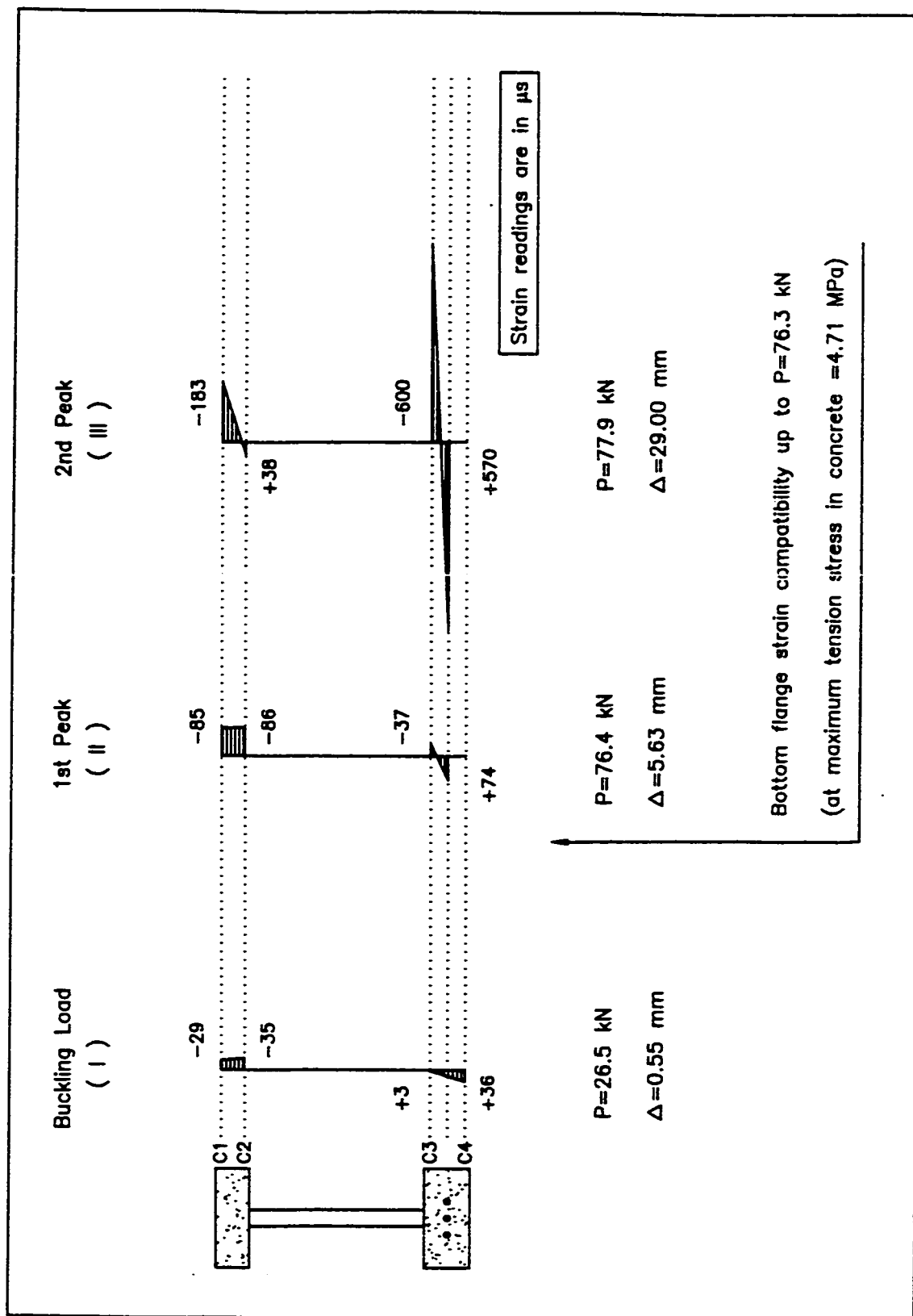


Figure 5.26 Strain profile at mid-span at different stages of loading, girder A-175

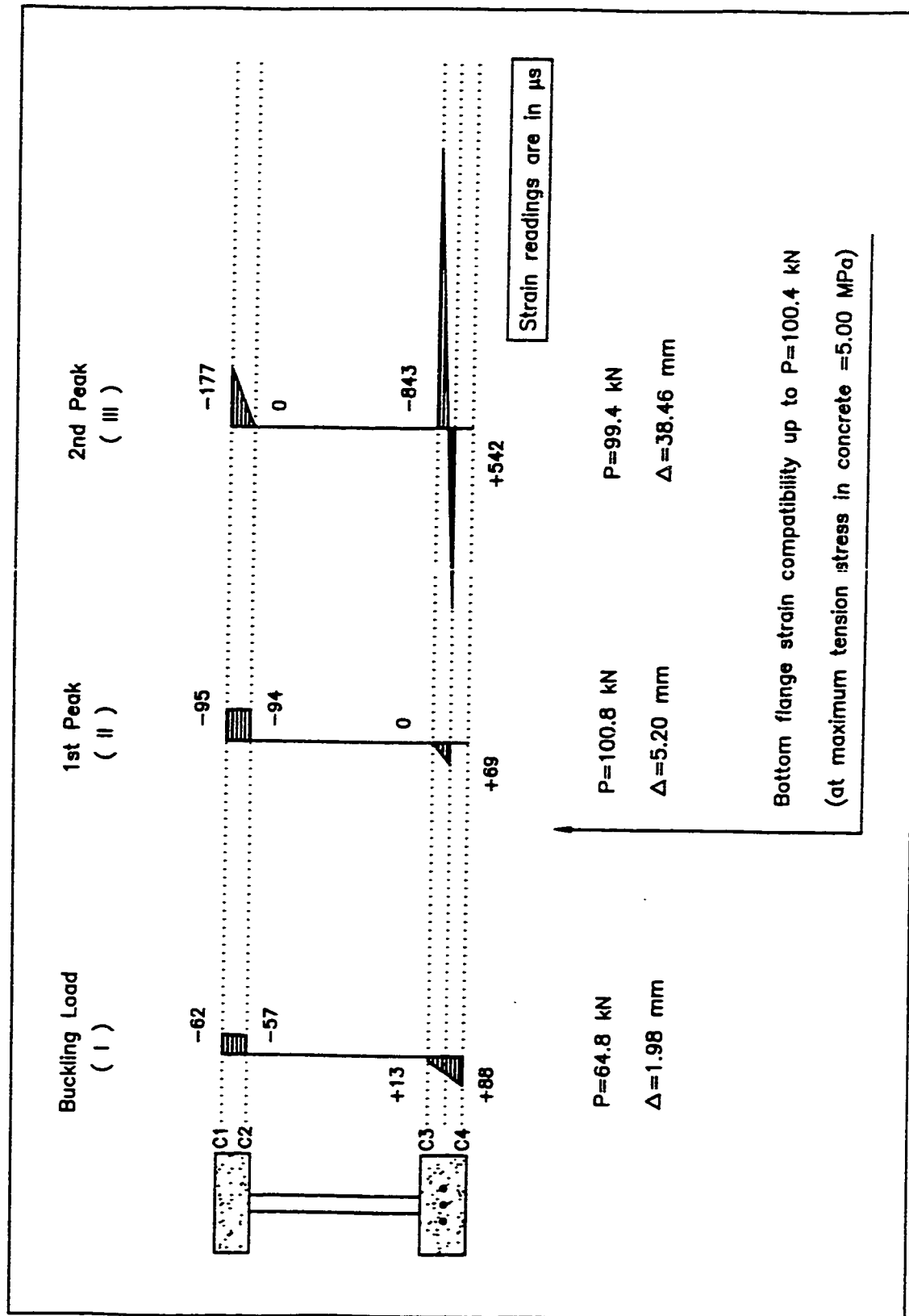


Figure 5.27 Strain profile at mid-span at different stages of loading, girder A-110

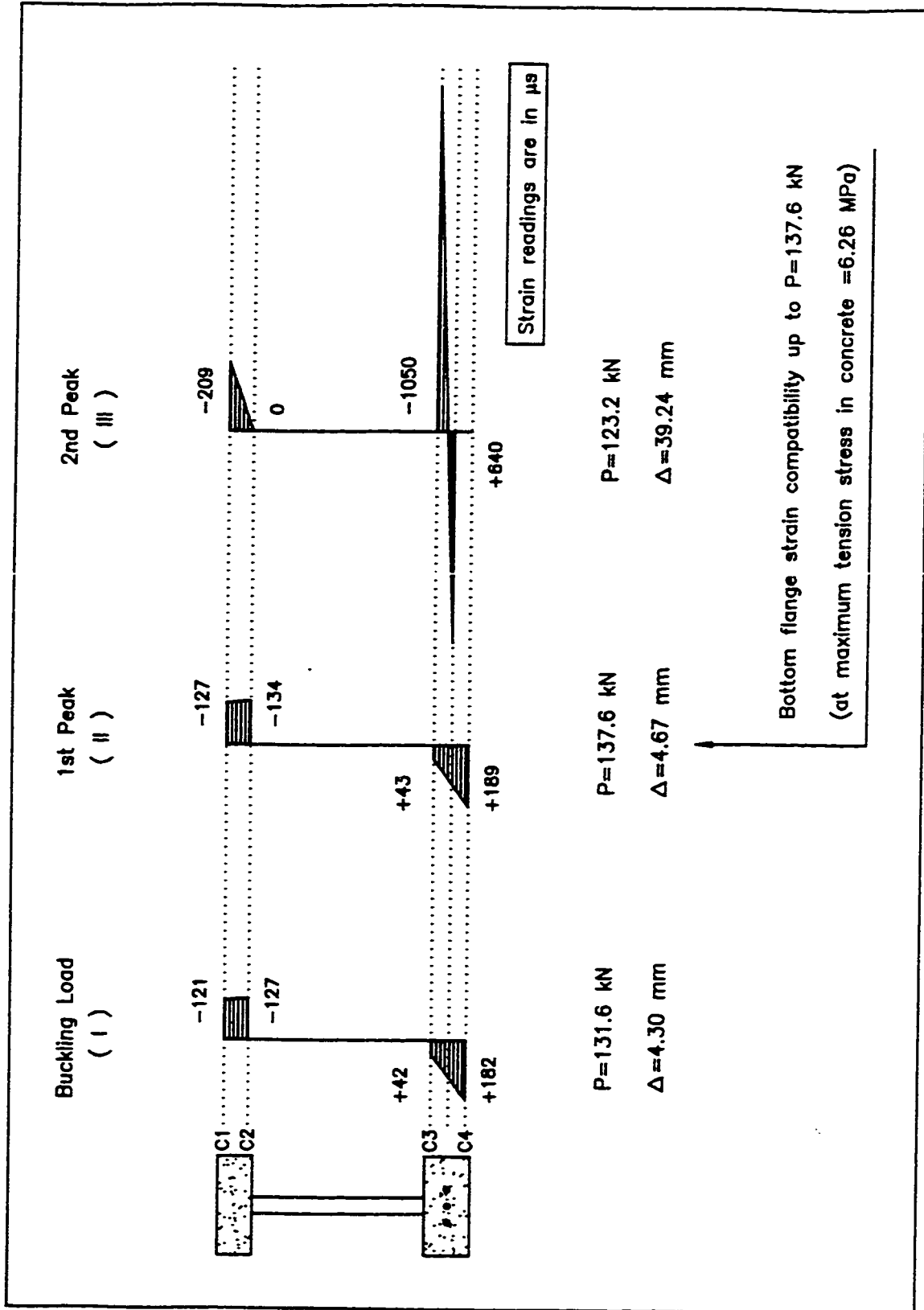


Figure 5.28 Strain profile at mid-span at different stages of loading, girder A-80

From all the above figures, the flexural behaviour is obviously going through the following stages:

(1) Up to the web buckling load

The stresses in the concrete flanges and in the strands are fairly proportional. The readings of the top flange gauges C1 and C2 show that the flange is entirely under compression. The readings of the bottom flange gauges C3 and C4 show that the flange is either entirely under tension or its top fibre is taking very small compression stresses. The readings of the concrete strains in the bottom flange and the strain in the prestressing strands show that the strain compatibility in the bottom flange is maintained during this stage.

(2) Following the web buckling and up to the first load peak

At the beginning of this stage, the stresses in the flanges and in the strands are still showing a proportional increase. Gauges C1, C2, C3 are showing a steadily increasing compression while gauge C4 and the gauges of the prestressing strands are showing a steadily increasing tension. Slightly before the end of this stage, the strains in the top flange C1 and C2 stopped increasing but maintained their compression readings until the point of the first load peak. The same thing applies to the bottom gauge of the bottom flange C4 which stopped increasing but maintained its tension reading up to the first load peak as well. Gauge C3 and the prestressing strand gauges did not stabilize but kept increasing in compression and tension respectively. Either just prior to the point of the first load peak or just after it, the tension strain readings of gauge C4 reached its cracking limit which slightly differ from one girder to the other, and the bottom flange cracked. From this point and on, the strain readings of gauge C4 were no longer compatible with those of gauge C3 and the prestressing strands' gauges. Although all girders have the same prestressing level in their bottom flanges, the cracking in that flange took place at different loads. The occurrence of the cracking was dependent on the first load peak instead of the prestressing level. This can be justified in lieu of the behaviour in the following third stage which shows that the bottom flange will, from this point on, take almost all the additional moment by itself. This means that the behaviour that these beams were



believed to show in flexure, and were designed for, was fairly correct up to this point but will no longer be maintained after it.

(3) Following the first load peak and up to the second load peak

The top flange is no longer carrying uniform compression. The bottom flange is taking almost all the additional moment through continuously increasing compression in its top fibre and continuously increasing tension in the strands.

It should be noted that the readings of the strain rosettes L1 through L4 for all three girders of phase II (see Appendix F) show almost zero horizontal membrane stresses in the corrugated web at the loading points (which is a maximum moment region) throughout the entire loading. This confirms that the web does not contribute to the flexural capacity. Therefore, the method that was used in the preliminary design of the girder in flexure is therefore fairly accurate up to the first load peak, which was previously chosen as the ultimate strength of the girder. In the ultimate limit state flexural design of such a girder, the maximum moment can be assumed to be carried by the top flange in uniform compression and by the strands in tension neglecting the tensile strength of the bottom flange. If this is applied to girders A-110 and A-80 assuming that they will be designed for a load equivalent to their first load peak, and calculating their mid-span moments as simple beams under two point loads, the uniform compressive stresses in the top flange of each girder should then be -5.5 MPa and -7.4 MPa respectively. The corresponding experimental values are -3.2 MPa and -4.4 MPa respectively. The reason of having smaller actual stresses than the calculated values (which is on the safe side) might be a consequence of having actual mid-span moments that are less than the calculated ones. The counteracting moment produced by the horizontal outward reaction forces which are acting on the top concrete flange at both loading points should reduce the actual overall moment of the girder at the mid-span. These horizontal outward reaction forces exist at the two loading points as a consequence of the tendency of the bottom flange of the transfer beam to bend outward under tension while the top concrete flange of the test girder tends to bend inward under compression.

Having studied both the shear and flexural behaviour and strengths of such a structural system, one can try to explain how the girder is still capable of taking more load after the first load peak. After this peak, which is associated with the compression buckling failure of the fold lines beneath the two loading points and in the mid-span region, the web continues to carry the additional shear according to the same load-carrying mechanism, i.e., the principal tension is anchored to the stiff concrete flanges and the stiff concrete end block while the principal compression is taken by the not failed yet fold lines in the shear-span. However, and due to the web failure in the mid-span region, each flange is now working independently and the main portion of the additional moment is taken by the bottom flange. As long as the bottom concrete flange is capable of carrying the major portion of the additional mid-span moment alone, and as long as the fold lines did not show a full collapse in the shear-span, the girder should be able to take more load.

## CHAPTER 6

### CONCLUSIONS AND RECOMMENDATIONS

#### 6.1 SUMMARY

The subject of this thesis is a research program that was planned and conducted at the University of Calgary to theoretically and experimentally investigate the strength of corrugated steel panels under different kinds of loading with a focus on the shear strength of corrugated webs in the composite girder construction. The increasing international interest in the use of corrugated panels as webs in prestressed composite bridge girders initiated the research idea. In the past twelve years, bridges with such girders were built in France, Japan, and Sweden. The available theoretical base for such an application is mainly the research that was previously conducted to investigate the shear strength of corrugated steel panels as shear diaphragm and as webs in small steel beams. Some research has recently been conducted in France and Japan to study the integrated behaviour of the new composite structural system. However, the author was not able to find any detailed published information out of these studies.

Out of the theoretical investigation, a plotting of the different governing strength modes for corrugated webs was developed. A general procedure was also developed to allow the optimum selection of the corrugation profile parameters based on *the least steel volume for a specific shear force* criterion.

The experimental part of the study involved conducting a series of tests, in two phases, on scaled prestressed concrete composite I-girders. A total of five, 5.5 m total length and 0.73 m total depth, prestressed concrete composite I-girders with custom-made corrugated steel webs have been built and statically tested under two, 210 mm wide, point loads. The zigzag web profile was chosen for the webs of the test girders due to its ease of fabrication. The webs of the five girders have the same thickness of 0.91 mm and the same corrugation angle of  $20^\circ$  with only the corrugation sub-panel (fold) width as a variable. The concrete cylinder strength for the top and bottom flanges were of average 55 MPa based on testing standard  $200 \times 100$  mm cylinders. The bottom concrete flange is prestressed with three, 13-mm diameter, 7-wire strands. A new technique of shear connector that utilizes transverse steel passing through holes in the web was used. In addition to the main investigation of the shear behaviour of the test girders, the experimental part of the program included the investigation of the flexural behaviour as well. Excellent agreement was observed between the theoretical prediction and the experimental results. The new system is clearly shown to be very light, very ductile, and the most important, structurally well predictable.

## **6.2 CONCLUSIONS**

### **6.2.1 Findings of The Theoretical Study**

- From the literature review, the shear buckling of corrugated steel panels was found to occur in either a global or a local buckling mode. The global mode involves the formation of diagonal buckles where each one crosses several corrugations. The local mode involves the formation of single diagonal buckles along each individual sub-panel. Compared with a flat plate steel web, the existence of a corrugation depth is responsible for providing higher stiffness against global buckling, while the narrow spaced fold lines that act as vertical stiffeners are responsible for providing higher stiffness against local buckling.

- The analysis of the available formula that predicts the global buckling strength of corrugated webs, using an orthotropic plate treatment, shows that a considerably higher resistance against global buckling can be provided by having only a relatively small corrugation depth. This justified a conclusion that the chosen corrugation profile, for any shear-carrying application, should have equal sub-panel widths in order to provide uniform resistance against the local buckling.
- The shear buckling of two corrugation profiles, the trapezoidal and the zigzag, was studied. A plotting of the shear buckling strength against the possible range of equal sub-panel widths that have the same thickness and corrugation angle was developed. The plotting clearly shows the existence of an intermediate region where both buckling strengths are much higher than the shear yield strength defined by the Huber-von Mises-Hencky yield criterion. It also shows that the major part of the possible range of sub-panel widths is governed by the local shear buckling mode which again justified the use of equal sub-panel widths.
- A single equation was proposed to define the shear strength of corrugated webs against both the local and the global buckling modes limited by the shear yield criterion. The equation is dependent on choosing a proper exponent  $n$  which controls the degree of transition from one limit to the other. The determination of the exponent value that simulates the actual transition was part of the experimental study. The suggested  $n$  values for the zigzag and the trapezoidal profiles are included in its findings.
- An optimization procedure that takes into account both modes of buckling as well as the shear yield limit was developed. The procedure allows one to choose the optimum corrugation profile parameters that provide the desired shear strength for the least volume of steel. The plotting of the criteria that defines the optimum corrugation profile, *the effective thickness*, against the possible range of corrugation angles shows that the shear resistance of such webs is largely insensitive to the initial imperfections in the

angle of corrugation. Almost the same shear strength and effective thickness can be achieved with profiles that have the same sub-panel width and the same thickness but corrugation angles that differ from the optimum angle in the range of about  $\pm 6^\circ$ . This also gives support to the method of analysis that assumes the corrugated webs are in a pure shear state. Even in regions where high moments exist, the accordion effect of the corrugation profile will geometrically adapt to the bending moment by increasing the corrugation angle toward the compression zone and reducing it toward the tension zone. Such a change in the corrugation angle is expected to be minimal, and should result in a negligible decrease in the shear strength. Therefore, the effect of the interaction of the moment and shear on the shear strength of such webs should be minimal and can be neglected.

### 6.2.2 Findings of The Experimental Study

- In the second phase of testing, which included the three girders with the webs of the narrowest sub-panel widths, the buckling strength of the webs was identified by three different means that showed excellent agreement among each other. All of the five webs of the five girders (with sub-panel widths of 285, 215, 175, 110, and 80 mm) were in the region that is theoretically governed by the local buckling mode with the last two webs very close to the intermediate region that is governed by the shear yield limit. A sub-panel width of 50 mm should theoretically correspond to the highest shear strength in the middle of the region governed by the shear yield. The ratio of the experimentally determined and the predicted buckling shears according to the local buckling mode ranged from 1.10 to 1.13 which gives confidence in the theoretical predictions.
- The values of the interaction exponent  $n = 2$  and  $n = 3$  were suggested for use with the trapezoidal profile and the zigzag profile respectively. This suggestion takes into account the higher resistance against global buckling that is usually provided by the trapezoidal profile which results in widening the region governed by the shear yield

limit. However, testing girders with webs whose strengths are governed by the shear yield is still needed to confirm these suggestions.

- The experimental load-deflection curves confirm the existence of a significant post-buckling shear strength, especially for webs with theoretical buckling strengths that is much lower than the shear yield limit. An almost linear load-deflection relationship was obtained up to the first load peak. The peak was followed by a dip, a second peak, a second dip, then by a continuous rise afterwards up to the termination of testing. The ductility of the girder was maintained even after high mid-span deflection was reached at the end of testing. The unloading was associated with a rapid recovery of as much as 55 % of the total mid-span deflection as was observed from the testing of the three girders of the second phase. According to the visual observations of the recovery of the two girders of the first phase of testing where the testing was terminated at smaller mid-span deflections, it can be concluded that much higher deflection recovery would be achieved if the testing was terminated just after the first load peak.
- The post-buckling contribution differed from one girder to the other depending on how close the buckling strength is to the shear yield limit. The ratios of the shear buckling to the first peak shear for the five girders A-285, A-215, A-175, A-110, and A-80 were 18 %, 26 %, 40 %, 70 %, and 96 % respectively. This means that although the optimization procedure was based on only the two buckling limits and the shear yield, and did not take into account the post-buckling strength, its results can still be very useful. With the interest focused in the intermediate zone where the shear yield governs (or even in its neighborhood from the local-buckling-governed-zone), less attention should be paid to the other regions where the post-buckling strength constitutes the major portion of the total shear strength.
- Up to the shear buckling load, the principal stresses in the web maintain a  $45^\circ$  angle to the horizontal which indicates a pure shear state. After the buckling takes place, the

angle of the principal tension becomes flatter while the perpendicular principal compression takes a steeper angle switching toward the stiff fold line. A uniform tension field takes place with the fold lines, acting as vertical stiffeners, resisting the vertical compression.

- In all five tests, the first load peak was associated with a vertical compression buckling of the lower edge of the web beneath the two point loads and extending to the girder's mid-span. This observation along with the fact that the web continued to carry more, and even higher, shear after that peak, suggests that another limit should be included in the design of such webs. The additional limit takes into account the vertical compression buckling of the fold lines. This can be compared to the design of flat plate webs where the vertical stiffeners are designed to carry the compressive load in the Pratt truss. In our corrugated web case, the vertical stiffeners are built-in, and their maximum strength should then be taken into account in the web design.
- The test A-80-b shows that the web can carry a significant amount of shear even if it is not fully connected. As long as the fold lines in the web splice region are able to act as vertical stiffeners to support the compression force, the load-carrying mechanism in both the pre-buckling and the post-buckling stages can be maintained in each individual web splice with the compression force transmitted to the fold lines of the unwelded web splice through its ends instead of through the whole web height.
- The analysis of the axial strains in both concrete flanges, prestressing strands, and in the corrugated web due to flexure clearly shows a negligible web contribution to the girder's flexural strength. Up to the first load peak, the axial compression is mainly carried by the top concrete flange while the axial tension is carried by the bottom concrete flange and the prestressing strands. After the compression buckling failure of the web in the mid-span region, the vertical movement of the top flange is not constrained to that of the bottom flange any more. The additional moment is then carried almost entirely by



the bottom flange.

- In the practical ultimate limit state design of such girders, the load corresponding to the first peak should be taken as the ultimate nominal strength. The factored ultimate strength can then be determined using a proper strength reduction factor. The flexural design can assume that the compression is entirely carried by the top flange, while the tension is entirely carried by the prestressing strands neglecting the tensile strength of the bottom flange.

### **6.3 RECOMMENDATIONS FOR FUTURE RESEARCH**

The following recommendations are suggested for future research in the corrugated web applications:

- More experimental studies are needed to confirm the suggested values for the interaction exponent. Testing of girders whose webs are governed by the shear yield is essential in such a study.
- The proposed vertical compression buckling strength of the web needs to be verified and refined using more experimental results.
- If sub-panels that have low theoretical shear buckling strengths were to be used in bridge girders, the fatigue problems due to traffic live loads need to be studied.
- A more detailed cost-efficiency study is needed for this new composite structural system. Such a study can include the costs of corrugation manufacturing, self weight of girder, required temporary and permanent supports, and girder erection and transportation. Other parameters can also be included such as the different shear connector methods, and the different material strengths.

- The new shear connector method is in need of design rules that are based on both theoretical and experimental investigations. As was mentioned in the literature review, the development of a such rules is in progress in Japan.
- The excellent ductile behaviour and the high degree of deflection recovery that were experimentally observed suggest that the more research should be conducted to investigate the different dynamic applications of such system. Composite shear walls in high risk earthquake zones might be a suitable new research topic.

## REFERENCES

1. Basler K., “ Strength of Plate Girders in Shear,” *Journal of the Structural Division*, ASCE, Vol. 87, No. ST7, October 1961, pp. 151-180.
2. Basler K., “ Strength of Plate Girders Under Combined Bending and Shear,” *Journal of the Structural Division*, ASCE, Vol. 87, No., ST7, October 1961, pp. 181-197.
3. Bergfelt, A., and Leiva-Aravena, L., *Shear Buckling of Trapezoidally Corrugated Girder Webs*, Publication S 84:2, Division of Steel and Timber Structures, Chalmers University of Technology, Göteborg, Sweden, 1984.
4. Bergfelt, A., Edlund B., and Leiva-Aravena, L., *Trapezoidally Corrugated Girder Webs – Shear Buckling, Patch Loading*, Summary Report, Division of Steel and Timber Structures, Chalmers University of Technology, Göteborg, Sweden, 1985.
5. Capra, A., and Leville, A., “ The Bridge at Dole,” *FIP Symposium, post-Tensioned Concrete Structures*, Proceedings, London, September 1996, Vol. 1, pp. 135-141.
6. Cheyrezy, M., and Combault, J., “ Composite Bridges with Corrugated steel Webs – Achievements and Prospects,” *IABSE Symposium, Mixed Structures: Including New Materials*, IABSE Reports, Brussels, 1990, Vol. 60, pp. 479-484.

7. Combault, J., "The Maupre Viaduct Near Charolles, France," *NEC/COP National Steel Construction Conference*, Proceedings, Miami Beach, 1988, pp. 12-1 – 12-22.
8. Easley, J. T., "Buckling Formulas for Corrugated Metal Shear Diaphragms," *Journal of the Structural Division*, ASCE, Vol. 101, No. ST7, July 1975, pp. 1403-1417.
9. Easley, J. T., and McFarland, D. E., "Buckling of Light-Gage Corrugated Metal Shear Diaphragms," *Journal of the Structural Division*, ASCE, Vol. 95, No. ST7, July 1969, pp. 1497-1516.
10. Elgaaly, M., and Dagher, H., "Beams and Girders with Corrugated Webs," *Annual Technical Session, Stability of Bridges*, Proceedings, Structural stability Research Council, St. Louis, Missouri, April 1990, pp. 37-53.
11. Elgaaly, M., and Seshadri, A., "Girders with Corrugated Webs Under partial Compressive Edge Loading," *Journal of Structural Engineering*, ASCE, Vol. 123, No. 6, June 1997, pp. 783-791.
12. Elgaaly, M., Hamilton, R., and Seshadri, A., "Shear Strength of Beams with Corrugated Webs," *Journal of Structural Engineering*, ASCE, Vol. 122, No. 4, April 1996, pp. 390-398.
13. Elgaaly, M., Seshadri, A., and Hamilton, R., "Beams with Corrugated Webs, Research to Practice," *Research Transformed into Practice: Implementation of NSF Research*, Proceedings, Conference sponsored by National Science Foundation, Arlington, Virginia, June 1995, pp. 601-612.

14. Elgaaly, M., Seshadri, A., and Hamilton, R., " Bending Strength of Steel Beams with Corrugated Webs," *Journal of Structural Engineering*, ASCE, Vol. 123, No. 6, June 1997, pp. 772-782.
15. Elgaaly, M., Smith, D., and Hamilton, R., " Beams and Girders with Corrugated Webs," *NSF Structures, Geomechanics, and Buildings System Grantees Conference*, Proceedings, San Juan, Puerto Rico, June 1992, pp. 126-128.
16. El-Metwally, A. S., and Loov, R. E., " Composite Girders – High Strength Concrete Combined with Corrugated Steel Webs," *International Symposium on High-Performance and Reactive Powder Concretes*, Proceedings, Sherbrooke, Quebec, Canada, August 1998, Vol. 1, pp. 197-215.
17. El-Metwally, A. S., and Loov, R. E., " Prestressed Composite Girders with Corrugated Steel Webs," *The Fifth International Conference on Short and Medium Span Bridges*, Proceedings, Calgary, Alberta, Canada, July 1998, Vol. 1, pp. 579-590.
18. Hamada, M., Nakayama, K., Kakiyama, M., Satoh, K., and Ohtake, F., " Development of Welded I-Beam with Corrugated Web," *The Sumitomo Search*, Tokyo, Japan, No. 29, 1984, pp. 75-90.
19. Hamilton, R., *Behaviour of Welded Girders with Corrugated Webs*, PhD Thesis, Department of Civil Engineering, University of Maine, Orono, Maine, 1993.
20. Hassanain, M. A., and Loov, R. E., " Optimal Design of Precast Bridge Girders Made of High-Performance Concrete," *The Annual General Meeting of Concrete Canada (The Network of Centres of Excellence on High-Performance Concrete)*, Proceedings, Moncton, New Brunswick, August 1996, pp. 115-124.

21. Heywood, P., "Corrugated Box Girder Web Lowers Bridge Weight, Cost," *Engineering News Record*, Vol. 219, No. 25, December 1987, pp. 32.
22. Honda, H., and Tanaka, H., "Mechanical Behaviour of Corrugated Web Girders by Change of Web Shape," *The New Technologies in Structural Engineering International Conference*, Proceedings, Lisbon, Portugal, July 1997, Vol. 1, pp. 397-402.
23. Hondani Bridge, *Construction Drawings*, English Version, Japan Highway Public Corporation, 1998.
24. Hussain, I. M., and Libove, C., "Stiffness Tests of Trapezoidally Corrugated Shear Webs," *Journal of the Structural Division*, ASCE, Vol. 103, No. ST7, May 1977, pp. 971-987.
25. Isiguro, W., Uehira, K., Sugo, T., and Murata, Y., "Stability of Prestressed Concrete Bridge with Corrugated Steel Web," *International Conference for Composite Construction – Conventional and Innovative*, Conference Report, Innsbruck, Australia, September 1997, pp. 205-210.
26. Johnson, R. P., and Cafolla, J., "Corrugated Webs in Plate Girders for Bridges," *Structures and Buildings*, The Institution of Civil Engineers, Vol. 123, May 1997, pp. 157-164.
27. Johnson, R. P., and Cafolla, J., "Fabrication of Steel Bridge Girders with Corrugated Webs," *The Structural Engineer*, Vol. 75, No. 8, 15 April 1997, pp. 133-135.

28. Johnson, R. P., and Cafolla, J., "Local Flange Buckling in Plate Girders with Corrugated Webs," *Structures and Buildings*, The Institution of Civil Engineers, Vol. 123, May 1997, pp. 148-156.
29. König, G., and Zink, M., "New Bridges for High-Speed Trains," *The Concrete Across Borders International Conference*, Proceedings, Odense, Denmark, June 1994, Vol. II, pp. 477-486.
30. König, G., Duda, H., and Zink, M., "Novel and Advanced Applications of Prestressed Concrete in Bridges," *Spannbetonbau in der Bundesrepublik Deutschland 1990-1994*, Deutscher Beton-Verein E. V., pp. 71-76.
31. Lebon, J. D., "Steel Corrugated Web Bridges – First Achievement," *The Fifth International Conference on Short and Medium Span Bridges*, Proceedings, Calgary, Alberta, Canada, July 1998, Vol. 1, pp. 101-111.
32. Lebon, J. D., and Leveille, A., "The Dole Bridge," *XII FIP Congress*, National Report, Washington D. C., 1994, pp. 353-357.
33. Leiva-Aravena, L., "Buckling of Trapezoidally Corrugated Webs," *ECCS Colloquium on Stability of Plates and Shell Structures*, Proceedings, University of Ghent, Belgium, April 1987, pp. 107-116.
34. Leiva-Aravena, L., *Buckling and Strength of Corrugated Steel Panels*, Thesis for The Degree of Licentiate of Engineering, Division of Steel and Timber Structures, Chalmers University of Technology, Göteborg, Sweden, 1987.

35. Leiva-Aravena, L., *Trapezoidally Corrugated Panels – Buckling Behaviour Under Axial Compression and Shear*, Publication S 87:1, Division of Steel and Timber Structures, Chalmers University of Technology, Göteborg, Sweden, 1987.
36. Linder, J., “ Lateral Torsional Buckling of Beams with Trapezoidally Corrugated Webs,” *The Fourth International Colloquium on Stability of Steel Structures*, Proceedings, Budapest, Hungary, 1990, pp. 305-308.
37. Linder, J., “ Shear Capacity of Beams with Trapezoidally Corrugated Webs and Openings,” Proceedings, Structural Stability Research Council, Chicago, 1991, pp. 403-412.
38. Loov, R. E., “ A General Stress-Strain Curve for Concrete, Implications for High Strength Concrete Columns,” *Annual Conference of The Canadian Society for Civil Engineering*, Proceedings, Vancouver, British Columbia, 1991, pp. 302-311.
39. Loov, R. E., *A General Stress-Strain Curve for Prestressing Strands*, Lecture Notes: Behaviour and Design of Prestressed Concrete Members (ENCI 637), Department of Civil Engineering, The University of Calgary, 1996.
40. Loov, R. E., and El-Metwally, A. S., “ High Strength Composite Beams with Corrugated Steel Webs,” *International Conference on High Performance High Strength Concrete*, Proceedings, Perth, Australia, August 1998, pp. 489-503.
41. Luo, R., and Edlund, B., “ Buckling Analysis of Trapezoidally Corrugated Panels Using Spline Finite Strip Method,” *Thin Walled Structures*, Vol. 18, 1994, pp.209-224.



42. Luo, R., and Edlund, B., “ Shear Capacity of Plate Girders with Trapezoidally Corrugated Webs,” *Thin Walled Structures*, Vol. 26, 1996, pp.19-44.
43. Luo, R., and Edlund, B., “ Ultimate Strength of Girders with Trapezoidally Corrugated Webs Under Patch Loading,” *Thin Walled Structures*, Vol. 24, 1996, pp.135-156.
44. Luo, R., and Edlund, B., *Numerical Simulation of Shear Tests on Plate Girders with Trapezoidally Corrugated Webs*, Publication, Division of Steel and Timber Structures, Chalmers University of Technology, Göteborg, Sweden, 1995.
45. Mo, Y., Wong, D., and Chen, C., “ Experimental Studies on Prestressed Concrete Box Bridges with Corrugated Steel Webs,” *American Concrete Institute (ACI) Convention*, Oral presentation handout, Los Angeles, October 1998.
46. Moreau, P., Thivans, P., Lacroix, R., Gesta, P., Attal, A., Mauboussin, J., Placidi, M., Marchetti, M., Virlogeux, M., Causse, G., and Calgaro, J., “ New Composite Structures – Concrete and Steel,” *The Twelfth IABSE Congress*, Proceedings, Vancouver, British Columbia, September 1984, pp. 305-312.
47. Naito, T., and Hattori, M., “ Prestressed Concrete Bridge Using Corrugated Steel Webs – Shinkai Bridge,” *XII FIP Congress*, National Report, Washington D. C., 1994, pp. 101-104.
48. Pasternak, H., and Branka, P., “ Girders with Corrugated Webs – Research, Production, Application,” *The New Technologies in Structural Engineering International Conference*, Proceedings, Lisbon, Portugal, July 1997, Vol. 1, pp. 521-526.

49. Rosignoli, M., " Prestressed Composite Girders for Highway Bridges," *Structural Engineering International*, Journal of the International Association for Bridges and Structural Engineering (IABSE), Vol. 7, No. 4, November 1997, pp. 278-283.
50. Sherman, D., and Fisher, J., " Beams with Corrugated Webs," *The First Special Conference on Cold-Formed Steel Structures*, Proceedings, University of Missouri-Rolla, August 1971, pp. 198-204.
51. Structural Stability Research Council, *Guide to Stability Design Criteria for Metal Structures*, Fourth Edition, Galambos, T. V., Editor, John Wiley & Sons, New York, 1988.
52. Tategami, H., Kajikawa, Y., Honda, H., and Uchira, K., " Dynamic Behaviour of a PC Box Girder Bridge Using a Corrugated Steel Web," *The New Technologies in Structural Engineering International Conference*, Proceedings, Lisbon, Portugal, July 1997, Vol. 2, pp. 715-722.
53. Timoshenko, S. P., and Gere, J. M., *Theory of Elastic Stability*, Second Edition, McGraw-Hill, New York, 1981.
54. Yoda, T., and Ohura, T., " Effects of Shear Connectors on Mechanical Behaviour of Composite Girders with Corrugated Steel Webs," *The Fourth Pacific Structural Steel Conference*, Proceedings, Singapore, October 1995, pp. 117-121.
55. Yoda, T., Ohura, T., and Sato, Y., " Torsional Behaviour of Composite PC Box Girders with Corrugated Steel Webs," *The Fourth ASCCS (Association for Research in Steel-Concrete Composite Structures) International Conference*, Proceedings, Kosice, Slovakia, June 1994, pp. 458-461.

56. Yoda, T., Ohura, T., and Sekii, K., " Analysis of Composite PC Box Girders with Corrugated Steel Webs," *The Fourth International Conference on Short and Medium Span Bridges*, Proceedings, Halifax, Nova Scotia, Canada, August 1994, pp. 1107-1115.
57. Yoda, T., Takeshitax, A., Sato, K., Sakurada, M., Shiga, H., and Nakasu, K., " Fatigue Tests of a New Type of Shear Connectors in a Composite Girder with a Corrugated Steel Web," *The Fifth International Conference on Short and Medium Span Bridges*, Proceedings, Calgary, Alberta, Canada, July 1998, Vol. 3, pp. 1651-1658.

## ***APPENDIX A***

### **Mathcad Worksheet for Calculating The Shear Strength of Trapezoidally Corrugated Webs in Composite Girders**

\*\*\*\*\*

This worksheet computes the shear strength of a **TRAPEZOIDALLY** corrugated web in a **COMPOSITE GIRDER** based on the different buckling modes and the yield strength. The worksheet considers only a trapezoidal profile that has a constant sub-panel width. The equations are those mentioned in chapter 3.

\* Eight input values are required:

- (1) The material properties of the web  $E$  ,  $F_y$  ,  $\nu$
- (2) The following geometrical properties of the corrugated profile  $h$  ,  $w$  ,  $\theta$
- (3) Two interactive buckling exponents  $n$  ,  $m$  (just to compare results)

\* The program will calculate and plot the different buckling strengths (as shear stress  $\tau$  and as shear force  $V$  on the Y-axis) against possible sub-panel widths  $a$  (on the X-axis).

\*The output values will also be saved as an ASCII text file in the same directory where this worksheet is stored. The results can then be plotted using other software.

+ The input data used below are those shown in figure 3.5.

\*\*\*\*\*

TOL=0.0001      ORIGIN=1

\*\*\*\*\*

### INPUT DATA

$E := 200000$	$F_y := 350$	$\nu := 0.30$	* All input data should be in: N , mm , MPa , degrees
			* $h$ should be a multiple of 10
$h := 1700$	$w := 9$	$\theta := 37$	* $\theta$ should be in the range (1° ...90°)
			* Do not make changes to the worksheet beyond this separator line
$n := 1$	$m := 2$		

\*\*\*\*\*

### VARIABLES

$$N := \frac{h}{10} \quad i = 1..N \quad a_i := 10 \cdot i$$

### SHEAR YIELD CRITERION

$$\tau_{y_i} = \frac{F_y}{\sqrt{3}} \quad V_{y_i} = w \cdot h \cdot \tau_{y_i}$$

### LOCAL BUCKLING CRITERION

$$k_{l_i} := 5.34 + 2.31 \cdot \left(\frac{a_i}{h}\right) - 3.44 \cdot \left(\frac{a_i}{h}\right)^2 + 8.39 \cdot \left(\frac{a_i}{h}\right)^3 \quad \tau_{le_i} = k_{l_i} \cdot \frac{\pi^2 \cdot E}{12 \cdot (1 - \nu^2) \cdot \left(\frac{a_i}{w}\right)^2} \quad V_{le_i} = w \cdot h \cdot \tau_{le_i}$$

### GLOBAL BUCKLING CRITERION

$$k_g := 68.4 \quad s_i := 4 \cdot a_i \quad c_i := 2 \cdot a_i \cdot (1 + \cos(\theta \text{ deg})) \quad H_i := a_i \cdot \sin(\theta \text{ deg})$$

$$I_{x_i} := 2 \cdot a_i \cdot w \cdot \left( \frac{H_i}{2} \right)^2 + \frac{w \cdot H_i^3}{6 \cdot \sin(\theta \text{ deg})} \quad D_{x_i} := \frac{E \cdot I_{x_i}}{c_i} \quad D_{y_i} := \frac{c_i}{s_i} \cdot \left( \frac{E \cdot w^3}{12} \right)$$

$$\tau_{ge_i} := k_g \cdot \frac{(D_{y_i})^{0.25} \cdot (D_{x_i})^{0.75}}{w \cdot h^2} \quad V_{ge_i} := w \cdot h \cdot \tau_{ge_i}$$

### INTERACTION EQUATION

$$j := 1..2 \quad n_j := \begin{bmatrix} n \\ m \end{bmatrix} \quad \tau_{in_{i,j}} := \left[ \frac{1}{(\tau_{le_i})^{n_j}} + \frac{1}{(\tau_{ge_i})^{n_j}} + \frac{1}{(\tau_{y_i})^{n_j}} \right]^{-\frac{1}{n_j}} \quad V_{in_{i,j}} := w \cdot h \cdot \tau_{in_{i,j}}$$

\*\*\*\*\*

### DETERMINING THE MAXIMUM STRENGTH AND ITS SUB-PANEL WIDTH

For the interaction exponent n:

$$\tau_{max1} := \max(\tau_{in}^{<1>}) \quad \Pi_i := \text{if}(\tau_{in_{i,1}} - \tau_{max1} \geq 0, i, 0) \quad I := \max(\Pi) \quad V_{max1} := w \cdot h \cdot \tau_{max1}$$

Then the maximum strength is  $\tau_{max1} = 173 \text{ MPa}$  corresponding to  $V_{max1} = 2.65 \cdot 10^6 \text{ N}$   
at a sub-panel width  $a_1 = 170 \text{ mm}$

For the interaction exponent m:

$$\tau_{max2} := \max(\tau_{in}^{<2>}) \quad JJ_i := \text{if}(\tau_{in_{i,2}} - \tau_{max2} \geq 0, i, 0) \quad J := \max(JJ) \quad V_{max2} := w \cdot h \cdot \tau_{max2}$$

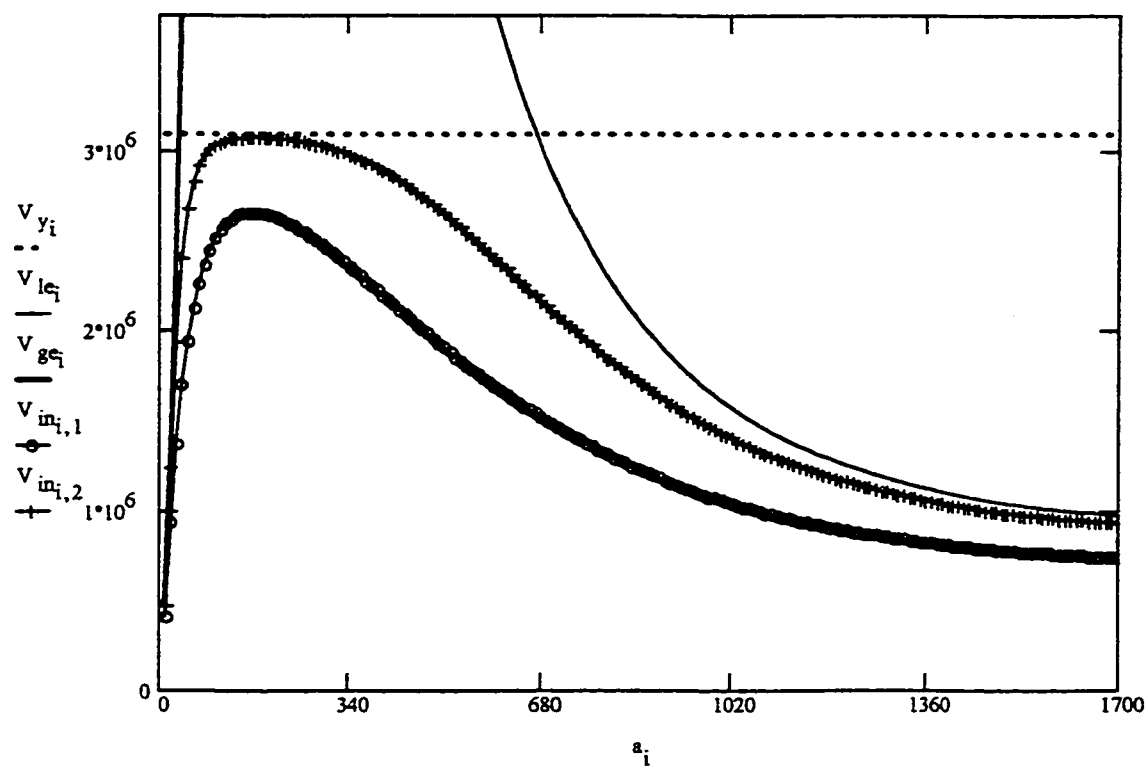
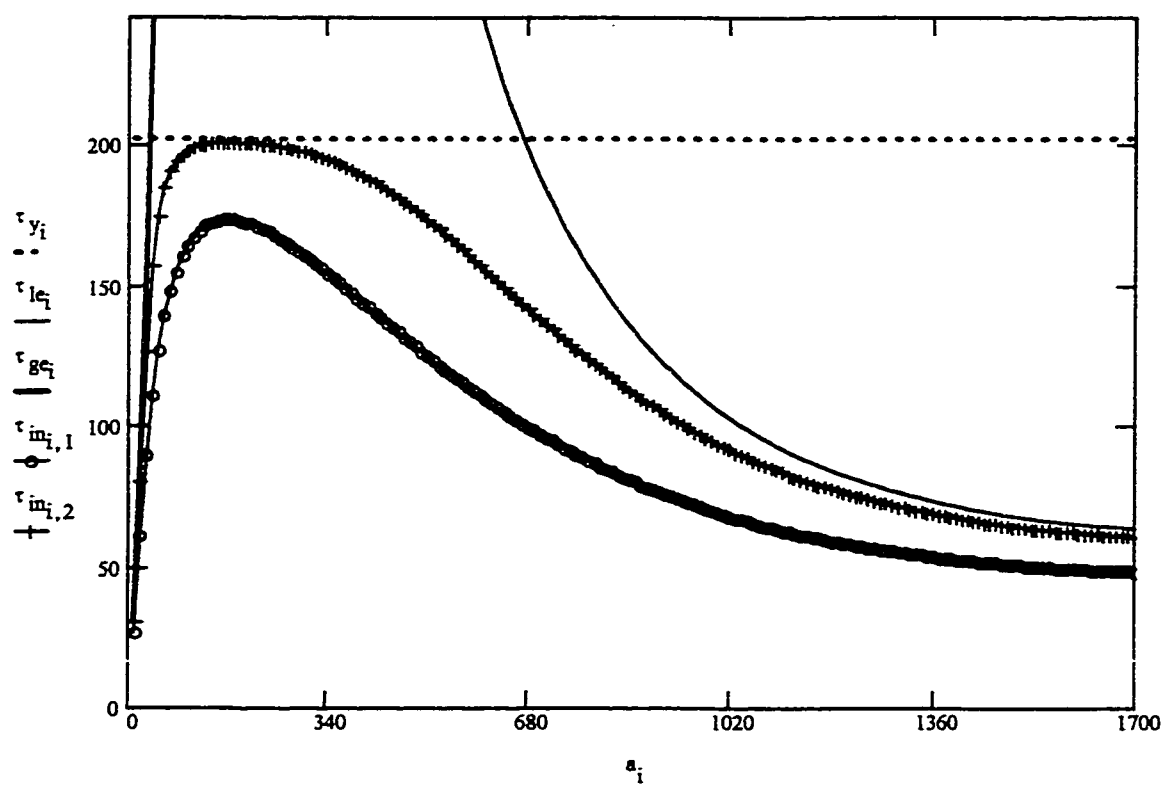
Then the maximum strength is  $\tau_{max2} = 201 \text{ MPa}$  corresponding to  $V_{max2} = 3.07 \cdot 10^6 \text{ N}$   
at a sub-panel width  $a_2 = 180 \text{ mm}$

\*\*\*\*\*

### WRITING ASCII TEXT FILE

WRITEPRN(TR) := a <sub>i</sub>	APPENDPRN(TR) := τ <sub>y<sub>i</sub></sub>
APPENDPRN(TR) := τ <sub>le<sub>i</sub></sub>	APPENDPRN(TR) := τ <sub>ge<sub>i</sub></sub>
APPENDPRN(TR) := τ <sub>in<sub>i,2</sub></sub>	APPENDPRN(TR) := V <sub>y<sub>i</sub></sub>
APPENDPRN(TR) := V <sub>ge<sub>i</sub></sub>	APPENDPRN(TR) := V <sub>in<sub>i,1</sub></sub>
	APPENDPRN(TR) := V <sub>in<sub>i,2</sub></sub>

## PLOTING RESULTS



***APPENDIX B*****Mathcad Worksheet for Calculating The Optimum  
Trapezoidally Corrugated Web Profile in Composite Girders**



\*\*\*\*\*

\*\*\*\*\*

\*\*\*\*\*

$$k_{l_i} = 5.34 + 2.31 \cdot \left(\frac{a_i}{h}\right) - 3.44 \cdot \left(\frac{a_i}{h}\right)^2 - 8.39 \cdot \left(\frac{a_i}{h}\right)^3 \quad z_i = k_{l_i} \cdot \frac{\pi^2 \cdot E}{12 \cdot (1 - \nu^2) \cdot (a_i)^2}$$

For the global buckling criterion:

$$k_g := 68.4$$

$$s_i := 4 \cdot a_i$$

$$c_{i,j} := 2 \cdot a_i \cdot (1 + \cos(\theta_j \cdot \text{deg}))$$

$$H_{i,j} := a_i \cdot \sin(\theta_j \cdot \text{deg})$$

$$x_{i,j} := \frac{E \cdot \left[ 2 \cdot a_i \cdot \left( \frac{H_{i,j}}{2} \right)^2 + \frac{(H_{i,j})^3}{6 \cdot \sin(\theta_j \cdot \text{deg})} \right]}{c_{i,j}}$$

$$y_{i,j} := \frac{E}{12} \cdot \frac{c_{i,j}}{s_i}$$

$$z_i := \frac{k_{l_i} \cdot \pi^2 \cdot E}{12 \cdot (1 - \nu^2) \cdot (a_i)^2}$$

Solve the interaction equation for  $w_{i,j}$ :

$$W_{i,j} := \text{root} \left[ V_n - \left[ \frac{1}{(w \cdot h \cdot \tau_y)^n} + \frac{1}{(w^3 \cdot h \cdot z_i)^n} + \frac{1}{\left[ \frac{k_g \cdot [(w)^3 \cdot y_{i,j}]^{0.25} \cdot (w \cdot x_{i,j})^{0.75}}{h} \right]^n} \right]^{\frac{1}{n}}, w \right]$$

Determine the corresponding effective thicknesses:

$$W_{\text{eff},i,j} := W_{i,j} \cdot \frac{s_i}{c_{i,j}}$$

\*\*\*\*\*

**DETERMINING THE OPTIMUM PROFILE PARAMETERS  $w_{\text{eff}}$ ,  $\theta$ ,  $a$ , and  $w$**

$$W_{\text{eff},\min} := \min(W_{\text{eff}})$$

*To determine the sub-panel width:*

$$W_{m_i} := \min \left[ (W_{\text{eff}}^T)^{<i>} \right] \quad \Pi_i := \text{if}(W_{\text{eff},\min} - W_{m_i} \neq 0, i, 0) \quad I := \max(\Pi)$$

*To determine the corrugation angle:*

$$W_{m_j} := \min(W_{\text{eff}}^{<j>}) \quad JJ_j := \text{if}(W_{\text{eff},\min} - W_{m_j} \neq 0, j, 0) \quad J := \max(JJ)$$

Therefore, the parameters of the optimum profile are:

$$\text{A sub-panel width} \quad a_1 = 250 \quad \text{mm}$$

$$\text{a corrugation angle} \quad \theta_j = 16 \quad \text{degrees}$$

$$\text{a plate thickness} \quad W_{I,J} = 9 \quad \text{mm}$$

$$\text{Which results in an effective plate thickness} \quad W_{\text{eff},I,J} = 9.1 \quad \text{mm}$$

\*\*\*\*\*

## WRITING ASCII TEXT FILE FOR SELECTED PROFILES

WRITEPRN(TROPT) :=  $\epsilon_j$

APPENDPRN(TROPT) :=  $W_{\text{eff}_{\text{floor}(\frac{1}{4}),j}}$

APPENDPRN(TROPT) :=  $W_{\text{eff}_{\text{floor}(\frac{1}{2.5}),j}}$

APPENDPRN(TROPT) :=  $W_{\text{eff}_{\text{floor}(\frac{1}{1.5}),j}}$

APPENDPRN(TROPT) :=  $W_{\text{eff}_{I,j}}$

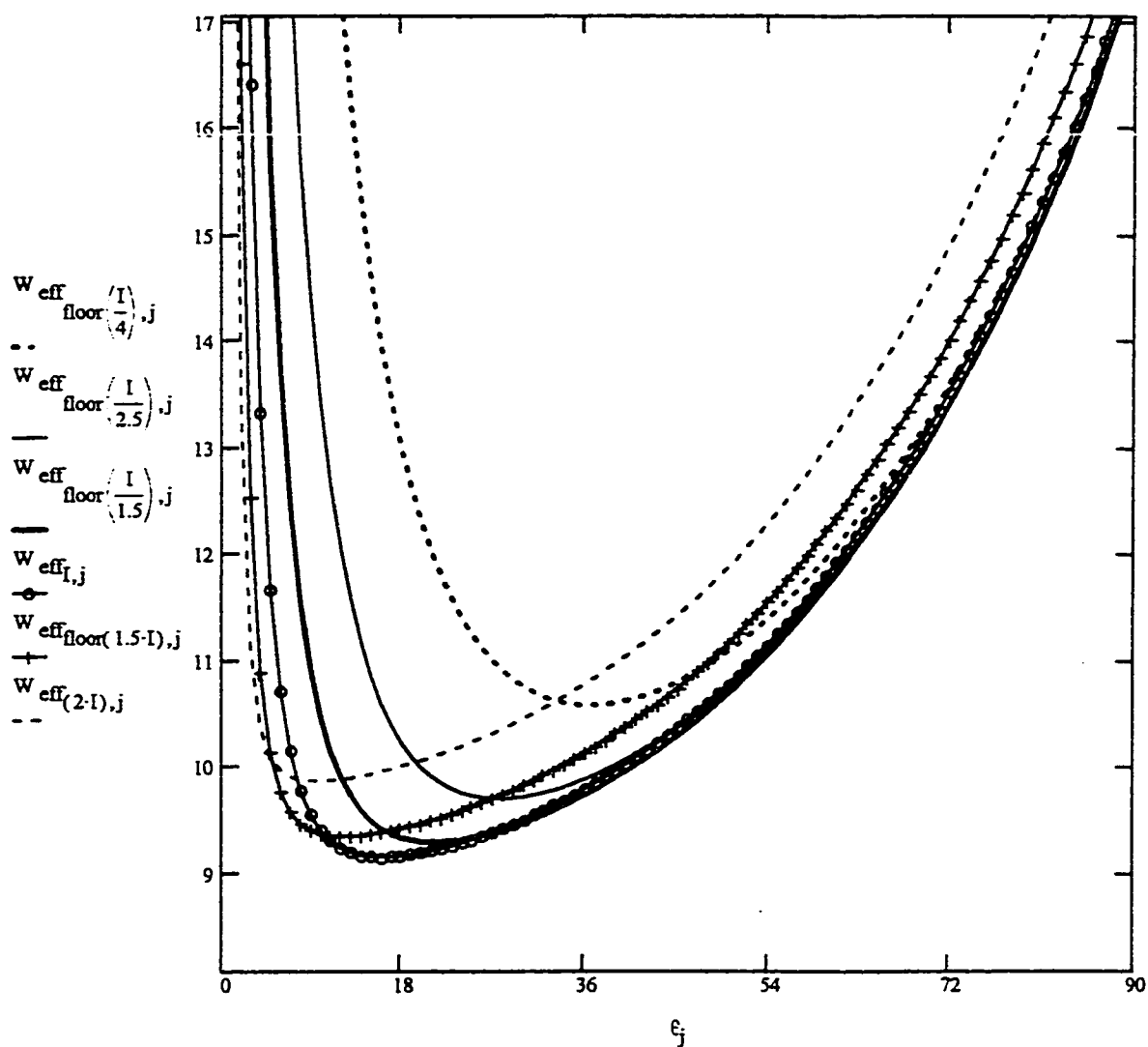
APPENDPRN(TROPT) :=  $W_{I,j}$

APPENDPRN(TROPT) :=  $W_{\text{eff}_{\text{floor}(1.5-I),j}}$

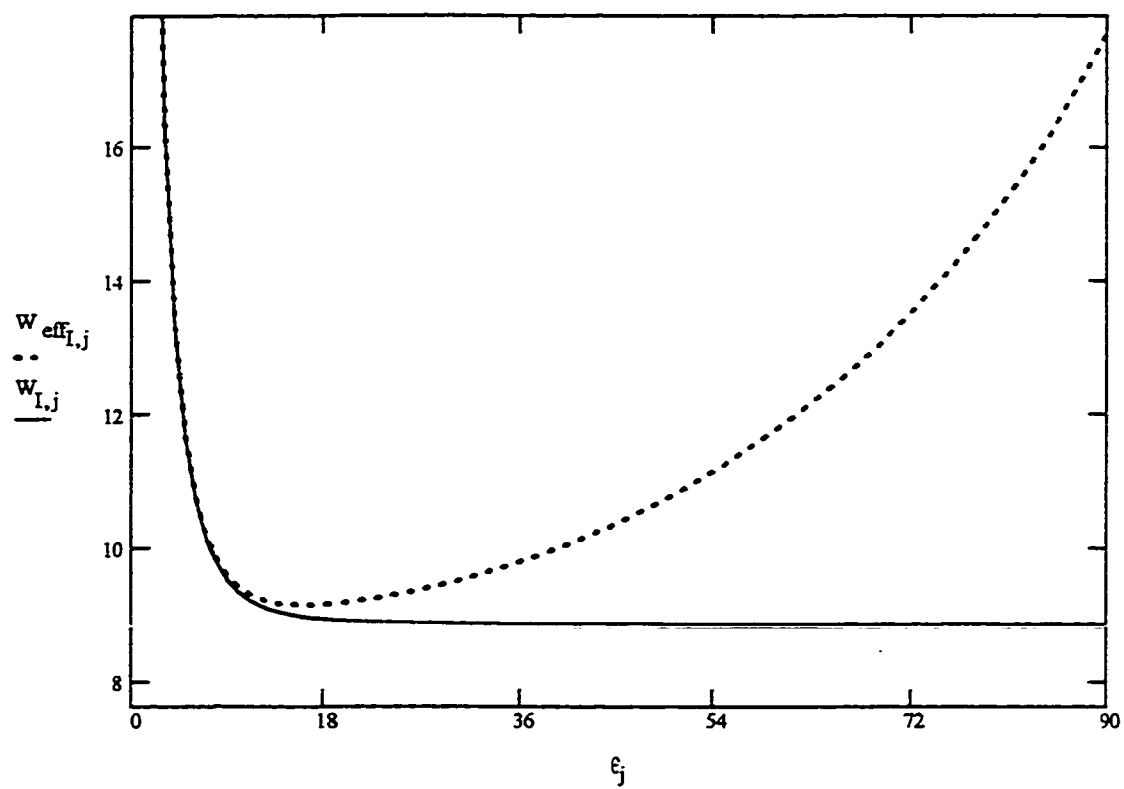
APPENDPRN(TROPT) :=  $W_{\text{eff}_{(2-I),j}}$

\*\*\*\*\*

## PLOTTING THE SELECTED COMBINATIONS



# PLOTTING $\underline{W}_{eff}$ AND $\underline{W}$ FOR THE OPTIMUM PROFILE



## ***APPENDIX C***

### **Mathcad Worksheet for Calculating The Optimum Zigzag Corrugated Web Profile in Composite Girders**

\*\*\*\*\*

This worksheet computes the thickness of **ZIGZAG** corrugated webs in **COMPOSITE GIRDERS** for all possible combinations of sub-panel widths and corrugation angles to withstand a known nominal shear force. The zigzag profile should be of constant sub-panel width. The equations are those mentioned in chapter 3.

\* Seven input values are required:

- (1) The material properties of the web  $E$ ,  $F_y$ ,  $\nu$
- (2) The web height  $h$ , the nominal design shear force  $V_n$ , and an initial input value of  $w$  for the solver to use
- (3) One interactive buckling exponents  $n$

\* The program will calculate and plot the web thickness (as  $w$  or  $w_{eff}$  on the Y-axis) against all possible corrugation angles  $\beta$  (on the X-axis). Each trace of  $w$  or  $w_{eff}$  will represent a different sub-panel width  $a$ .

\*The output values will also be saved as an ASCII text file in the same directory where this worksheet is stored. The results can then be plotted using other software.

+ The input data used below are based on the preliminary dimensioning of the test girder.

\*\*\*\*\*

TOL=0.0001      ORIGIN=1

\*\*\*\*\*

### INPUT DATA

$E = 210000$      $F_y = 350$        $\nu = 0.30$

\* All input and output are in: N, mm, MPa, Degree

\*  $h$  should be a multiple of 10

$h = 500$        $V_n = 95 \cdot 10^3$        $n = 2$        $w = 1$

\* Do not make changes to the worksheet beyond this separator line

\*\*\*\*\*

### VARIABLES

$N = \frac{h}{10}$        $i = 1..N$        $a_i = 10 \cdot i$        $j = 1..45$        $\beta_j = j$

### CALCULATIONS

For the shear yield criterion:

$$\tau_y = \frac{F_y}{\sqrt{3}}$$

For the local buckling criterion:

$$k_{l_i} = 5.34 + 2.31 \cdot \left( \frac{a_i}{h} \right) - 3.44 \cdot \left( \frac{a_i}{h} \right)^2 + 8.39 \cdot \left( \frac{a_i}{h} \right)^3$$

$$z_i = k_{l_i} \cdot \frac{\pi^2 \cdot E}{12 \cdot (1 - \nu^2) \cdot \left( \frac{a_i}{h} \right)^2}$$

For the global buckling criterion:

$$k_g = 68.4$$

$$s_i = 2 \cdot a_i$$

$$c_{i,j} = 2 \cdot a_i \cdot \cos(\beta_j \cdot \text{deg})$$

$$H_{i,j} = a_i \cdot \sin(\beta_j \cdot \text{deg})$$

$$x_{i,j} = \frac{E \cdot \left[ \frac{(H_{i,j})^3}{6 \cdot \sin(\beta_j \cdot \text{deg})} \right]}{c_{i,j}}$$

$$y_{i,j} = \frac{E}{12} \cdot \frac{c_{i,j}}{s_i}$$

$$z_i = \frac{k_{l_i} \cdot r^2 \cdot E}{12 \cdot (1 - \nu^2) \cdot (a_i)^2}$$

Solve the interaction equation for  $w_{i,j}$ :

$$W_{i,j} = \text{root} \left[ V_n - \left[ \frac{1}{(w \cdot h \cdot \tau_y)^n} + \frac{1}{(w^3 \cdot h \cdot z_i)^n} + \frac{1}{\left[ \frac{k_g \cdot [(w)^3 \cdot y_{i,j}]^{0.25} \cdot (w \cdot x_{i,j})^{0.75}}{h} \right]^n} \right]^{\frac{1}{n}}, w \right]$$

Determine the corresponding effective thicknesses:

$$W_{\text{eff},i,j} = W_{i,j} \cdot \frac{s_i}{c_{i,j}}$$

\*\*\*\*\*

**DETERMINING THE OPTIMUM PROFILE PARAMETERS  $w_{\text{eff}}$ ,  $\theta$ ,  $a$ , and  $w$**

$$W_{\text{eff},\min} = \min(W_{\text{eff}})$$

*To determine the sub-panel width:*

$$W_{m_i} = \min \left[ (W_{\text{eff}}^I)^{<I>} \right] \quad \Pi_i = \text{if}(W_{\text{eff},\min} - W_{m_i} \leq 0, i, 0) \quad I = \max(\Pi)$$

*To determine the corrugation angle:*

$$W_{m_j} = \min \left[ (W_{\text{eff}}^{<J>})^{<J>} \right] \quad JJ_j = \text{if}(W_{\text{eff},\min} - W_{m_j} \leq 0, j, 0) \quad J = \max(JJ)$$

Therefore, the parameters of the optimum profile are:

A sub-panel width  $a_I = 50$  mm

a corrugation angle  $\beta_J = 23$  Degree

a plate thickness  $W_{I,J} = 1.1$  mm

Which results in an effective plate thickness  $W_{\text{eff},I,J} = 1.2$  mm

\*\*\*\*\*

### WRITING *ASCII* TEXT FILE FOR SELECTED PROFILES

WRITEPRN(ZGOPT) :=  $\beta_j$

APPENDPRN(ZGOPT) :=  $W_{\text{eff}_{\text{floor}(\frac{I}{4}),j}}$

APPENDPRN(ZGOPT) :=  $W_{\text{eff}_{\text{floor}(\frac{I}{1.5}),j}}$

APPENDPRN(ZGOPT) :=  $W_{\text{eff}_{I,j}}$

APPENDPRN(ZGOPT) :=  $W_{I,j}$

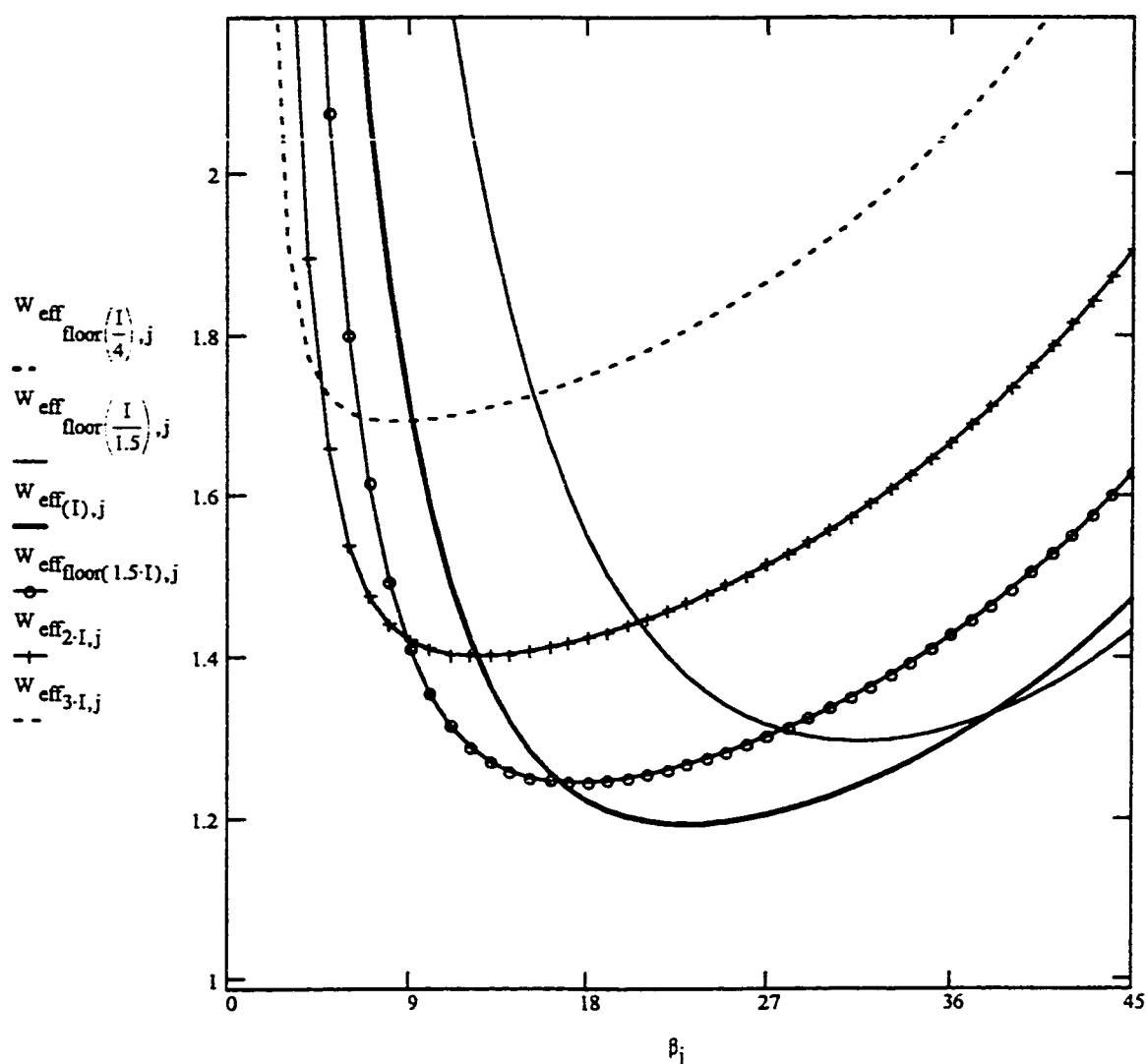
APPENDPRN(ZGOPT) :=  $W_{\text{eff}_{\text{floor}(1.5 \cdot I),j}}$

APPENDPRN(ZGOPT) :=  $W_{\text{eff}_{2 \cdot I,j}}$

APPENDPRN(ZGOPT) :=  $W_{\text{eff}_{3 \cdot I,j}}$

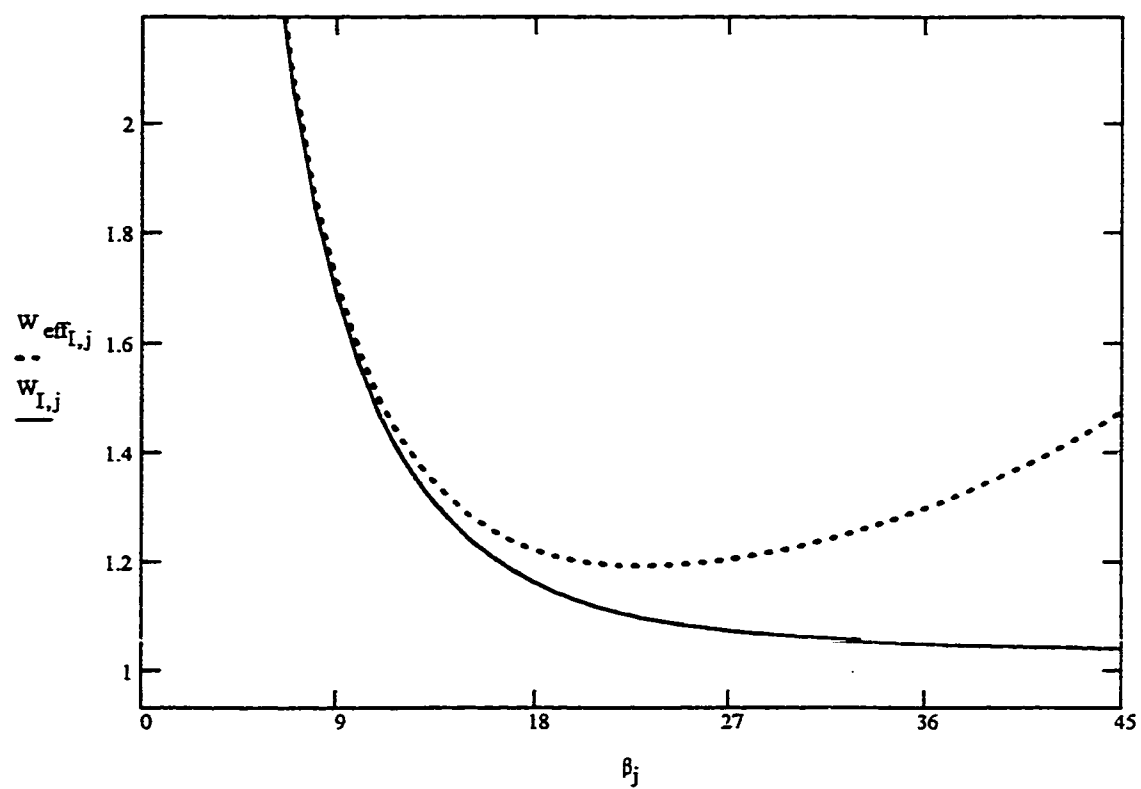
\*\*\*\*\*

### PLOTTING THE SELECTED COMBINATIONS





# PLOTTING $\underline{W}_{eff}$ AND $\underline{W}$ FOR THE OPTIMUM PROFILE



***APPENDIX D*****Mathcad Worksheet for Calculating The Shear Strength of  
Zigzag Corrugated Webs in Composite Girders**

\*\*\*\*\*

This worksheet computes the shear strength of a **ZIGZAG** corrugated web in a **COMPOSITE GIRDER** based on the different buckling modes and the yield strength of the web material. The zigzag profile should be of constant sub-panel width. The equations are those mentioned in chapter 3.

\* Eight input values are required:

- (1) The material properties of the web  $E$  ,  $F_y$  ,  $\nu$
- (2) The following geometrical properties of the corrugated profile  $h$  ,  $w$  ,  $\beta$
- (3) Two interactive buckling exponents  $n$  ,  $m$  (just to compare results)

\* The program will calculate and plot the different buckling strengths (as shear stress  $\tau$  and as shear force  $V$  on the Y-axis) against possible sub-panel widths  $a$  (on the X-axis).

\*The output values will also be saved as an ASCII text file in the same directory where this worksheet is stored. The results can then be plotted using other software.

+ The input data used below are for the webs of the test girders.

\*\*\*\*\*

TOL=0.0001      ORIGIN=1

\*\*\*\*\*

### INPUT DATA

$E = 210000$	$F_y = 350$	$\nu = 0.30$	* All input and output are in: N , mm , MPa , Degree
			* $h$ should be a multiple of 10
$h = 500$	$w = 0.91$	$\beta = 20$	* $\beta$ should be in the range (1° ...45°)
			* Do not make changes to the worksheet beyond this separator line
$n = 1$	$m = 2$		

\*\*\*\*\*

### VARIABLES

$$N = \frac{h}{10} \quad i = 1 \dots N \quad a_i = 10 \cdot i$$

### SHEAR YIELD CRITERION

$$\tau_{y_i} = \frac{F_y}{\sqrt{3}} \quad V_{y_i} = w \cdot h \cdot \tau_{y_i}$$

### LOCAL BUCKLING CRITERION

$$k_{l_i} = 5.34 - 2.31 \cdot \left(\frac{a_i}{h}\right) - 3.44 \cdot \left(\frac{a_i}{h}\right)^2 - 8.39 \cdot \left(\frac{a_i}{h}\right)^3 \quad \tau_{le_i} = k_{l_i} \cdot \frac{\pi^2 \cdot E}{12 \cdot (1 - \nu^2) \cdot \left(\frac{a_i}{w}\right)^2} \quad V_{le_i} = w \cdot h \cdot \tau_{le_i}$$

### GLOBAL BUCKLING CRITERION

$$k_g := 68.4$$

$$s_i := 2 \cdot a_i$$

$$c_i := 2 \cdot a_i \cdot \cos(\beta \cdot \text{deg})$$

$$H_i := a_i \cdot \sin(\beta \cdot \text{deg})$$

$$I_{x_i} := \frac{w \cdot (H_i)^3}{6 \cdot \sin(\beta \cdot \text{deg})}$$

$$D_{x_i} := \frac{E \cdot I_{x_i}}{c_i}$$

$$D_{y_i} := \frac{c_i}{s_i} \cdot \left( \frac{E \cdot w^3}{12} \right)$$

$$\tau_{ge_i} := k_g \cdot \frac{(D_{y_i})^{0.25} \cdot (D_{x_i})^{0.75}}{w \cdot h^2}$$

$$V_{ge_i} = w \cdot h \cdot \tau_{ge_i}$$

### INTERACTION EQUATION

$$j := 1..2 \quad n_j := \begin{bmatrix} n \\ m \end{bmatrix} \quad \tau_{in_{i,j}} := \left[ \frac{1}{(\tau_{le_i})^{n_j}} + \frac{1}{(\tau_{ge_i})^{n_j}} + \frac{1}{(\tau_{y_i})^{n_j}} \right]^{-\frac{1}{n_j}} \quad V_{in_{i,j}} = w \cdot h \cdot \tau_{in_{i,j}}$$

\*\*\*\*\*

### DETERMINING THE MAXIMUM STRENGTH AND ITS SUB-PANEL WIDTH

For the interaction exponent n:

$$\tau_{max1} := \max(\tau_{in}^{<1>}) \quad \Pi_i := \text{if}(\tau_{in_{i,1}} - \tau_{max1} \neq 0, i, 0) \quad I = \max(\Pi) \quad V_{max1} = w \cdot h \cdot \tau_{max1}$$

Then the maximum strength is  $\tau_{max1} = 92 \text{ MPa}$  corresponding to  $V_{max1} = 4.21 \cdot 10^4 \text{ N}$

at a sub-panel width  $a_1 = 50 \text{ mm}$

For the interaction exponent m:

$$\tau_{max2} := \max(\tau_{in}^{<2>}) \quad JJ_i := \text{if}(\tau_{in_{i,2}} - \tau_{max2} \neq 0, i, 0) \quad J = \max(JJ) \quad V_{max2} = w \cdot h \cdot \tau_{max2}$$

Then the maximum strength is  $\tau_{max2} = 155 \text{ MPa}$  corresponding to  $V_{max2} = 7.04 \cdot 10^4 \text{ N}$

at a sub-panel width  $a_2 = 50 \text{ mm}$

\*\*\*\*\*

### WRITING ASCII TEXT FILE

$$\text{WRITEPRN}(ZG) := a_i$$

$$\text{APPENDPRN}(ZG) := \tau_{y_i}$$

$$\text{APPENDPRN}(ZG) := \tau_{le_i}$$

$$\text{APPENDPRN}(ZG) := \tau_{ge_i}$$

$$\text{APPENDPRN}(ZG) := \tau_{in_{i,1}}$$

$$\text{APPENDPRN}(ZG) := \tau_{in_{i,2}}$$

$$\text{APPENDPRN}(ZG) := V_{y_i}$$

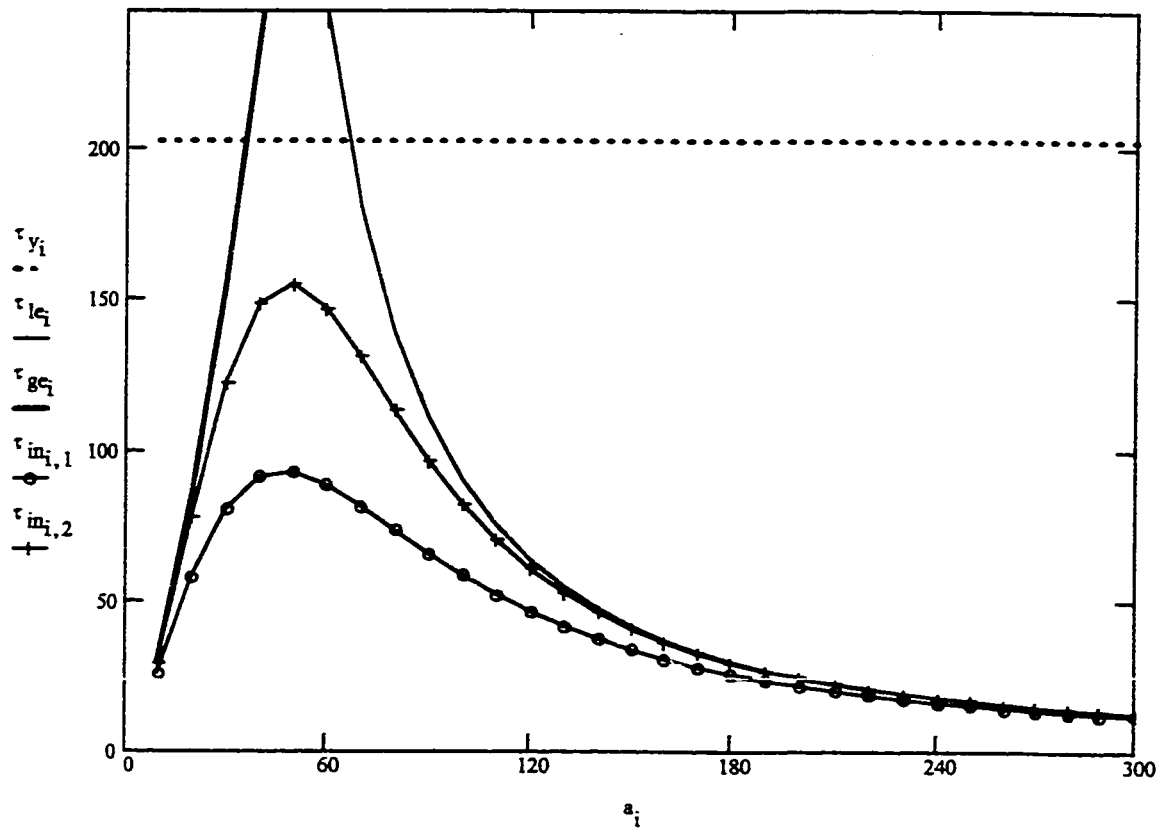
$$\text{APPENDPRN}(ZG) := V_{le_i}$$

$$\text{APPENDPRN}(ZG) := V_{ge_i}$$

$$\text{APPENDPRN}(ZG) := V_{in_{i,1}}$$

$$\text{APPENDPRN}(ZG) := V_{in_{i,2}}$$

### PLOTTING STRESS RESULTS



For the interaction exponent  $n$ :

$$\tau_{in_{28,1}} = 13 \quad \text{MPa} \qquad \tau_{in_{21,1}} = 20 \quad \text{MPa} \qquad \tau_{in_{17,1}} = 28 \quad \text{MPa}$$

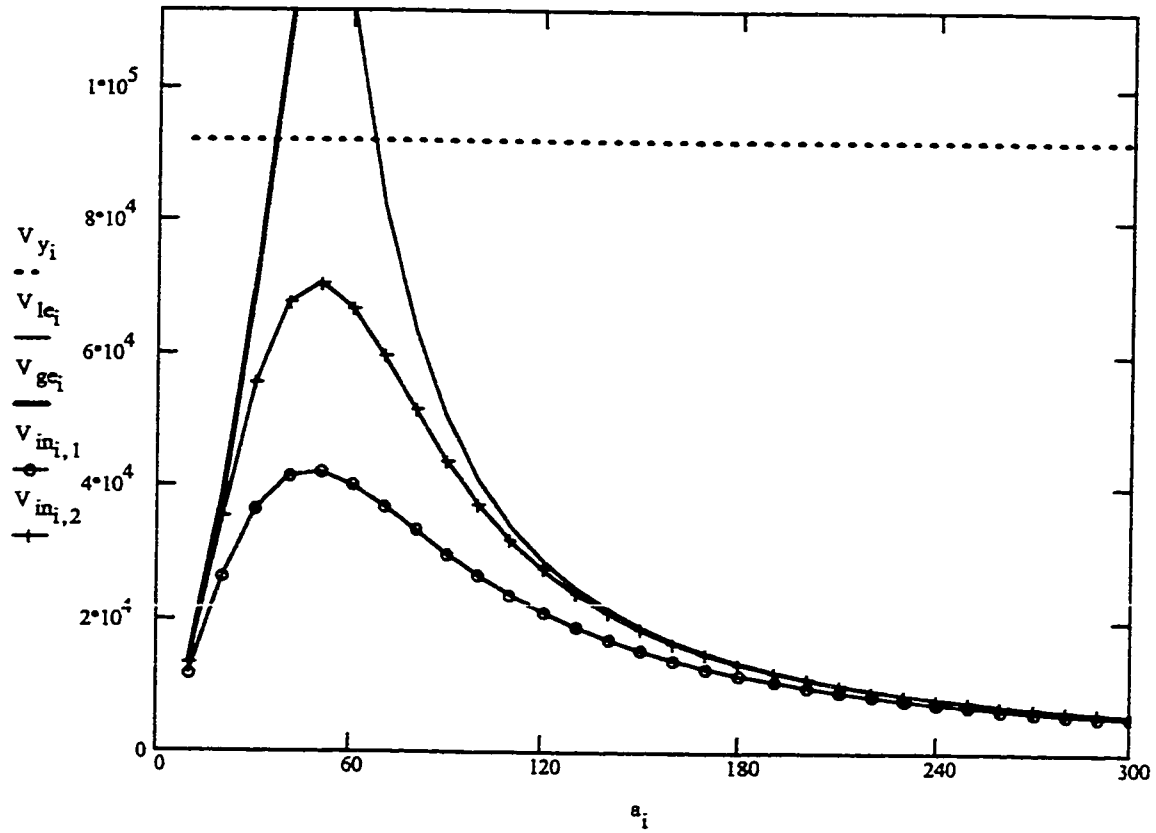
$$\tau_{in_{11,1}} = 52 \quad \text{MPa} \qquad \tau_{in_{8,1}} = 73 \quad \text{MPa}$$

For the interaction exponent  $m$ :

$$\tau_{in_{28,2}} = 14 \quad \text{MPa} \qquad \tau_{in_{21,2}} = 22 \quad \text{MPa} \qquad \tau_{in_{17,2}} = 33 \quad \text{MPa}$$

$$\tau_{in_{11,2}} = 70 \quad \text{MPa} \qquad \tau_{in_{8,2}} = 113 \quad \text{MPa}$$

# PLOTING FORCE RESULTS



For the interaction exponent  $n$ :

$$V_{in_{28,1}} = 5.98 \cdot 10^3 \quad N$$

$$V_{in_{21,1}} = 9.16 \cdot 10^3 \quad N$$

$$V_{in_{17,1}} = 1.27 \cdot 10^4 \quad N$$

$$V_{in_{11,1}} = 2.37 \cdot 10^4 \quad N$$

$$V_{in_{8,1}} = 3.34 \cdot 10^4 \quad N$$

For the interaction exponent  $m$ :

$$V_{in_{28,2}} = 6.4 \cdot 10^3 \quad N$$

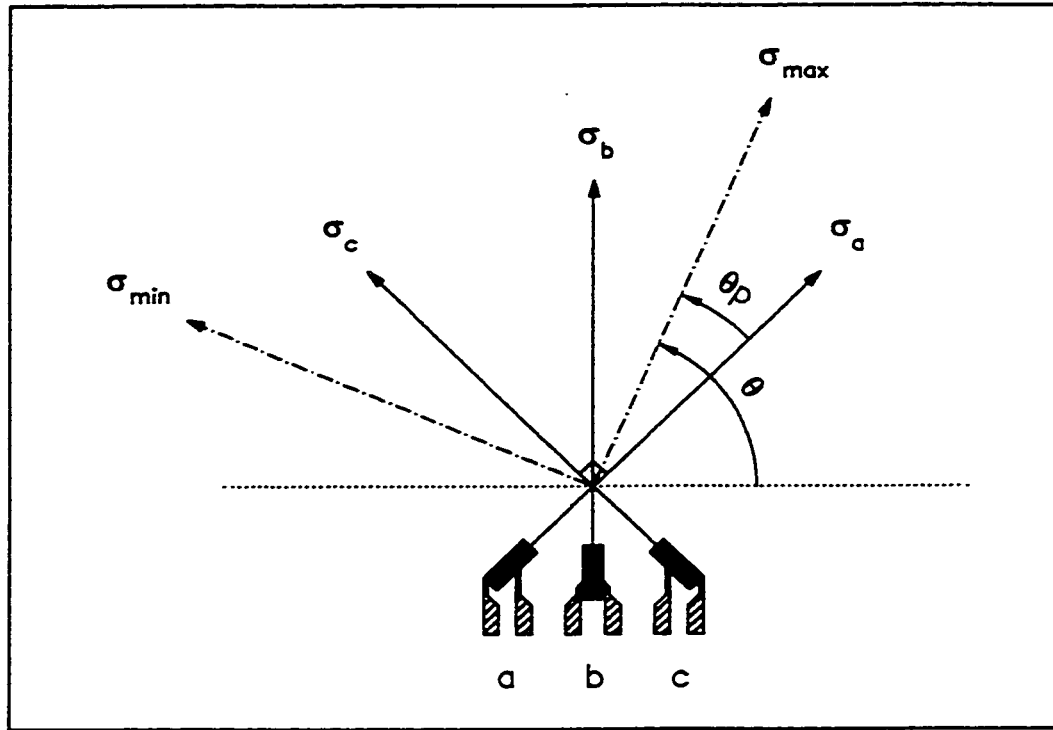
$$V_{in_{21,2}} = 1.02 \cdot 10^4 \quad N$$

$$V_{in_{17,2}} = 1.48 \cdot 10^4 \quad N$$

$$V_{in_{11,2}} = 3.19 \cdot 10^4 \quad N$$

$$V_{in_{8,2}} = 5.13 \cdot 10^4 \quad N$$

***APPENDIX E*****Stress Calculation and Transformation Formulas for  
Three-Way 45 ° Strain Rosettes**



$$\sigma_a = \frac{E}{1-\nu^2} (\varepsilon_a + \nu \varepsilon_c) \quad \text{and} \quad \sigma_c = \frac{E}{1-\nu^2} (\varepsilon_c + \nu \varepsilon_a)$$

$$\tau_{ac} = \frac{E}{2(1+\nu)} (2\varepsilon_b - \varepsilon_a - \varepsilon_c)$$

$$\sigma_{\max/\min} = \frac{\sigma_a + \sigma_c}{2} \pm \sqrt{\left(\frac{\sigma_a - \sigma_c}{2}\right)^2 + (\tau_{ac})^2}$$

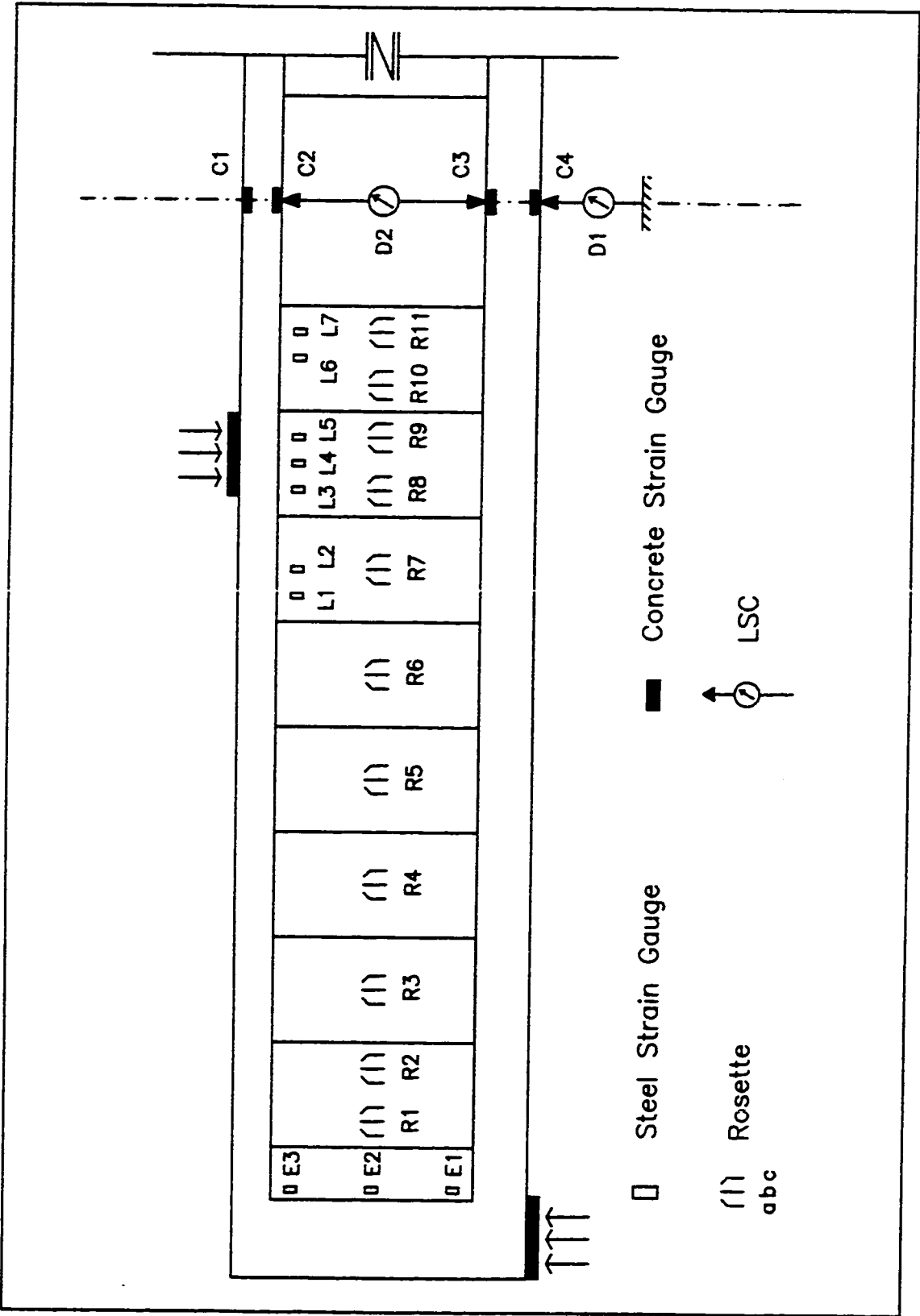
$$\text{If } \varepsilon_a \geq \varepsilon_c \quad \text{then} \quad \theta_p = \frac{1}{2} \tan^{-1} \left( \frac{2\tau_{ac}}{\sigma_a - \sigma_c} \right)$$

$$\text{If } \varepsilon_a < \varepsilon_c \quad \text{then} \quad \theta_p = \left[ \frac{1}{2} \tan^{-1} \left( \frac{2\tau_{ac}}{\sigma_a - \sigma_c} \right) \right] - \frac{\pi}{2}$$

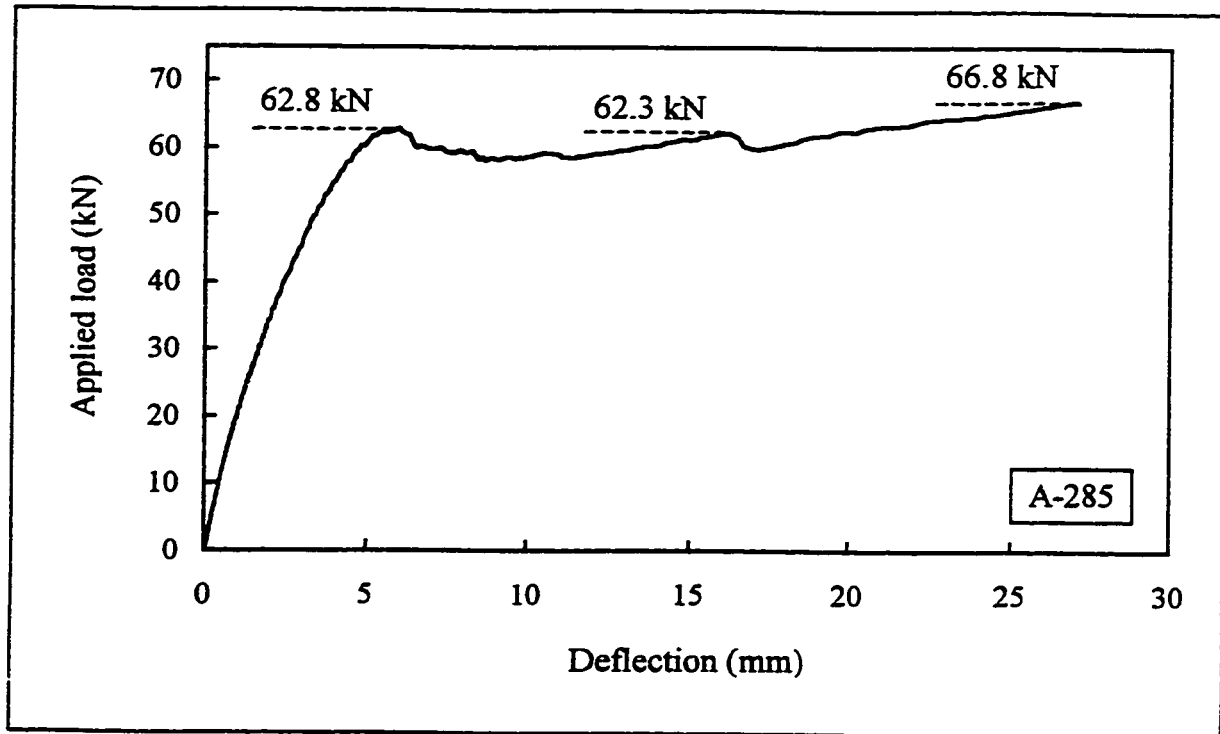
$$\tau_{\max} = \sqrt{\left(\frac{\sigma_a - \sigma_c}{2}\right)^2 + (\tau_{ac})^2}$$



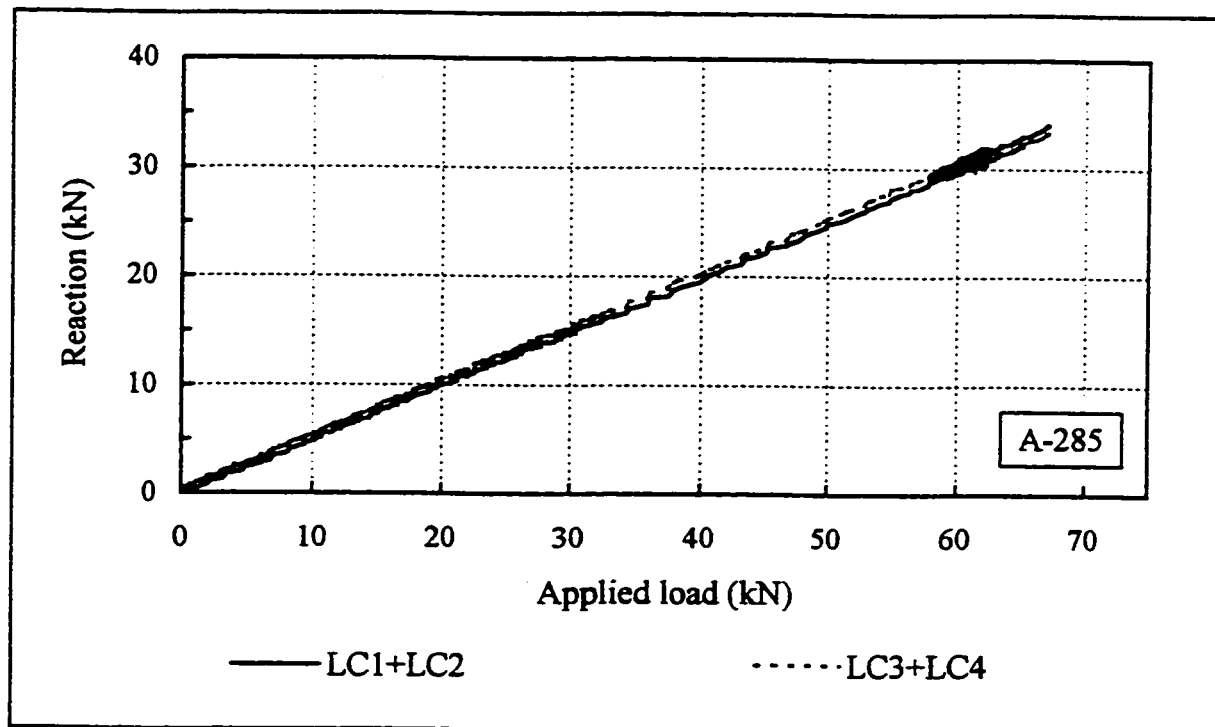
***APPENDIX F*****Complete Experimental Results**



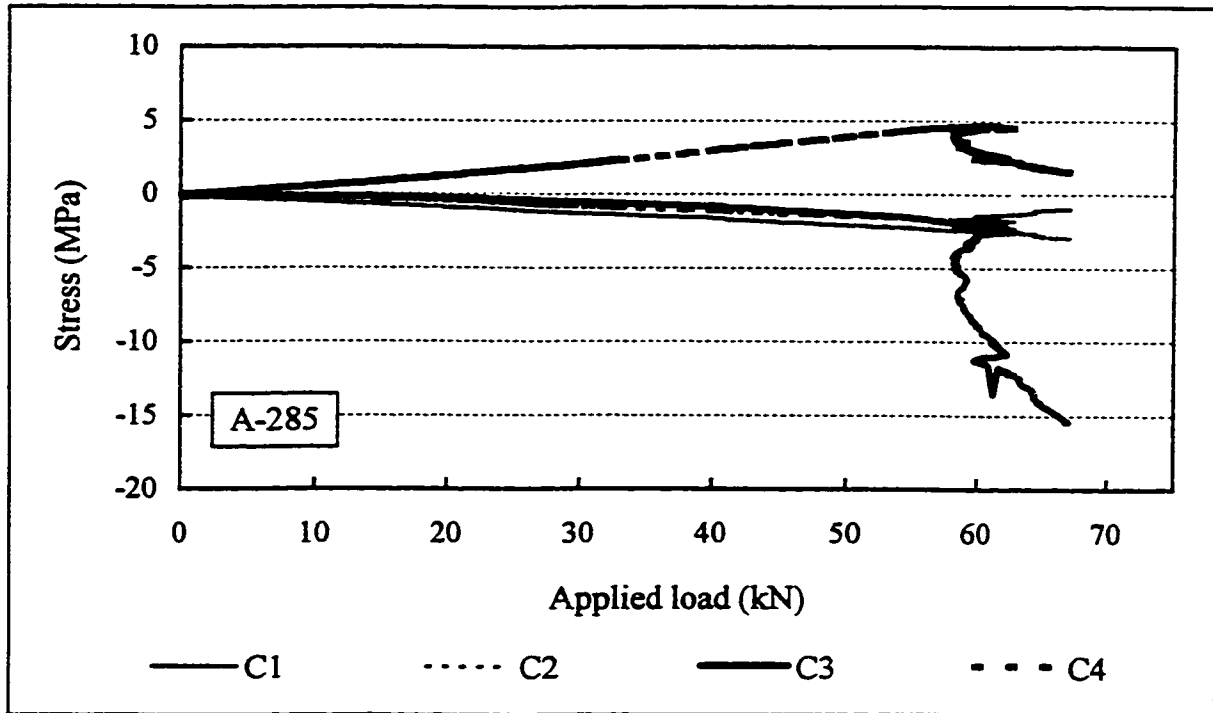
Instrumentation details, girders A-285 and A-215

**Results : Girder A-285**

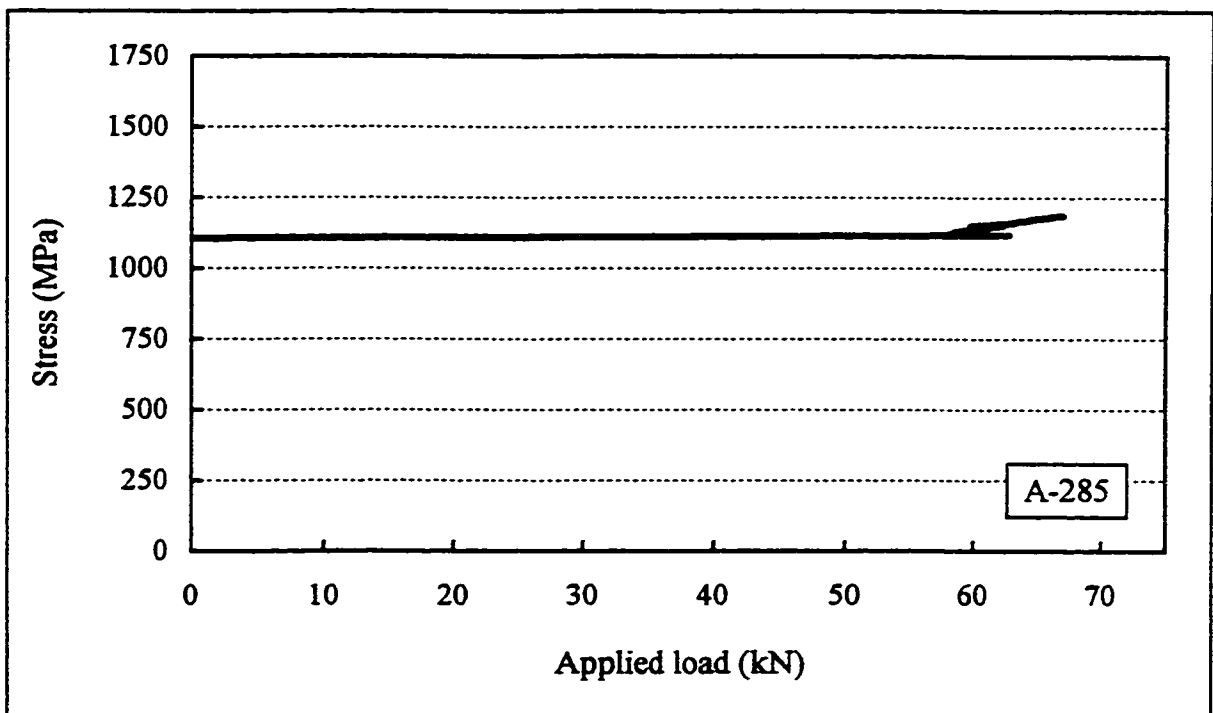
Applied load vs mid-span vertical deflection



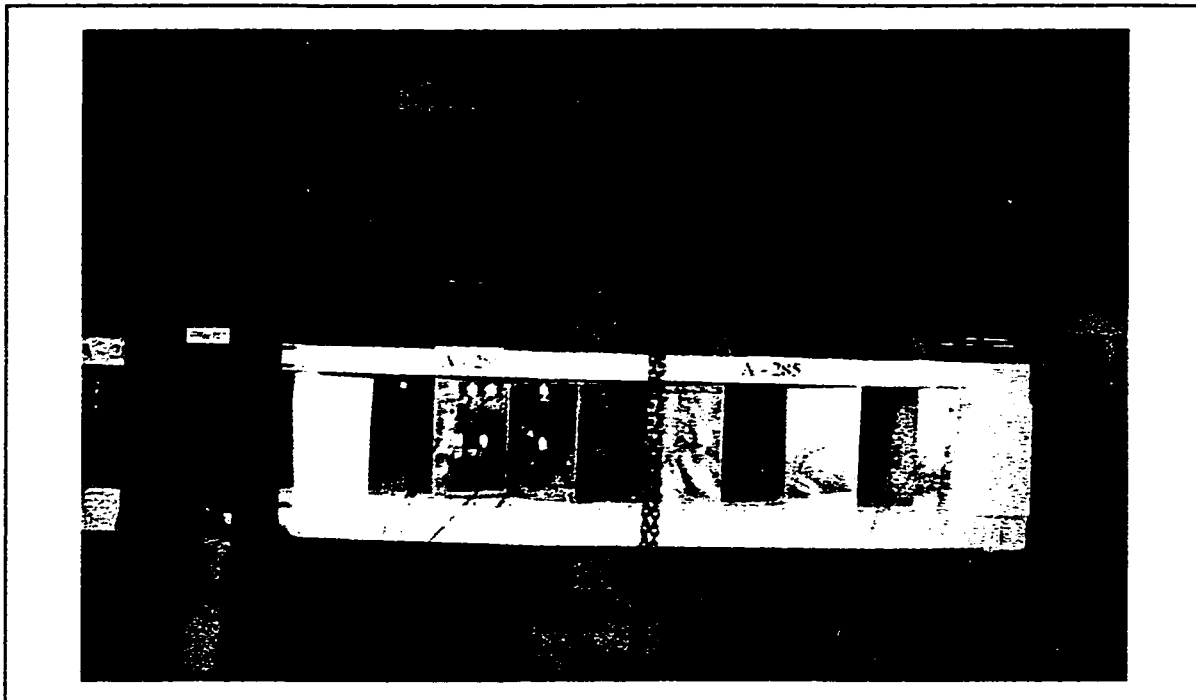
Applied load vs load cells' reactions



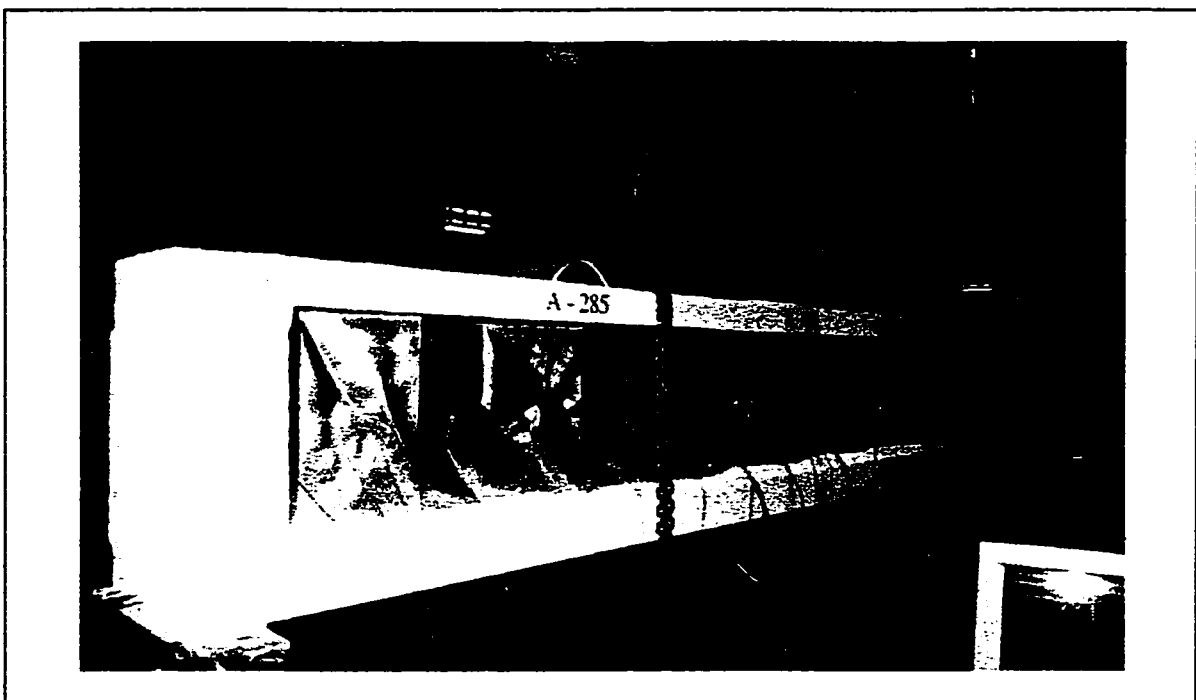
Applied load vs stresses in concrete flanges



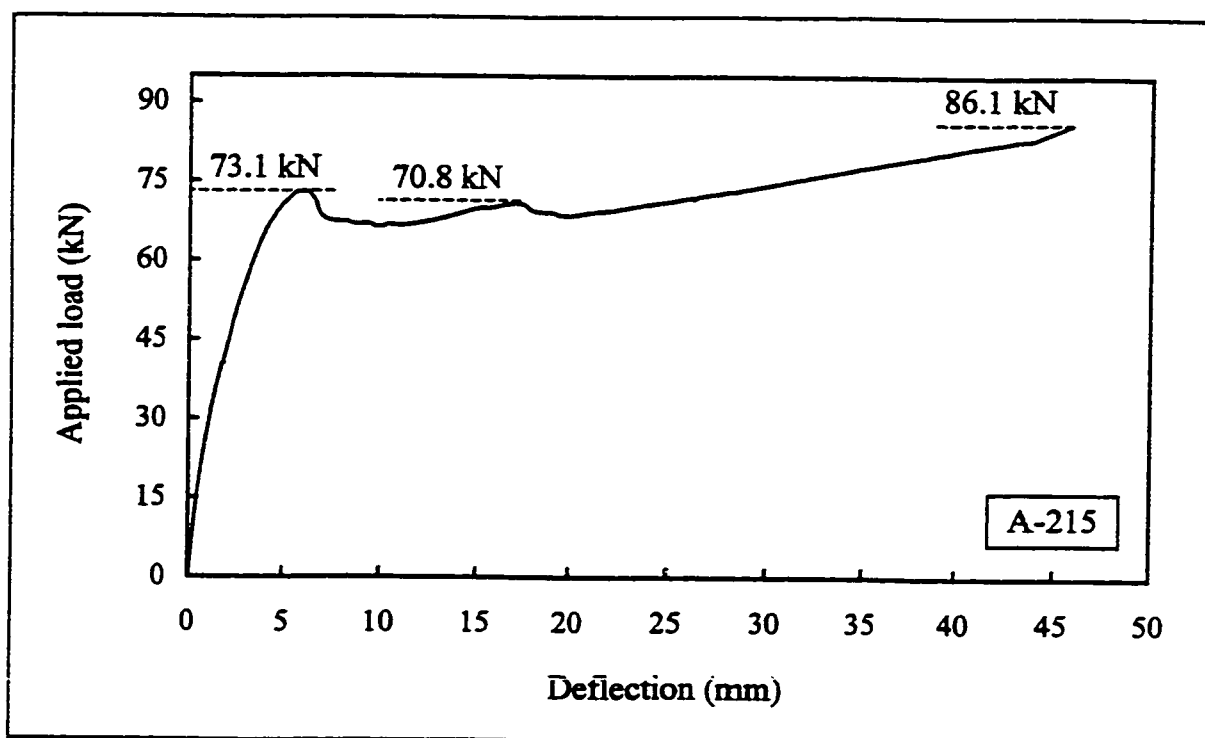
Applied load vs average stress in prestressing strands



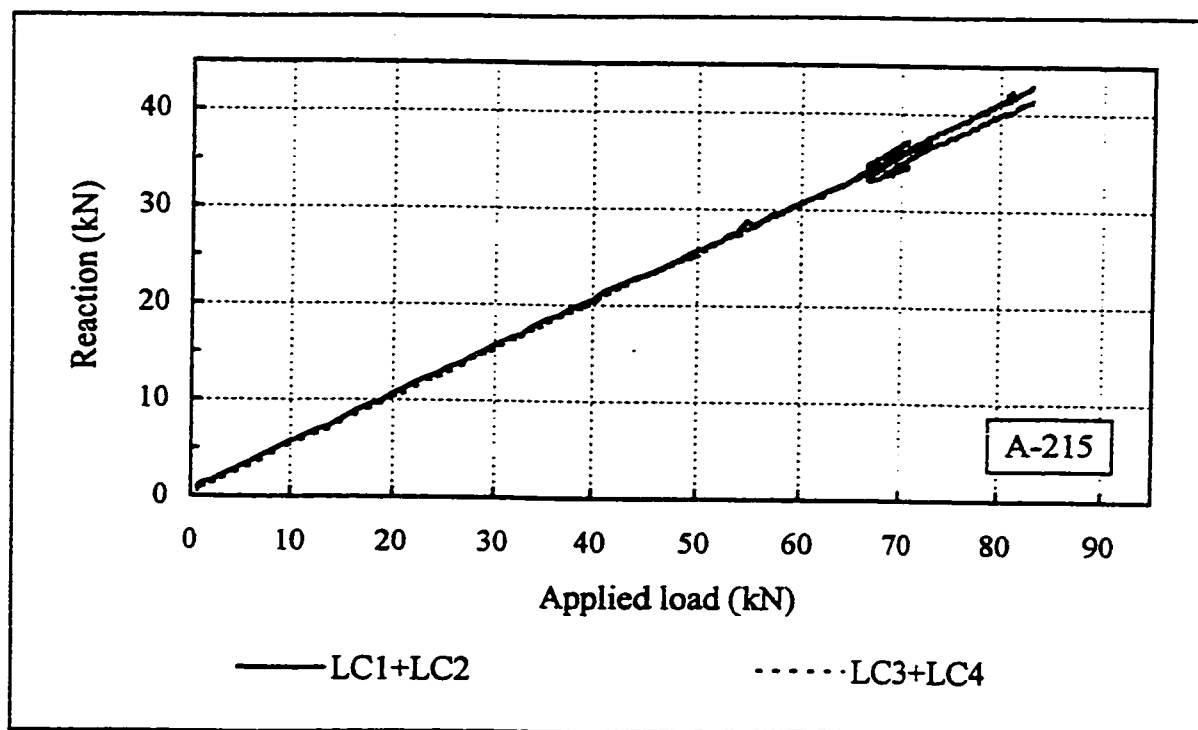
Girder A-285 before testing



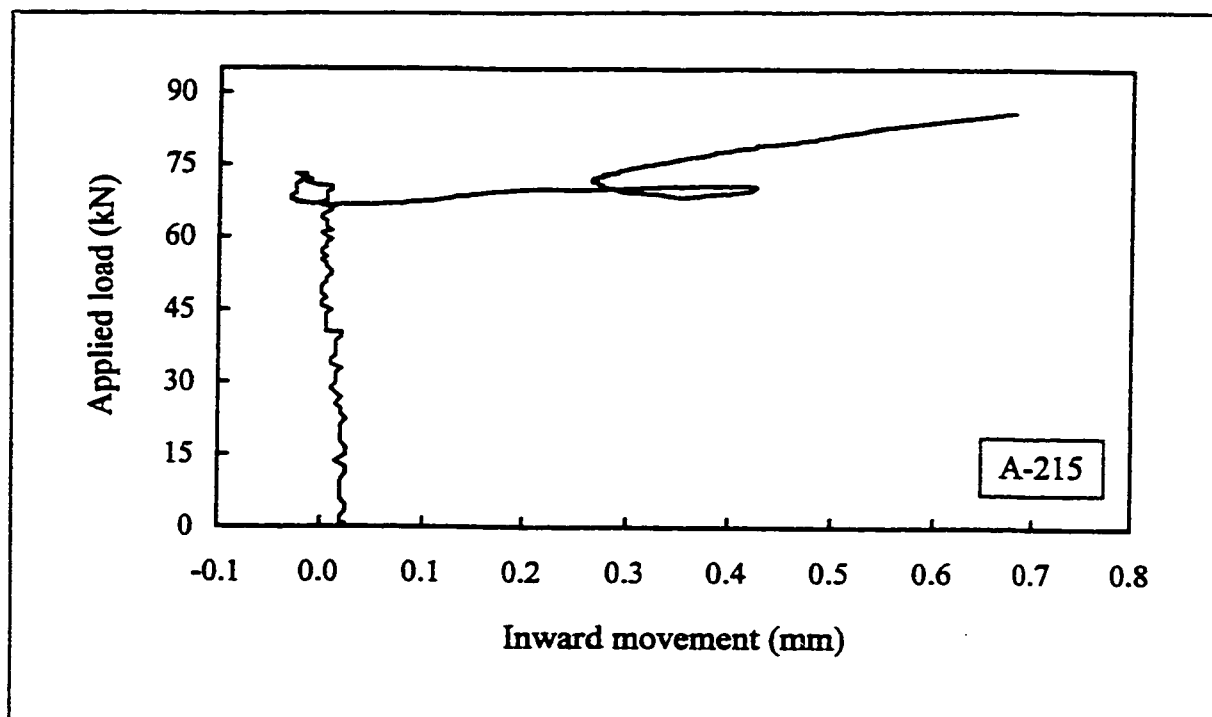
Girder A-285 after testing

**Results : Girder A-215**

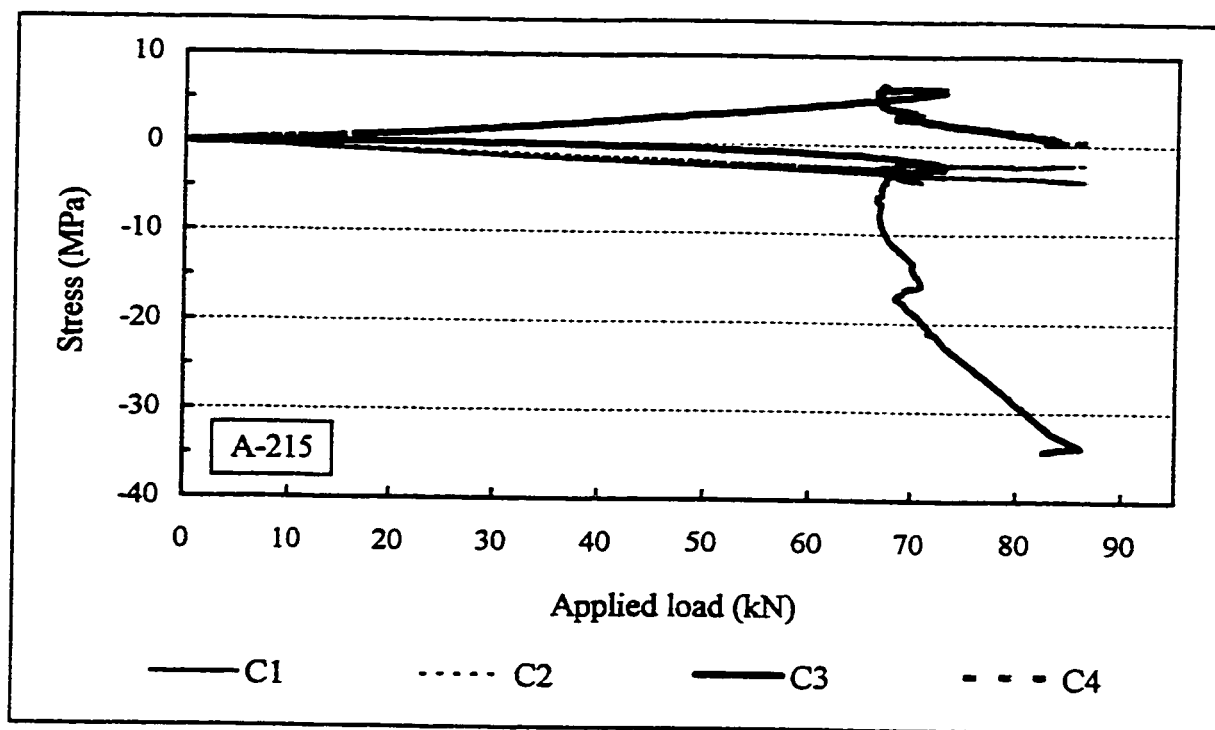
Applied load vs mid-span vertical deflection



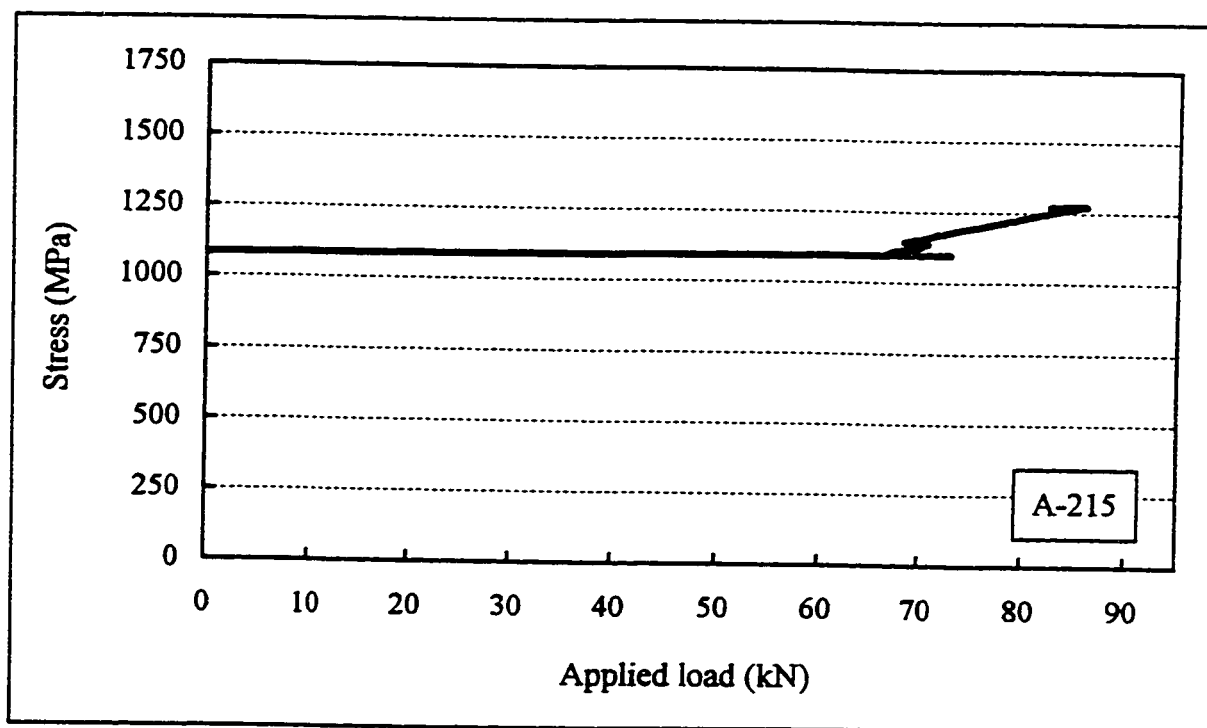
Applied load vs load cells' reactions



Applied load vs relative inward movement of flanges at mid-span

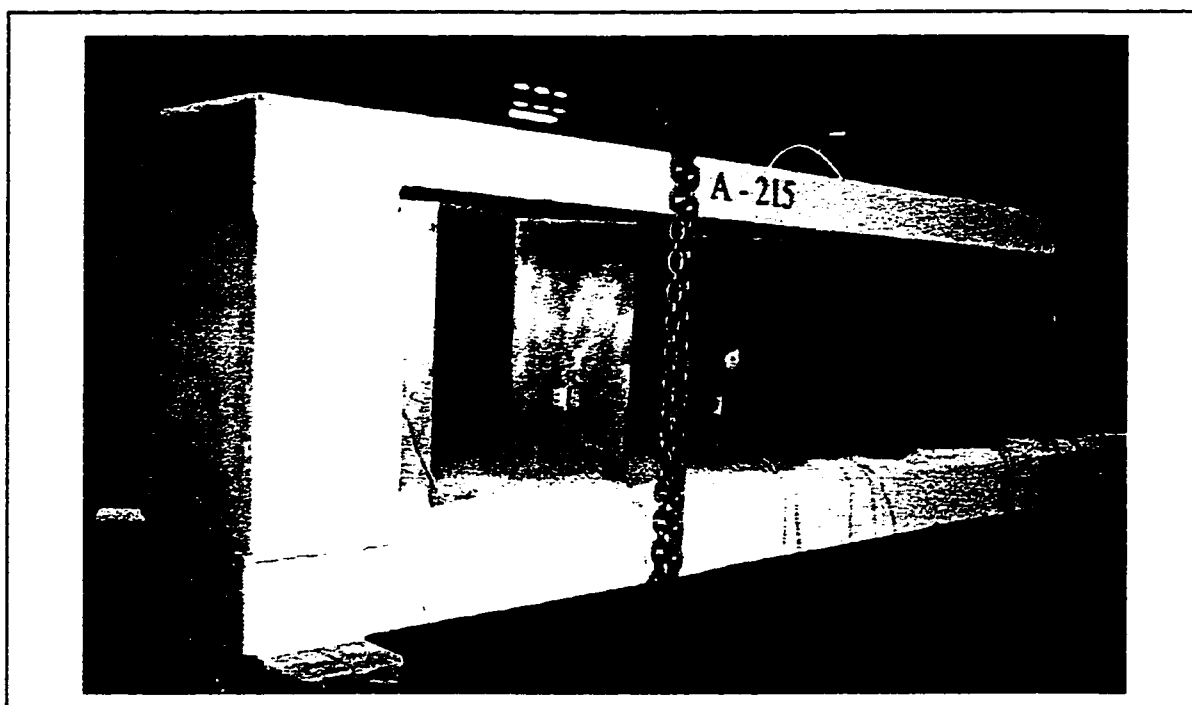


Applied load vs stresses in concrete flanges

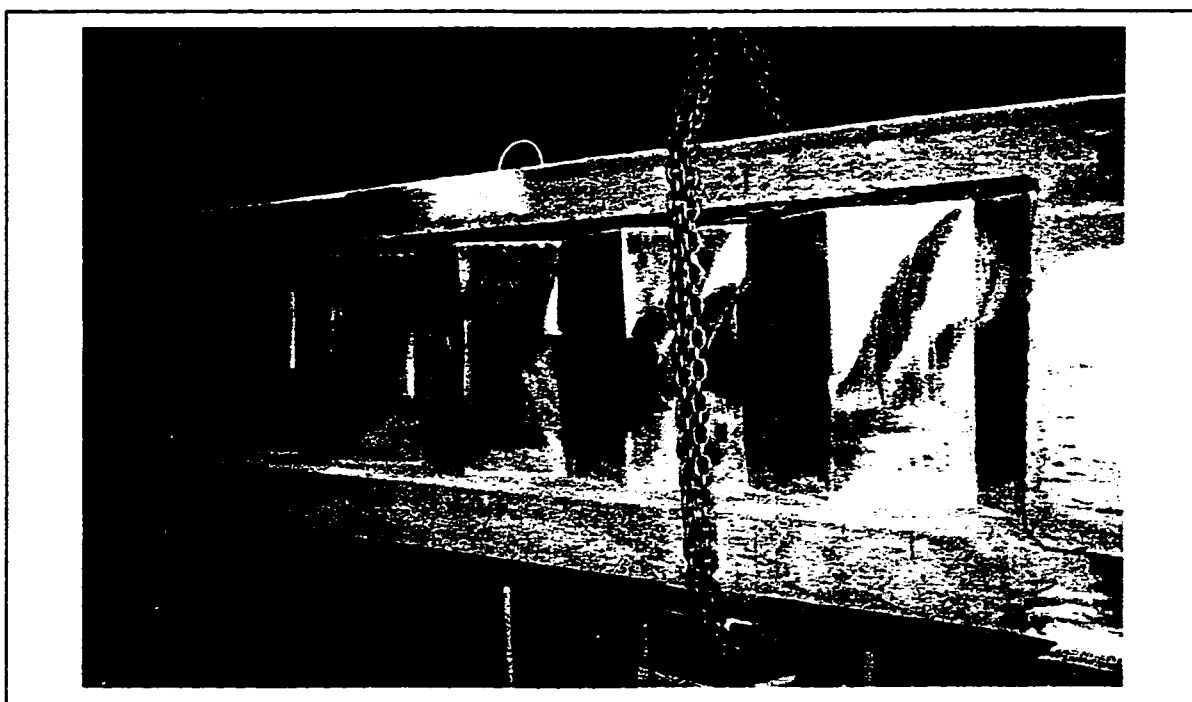


Applied load vs average stress in prestressing strands

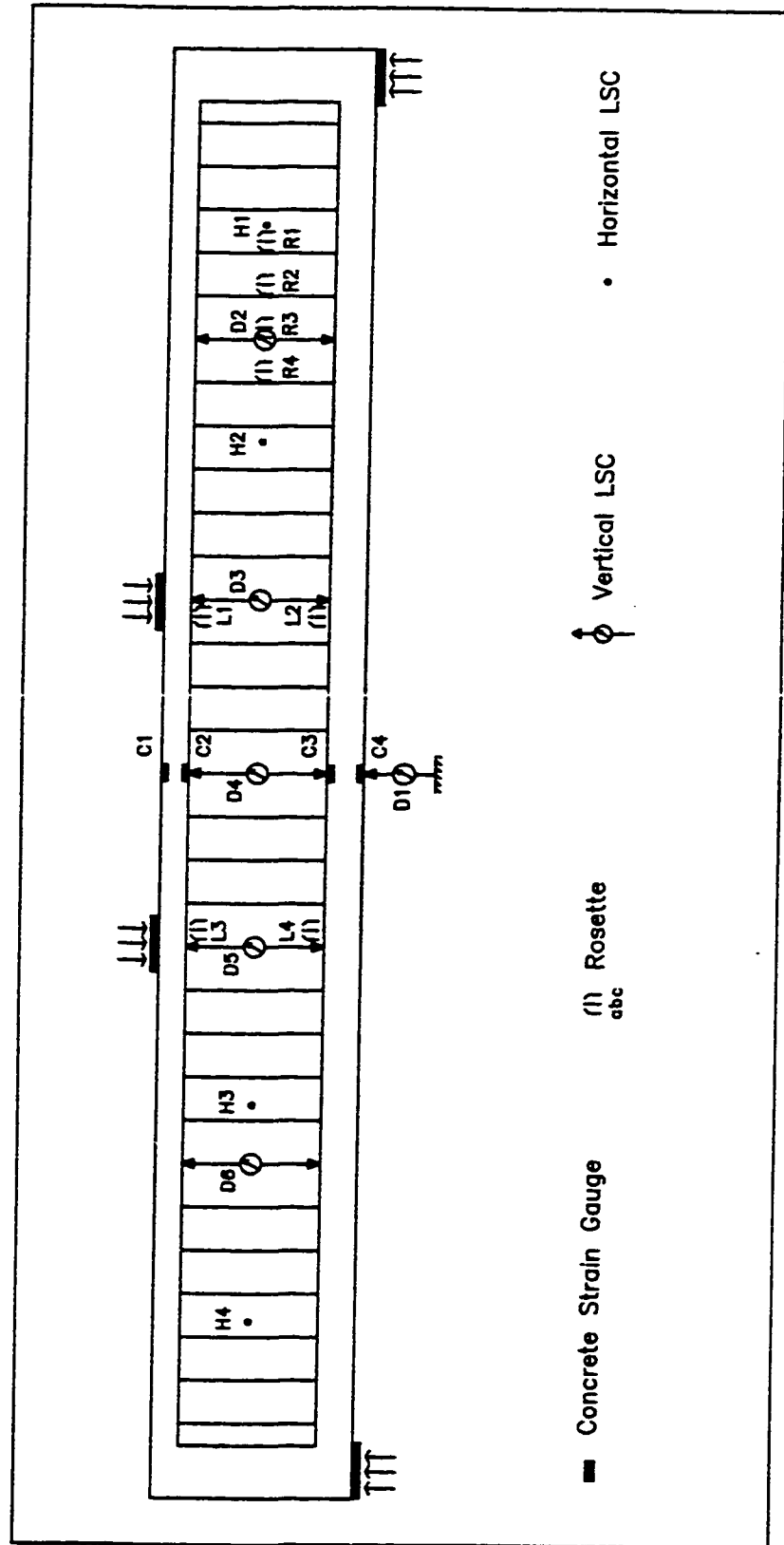




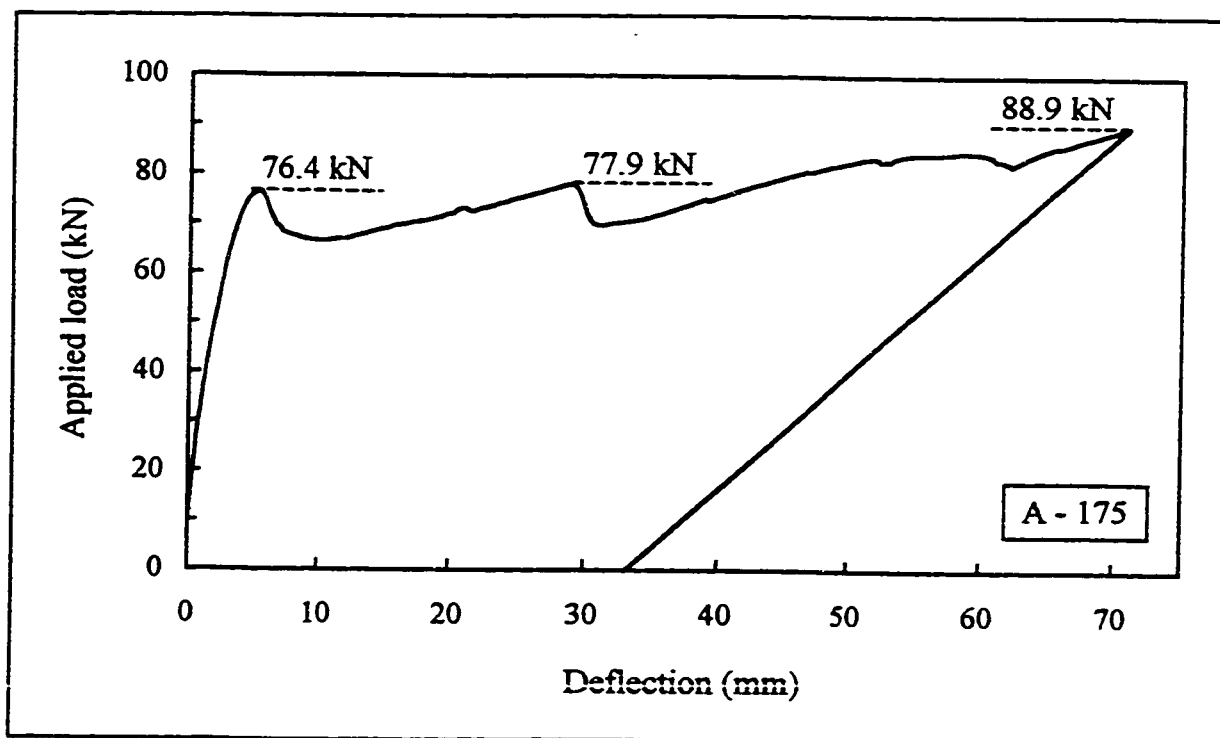
Girder A-215 before testing



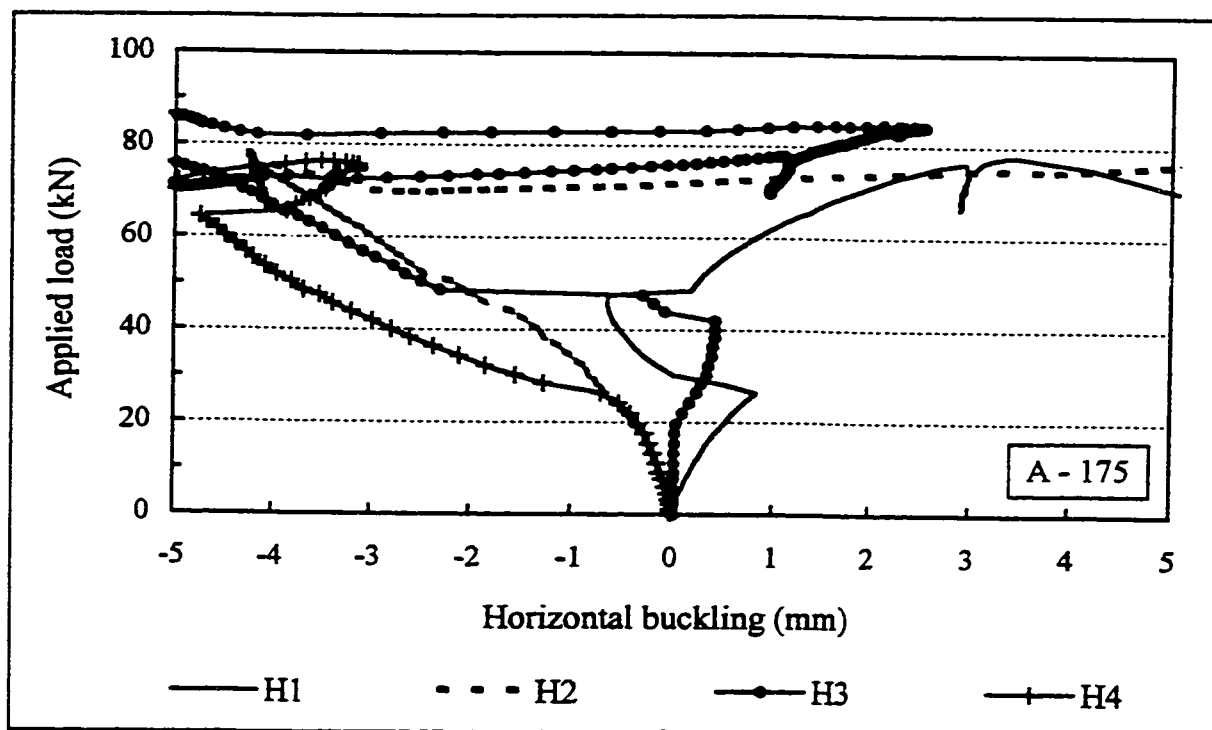
Girder A-215 during testing



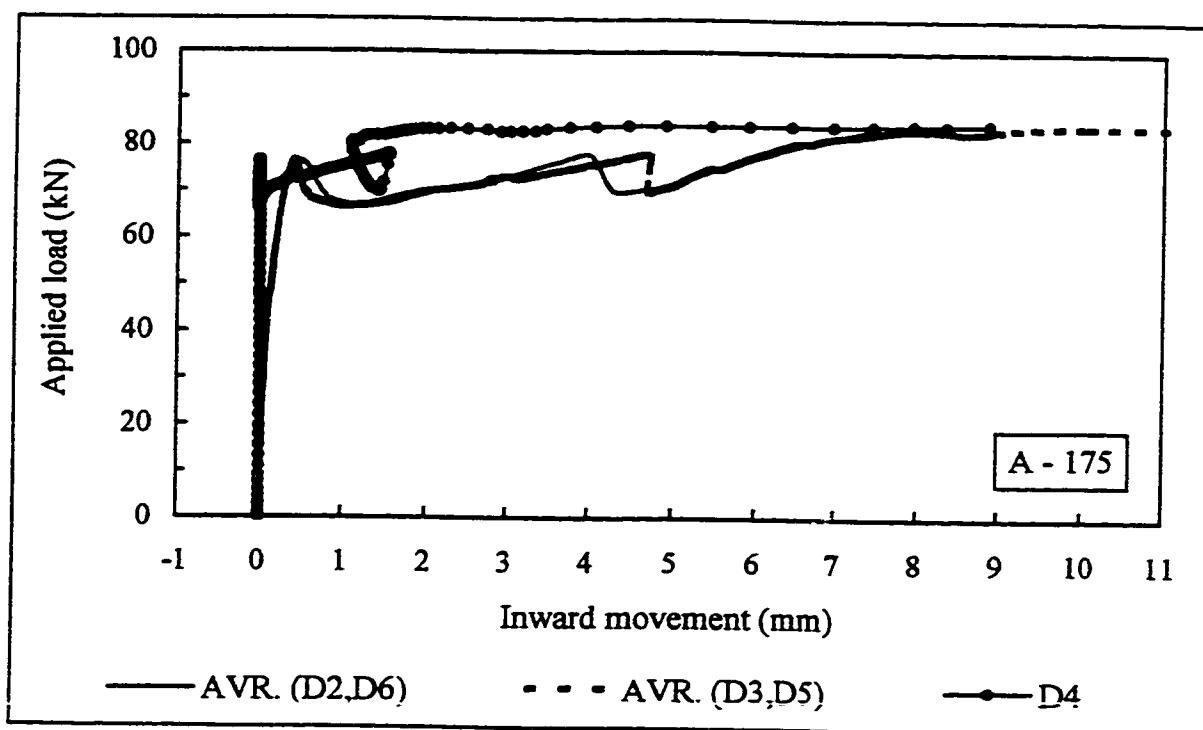
Instrumentation details, girders A-175, A-110, and A-80

**Results : Girder A-175**

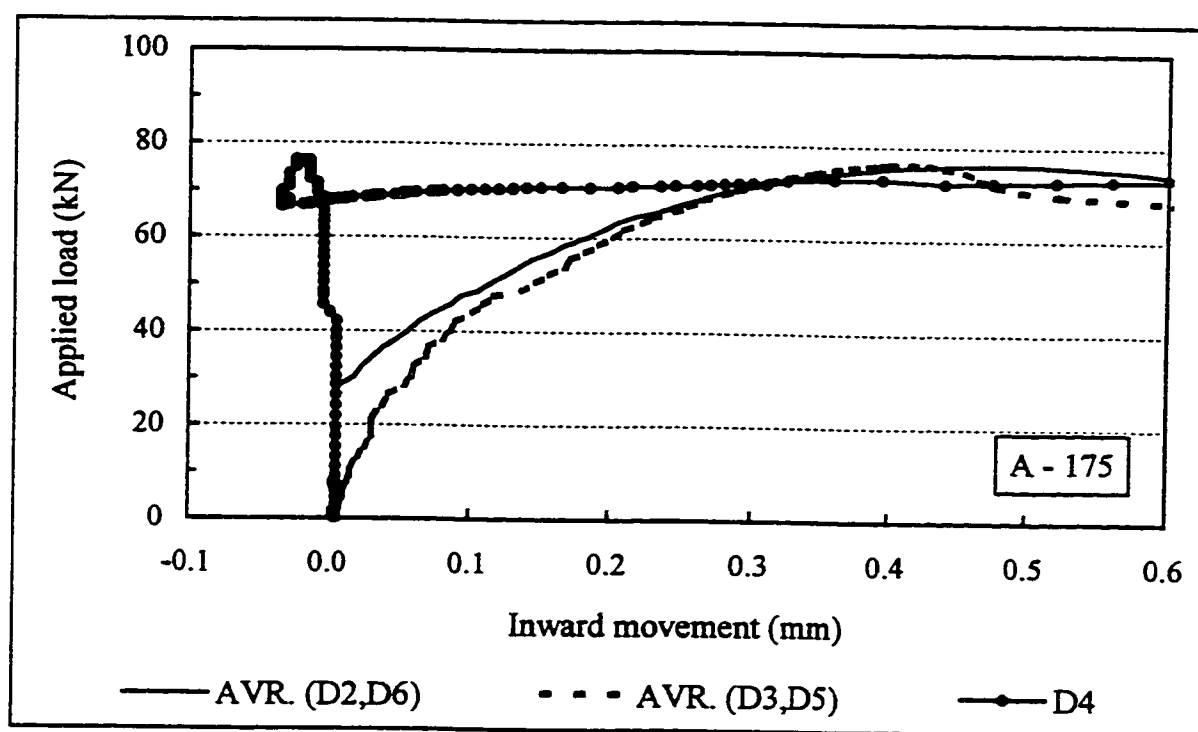
Applied load vs mid-span vertical deflection



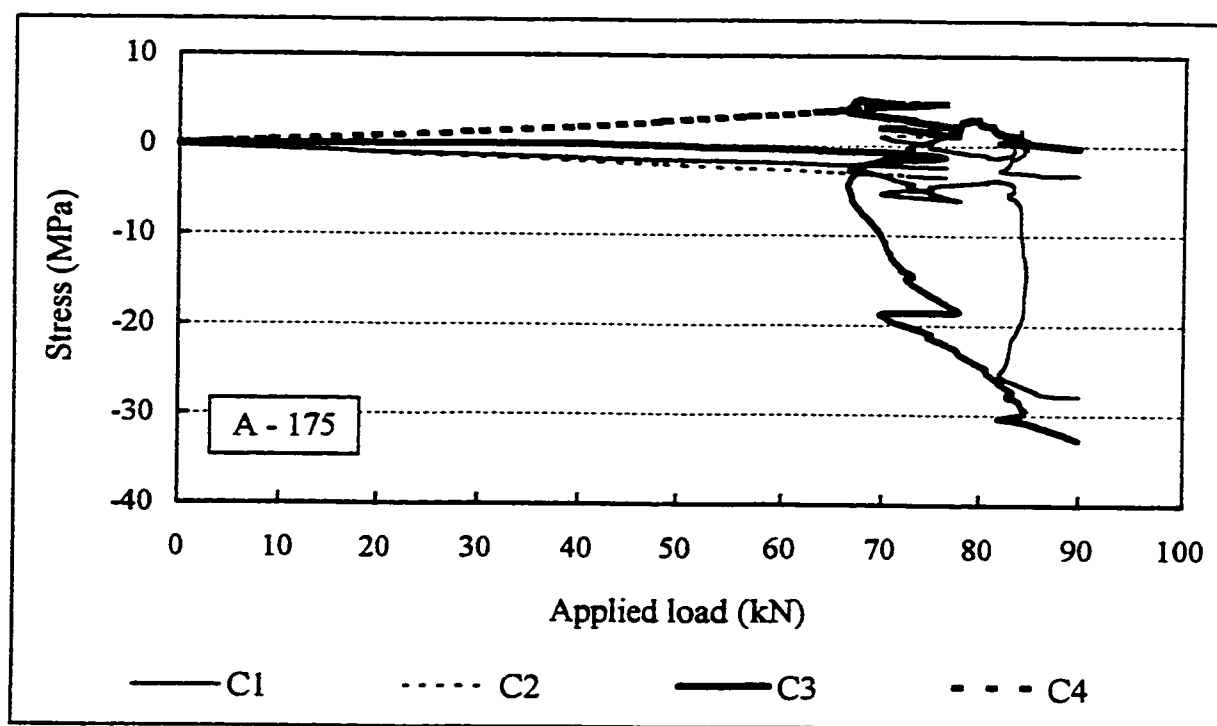
Applied load vs horizontal web buckling



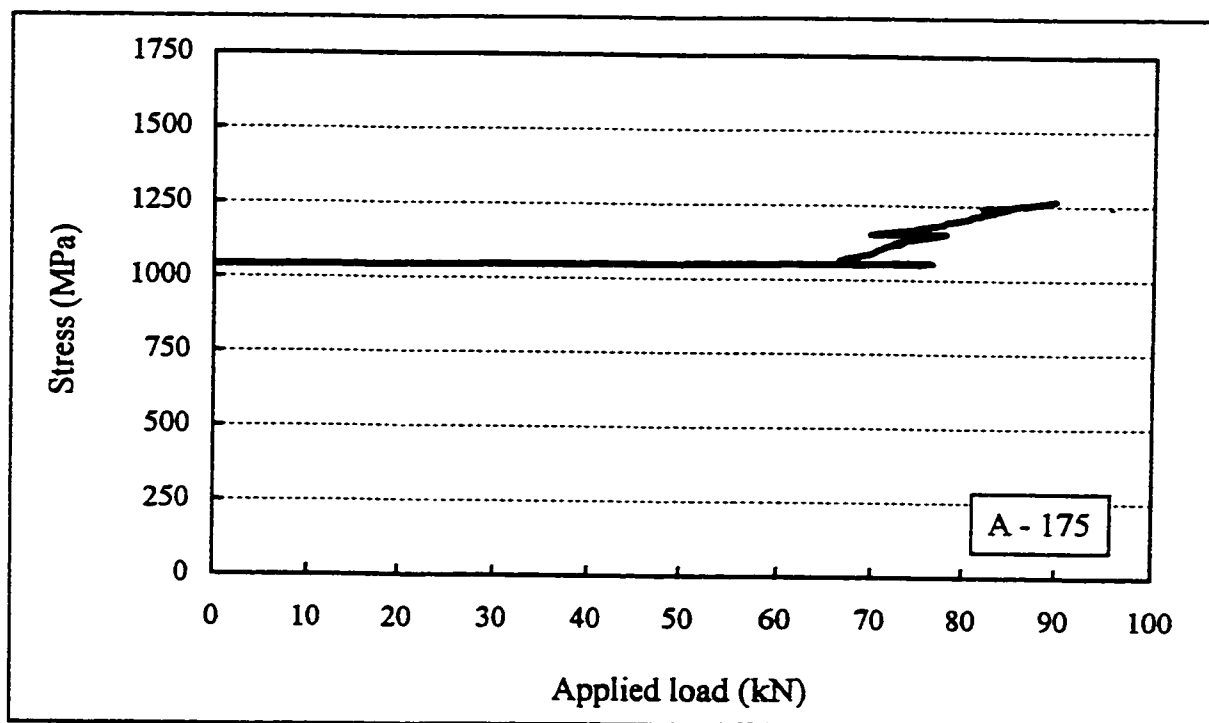
Applied load vs relative inward movement of flanges



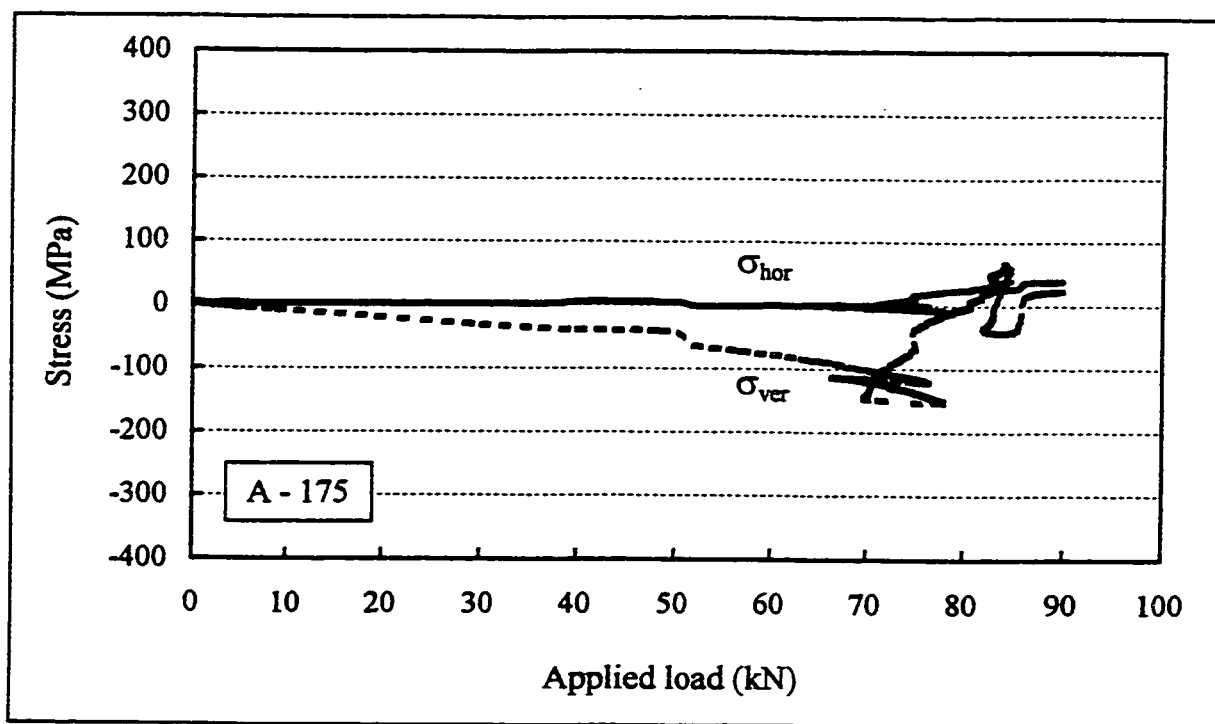
Applied load vs relative inward movement of flanges (zoomed)



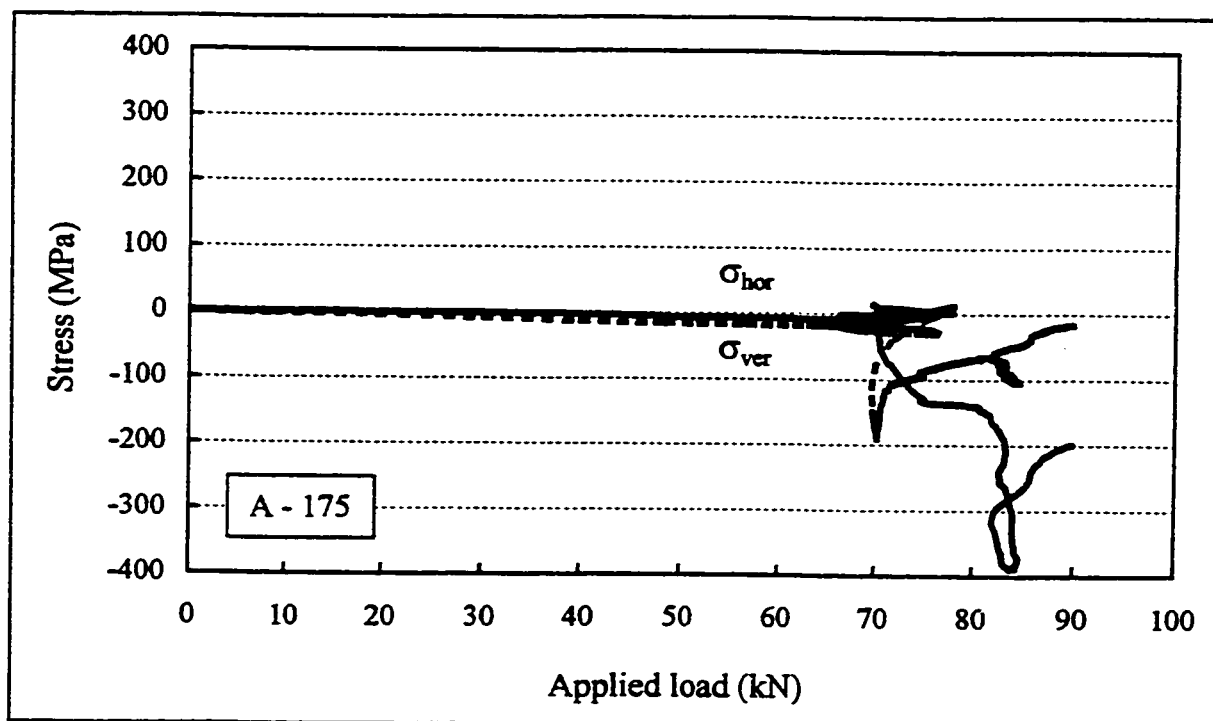
Applied load vs stresses in concrete flanges



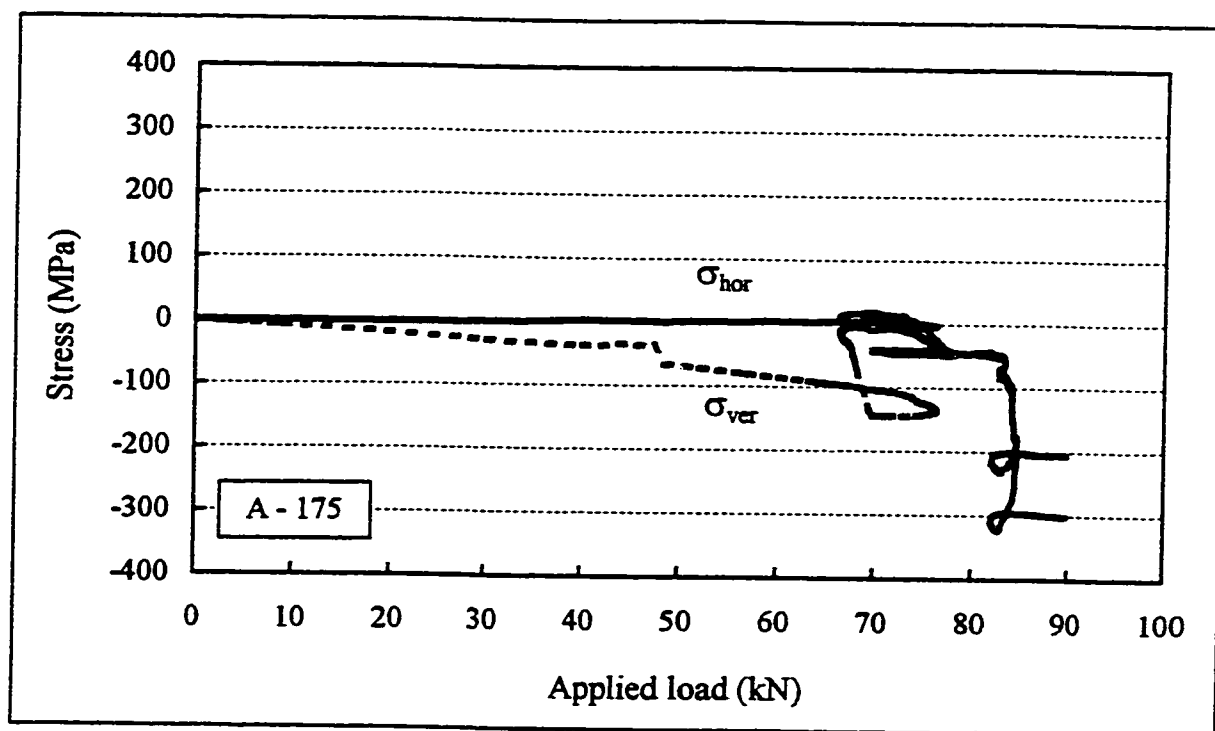
Applied load vs average stress in prestressing strands



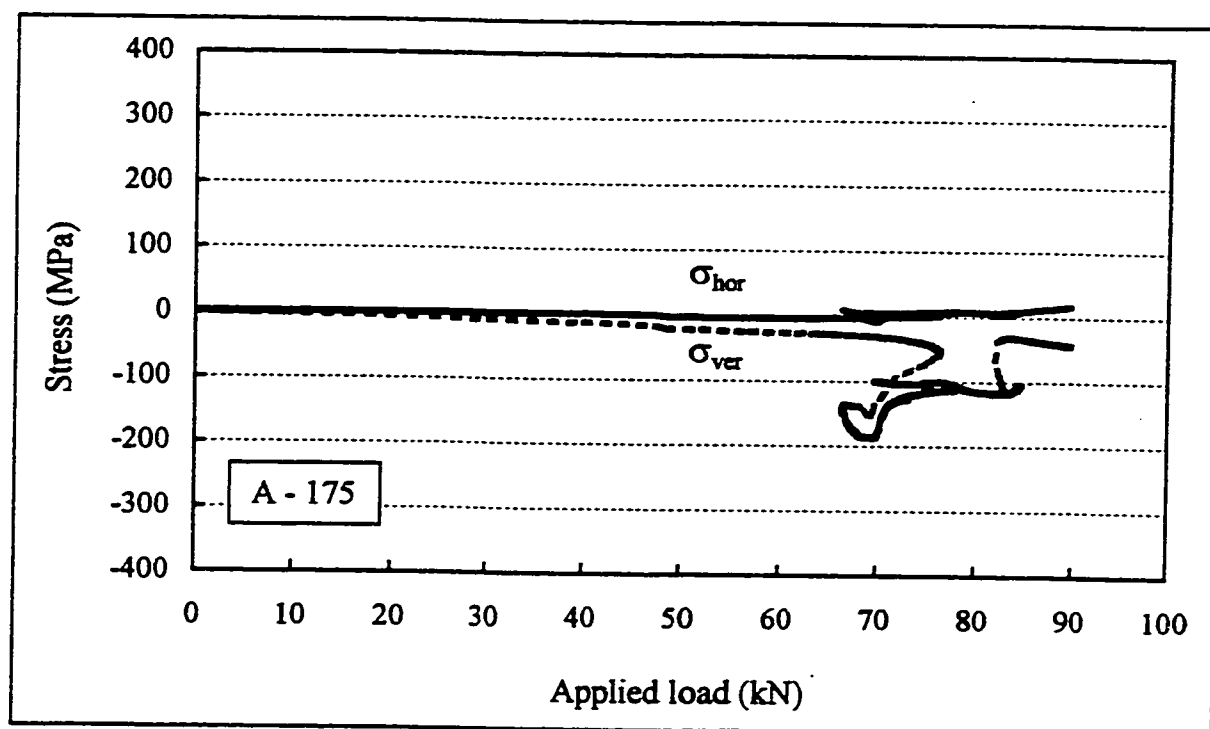
Horizontal and vertical membrane stresses beneath loading points, rosette L1



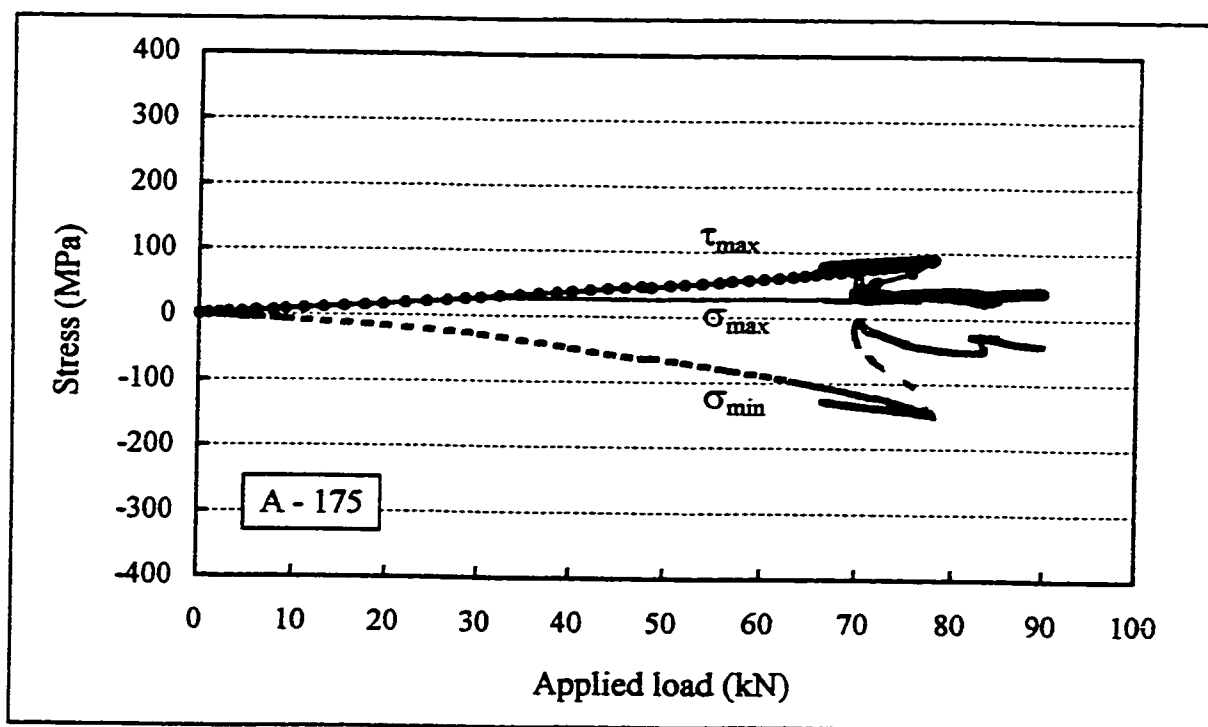
Horizontal and vertical membrane stresses beneath loading points, rosette L2



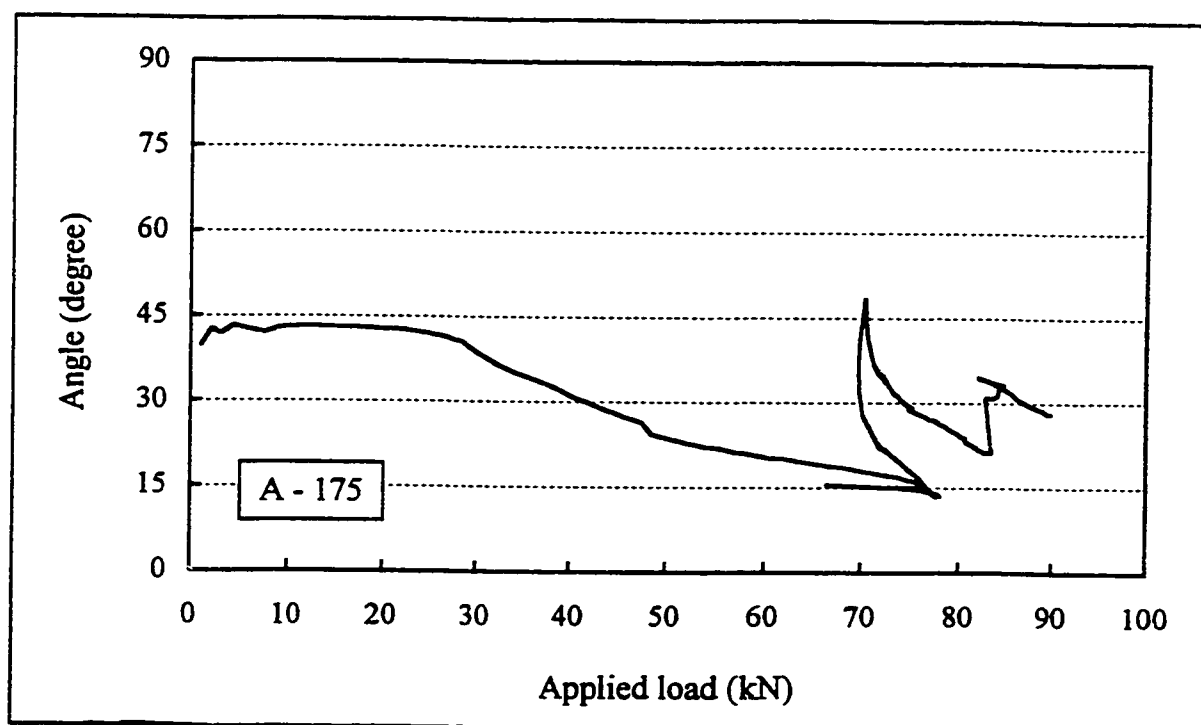
Horizontal and vertical membrane stresses beneath loading points, rosette L3



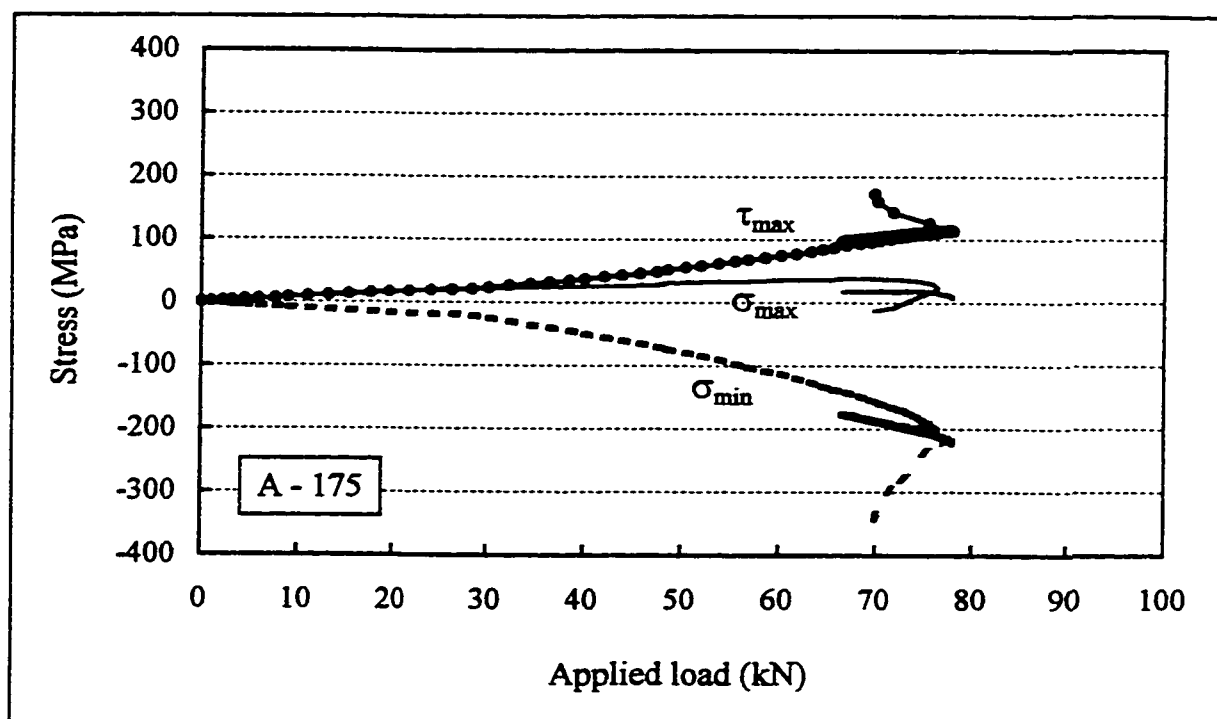
Horizontal and vertical membrane stresses beneath loading points, rosette L4



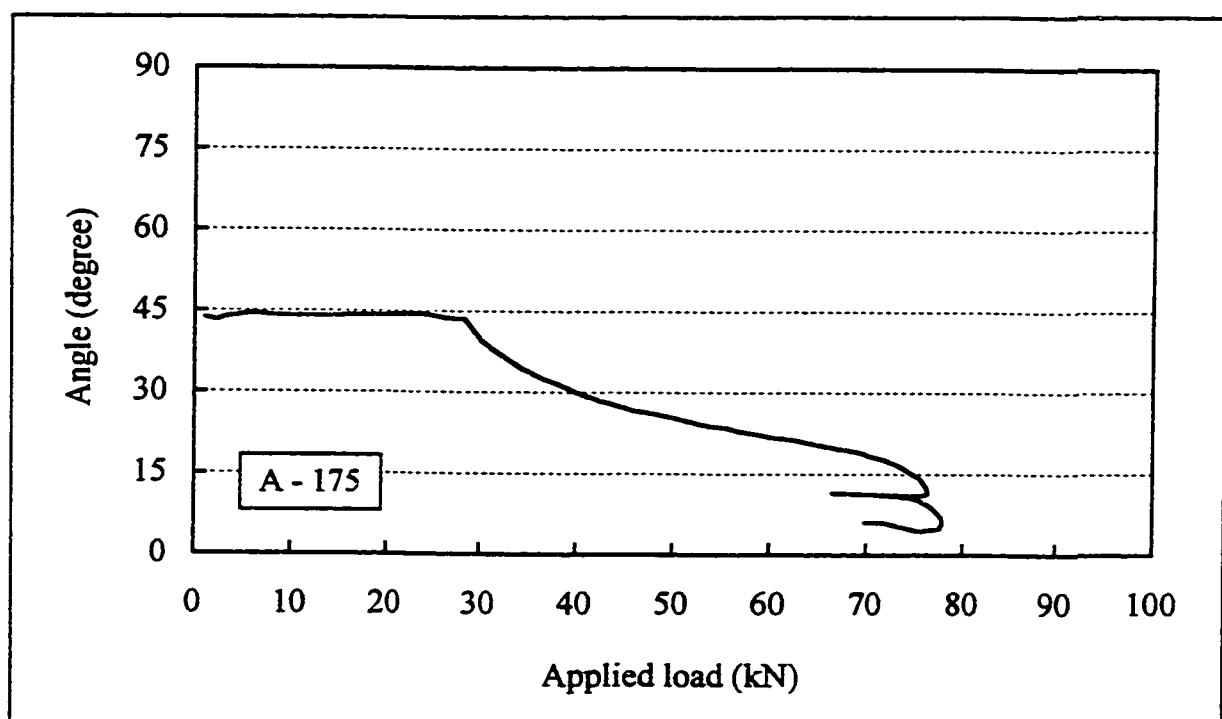
Principal membrane stresses in shear span, rosette R1

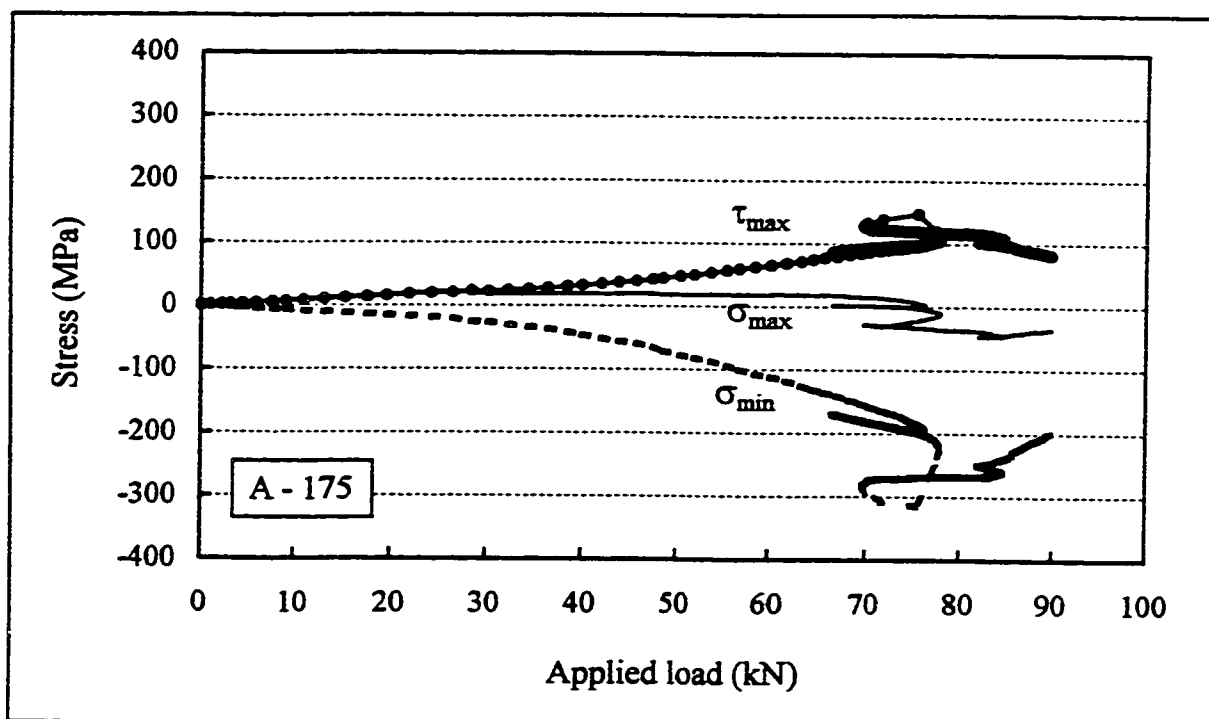
Angle of  $\sigma_{max}$  w.r.t. horizontal direction, rosette R1



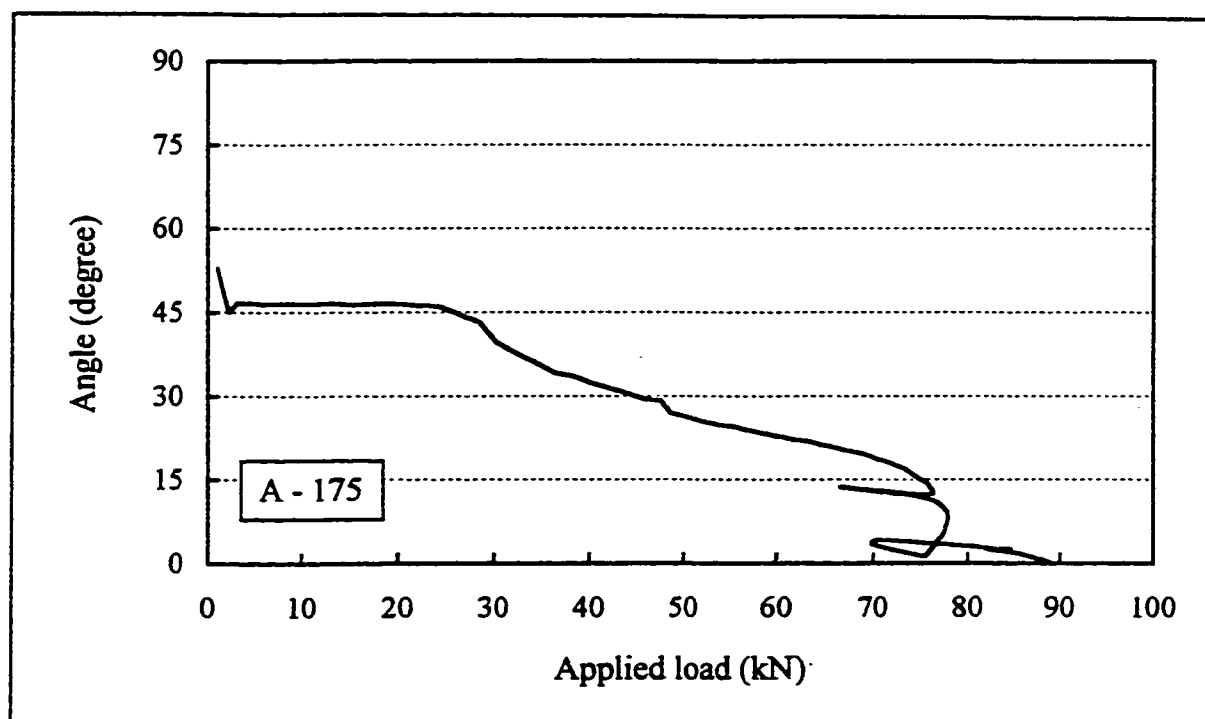


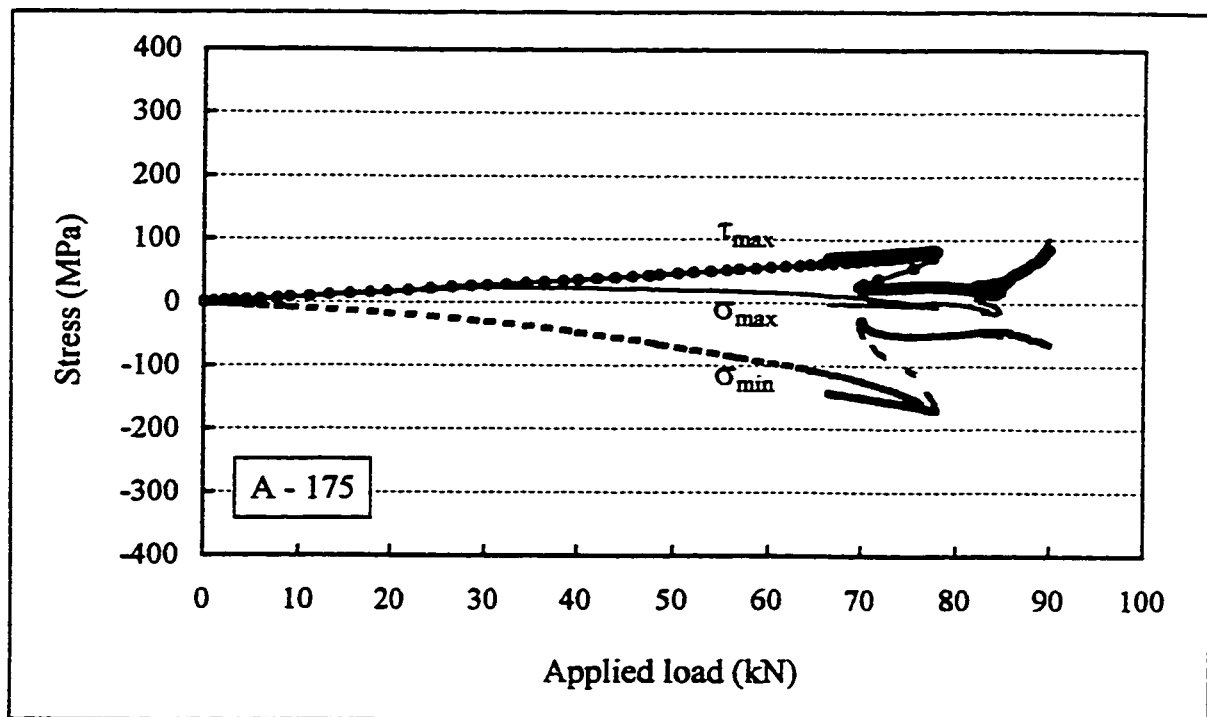
Principal membrane stresses in shear span, rosette R2

Angle of  $\sigma_{max}$  w.r.t. horizontal direction, rosette R2

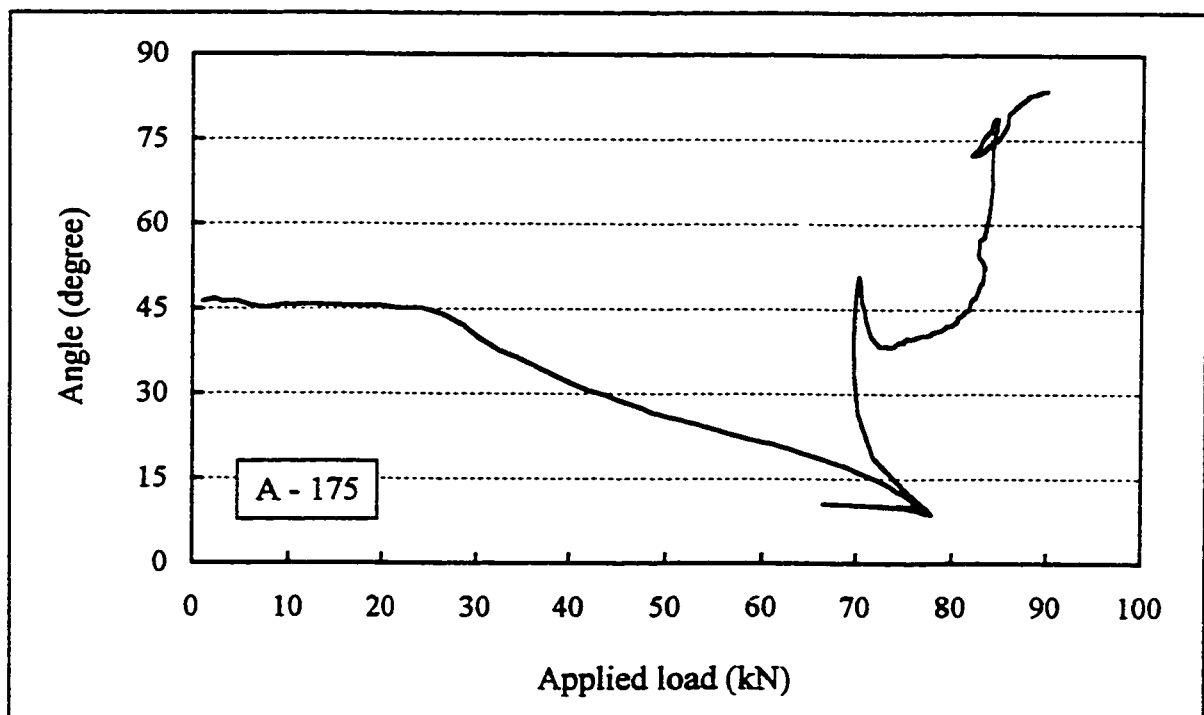


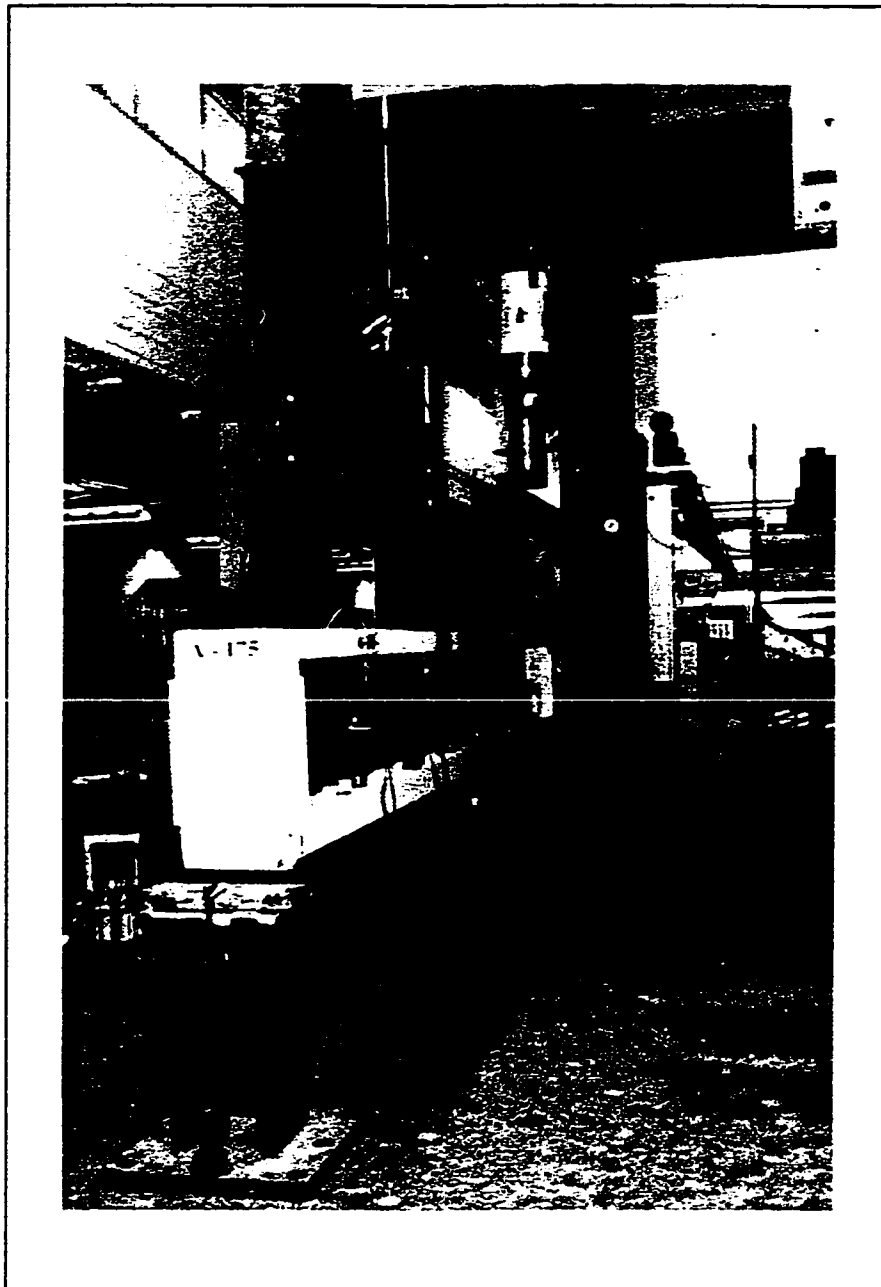
Principal membrane stresses in shear span, rosette R3

Angle of  $\sigma_{max}$  w.r.t. horizontal direction, rosette R3

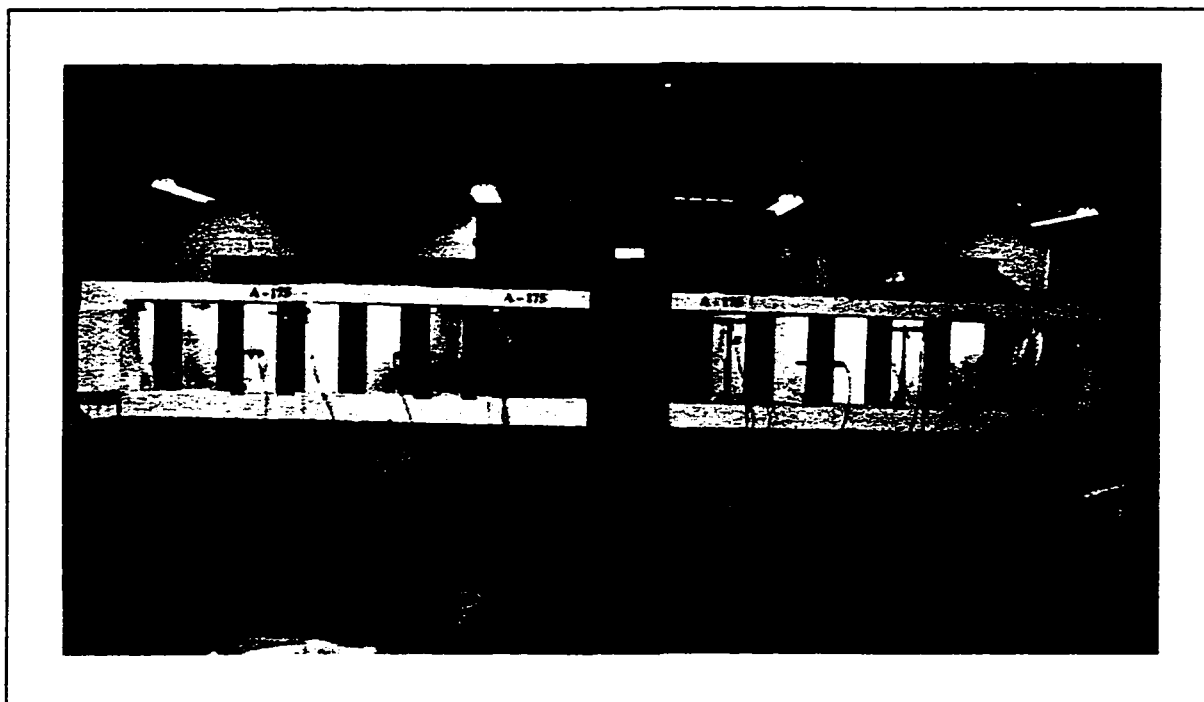


Principal membrane stresses in shear span, rosette R4

Angle of  $\sigma_{max}$  w.r.t. horizontal direction, rosette R4



Girder A-175 and loading frame (side view)

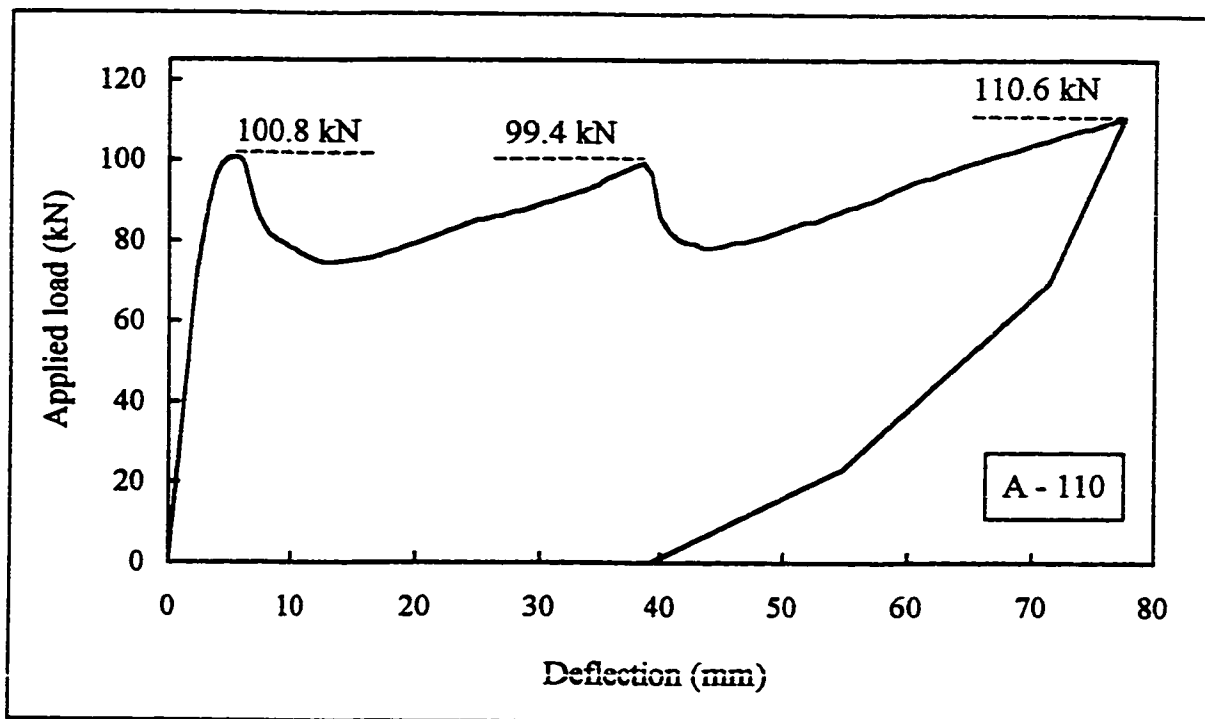


Girder A-175 before testing

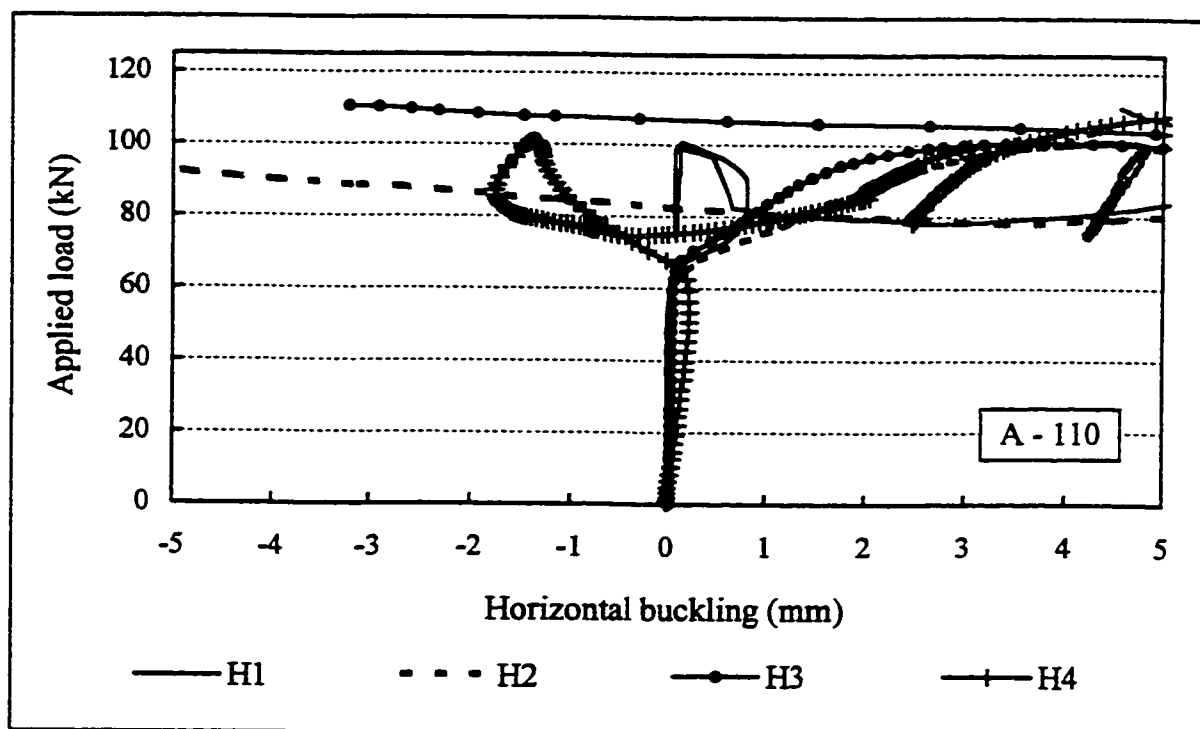


Girder A-175 after testing

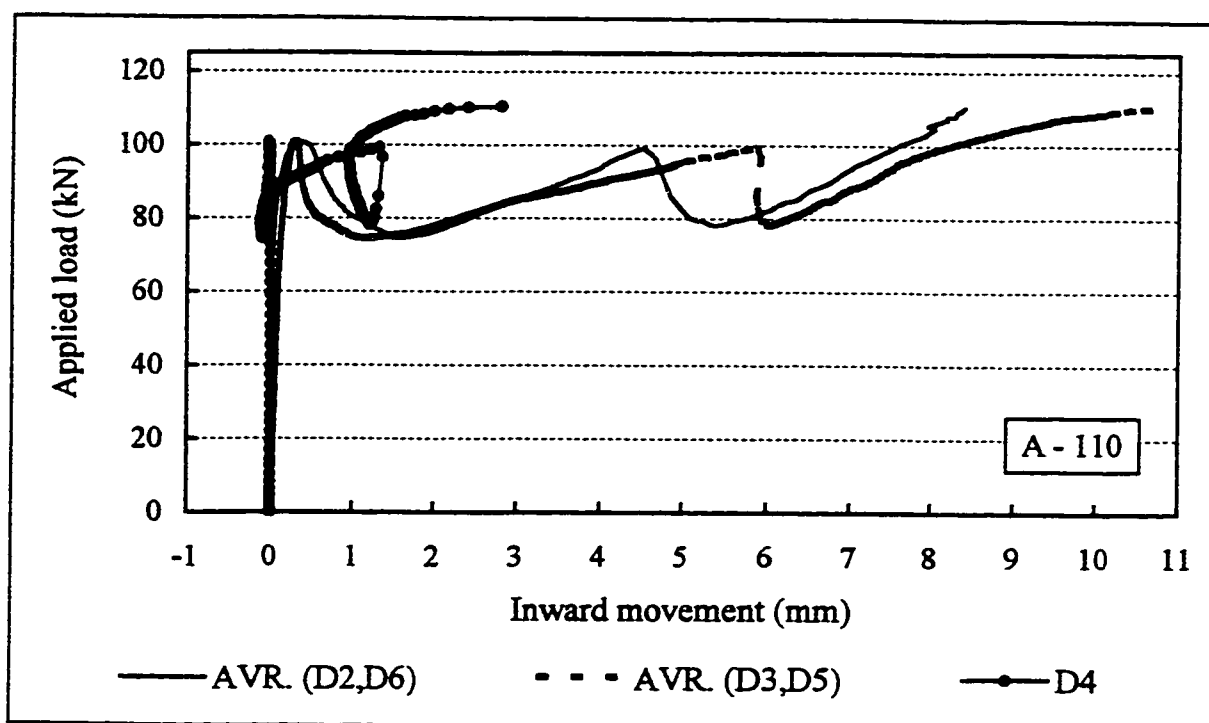
### Results : Girder A-110



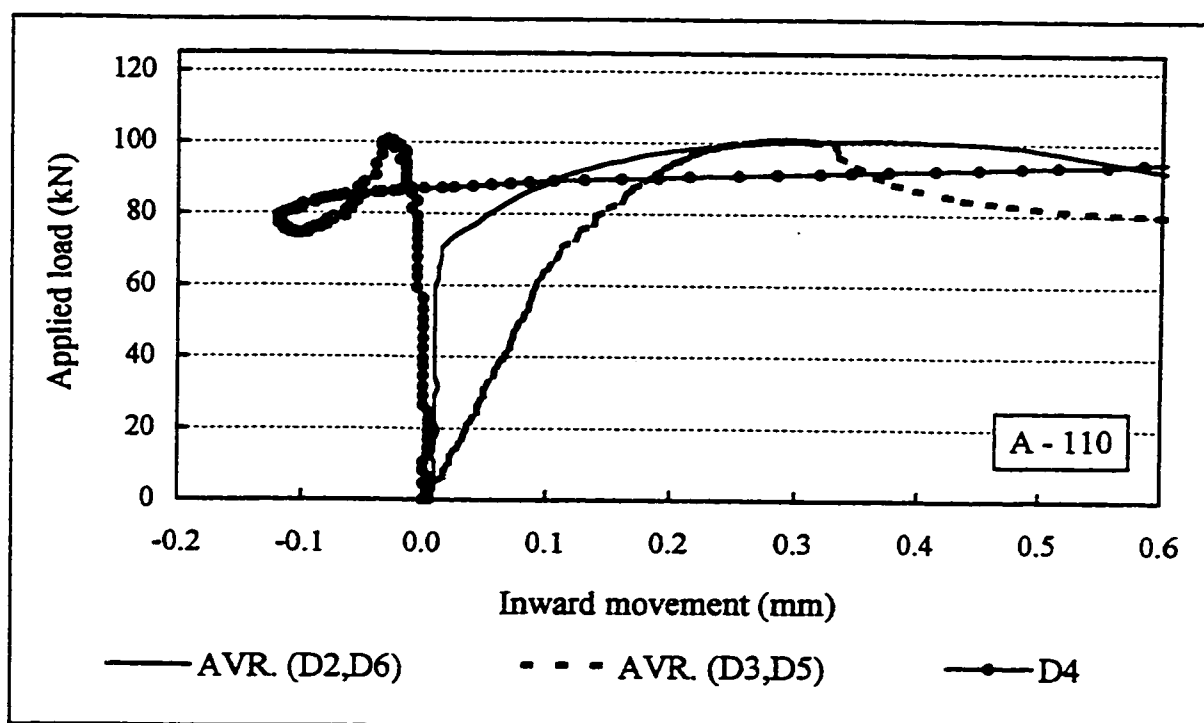
Applied load vs mid-span vertical deflection



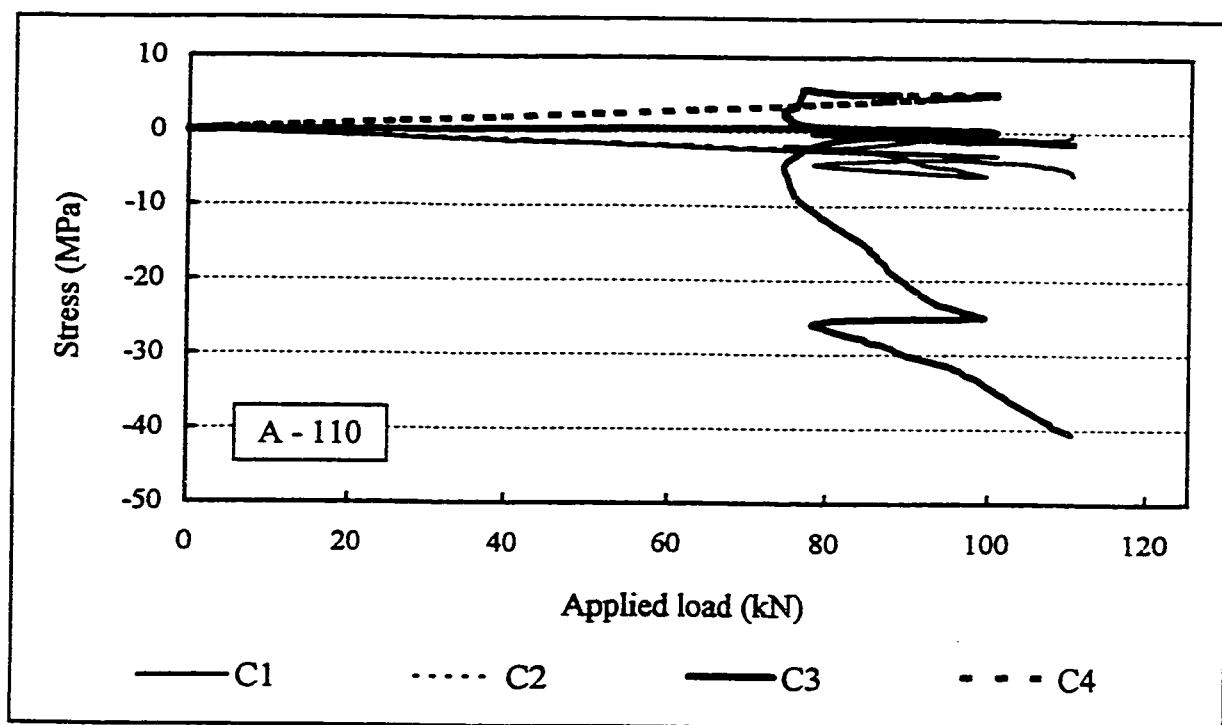
Applied load vs horizontal web buckling



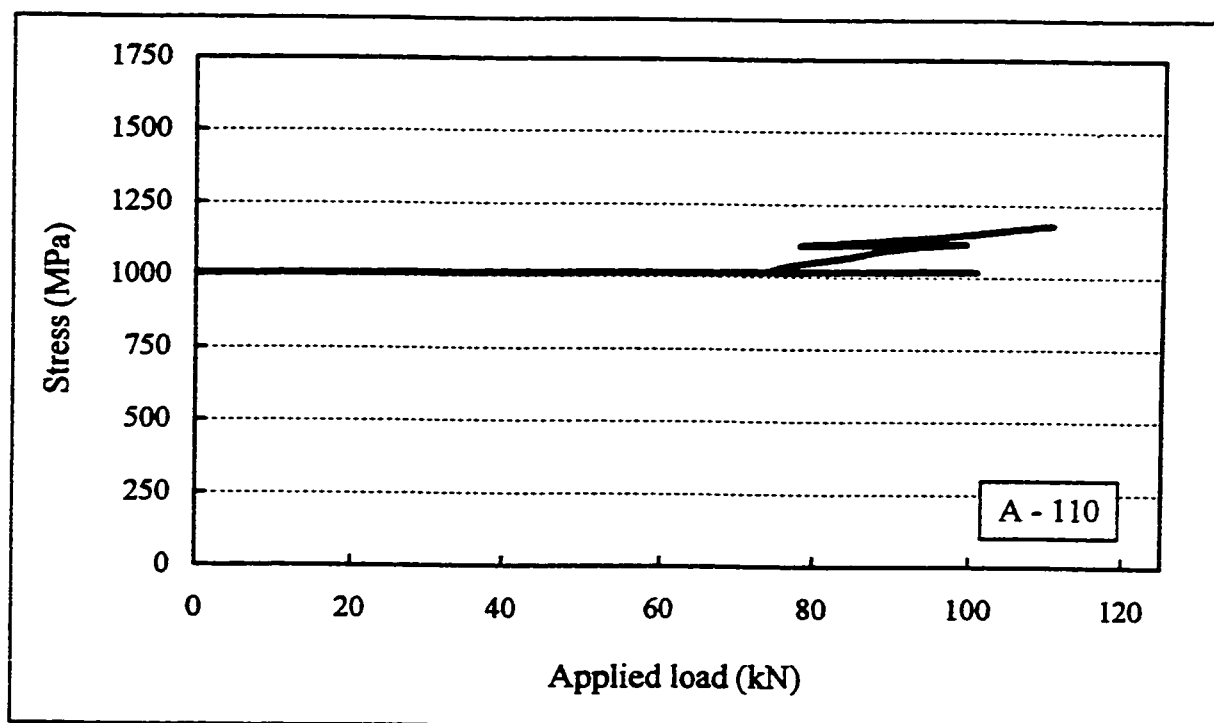
Applied load vs relative inward movement of flanges



Applied load vs relative inward movement of flanges (zoomed)

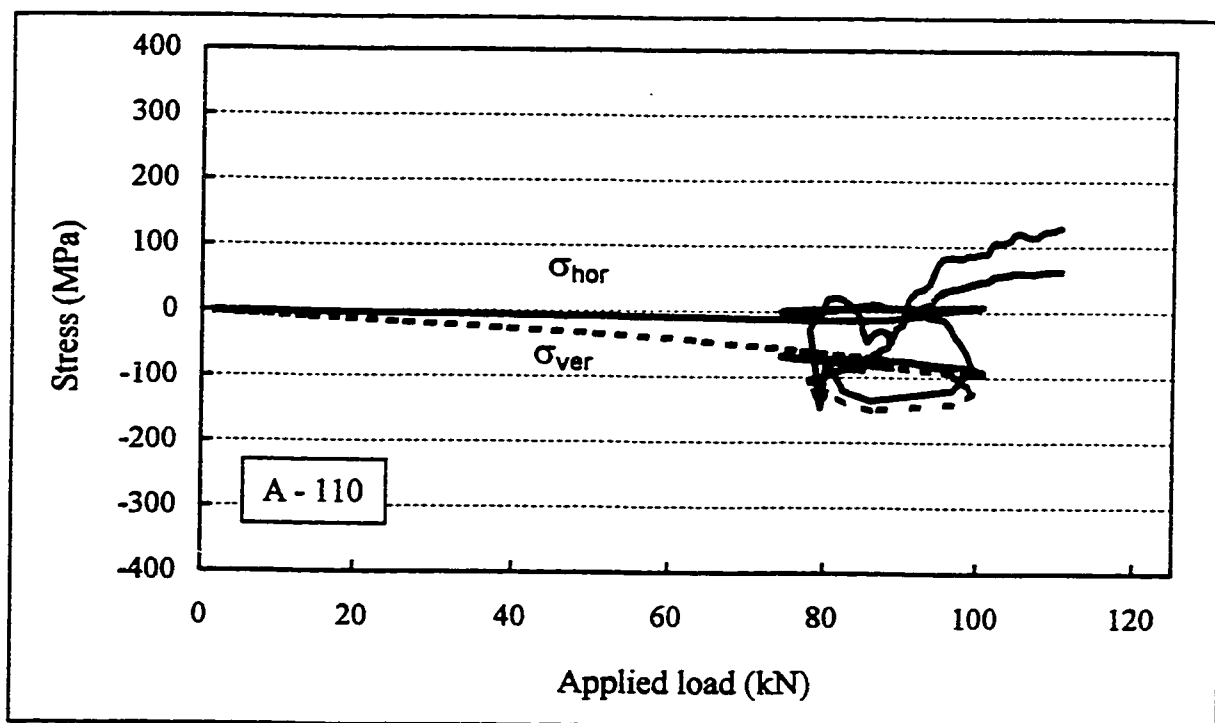


Applied load vs stresses in concrete flanges

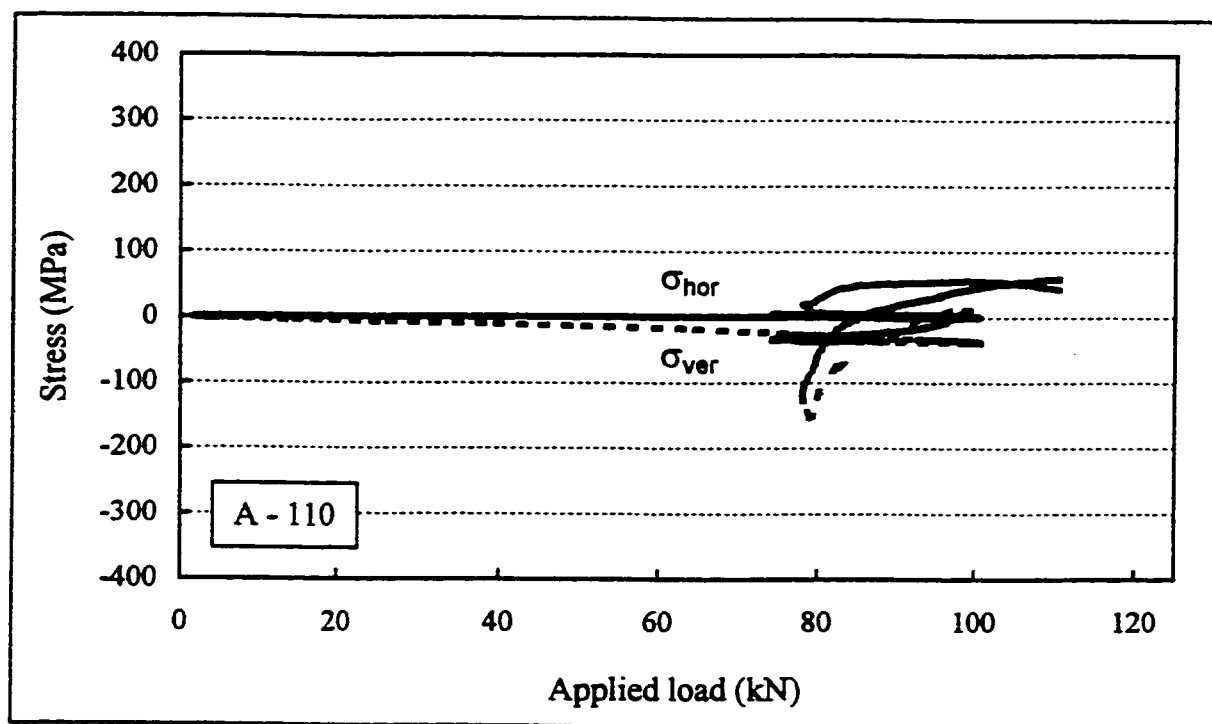


Applied load vs average stress in prestressing strands

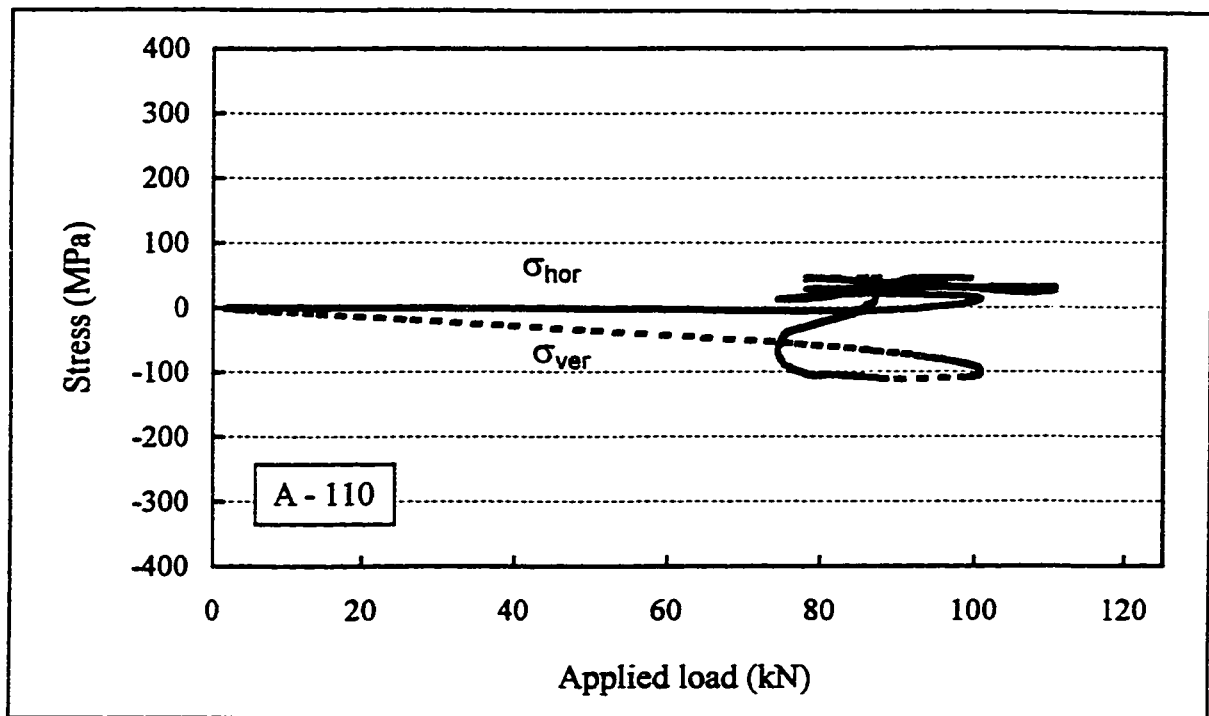




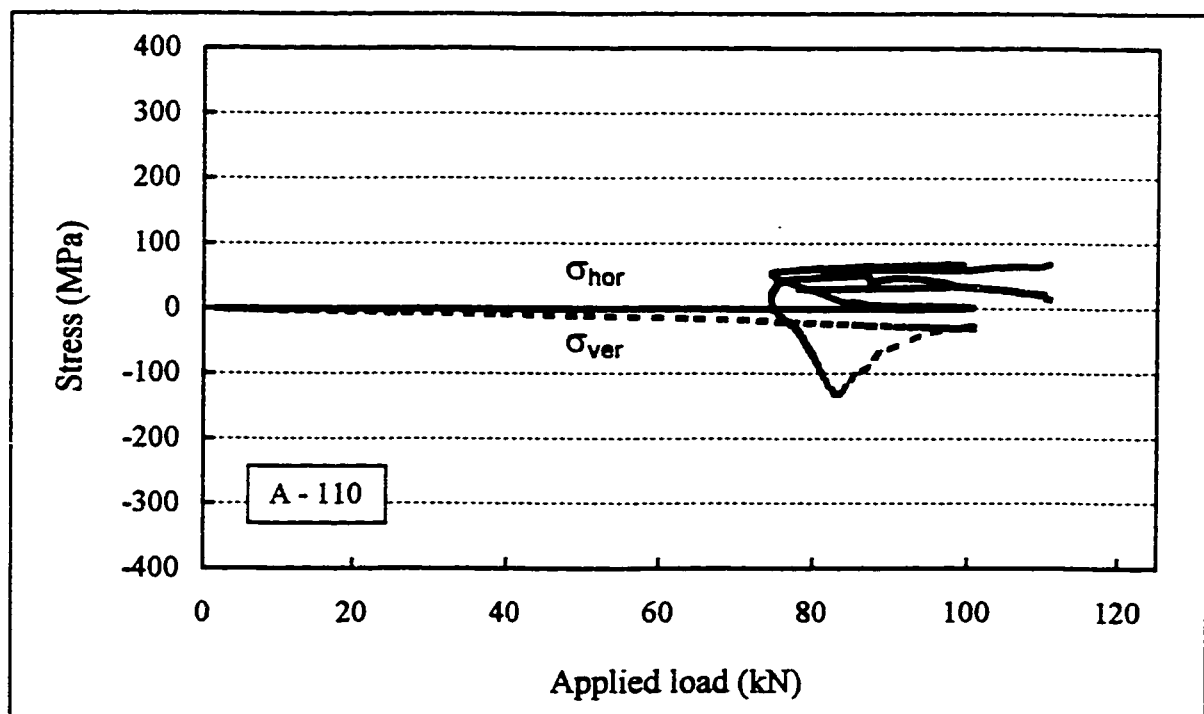
Horizontal and vertical membrane stresses beneath loading points, rosette L1



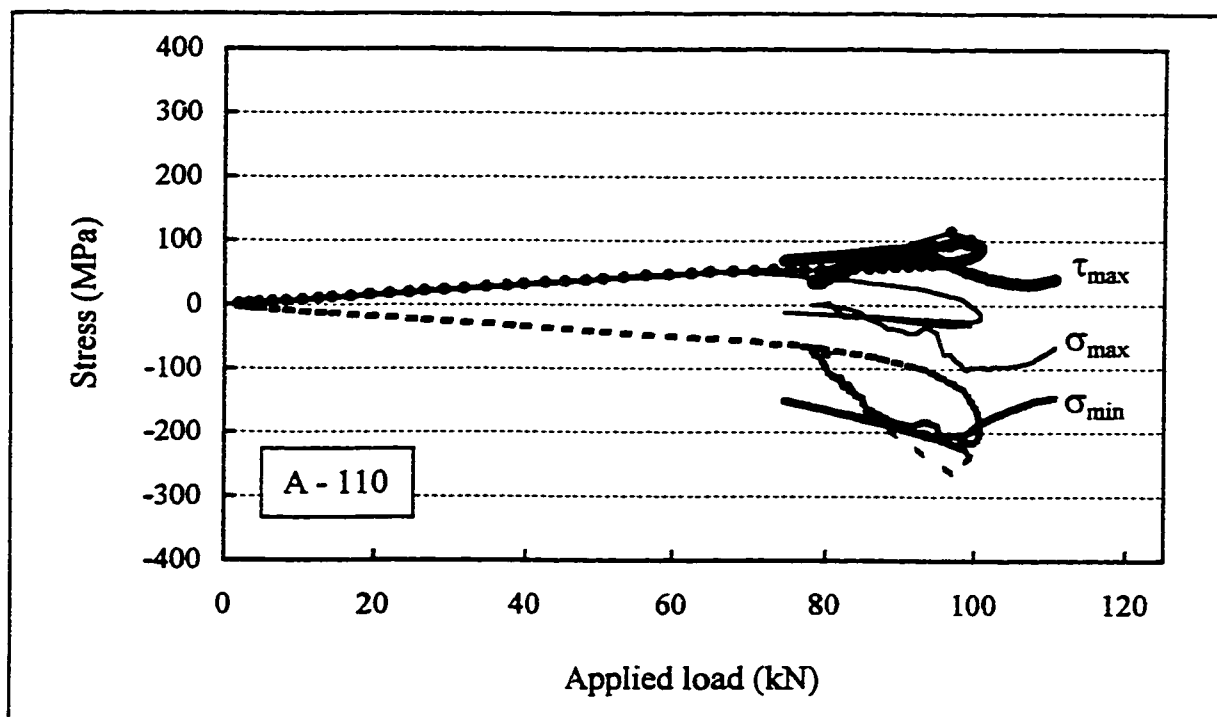
Horizontal and vertical membrane stresses beneath loading points, rosette L2



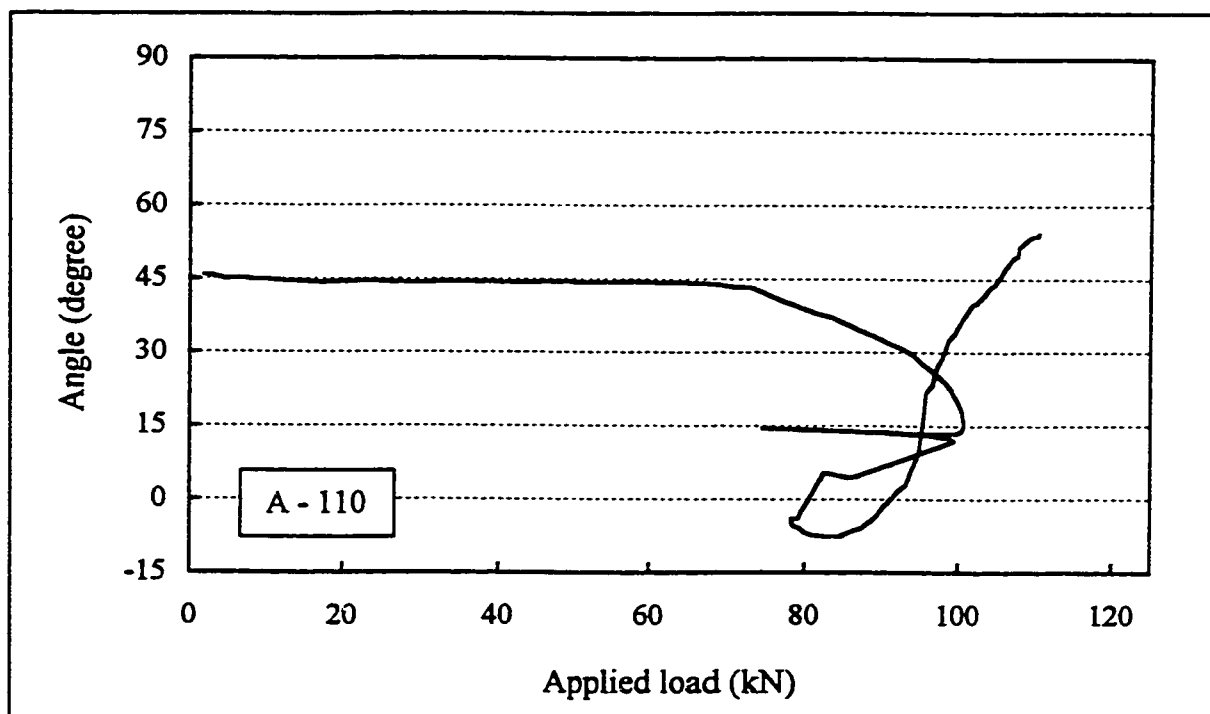
Horizontal and vertical membrane stresses beneath loading points, rosette L3

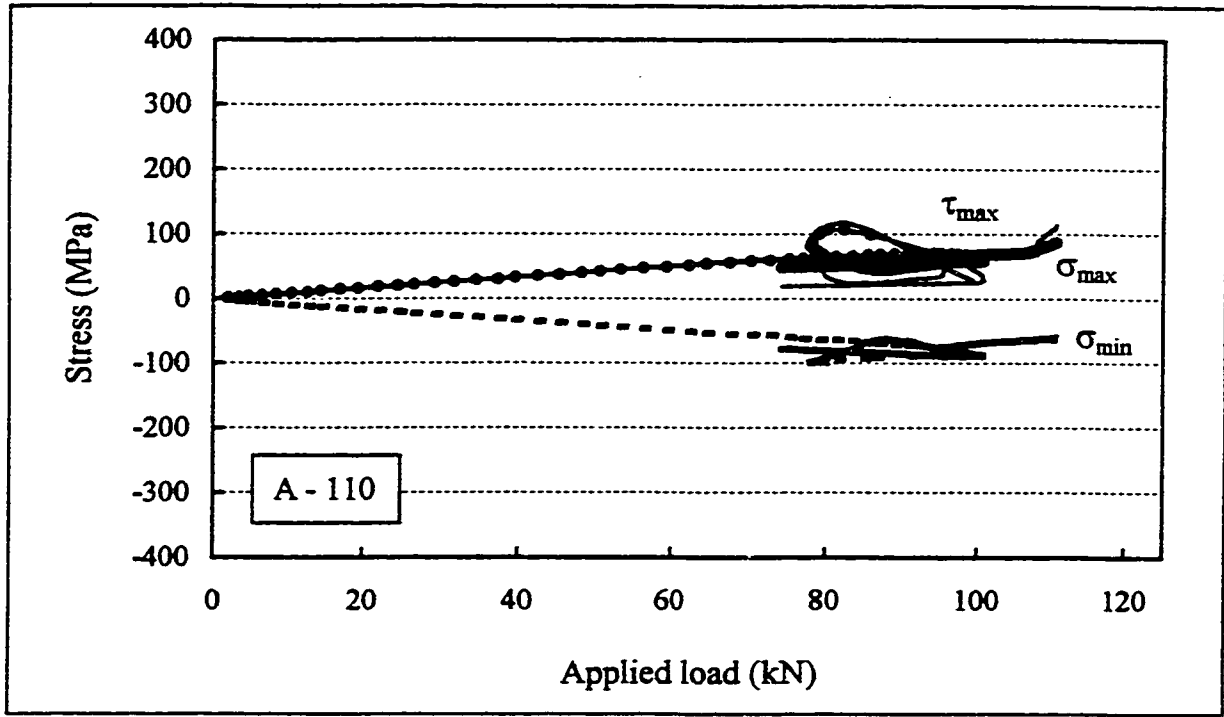


Horizontal and vertical membrane stresses beneath loading points, rosette L4

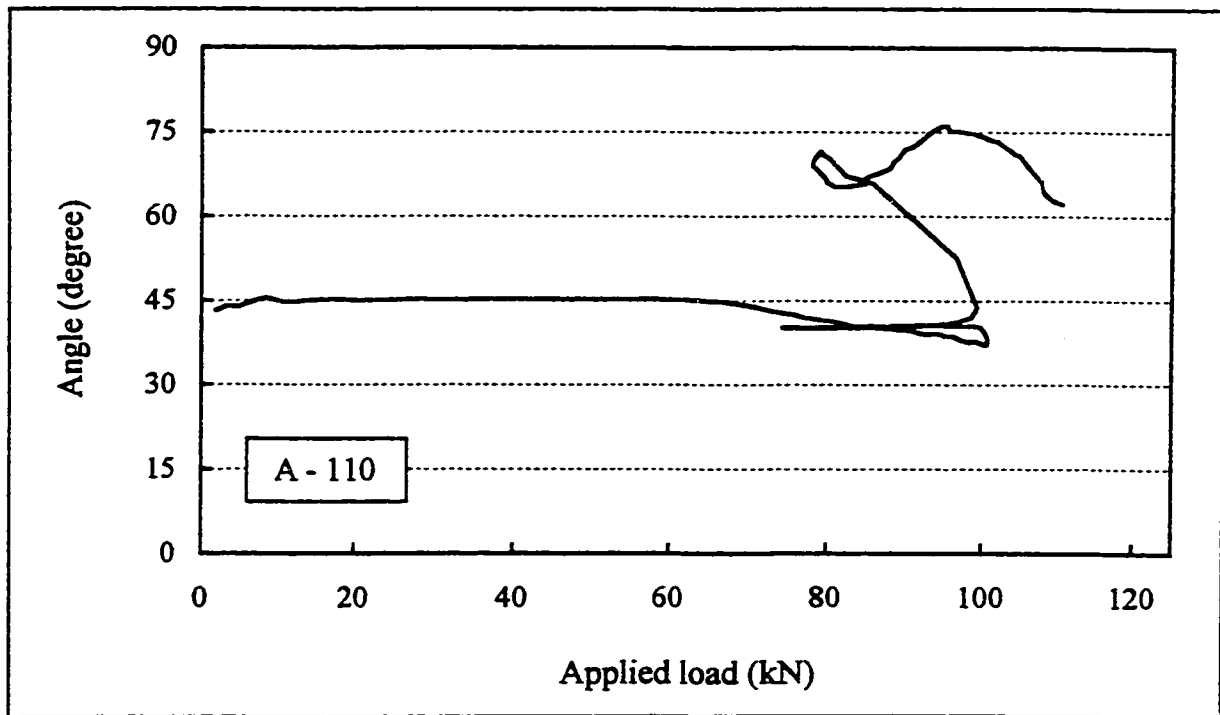


Principal membrane stresses in shear span, rosette R1

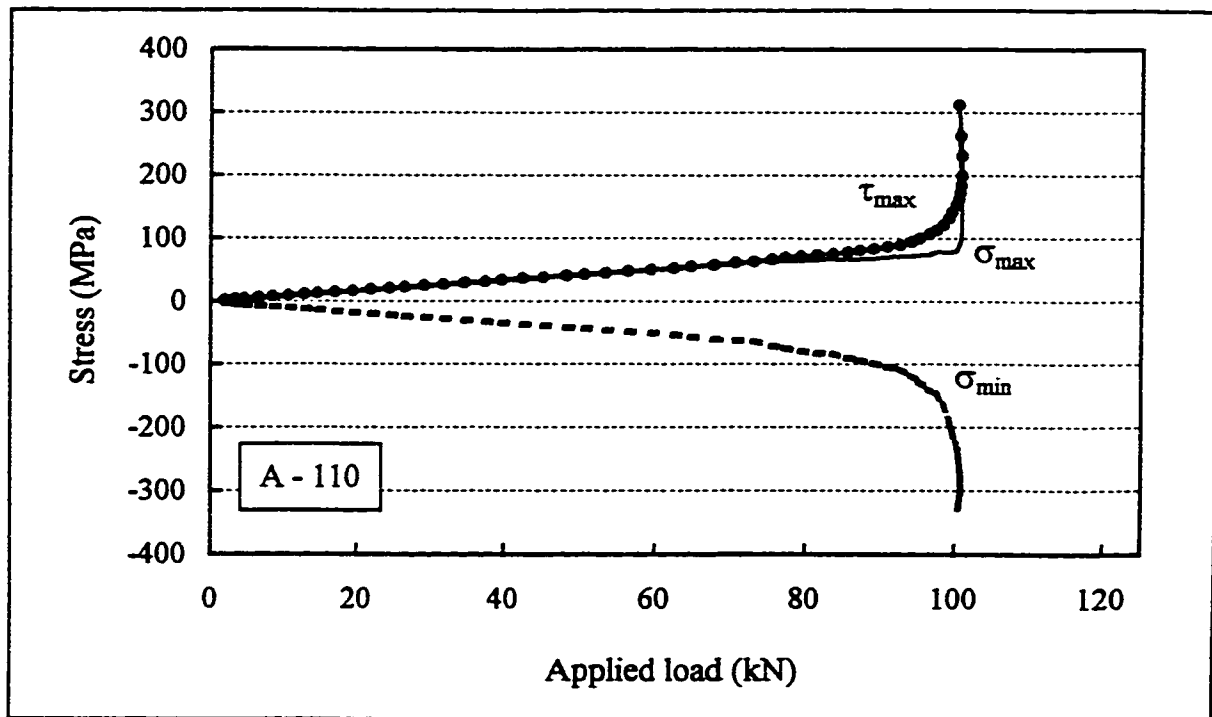
Angle of  $\sigma_{\max}$  w.r.t. horizontal direction, rosette R1



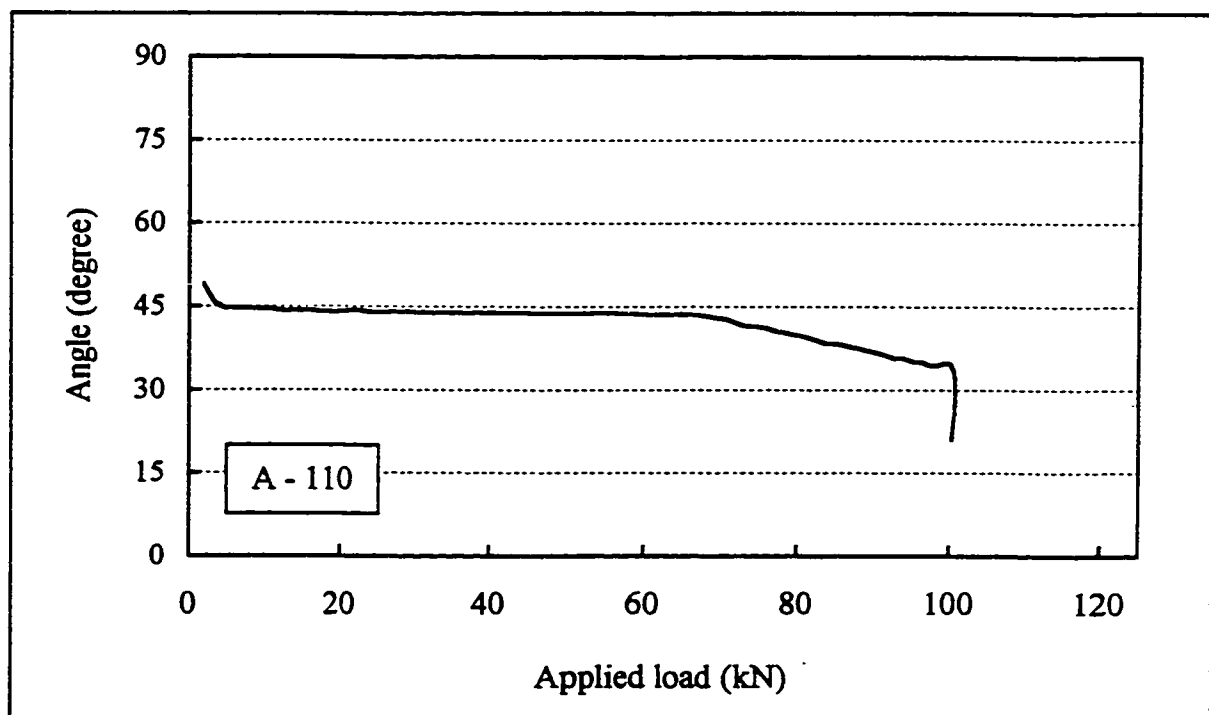
Principal membrane stresses in shear span, rosette R2

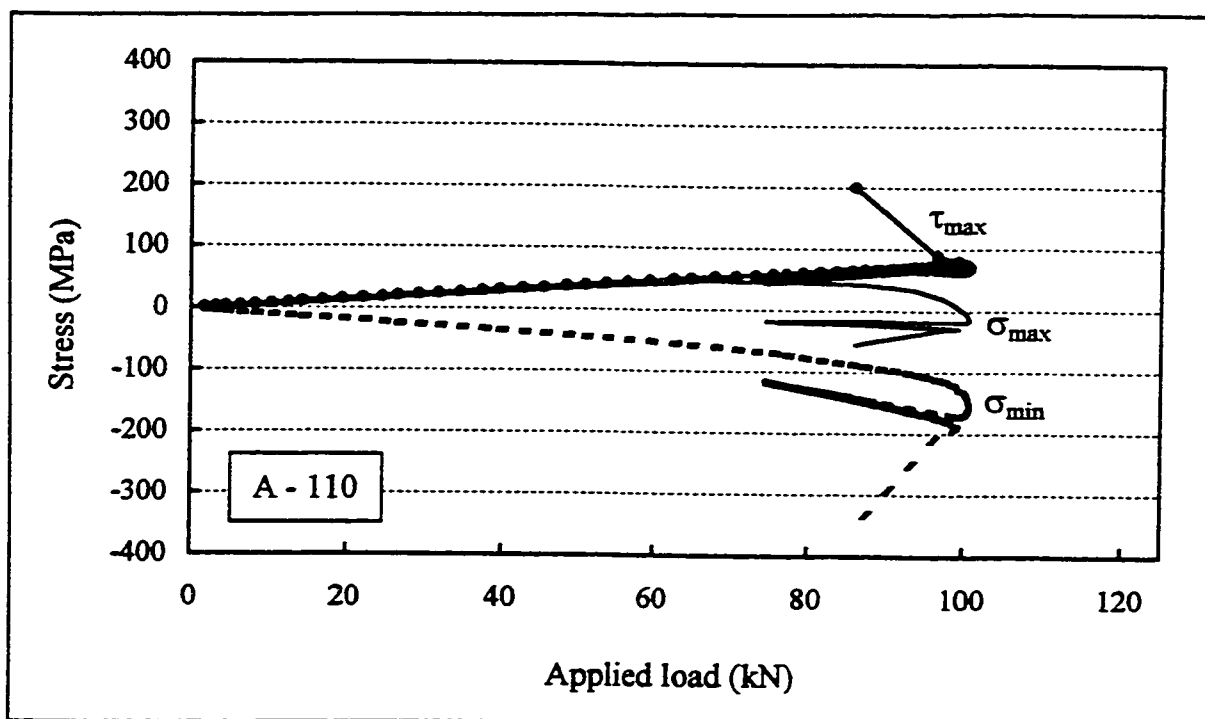


Angle of  $\sigma_{max}$  w.r.t. horizontal direction, rosette R2

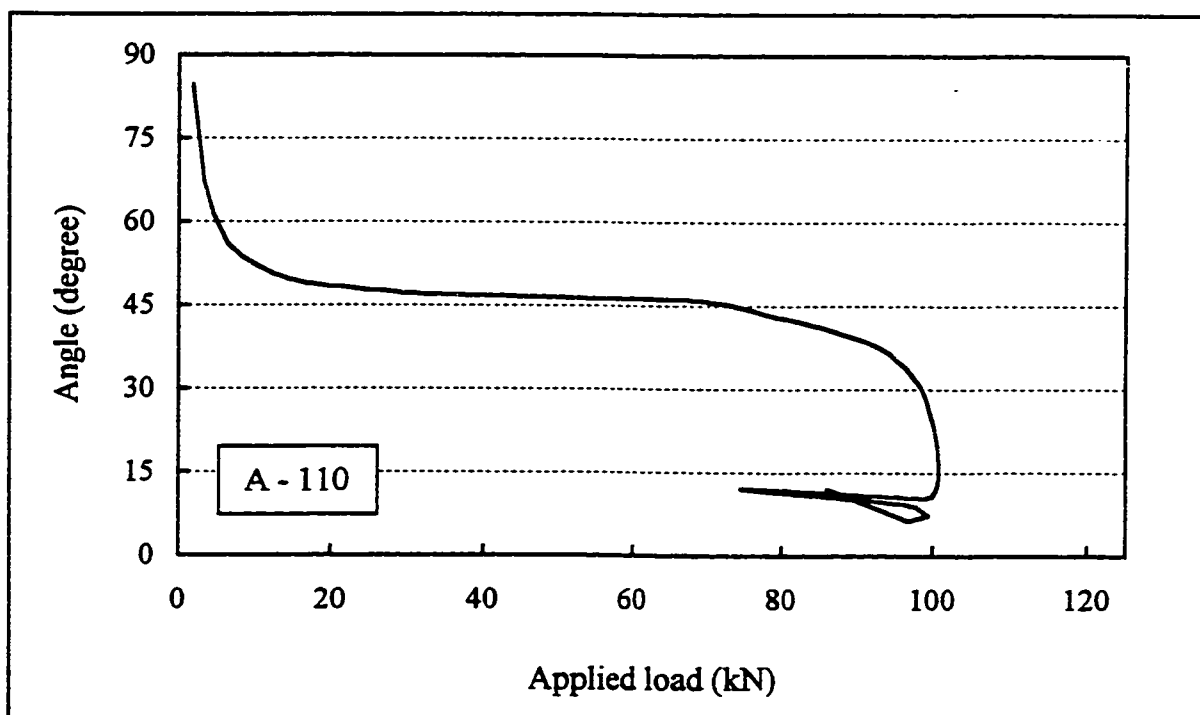


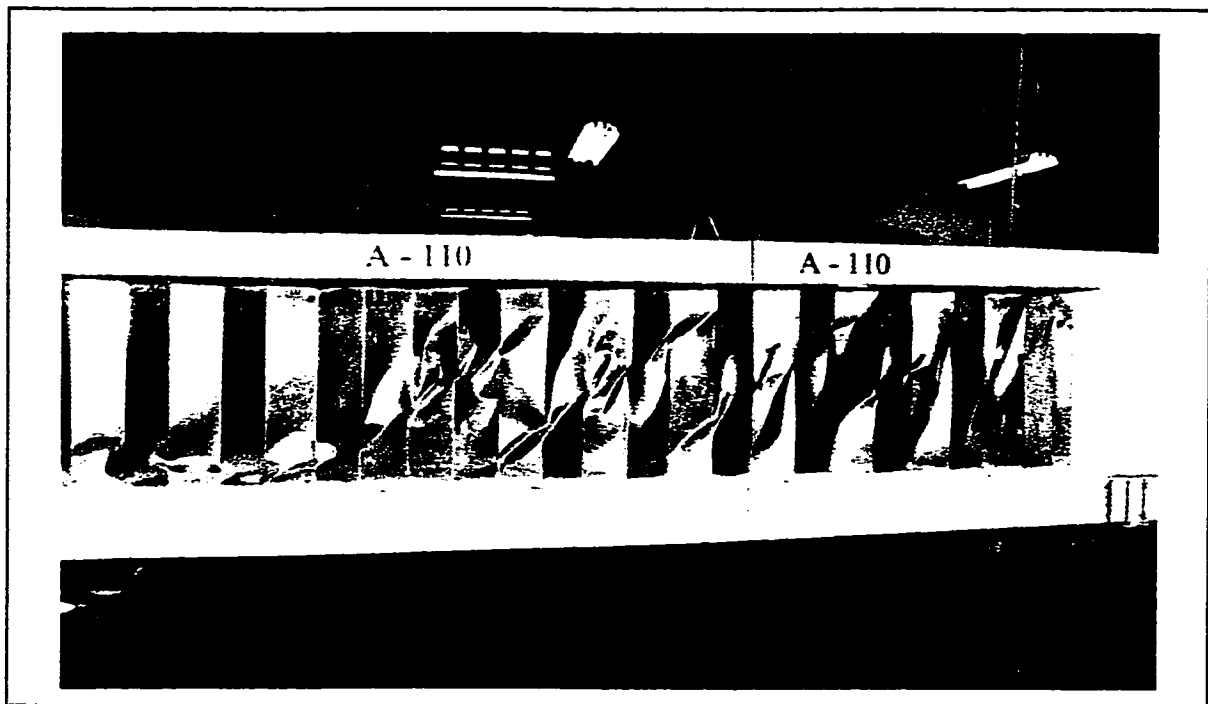
Principal membrane stresses in shear span, rosette R3

Angle of  $\sigma_{\max}$  w.r.t. horizontal direction, rosette R3



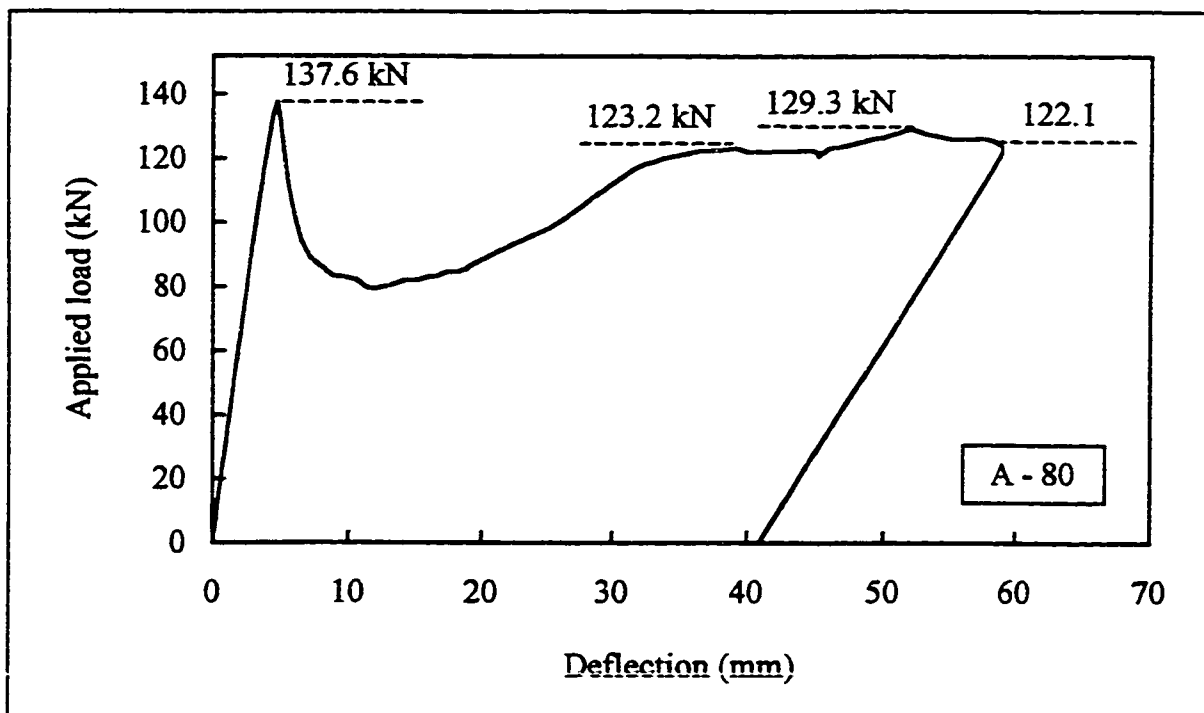
Principal membrane stresses in shear span, rosette R4

Angle of  $\sigma_{\max}$  w.r.t. horizontal direction, rosette R4

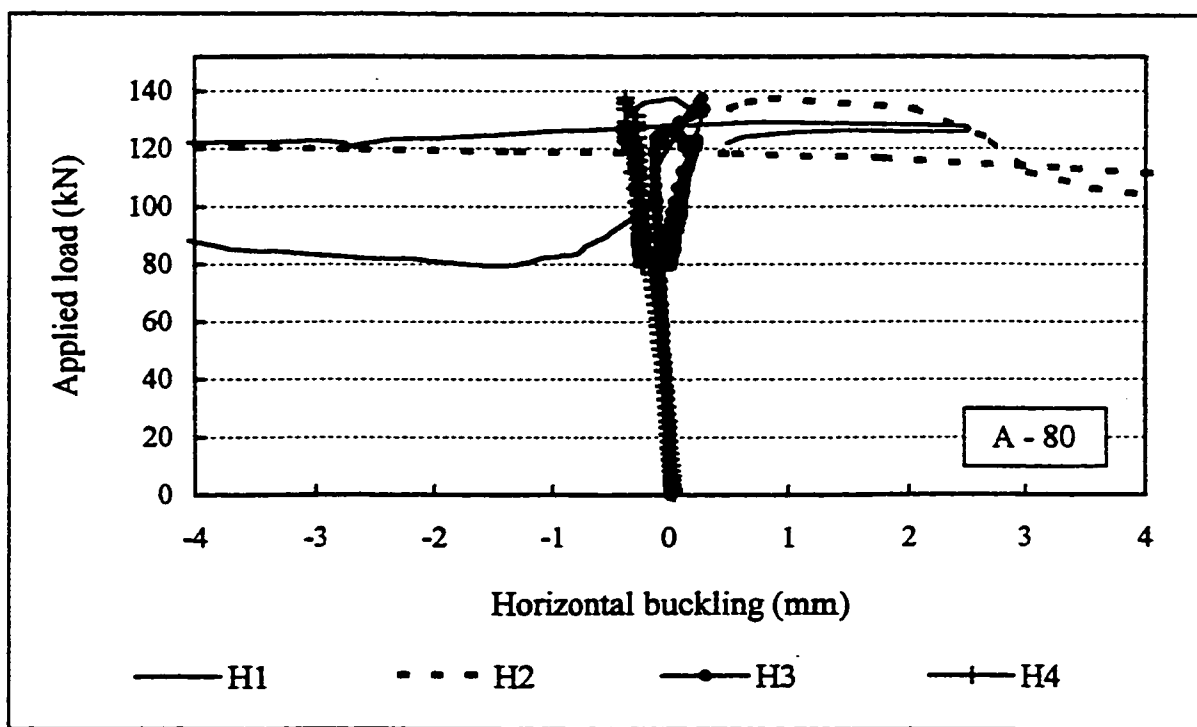


Girder A-110 after testing

# Results : Girder A-80

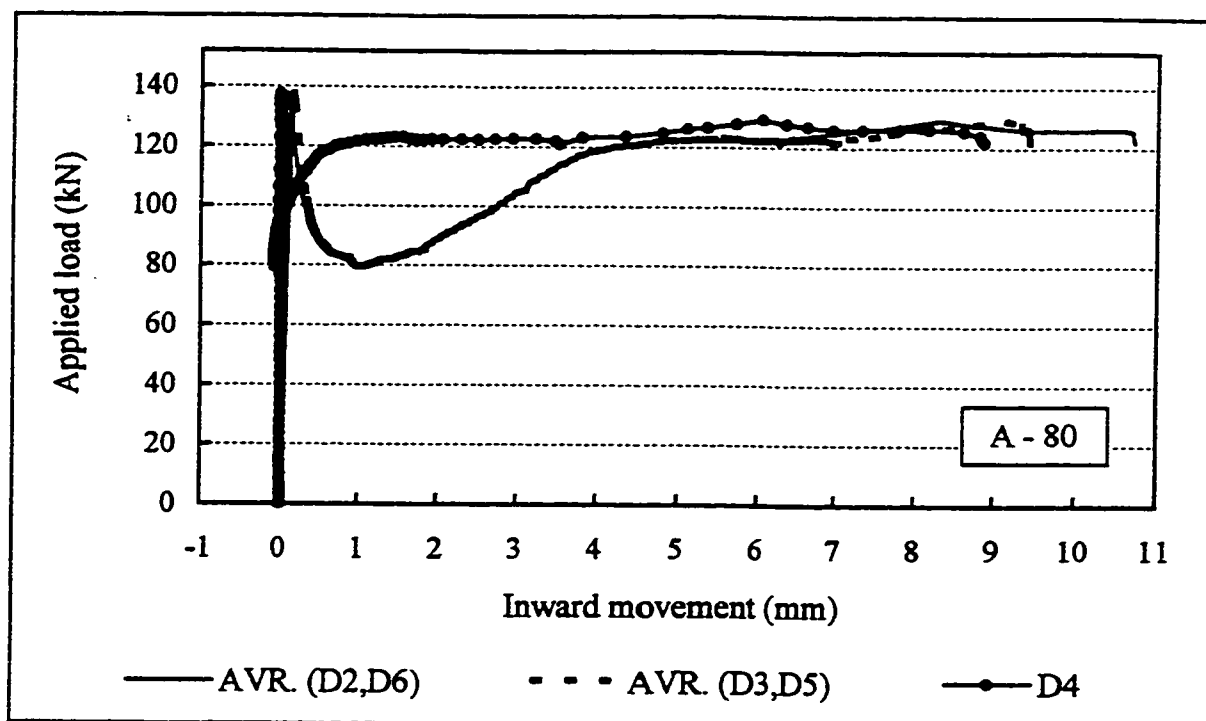


Applied load vs mid-span vertical deflection

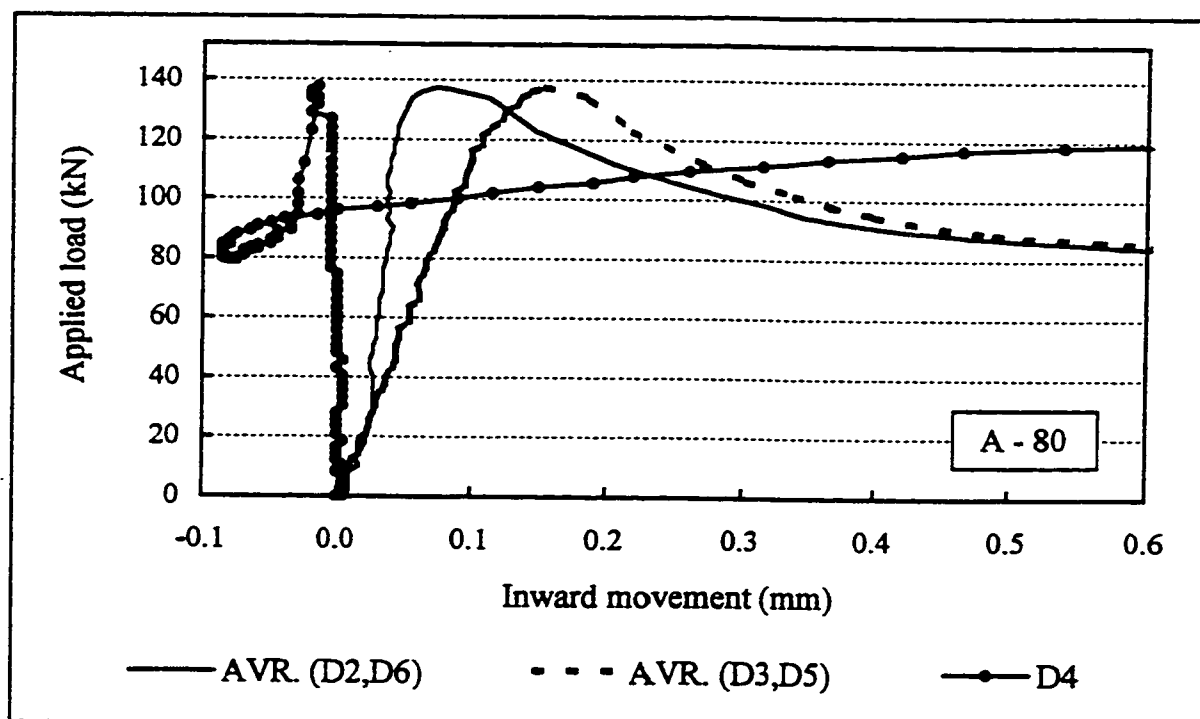


Applied load vs horizontal web buckling

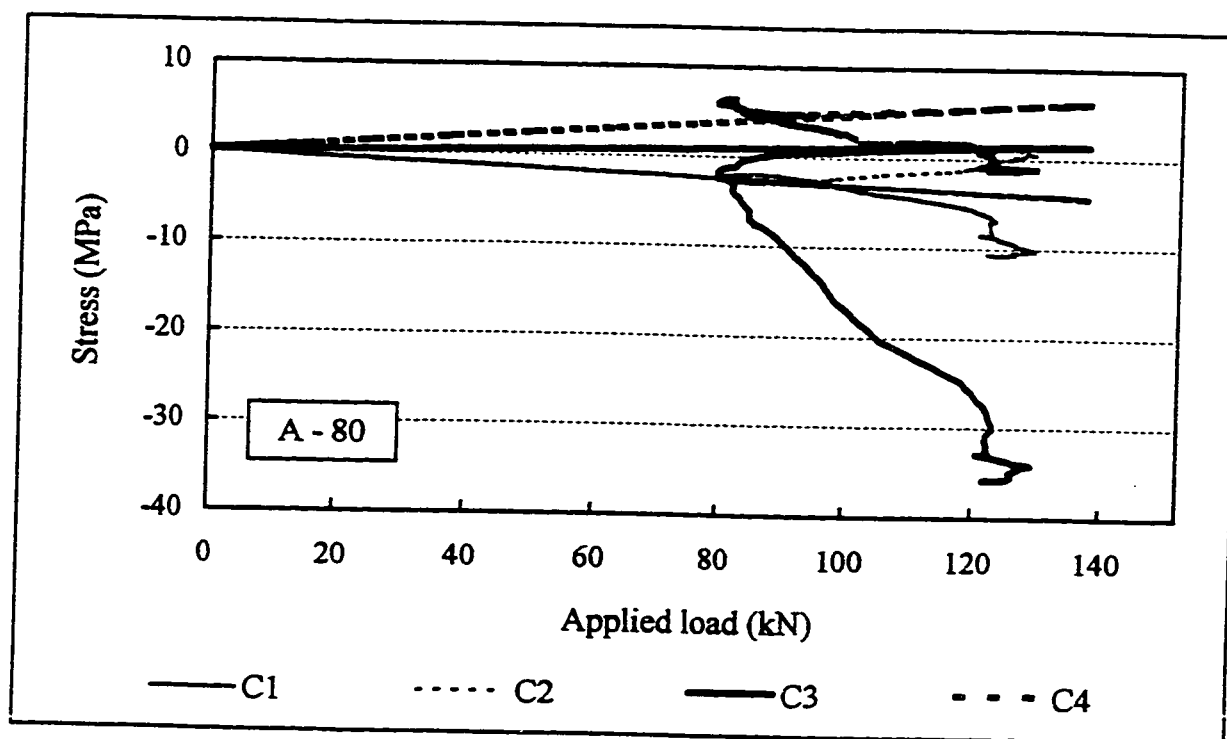




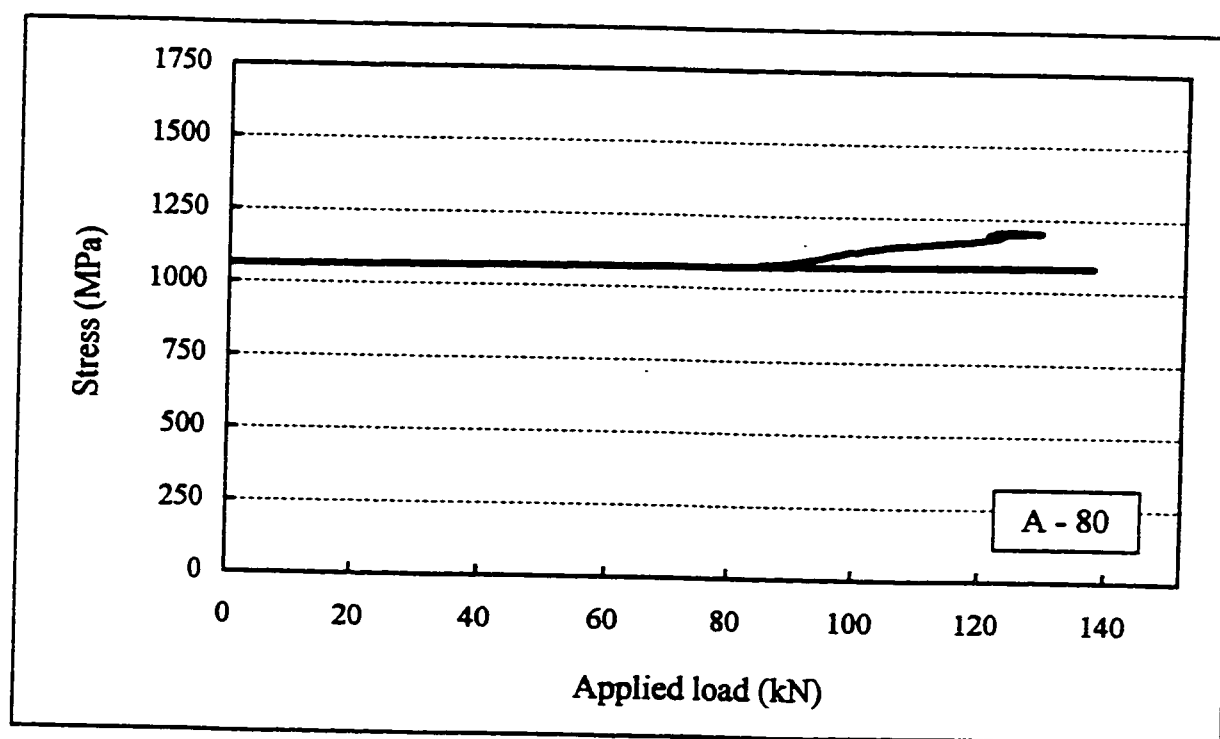
Applied load vs relative inward movement of flanges



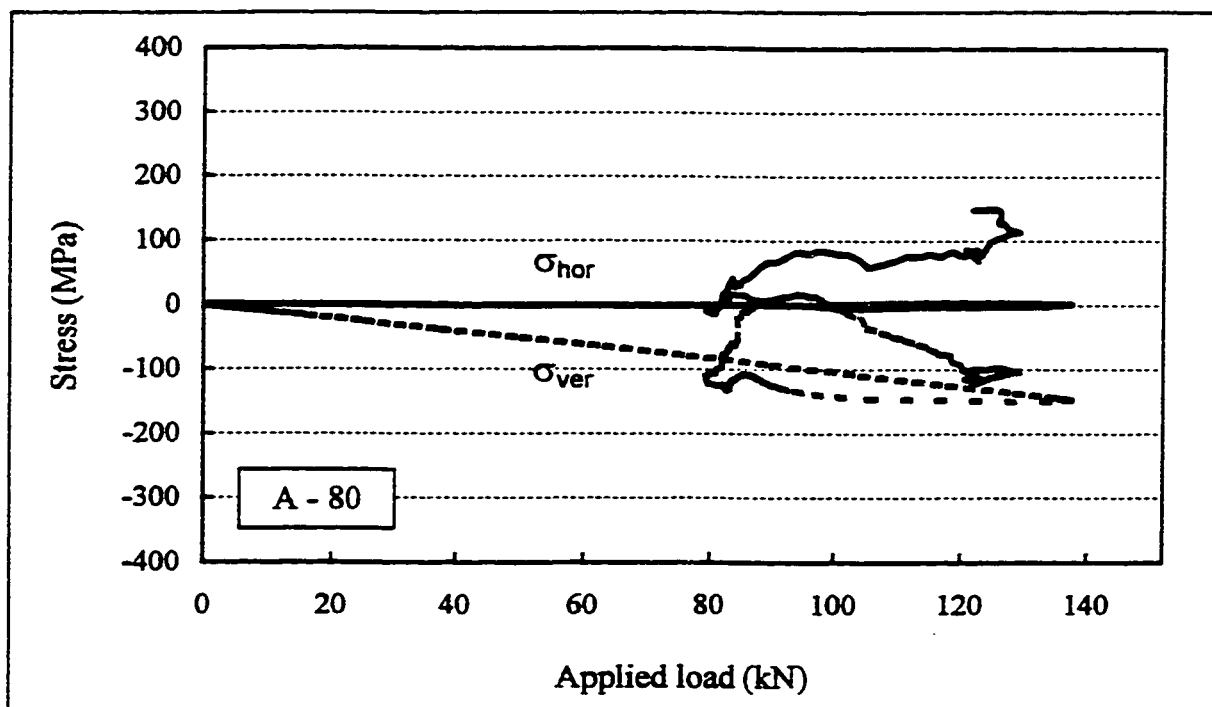
Applied load vs relative inward movement of flanges (zoomed)



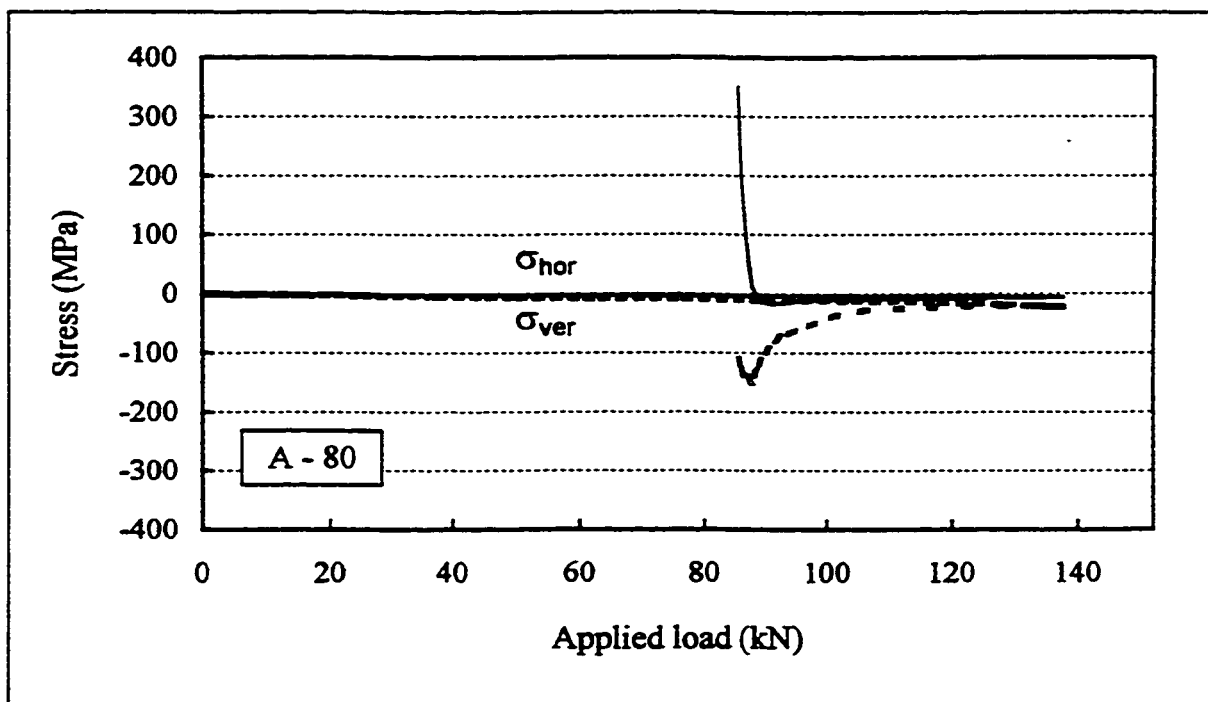
Applied load vs stresses in concrete flanges



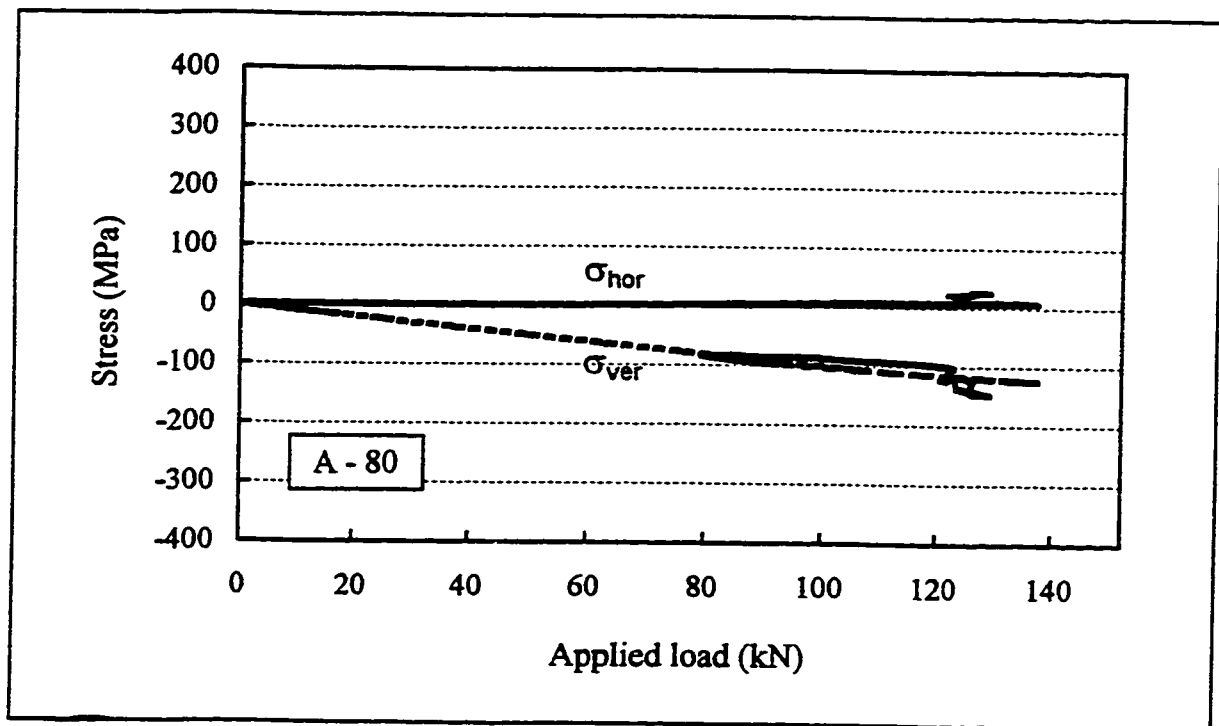
Applied load vs average stress in prestressing strands



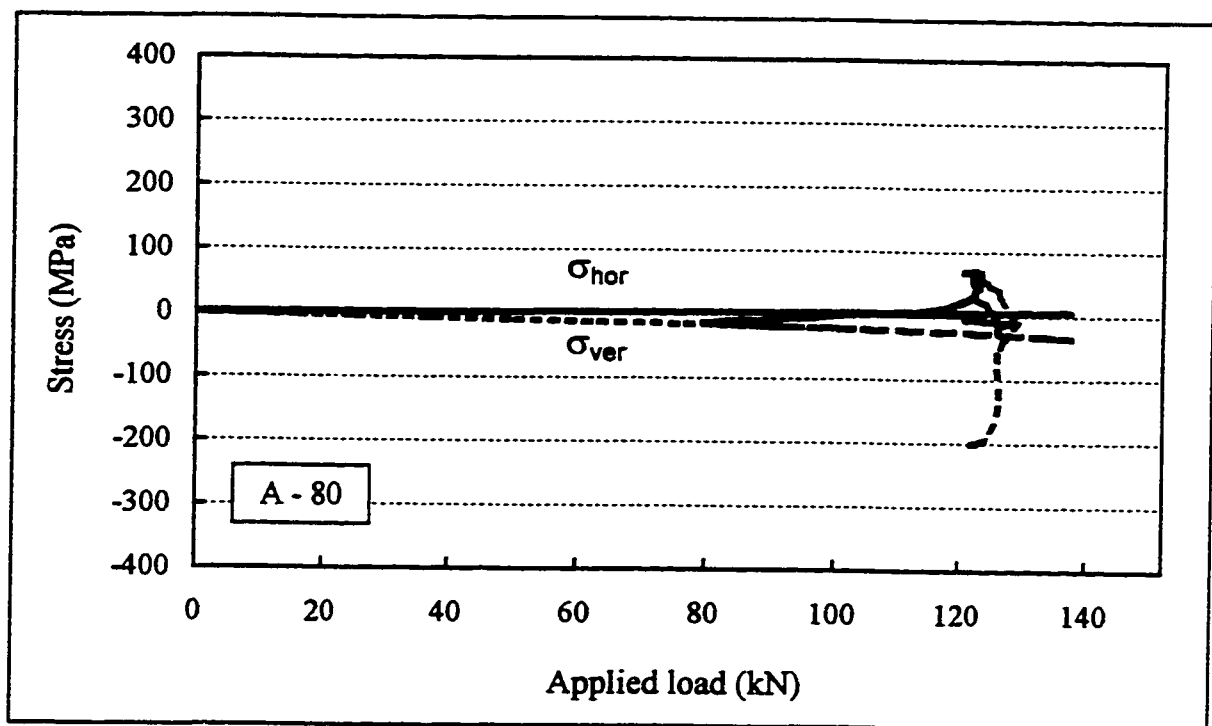
Horizontal and vertical membrane stresses beneath loading points, rosette L1.



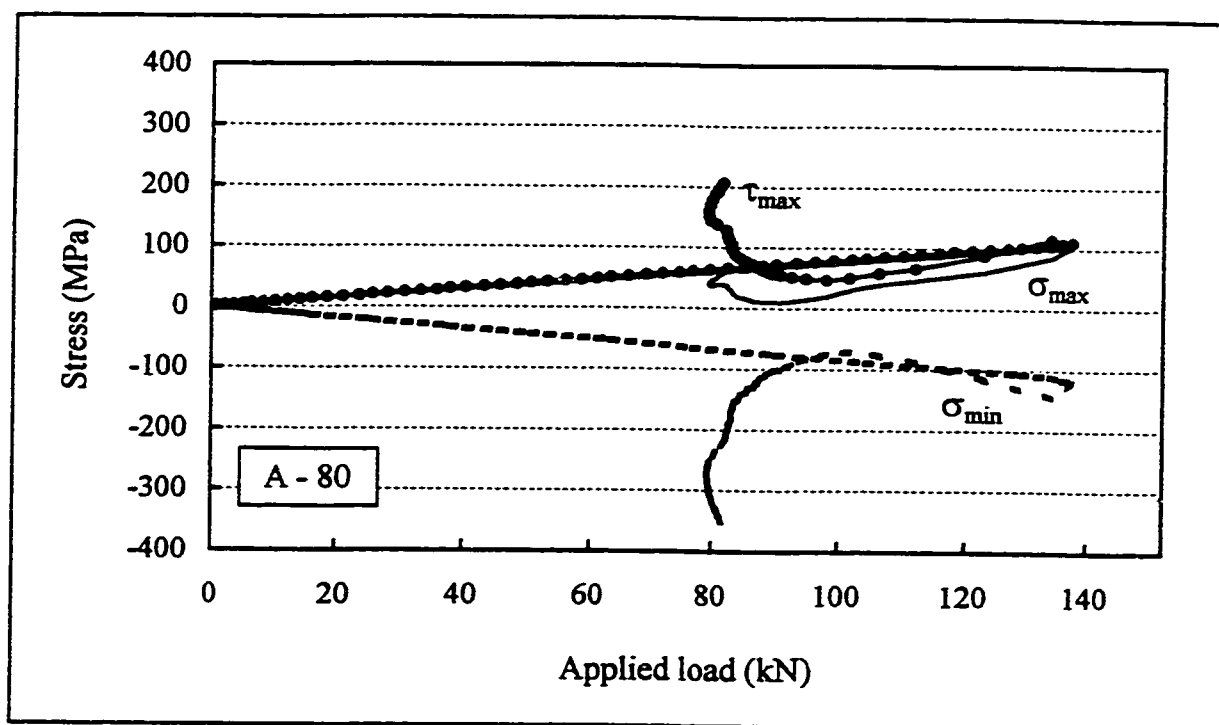
Horizontal and vertical membrane stresses beneath loading points, rosette L2



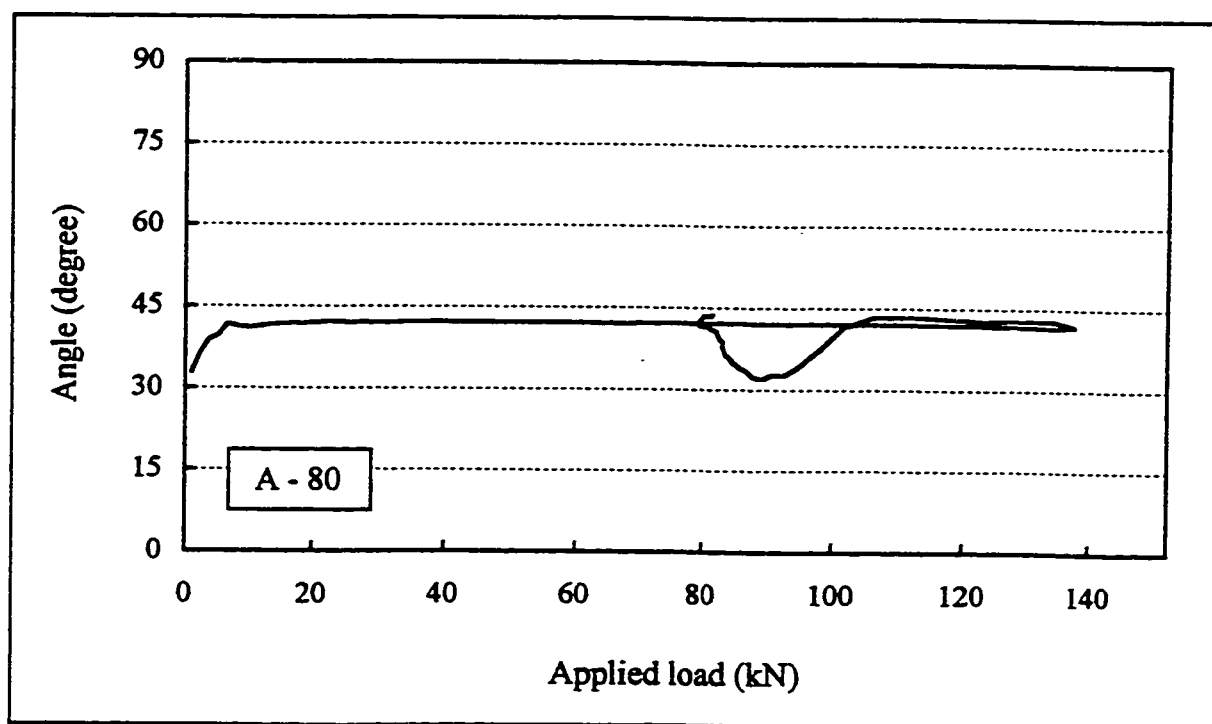
Horizontal and vertical membrane stresses beneath loading points, rosette L3

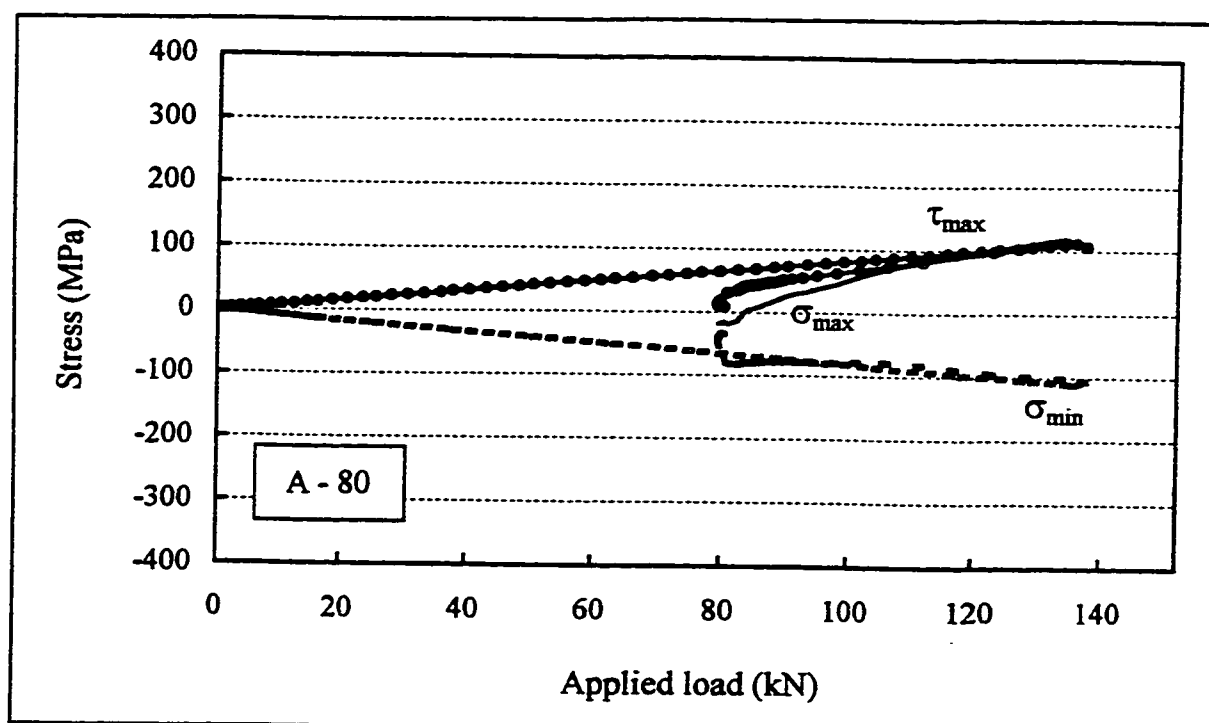


Horizontal and vertical membrane stresses beneath loading points, rosette L4

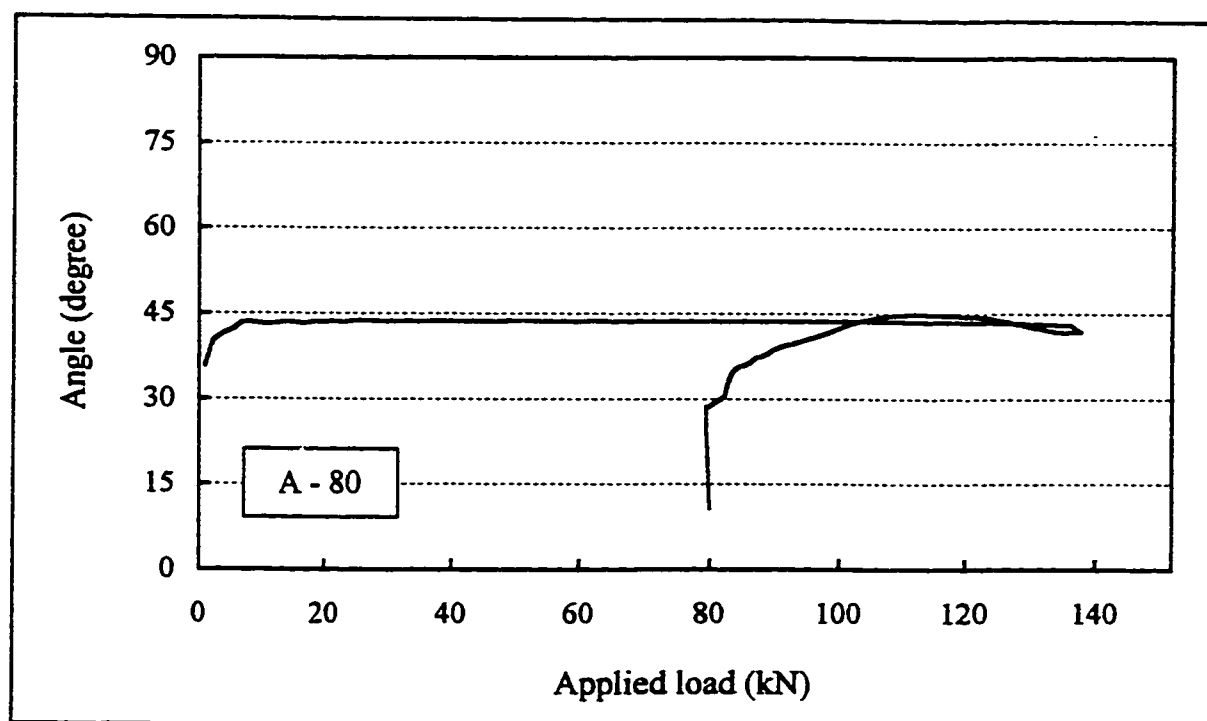


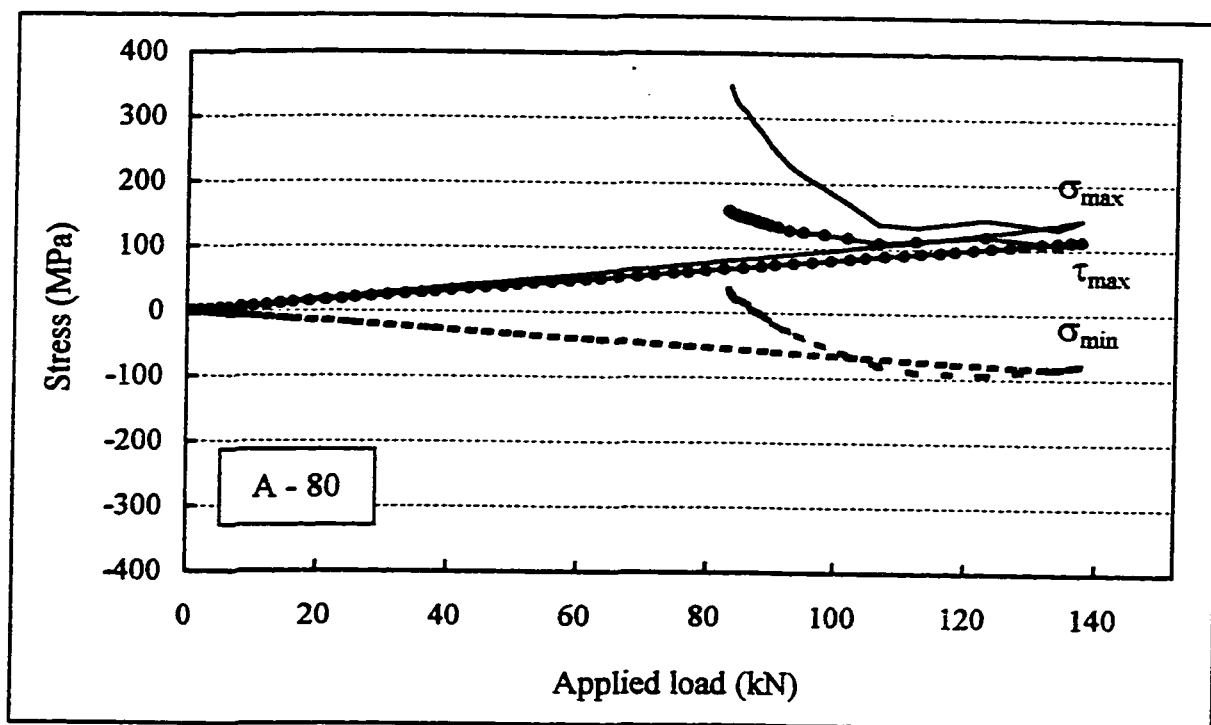
Principal membrane stresses in shear span, rosette R1

Angle of  $\sigma_{max}$  w.r.t. horizontal direction, rosette R1

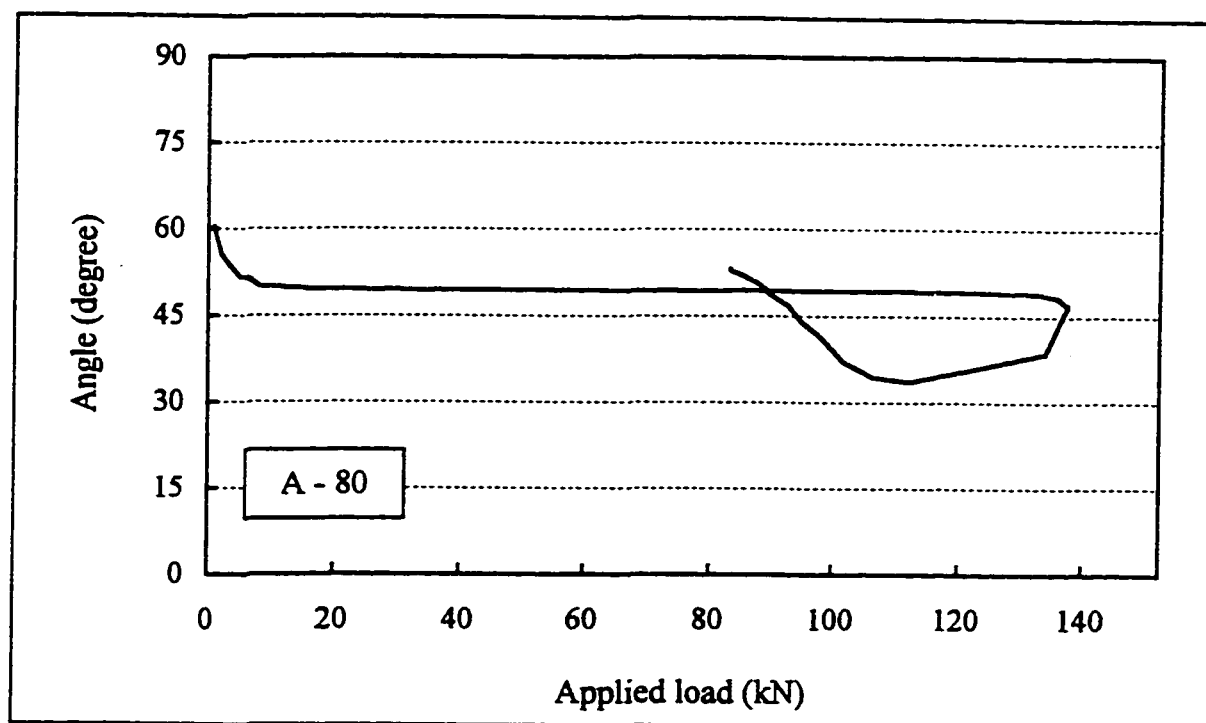


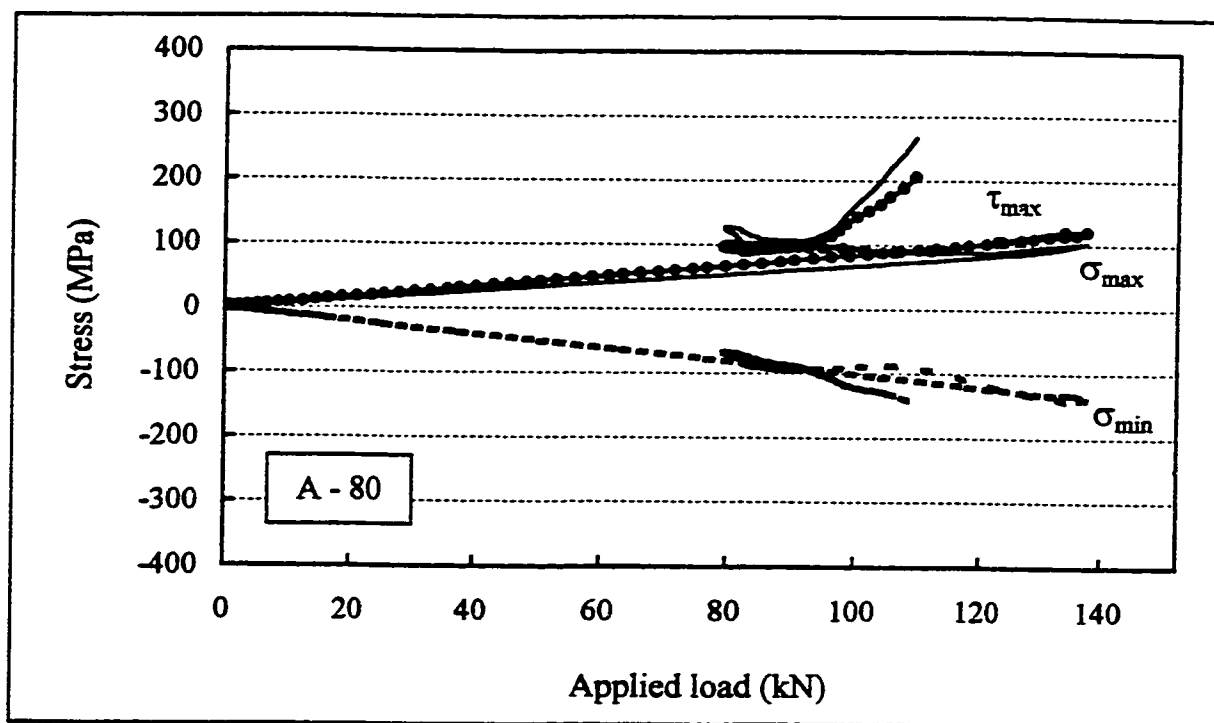
Principal membrane stresses in shear span, rosette R2

Angle of  $\sigma_{\max}$  w.r.t. horizontal direction, rosette R2

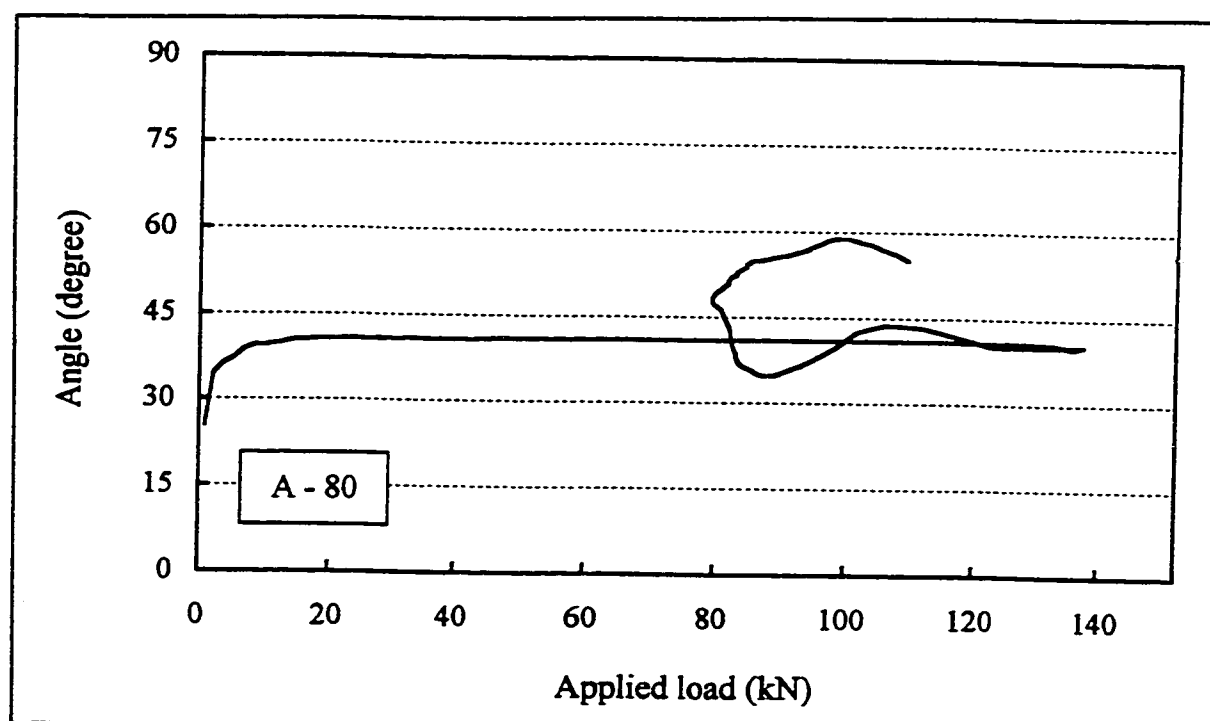


Principal membrane stresses in shear span, rosette R3

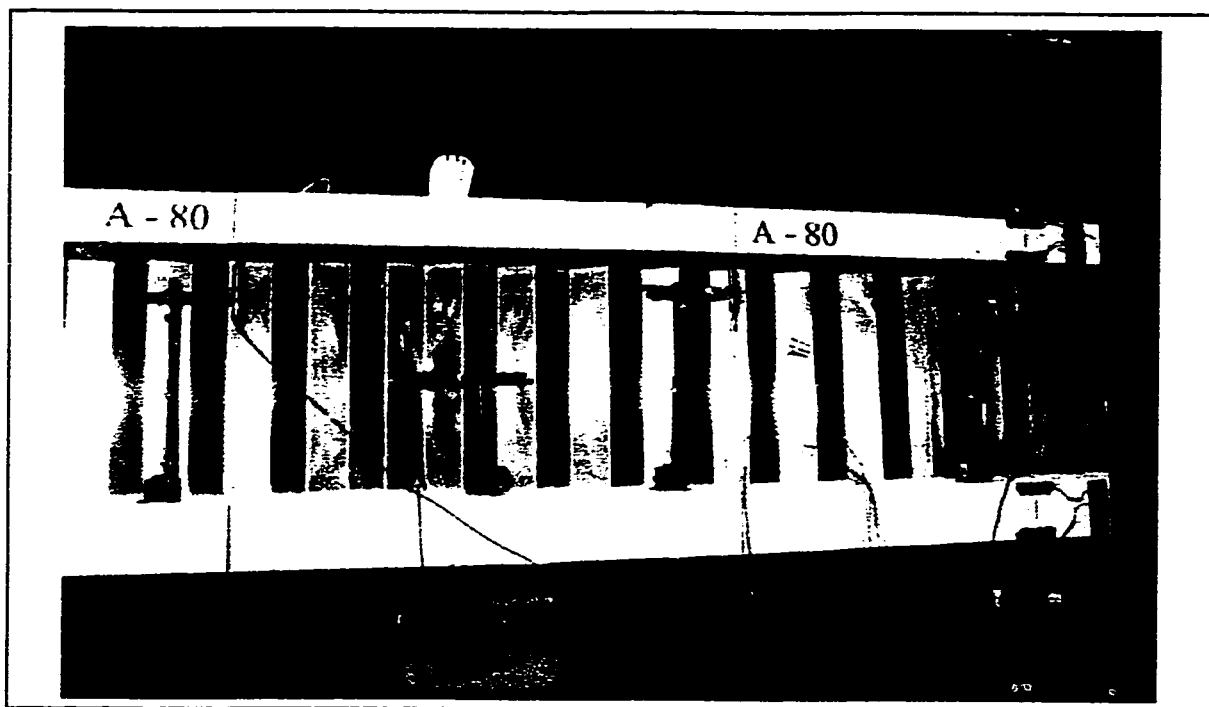
Angle of  $\sigma_{\max}$  w.r.t. horizontal direction, rosette R3



Principal membrane stresses in shear span, rosette R4

Angle of  $\sigma_{\max}$  w.r.t. horizontal direction, rosette R4

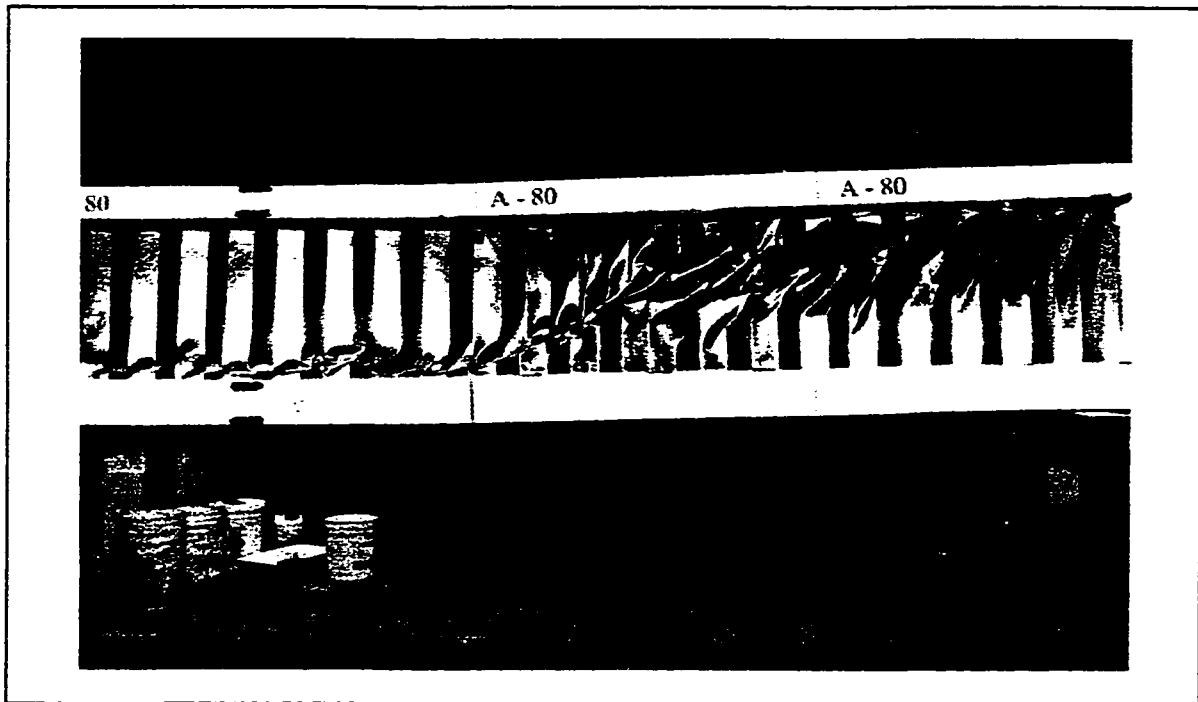




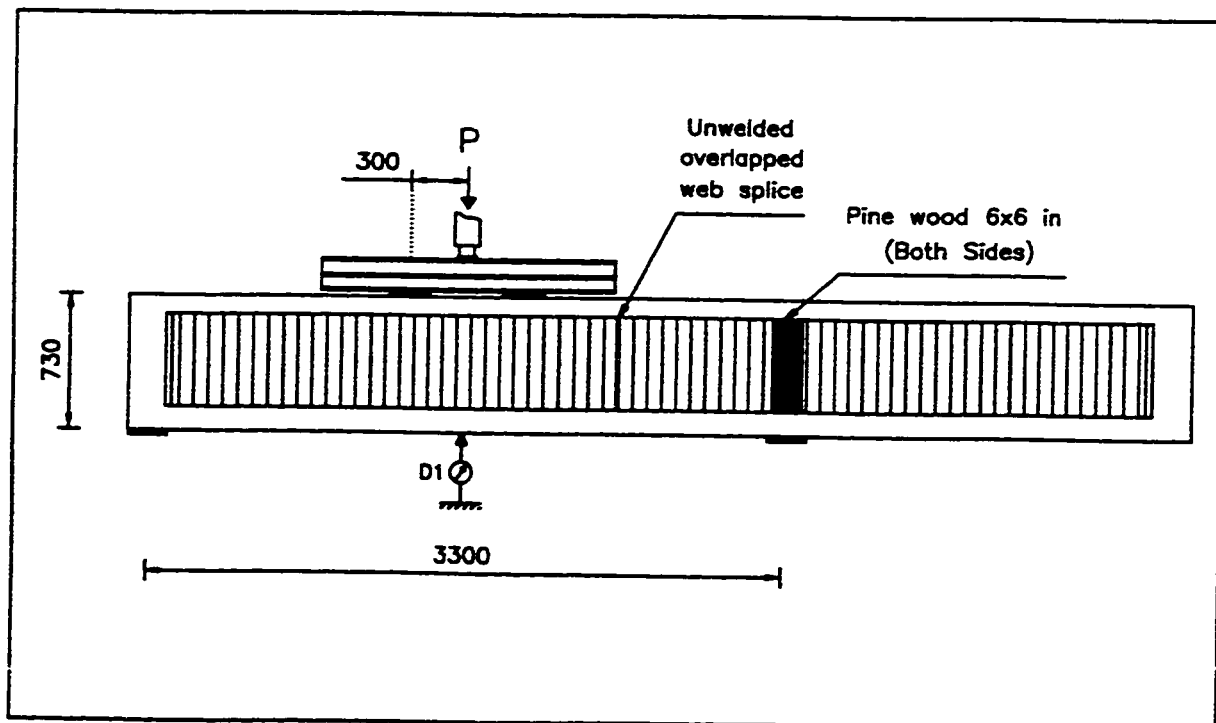
Girder A-80 before testing



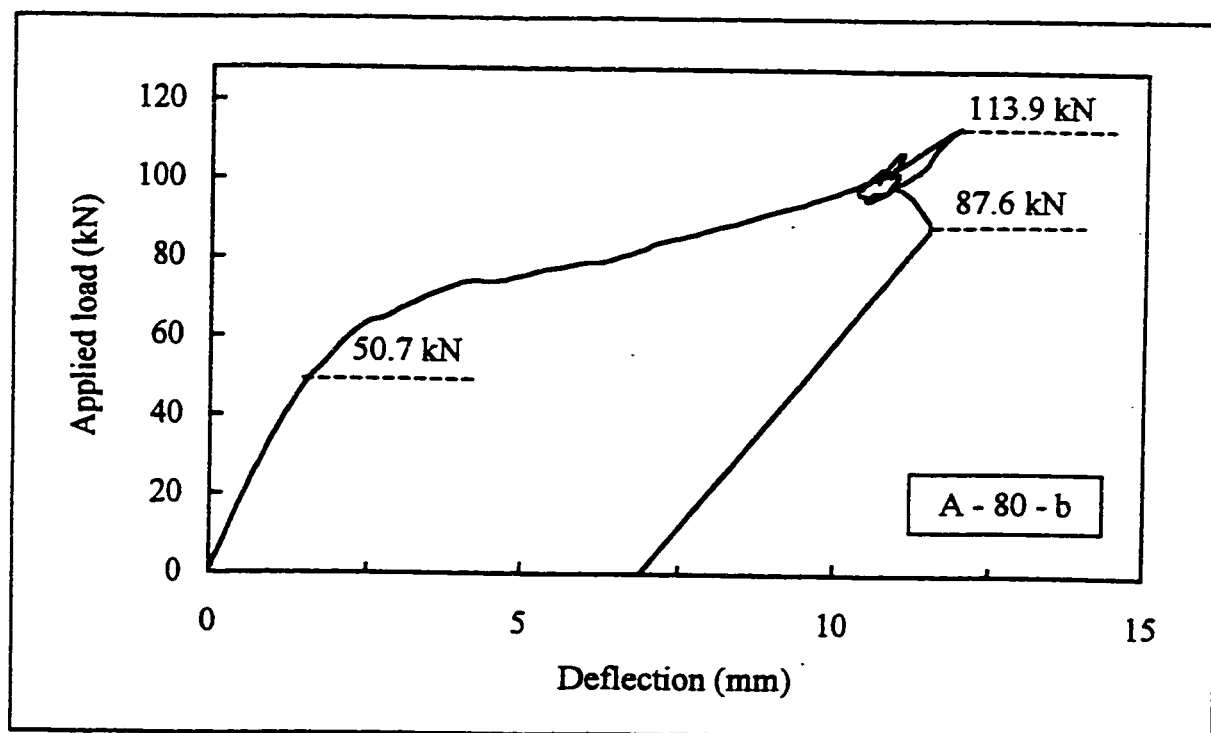
Girder A-80 after testing



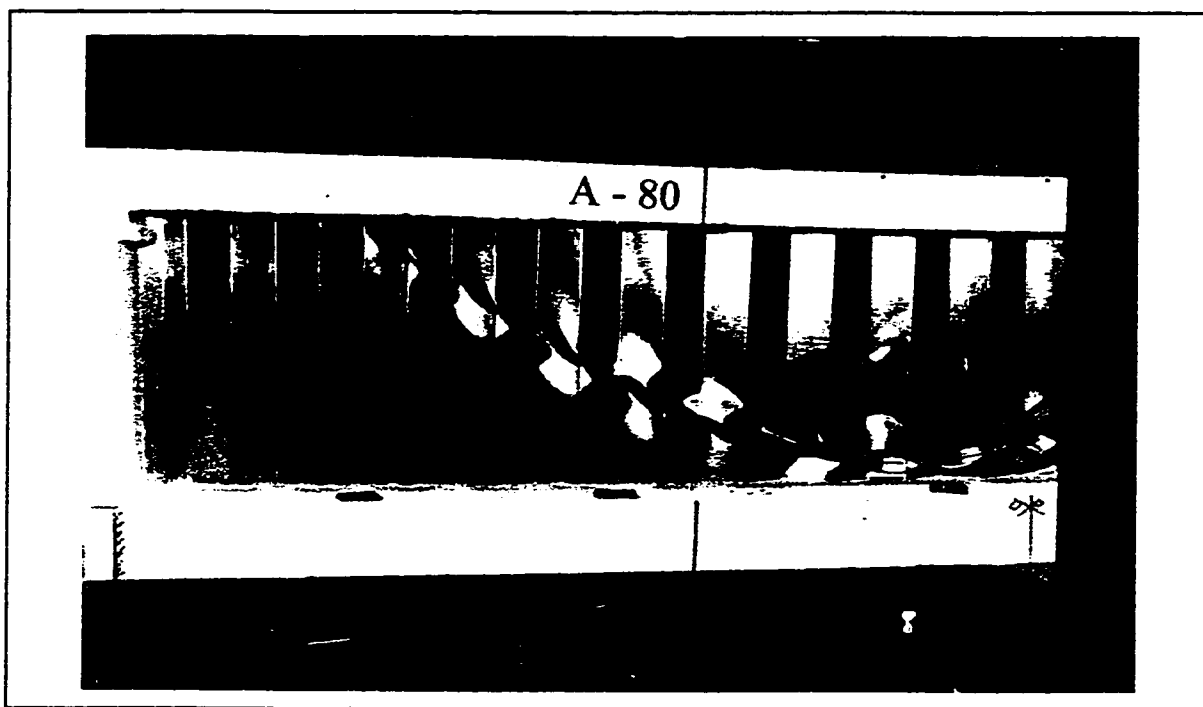
Girder A-80 after testing (zoomed)

**Results : Girder A-80-b**

Instrumentation and test setup



Applied load vs mid-span vertical deflection



Girder A-80-b during testing